Doctoral Dissertation
Doctoral Program in Aerospace Engineering (32nd Cycle)

Development of accurate and efficient structural models for analysis of multilayered and sandwich structures of industrial interest

Andrea Urraci

* * * * * *

Supervisor
Prof. Ugo Icardi

Doctoral Examination Committee:
Prof. Alessandro Airoldi, Referee, Politecnico di Milano
Prof. Maria Kashtalyan, Referee, University of Aberdeen
Prof. Daniele Fanteria, Referee, Università di Pisa
Prof. Luigi Lazzeri, Referee, Università di Pisa
Prof. Dimitris Saravanos, Referee, Panepistimio Patron - University of Patras

Politecnico di Torino
December 2, 2019

I hereby declare that, the contents and organisation of this dissertation constitute my own original work and does not compromise in any way the rights of third parties, including those relating to the security of personal data.

……………………………………....

Andrea Urraci

Turin, December 2, 2019

Acknowledgement

Firstly, my most sincere acknowledgment is dedicated to my supervisor, Prof. Ugo Icardi, for his guidance and support. Since my bachelor and master degree theses, he has been my mentor. During my PhD course, not only my knowledge has improved, but I feel I have become a better man.

Sincere thanks also to Politecnico di Torino and DIMEAS, that charged my education. Special acknowledgement to professors, (here reported in alphabetical order) Prof. Enrico Cestino, Prof. Marco Di Sciuva, Prof. Giacomo Frulla, Prof. Marco Gherlone, Prof. Giulio Romeo, which honored me with the opportunity to permorm class exercises and then to learn the art of teaching.

I acknowledge also PhD colleagues for the good times spent together outside the research activity: Reza Malekimoghadam, Filippo Masseni. Very special thanks to Alessandro Bacchini, for his help and cooperation for training activities during these years.

Finally, my biggest recognition is dedicated to my family for their encouragement to follow my dreams.

Abstract

The purpose of this thesis is the development of accurate and efficient structural models for the analysis of multilayered and sandwich structures. Starting from the 3-D zig-zag adaptive (ZZA) theory by Icardi and Sola, a number of variants are created, in order to understand when transverse displacement representation is essential, or, vice versa, a simpler kinematics can be assumed. Higher-order theories are developed both in mixed and displacement-based forms and their coefficients are redefined for each layer across the thickness and calculated by imposing the full set of physical constraints of the parent theory (ZZA). Using this approach, zig-zag functions can be changed or omitted, those describing the variation of displacements across the thickness can be assumed differently for each displacement component and from point to point across the thickness. On the contrary, the accuracy of lower-order theories that do not have these features become strongly case dependent. Such findings are confirmed by means of numerous challenging benchmarks. Different loading (both localized and distributed) and boundary conditions are examined for elastostatic cases, where laminations with strongly asymmetries are also studied. Also damaged lay-ups are analysed, because this conditions could occur during service life and structural models should be able to accurately capture this. Moreover, the capability of theories to precisely calculate natural frequencies, to describe response to impulsive blast pulse loading and to catch effects on pumping vibrations of soft-core sandwiches are tested. Impact damage analysis and two-material wedge problems are also approached. A generalization of the adaptive zig-zag theory by Icardi and Sola is also presented, whose particularizations have the same accuracy of the parent theory but lower processing time, thus a higher efficiency. Such theory is able to match the results of most used formulations in the literature and, thanks to its simple displacement field, is the most suitable to apply the Strain Energy Update Technique. Such technique allows to get accurate C0 finite elements and to improve the results of the analyses obtained by means of commercial finite elements software.

Motivations, objectives, steps and major achievements of research

Motivations

Nowadays, composite and sandwich materials are widespread in a lot of engineering fields, thanks to their specific properties. Anyway, their modeling is complex because of their intrinsically multi-phase construction, so, they exhibit different local failure and damage propagation behaviour compared to metals. They are also strongly influenced by local effects, at fiber-matrix and layer interface level. Moreover, displacements have to be C^0-continuous across the thickness (zig-zag effect), in order to guarantee the continuity of out-of-plane stresses and of the gradient of transverse normal stress across the thickness.

The design of complex structures made of these materials is carried out by utilizing commercial finite element software, using 1-D and 2-D elements based on simple equivalent single layer theories, which disregard layerwise effects. Indeed, these elements are not accurate, e.g. when thin-walled structures or soft-core sandwiches are analyzed (according to papers by Carrera and co-workers [1], [2], [3]). Commercial 3-D finite elements are more accurate, but they are very expensive and in any case they do not respect out-of-plane stresses prescriptions by the theory of elasticity.

For these reasons, aerostructural research has been focusing on the development of accurate and efficient models to describe behavior of these materials during service life; among the many modeling approaches zig-zag theories stand out because offer a good balance between precision and computational costs. Particularly, refined zig-zag adaptive theory ZZA by Icardi and Sola [4], which is developed under physical considerations and has the same number of d.o.f. of FSDT, has demonstrated its superior accuracy and a high capability to describe layerwise effects. Anyway, it cannot analyse complex structures of industrial interests, e.g. wings, as like as any other analytical model.

In order to overcome these issues, finite elements can be obtained by this theory. However, because of its layerwise and higher-order terms that impose physical constraints (compatibility and boundary conditions on out-of-plane stresses and fulfilment of local equilibrium equation) there are a lot of higher order derivatives into strain energy (see Icardi and Ferrero [5]). As a consequence, a high number of nodal d.o.f. is required, so, they cannot be used to analyze very complex structures. Mixed finite elements able to obtain accurate displacements and stresses can be developed (see e.g. mixed 3-D C0 element by Icardi and Atzori [6], Icardi [7], Icardi and Sola [8]). Anyway, even though their shape functions are simple, they still require a greater number of d.o.f. than commercial ones. Thus, with the intended aim to exploit the power of commercial finite element software and to increase their performance, a novel Strain Energy Update Technique (SEUPT) has been developed.

Objectives

In order to apply SEUPT, corrective terms are introduced into the displacement field of a simplified model, so that the same amount of strain energy of a higher-order theory (e.g. ZZA) is obtained.

Regarding its original form (see Icardi [9] and Icardi and Ferrero [10]), precision of results obtained by commercial finite elements was improved using an iterative post-processing tool. In order to apply this version of SEUPT, the next steps have to be followed:

- Choice of the region to which apply SEUPT;
- Polynomial spline interpolation of the results (e.g. displacements, strains, stresses) obtained by finite elements;
- Calculation of energy contributions of zig-zag theory, using finite element results;
- Calculation of energy contributions of finite elements;
- Corrective terms are introduced into energy contribution by finite elements.
- Calculation of corrective terms, through an iterative process that makes energy contributions equal.
- When the convergence has been achieved, nodal d.o.f. of finite elements are updated;

- A great improvement of results is obtained.

A modified and upgraded version of SEUPT was developed by Icardi and Sola (see [11], [12], [13]). Unlike the previous version, a priori technique is performed, with the aim to obtain an accurate C0 lagrangian finite element.

Firstly, a higher-order theory (e.g. ZZA) is chosen and referred as original model OM. The purpose is to obtain a modified C0 counterpart (without any d.o.f. derivatives) referred as equivalent model EM. In other words, the aim is to obtain a modified expression of displacements of EM, without d.o.f. derivatives, through energy balances, that equalize strain energy, work of inertial and external forces between the two models. Indeed, the basic assumption of SEUPT is that each derivative of d.o.f. in OM can be removed, obtaining a C0 equivalent model, because its energy contributions can be incorporated through corrective terms, irrespective the order of derivatives. So, EM and OM have the same amount of energy and the same d.o.f. and provide the same results. To achieve this, the following steps have to be followed:

- The closed-form expressions of displacements of OM model are obtained, through symbolic calculus tool. They are functions of five d.o.f. of ZZA and their derivatives;
- The closed-form expressions of displacements of EM model are written. This displacement field depends only from d.o.f.
- Derivatives of d.o.f. into displacement field of OM are substituted with corrective terms, whose expression is unknown. So, this rewritten C0 displacement field does not contain any derivative of d.o.f. and it constitutes modified displacement field of EM (but corrective terms are not yet calculated);
- Strain energy of the two models is computed. Through an energy balance and integrating by parts, it is possible to obtain a closed form solution for each corrective term. Thanks to symbolic calculus tool, they are calculated once and for all;
- The same steps can be used also for work of inertial and external forces;
- Because of corrective terms, both models have the same amount of energy. As a consequence they provide the same results.

Because no derivatives are involved as nodal d.o.f., it is possible to obtain a simple C0 lagrangian finite element. Its shape functions are the same as commercial elements, but its precision is similar to a layerwise model

A further version of SEUPT (still under development) consists of a novel approach that strongly integrates commercial finite elements software in the improvement process. Like the previous version of SEUPT, structure is analyzed by using commercial software, so, the next steps are followed:

- Choice of the region to which apply SEUPT;
- Polynomial spline of displacements calculated by finite elements;
- Spline functions are normalized and then they are assumed as trial functions of a higher-order theory (e.g. ZZA), whose amplitudes are unknown and have to be calculated by solving problems;
- Equivalent external load are applied to the model;
- Amplitudes are calculated by applying Rayleigh-Ritz method;
- Corrective elastic moduli are calculated, in order to equal strain energies of higher-order theory and of finite elements;
- Corrective elastic moduli are substituted into commercial finite elements software; a new calculation is done, improving results because the same energy of a higher-order models is obtained.

So, this technique is very interesting, especially for industrial applications, because there is a greater use of commercial codes during design process as pre- and post-processors. Anyway, in order to properly apply SEUPT, modifications and improvements to ZZA theory are mandatory.

As previously stated, ZZA demonstrates a great accuracy. However, its displacement field is very complex and contains a large number of higher order derivatives of d.o.f. Because of summations of layerwise terms of ZZA, very long processing time could occur when structures of industrial interest with a very high number of layers are analyzed. Indeed, computational cost to compute strain energy dramatically increases with increasing the number of constituent layers.

So, the main focus of this thesis is the development of generalized, efficient and accurate theories, with features optimized to be an integral part of process of SEUPT and as a consequence, valuable tools for engineering design of complex components and able to compete with more famous ones in Literature [14]. In order to do this, a lot of studies were necessary and they are briefly outlined in the next section.

Steps of research

During research activity, the following steps were taken:

1. Firstly, mixed version of ZZA are created (see Icardi and Urraci [15]), because according to Literature, simplified but still accurate theories could be obtained by assuming displacements, strains and stresses apart, using Hellingher-Ressner (HR) or Hu-Washizu (HW) variational theorems. Also mixed theories based on kinematic considerations are created (a priori change of slope of displacements is enforced), but physically-based ones demonstrate their superiority [15]. Only HW mixed higher-order zig-zag adaptive theory (HWZZ), that imposes the full set of physical constraints of ZZA and has all coefficients redefined for each layer across the thickness obtains indistinguishable results from those of ZZA but with a lower computational cost (10% less than ZZA).
2. Even though HWZZ has the same accuracy of ZZA but lower processing time, other studies are required, because of cost saving of HWZZ is not very high. Indeed, processing time is mainly determined by integration of strain energy that strongly depends by complexity of fields of the theory and of zig-zag functions. Summations and layerwise functions into displacements of ZZA and HWZZ strongly increase processing time of integration of upper layers, especially when their number is very high. So, with the intended aim to lower computational effort of integration of strain energy, new theories were developed by assuming different and more simple layerwise functions. Particularly, a variant of HWZZ, called HWZZM (Icardi and Urraci [16]) is developed by assuming Murakami's zig-zag functions instead of those of HWZZ. Similarly, a modified ZZA theory, called ZZA* (Icardi and Urraci [17]) is developed, where first and second order power functions are assumed as layerwise functions. Indistinguishable results than parent theory are obtained by ZZA* and HWZZM, irrespective zig-zag functions chosen, as coefficients are redefined for each layer across the thickness and the full set of physical constraints

of ZZA is imposed. Moreover, lower processing time than ZZA and HWZZ are obtained by these theories. Anyway, further studies are required, in order to get a more generalized and simple version of ZZA, optimized for SEUPT process.

3. With the intended aim to create a general version of ZZA, a lot of theories were developed and tested. According to Icardi and Urraci [18], [19], [20], [21], [22] [23] these theories assume:
    a. different representations of global functions across the thickness, such as exponential, trigonometric, power series or a combination of them instead of polynomial;
    b. different representations of transverse variation of displacements that can be assumed differently from a point to point across the thickness and for each displacement.

Regarding calculation of coefficients, there are several differences between ZZA, HWZZ, HWZZM, ZZA* and theories of [18], [19], [20], [21], [22] [23].
Indeed, ZZA, HWZZ, HWZZM, ZZA* are developed adding terms to FSDT kinematics, which are subdivided into *higher-order* and *continuity* terms, according to the role assumed in the imposition of physical constraints:

- Coefficients of the continuity terms (which multiply the zig-zag functions) are calculated by imposing the compatibility of out-of-plane stresses and displacements at the interfaces across the thickness.
- Coefficients of higher-order terms (which multiply the global functions that describe the variations of displacements across the thickness) are calculated by imposing the fulfillment of local equilibrium equations at different points across the thickness and of boundary conditions on out-of-plane stresses.

So, coefficients of terms of ZZA, HWZZ, HWZZM, ZZA* theories assume a specific role and, as a consequence, are calculated by imposing the fulfillment of specific physical constraints. E.g., Φ_{α} of ZZA is calculated by imposing compatibility of transverse shear stress at interfaces, while C_{α} by enforcing the fulfillment of local equilibrium equation at inner layers.

Numerical assessments in [18], [19], [20], [21], [22] [23] demonstrated that roles of coefficients of theories ZZA, HWZZ, HWZZM, ZZA* can be freely modified without losing accuracy. E.g., Φ_{α} can be calculated by imposing the fulfillment of local equilibrium equation at inner layers, while C_{α} by enforcing compatibility of transverse shear stress at interfaces.
As a consequence, for theories developed in [18], [19], [20], [21], [22] [23] it is not necessary to a priori assign a specific role to terms of the displacement field. So, the rigid subdivision of coefficients is completely abandoned.
Indeed, coefficients of theories in [18], [19], [20], [21], [22] [23] are calculated by solving a unique algebraic system whose equations are all the physical conditions expressed in strong point-wise sense. By solving the system in matrix form, it is possible to calculate the explicit expression of the coefficients, which depend on geometry, on mechanical properties of constituent layers, on loading and on d.o.f. that must be calculated through Rayleigh-Ritz method. So, for theories [18], [19], [20], [21], [22] [23]:

c. there is no need to assign a specific role to coefficients.

As a result, two generalized version of ZZA are obtained and called ZZA-XX and ZZA-XX', whose functions that represent transverse variation of displacements along thickness coordinate can be freely assumed by user as input of analysis and coefficients are redefined for each layer across the thickness and calculated on a physical basis. Expansion order of displacements across the thickness is chosen by user, even if at least a cubic/fourth-order should be enforced to impose the full set of physical constraints of ZZA, and as a consequence, to obtain indistinguishable results than the parent theory.

4. A more general version of the ZZA, called ZZA_GEN can be obtained, omitting linear contribution of FSDT (that is included into ZZA and all theories derived from it). Nevertheless, five coefficients of the first layer from below are assumed as fixed d.o.f. of this theory, which have the same number of unknowns of ZZA and the same features than ZZA-XX and ZZA-XX'.

Major achievements of research

All the previous findings (1 to 4) are valid when coefficients are redefined for each layer across the thickness and calculated by enforcing the full set of physical constraints of ZZA. Under these conditions:

- zig-zag functions can be changed or omitted
- functions that describe variation of displacements across the thickness can be changed, so, exponential, power series and sinusoidal functions, or a combination of them, can be assumed differently for each displacement and from point to point across the thickness
- there is no need to assign a specific role to coefficients, indeed it can be freely switched.

without any loss of accuracy and indistinguishable results than ZZA are obtained.

On the contrary, if the fulfilment of physical constraint is only partial and/or coefficients are not redefined across the thickness, accuracy of theories (which are defined lower-order) become strongly dependent on the assumptions.

ZZA_GEN, of which a new particularization is developed and reported into this thesis (ZZA_GEN2*), is the most general version of theories obtained from ZZA, which assures the same accuracy of parent theory, but with low computational burden, thanks to its assumptions.

For these reasons they represent the most suitable theories, to which SEUPT processes should be applied. The application of different version of SEUPT techniques will be briefly outlined in chapter 8. Indeed, the focus of this thesis is the development of optimized models for SEUPT process (e.g. ZZA_GEN).

Previous achievements are also contained into these papers, published during PhD research:

Authors	Title	Journal	Years
U. Icardi and A. Urraci	Impact Damage Analysis with Stress Continuity Constraints Fulfilment at Damaged-Undamaged Regions and at Layer Interfaces	Latin American Journal of Solids and Structures	2017
U. Icardi and A. Urraci	Novel HW mixed zig-zag theory accounting for transverse normal deformability and lower-order counterparts assessed by old and new elastostatic benchmarks.	Aerospace Science and Technology	2018
U. Icardi and A. Urraci	Free and Forced Vibration of Laminated and Sandwich Plates by Zig-Zag Theories Differently Accounting for Transverse Shear and Normal Deformability	Aerospace, MDPI	2018
A. Urraci and U. Icardi	New 3-D zig zag theories: elastostatic assessment of strategies differently accounting for layerwise effects of laminated and sandwich composites	International Journal of Engineering Research and Application	2019
A. Urraci and U. Icardi	Approximate 3-D model for analysis of laminated plates with arbitrary lay-ups, loading and boundary conditions	International Journal of Engineering Research & Science	2019
A. Urraci and U. Icardi	Zig-zag theories differently accounting for layerwise effects of multilayered composites	International Journal of Engineering Research & Science	2019
U. Icardi and A. Urraci	Free Vibration of flexible soft-core sandwiches according to layerwise theories differently accounting for the transverse normal deformability	Latin American Journal of Solids and Structures	2019
U. Icardi and A. Urraci	Elastostatic assessment of several mixed/displacement-bases laminated plate theories, differently accounting for trasverse normal deformability	Aerospace Science and Technology	2020
U. Icardi and A. Urraci	Considerations about the choice of layerwise and through-thickness global functions of 3-D physically-based zig-zag theories	Under Review	-
A. Urraci and U. Icardi	Physically-based approximate 3-D multilayered structural models derived as a generalization and an improvement of zig-zag theories	Under Review	-

Overview of research

Brief description of theories developed

It should be noticed that in order to demonstrate previous findings, various theories were developed in papers [15] to [23]. Their accuracy was tested studying many challenging elastostatic and dynamic problems. A brief summary of theories developed in papers [15] to [23] and in this thesis is reported in Tables 1 to 5.

Regarding Tables 1a to 1c that briefly reports the features of theories, models in bold are retaken also into this thesis, while light blue highlighted ones are new theories developed in this thesis.

Particularly, Table 1a, reports higher-order zig-zag theories obtained from ZZA, whose coefficients are redefined for each layer and calculated by imposing the full set of physical constraints. In-plane displacements are piecewise cubic, transverse one is piecewise fourth-order.

Name and reference

HSDT_34 [19]		**ZZA*** [17]	
HWZZ [15]		ZZA*_43 [19]	
HWZZ_RDF [19]		ZZA*_43PRM [22]	
HWZZ_RDFX [20]		ZZA*_43X [20]	
HWZZM [17]		ZZA1 [16]	
HWZZM* [17]		ZZA2 [16]	
ZZA_RDF [19]		**ZZA3** [16]	
ZZA_RDFX [20]		ZZAS4 [18]	
ZZA-XX [19]		***ZZM***	
ZZA-XX' [19]			

Zig-zag omitted

Mixed HW

Mixed HW with different role of coefficients

Mixed HW with different role of coefficients and different representation from point to point across the thickness

Mixed HW, Different zig-zag functions

Mixed HW, Zig-zag omitted

Different role of coefficients

Different role of coefficients and different representation from point to point across the thickness

Different representation from point to point across the thickness, zig-zag omitted

Different expansion order (4th in-plane, 3rd transverse displacements)

Different expansion order (4th in-plane, 3rd transverse displacements), zig-zag omitted, different role of coefficients

Different expansion order (4th in-plane, 3rd transverse displacements), zig-zag omitted

Different zig-zag functions

Table 1a. Higher-order theories developed in [15] **to** [23]**. In bold theories reported in this paper.**

Table 1b reports two generalizations of ZZA developed in this thesis:

Theory	Particularizations
ZZA_GEN	[23]: ZZA_GEN1 and ZZA_GEN2 New particularization: ZZA_GEN2*
ZZA_X [18]	[18]: ZZA_PP34, ZZA_PT34, ZZA_PM34, ZZA_PMTP34, ZZA_PPM34, NOZZG [19]: ZZA_X1 to _X4. [22]: ZZA_X1* to _X4*. [20]: ZZA_X_1 to X_4. New particularizations: ZZA_XN1, ZZA_XN2, ZZA_XN3, ZZA_XN4, ZZA_XN5, ZZA_XN6, ZZA_XN7, ZZA_XN8, ZZA_XN9, ZZA_XN10.

Table 1b. New higher-order theories developed in this thesis.

Table 1c contains features of lower-order zig-zag theories.

Mixed theories with piecewise cubic in-plane displacements

HRZZ [15]	**MHR±** [17]
HRZZ4 [15]	**MHR4±** [17]
HWZZM(♥) [17]	**MHWZZA** [15]
MHR [15]	**MHWZZA4** [15]
MHR4 [15]	

Mixed HR with simplified transverse displacement.

Mixed HW versions of HWZZM with some zig-zag amplitudes calculated, other imposed. Particularizations: ♥=0,A,B,C, B2, C2

Mixed HW with displacements, kinematics with periodic change of slope of displacements, strains and stresses like HWZZ

Mixed HR with simplified transverse displacement, periodic change of slope of displacements and coefficients not redefined.

Mixed HR with simplified transverse displacement, the correct sign of zig-zag functions is assumed on a physical basis and coefficients not redefined.

Lower-order of representation

ZS1 [18]	ZS3 [18]
ZS1_1 [18]	ZS3_1 [18]
ZS1_2 [18]	ZS3_2 [18]
ZS1_3 [18]	PP23 [18]
ZS1_4 [18]	HSDT_32 [19]
ZS2 [18]	HSDT_33 [19]

Piecewise linear in-plane displacements and piecewise parabolic transverse one
Piecewise parabolic in-plane displacements. Zig-zag functions omitted.
Piecewise cubic in-plane displacements. Zig-zag functions omitted.

Piecewise cubic in-plane displacements and piecewise fourth-order transverse one

ZZ_NA1 [16]	ZZAM_P3P4 [18]
ZZ_NA2 [16]	ZZAS2 [18]
ZZAS1 [18]	ZZAS3 [18]

Not redefined coefficients.
Equilibrium enforced in integral form.
Some layers assume a linear in-plane displacement and a uniform transverse one.
Some layers assume a linear in-plane displacement and a parabolic transverse one.
Some layers assume a parabolic in-plane displacement and a cubic transverse one.

Table 1c. Lower-order theories developed in [15] to [23]. Accuracy strongly case dependent. In grey theories reported in this paper.

Contents

List of Tables

List of Figures

Nomenclature

Symbol	
$(.)_{,i}$	Derivative
α , β	In-plane coordinates
b^i	Body forces
C^i	Differentiability class of functions
C_{ij}	Elastic moduli
E_{ij}	Young's modulus
ε_{ij}	Strains
$\{F^e\}$	Vector of nodal forces
G_{ij}	Transverse shear modulus
Γ_α , Γ_β	Shear rotations of then normal
h	Overall thickness
$[K^e]$	Stiffness element matrix
$[M^e]$	Mass matrix
N_i	Shape functions
ν_{ij}	Poisson ratios
σ_{ij}	Stresses
θ	Orientation angle
$\{q^e\}$	Vector of nodal d.o.f.
$\Re^i$	Trial functions
S	Surface
t_i	Tractions
u_α^0 , u_β^0 , w^0	Middle plane displacements
u_α , u_ς	In-plane and transverse displacements
V	Volume
ς	Transverse coordinate

Acronyms, abbreviations and appellations of theories

Symbol	Explanation
3-D FEA	Mixed solid 3-D elements (see [6]).
CUF	Carrera Unified Formulation.
DL	Discrete-layer theories.
d.o.f.	Degrees of freedom
DZZ	Di Sciuva's like (or physically-based) zig-zag theories.
ESL	Equivalent Single Layer theories.
FSDT	First-order shear deformation theory (see 1.6).
HR	Hellinger-Ressner variational theorem
HRZZ	HR zig-zag mixed theory with uniform transverse displacement (see 2.3 and 2.3.1).
HRZZ4	HR zig-zag mixed theory with fourth-order polynomial transverse displacement (see 2.3 and 2.3.1).
HSDT	Higher-order shear deformation theory (see 1.6).
HSDT_32	Refined variant of HSDT with piecewise cubic in-plane displacements and piecewise parabolic transverse one (see 3.2.1 and 3.2.3).
HSDT_33	Refined variant of HSDT with piecewise cubic in-plane displacements and piecewise cubic transverse one (see 3.2.1 and 3.2.3).
HSDT_34	Refined variant of HSDT with piecewise cubic in-plane displacements and piecewise fourth-order polynomial transverse one (see 3.2.2 and 3.2.3).
HT	Hierarchical theories
HW	Hu-Washizu variational theorem
HWZZ	HW zig-zag mixed theory obtained from ZZA (see 2.4 and 2.4.1).
HWZZ_RDF	HWZZ whose coefficients assume different roles than ZA (see 3.3 and 3.3.1).
HWZZM	HW zig-zag mixed theory obtained from ZZM (see 3.1.1 and 3.1.3).
HWZZM*	HW zig-zag mixed theory obtained from ZZA* (see 3.1.2 and 3.1.3).
MHR	HR mixed theory with Murakami's zig-zag function (see 2.5 and 2.5.1)

Continuation:

Symbol	**Explanation**
MHR±	MHR with slope defined on a physical basis (see 2.6 and 2.6.1).
MHR4	MHR with fourth-order piecewise polynomial transverse displacement (see 2.5 and 2.5.1).
MHR4±	MHR4 with slope defined on a physical basis (see 2.6 and 2.6.1).
MHWZZA	HW mixed theory with displacements from MHR, strain and stresses like HWZZ (see 2.6 and 2.6.1).
MHWZZA4	HW mixed theory with in-plane displacements from MHR, transverse one from ZZA, strain and stresses like HWZZ (see 2.6 and 2.6.1).
MZZ	Murakami0s like or kinematic-based zig-zag theories
NOZZG	Generalized theory with features similar to DL and exponential representation (see [18]).
NOZZG’	Generalized theory with features similar to DL (see [18]).
SEUPT	Strain Energy Update Technique
TPE	Total Potential Energy
ZZ	Zig-zag theories.
ZZA	Zig-zag adaptive theory (see 1.6).
ZZA_GEN	Generalized zig-zag theory (see 3.5.1 and 3.5.2).
ZZA_RDF	ZZA whose coefficients assume different roles than ZA (see 3.3 and 3.3.1).
ZZA_X	Generalized zig-zag theory (see 3.5.3 and 3.5.4).
ZZA*	Modified ZZA theory without zig-zag functions (see 3.1.2 and 3.1.3).
ZZA****	Modified ZZA theory with different representation (see 3.4 and 3.4.1).
ZZM	Modified ZZA theory with Murakami’s zig-zag functions (see 3.1.1 and 3.1.3).

Outline

PART I – Introduction

Chapter 1: this chapter contains general assumptions about modelling of composites, as well as an in-depth description of ZZA. Also a brief explanation of FSDT, HSDT theories and of the mixed solid element by Icardi and Atzori [6] are given.

PART II – Zig-zag theories and applications

Chapter 2: most significant theories are reported in this chapter, which show progressive refinement of ZZA. Particularly, mixed theories are developed both in physically- and kinematic-based forms.

Chapter 3: most significant theories are reported in this chapter, which are a general and efficient version of ZZA.

Chapter 4: in this chapter, elastostatic assessment of theories of chapters 2 and 3 are reported. Challenging benchmarks are chosen to highlight discrepancies of predictions of theories, assuming low length-to-thickness ratios and different loading and boundary conditions. A functionally-graded sandwich plate not previously published is also analyzed.

Chapter 5: this chapter contains dynamic assessment of theories of chapters 2 and 3. Similarly to previous chapter, dynamic benchmarks are chosen to highlight discrepancies of predictions among theories. Moreover, the capability of theories to calculate pumping modes and response to blast pulse impulsive loading are explored.

Chapter 6: in this chapter, applications of most advanced and generalized theories for impact and material wedge problems (Icardi and Urraci [24]) are reported.

PART III – Approximate 3-D solutions

Chapter 7: in this chapter, approximate 3-D solutions are developed and outlined, whose purpose is to be an alternative solution for comparison if exact one is not available.

PART IV – SEUPT

Chapter 8: in this chapter, different versions of SEUPT are presented. A novel approach is also developed, whose purpose is to improve accuracy of commercial finite elements results, without no iterative post-processing techniques.

Chapter 1 - Modelling of composite

1.1 Features of composite and how they are modelled

Nowadays, composite and sandwich materials are overused in a lot of engineering fields, thanks to their excellent specific properties. Because of their intrinsically multi-phase construction, they have complex behavior that is strongly influenced by local effects, moreover, local failure and damage propagation are different than metals. Furthermore, displacements have to be C^0-continuous across the thickness (zig-zag effects) in order to guarantee the continuity of out-of-plane stresses and of the gradient of transverse normal stress across the thickness, which is needed to impose fulfillment of local equilibrium equations. Thus, their modelling is very complex and a lot of theories were proposed, in order to precisely calculate displacements and stresses and to prevent loss during service life. Readers can find detailed description of composite modelling in papers by Reddy [25], Reddy and co-workers [26], [27], Vasilive and Lur'e [28], Noor et al. [29], Carrera [30], [31], Qatu [32], Qatu et al. [33], Wanji and Zhen [34], Khandan et al. [35]. So, theories can be subdivided in different categories, depending on their features.

<u>Equivalent single-layer</u> (ESL) theories do not take into account layerwise effects but they are still used because of their simplicity ([36] and [37] are recent examples). Anyway, they require post-processing techniques and a shear correction factor (that is strongly case-dependent [38]) in order to get a realistic stress field; however, they can't get accurate results if there are strong layerwise effects, for some lay-ups (e.g. for soft-core sandwiches [39]) and certain loading conditions.

Instead, <u>Discrete-Layer</u> (DL) theories (e.g. [40], [41]) always obtain very accurate results. However, they require a very high computational cost when laminates with a lot of layers are analysed, because of their number of unknowns.

So, <u>zig-zag</u> (ZZ) theories have been developed adding layerwise and higher-order contributions to ESL, in order to obtain simple and accurate models that are able to analyse also structures of industrial interest with a low computational burden. The number of variables is low but predictive ability is very high. They can be subdivided into Di Sciuva's like [42] (DZZ or physically-based) and Murakami's like [43] (MZZ or kinematic-based) zig-zag theories. As regards the first ones, zig-zag contributions are the product of linear or non-linear zig-zag functions and zig-zag amplitudes that are calculated by imposing the continuity of out-of-plane stresses and of gradient of transverse normal stress at layer interfaces. As regards MZZ, these theories assume zig-zag functions that force a priori changing of slope of displacements at layer interfaces. Finally, ZZ theories can be also distinguished into displacement-based (strains and stresses are calculated using displacement-strain and constitutive stress-strain relations) and mixed form (strain and stress fields can be assumed separately from displacements and are developed through variational theorems). In-depth studies about accuracy of DZZ and MZZ theories in mixed and displacement-based forms will be reported in the next chapters. Results will confirm previous analyses by Gherlone [44] and Groh and Weaver [45] about the superiority of DZZ on MZZ, if the same expansion order of displacements across the thickness is assumed.

Recently, also hierarchical theories (HT) were proposed, where papers by Giunta et al. [46], Carrera et al. [47], Catapano et al. [48] and de Miguel et al. [49] are cited as significant examples. The variation of the displacement field across the thickness is postulated a priori, by choosing a hierarchical set of locally defined polynomials. In this case, layerwise functions are not included into displacement field, no physical or kinematic constraints are imposed, differently to ZZ. The main advantage of this approach is that no post-processing techniques are needed, as long as an appropriate expansion order of displacements across the thickness (and as a consequence an appropriate number of unknowns) is imposed [48]. Moreover, the accuracy of non-polynomial representations of displacements across the thickness was studied by Candiotti et al. [50], where exponential, sinusoidal and hyperbolic expansions were assumed using an axiomatic/asymptotic method, in order to understand which was the best choice for the analysed problems. Sinusoidal expansion was designed as the best option among the considered models.

It should be noticed that [46], [47], [48], [49], [50] are obtained as particularizations of Carrera's unified formulation (CUF) [14]. Indeed, CUF allows to express displacements to take arbitrary forms, as product of unknown coefficients (that are assumed as d.o.f.) and functions that describe variation of displacements along transverse coordinate. So, ESL, MZZ, HT, DL and also some existing theories can be obtained as its particularizations, because of its generalized formulation. Instead, DZZ cannot be obtained from [14], because of enforcement of physical constraints.

However, as it will be shown in-depth in chapters 4 and 5, recent refined physically-based zig-zag theories [18]- [23] can get accurate results, very close to exact or 3-D mixed finite elements solutions, also omitting zig-zag functions and without requiring post-processing procedure, resulting also more efficient than MZZ and HT, requiring only five d.o.f. Furthermore, they can assume an arbitrary representation of the displacements (that can be also assumed differently from a point to point across the thickness), where power, exponential and trigonometric series are tested, obtaining indistinguishable results still comparable to those provided by mixed 3-D finite elements, as long as coefficients are redefined across the thickness and the full set of physical constraints of ZZA is imposed. Generalized theories of [18]- [23] are able to replicate formulations widespread in literature [14], resulting very interesting, because of computational burden is still similar to ESL ones (only five d.o.f. required). Finally, since a lot of unknowns are involved in CUF and its particularizations [14] (see e.g. [46]- [49], [51]), such approaches will not be used into this thesis. For these reasons, the main topic of this research is the development and assessment of accurate, efficient, physically-based, generalized zig-zag theories.

Particularly, zig-zag adaptive 3-D theory (ZZA) developed by Icardi and Sola [52] is assumed as starting point of research activity of this thesis. This theory that is both displacement-based and physically-based is chosen because it demonstrates its superiority in a lot of cases, irrespective loading and boundary conditions assumed. Very low computational effort is needed, requiring only five degrees of freedom (d.o.f.) to obtain accurate results. It should be also noticed that ZZA and all theories derived from it contain a lot of derivatives of d.o.f. into displacement field, as a consequence of enforcement of physical constraints, that apparently inhibit the chance to get simple finite elements.

1.2 Assumptions adopted in this study

To develop theories, the following assumptions are adopted in this PhD thesis. The reference frame is a rectangular right-handed Cartesian coordinate reference system. It is placed on middle reference plane at lower left edge, so, $\alpha \in [0, L_\alpha]$, $\beta \in [0, L_\beta]$ and $\varsigma \in \left[-\frac{h}{2}, \frac{h}{2}\right]$, where L_α and L_β are the length of edges along α and β axes respectively. Thickness of k-th layer is indicated as h^k; constituent layers are perfectly bonded to each other and the effects of bonding resin are not considered. Similarly, sandwich laminates are analysed as multi-layered beams and plates with one or more intermediate weak cores, whose cell-scale effects are not considered. Differently to many papers in literature, multi-layered faces are not modelled as single layers, in order to prevent any loss of accuracy.

Spatial derivatives are indicated as $(.)_{,\alpha} = \partial / \partial\alpha$, $(.)_{,\beta} = \partial / \partial\beta$, $(.)_{,\varsigma} = \partial / \partial\varsigma$, while Newton's notation is used for time derivatives. Each theory of this thesis contains only five functional degrees of freedom (u_α^0, u_β^0, w^0, $\Gamma_\alpha^0 = \gamma_\alpha^0(\alpha,\beta)$ $-w^0(\alpha,\beta)_{,\alpha}$ and $\Gamma_\beta^0 = \gamma_\beta^0(\alpha,\beta) - w^0(\alpha,\beta)_{,\beta}$) that are the middle plane displacement components and rotations of the normal.

1.3 Strain-displacement and constitutive relations

In this section, strain-displacement equations and constitutive stress-strain relations assumed in this thesis are reported:

$$\begin{Bmatrix} \varepsilon_{\alpha\alpha} \\ \varepsilon_{\beta\beta} \\ \varepsilon_{\varsigma\varsigma} \\ \gamma_{\alpha\varsigma} \\ \gamma_{\beta\varsigma} \\ \gamma_{\alpha\beta} \end{Bmatrix} = \begin{bmatrix} \partial/\partial_{\alpha} & 0 & 0 \\ 0 & \partial/\partial_{\beta} & 0 \\ 0 & 0 & \partial/\partial_{\varsigma} \\ \partial/\partial_{\varsigma} & 0 & \partial/\partial_{\alpha} \\ 0 & \partial/\partial_{\varsigma} & \partial/\partial_{\beta} \\ \partial/\partial_{\beta} & \partial/\partial_{\alpha} & 0 \end{bmatrix} \begin{Bmatrix} u_{\alpha} \\ u_{\beta} \\ u_{\varsigma} \end{Bmatrix} \tag{1.1}$$

$$\begin{Bmatrix} \sigma_{\alpha\alpha} \\ \sigma_{\beta\beta} \\ \sigma_{\varsigma\varsigma} \\ \sigma_{\alpha\varsigma} \\ \sigma_{\beta\varsigma} \\ \sigma_{\alpha\beta} \end{Bmatrix} = \begin{bmatrix} C_{11} & C_{12} & C_{13} & C_{14} & C_{15} & C_{16} \\ & C_{22} & C_{23} & C_{24} & C_{25} & C_{26} \\ & & C_{33} & C_{34} & C_{35} & C_{36} \\ & & & C_{44} & C_{45} & C_{46} \\ & & & & C_{55} & C_{56} \\ & & & & & C_{66} \end{bmatrix} \begin{Bmatrix} \varepsilon_{\alpha\alpha} \\ \varepsilon_{\beta\beta} \\ \varepsilon_{\varsigma\varsigma} \\ \gamma_{\alpha\varsigma} \\ \gamma_{\beta\varsigma} \\ \gamma_{\alpha\beta} \end{Bmatrix} \begin{matrix} (C_{ij} = C_{ji}) \\ ([C]^{-1} = \ [S]) \end{matrix} \tag{1.2}$$

Strains are assumed to be infinitesimal and regarding elastic moduli C_{ij}, they are calculated starting from Young's and shear moduli and Poisson's ratios, so, $[S']$ matrix is defined (the following relations are valid for orthotropic materials):

$$[S] = \begin{bmatrix} 1/E_1 & -\nu_{12}/E_1 & -\nu_{13}/E_1 & 0 & 0 & 0 \\ -\nu_{12}/E_1 & 1/E_2 & -\nu_{23}/E_2 & 0 & 0 & 0 \\ -\nu_{13}/E_1 & -\nu_{23}/E_2 & 1/E_3 & 0 & 0 & 0 \\ 0 & 0 & 0 & 1/G_{13} & 0 & 0 \\ 0 & 0 & 0 & 0 & 1/G_{23} & 0 \\ 0 & 0 & 0 & 0 & 0 & 1/G_{12} \end{bmatrix} \tag{1.2a}$$

Considering that each layer has an arbitrary orientation θ, the following rotation matrix $[T]$ is defined:

$$[T] = \begin{bmatrix} c^2 & s^2 & 0 & 0 & 0 & +2cs \\ s^2 & c^2 & 0 & 0 & 0 & -2cs \\ 0 & 0 & 1 & 0 & 0 & 0 \\ 0 & 0 & 0 & c & s & 0 \\ 0 & 0 & 0 & -s & c & 0 \\ -cs & cs & 0 & 0 & 0 & c^2 - s^2 \end{bmatrix} \tag{1.2b}$$

$$c = cos(\theta); \qquad s = sin(\theta)$$

Thus, $[C]$ can be calculated using the following expression:

$$[C] = [T][S']^{-1}[T]^T \tag{1.2c}$$

So, using standard techniques, it is possible to obtain their expression, where $[C']=[S']^{-1}$:

$$
\begin{aligned}
C_{11} &= c^4 C_{11}' + 2c^2 s^2 \left(C_{12}' + 2C_{66}' \right) + s^4 C_{22}' \\
C_{12} &= c^2 s^2 \left(C_{11}' + C_{22}' - 4C_{66}' \right) + \left(c^4 + s^4 \right) C_{12}' \\
C_{13} &= c^2 C_{13}' + s^2 C_{23}' \\
C_{16} &= -cs \left[c^2 C_{11}' - s^2 C_{22}' - \left(c^2 - s^2 \right) \left(C_{12}' + 2C_{66}' \right) \right] \\
C_{22} &= s^4 C_{11}' + 2c^2 s^2 \left(C_{12}' + 2C_{66}' \right) + c^4 C_{22}' \\
C_{23} &= s^2 C_{13}' + c^2 C_{23}' \\
C_{26} &= -cs \left[s^2 C_{11}' - c^2 C_{22}' - \left(c^2 - s^2 \right) \left(C_{12}' + 2C_{66}' \right) \right] \\
C_{33} &= C_{33}' \\
C_{36} &= cs \left(C_{23}' - C_{13}' \right) \\
C_{44} &= c^2 C_{44}' + s^2 C_{55}' \\
C_{55} &= s^2 C_{44}' + c^2 C_{55}' \\
C_{45} &= cs \left(C_{44}' - C_{55}' \right) \\
C_{66} &= c^2 s^2 \left(C_{11}' + C_{22}' - 2C_{12}' \right) + \left(c^2 - s^2 \right)^2 C_{66}'
\end{aligned}
\tag{1.2d}
$$

(1.1) and (1.2) can be rewritten using tensor notation:

$$\varepsilon_{ij}^{\ u} = \frac{1}{2}[u_{i,j} + u_{j,i}] \tag{1.3}$$

$$\sigma_{ij}^{\ \varepsilon} = C_{ijkl}\ \varepsilon_{kl} \tag{1.4}$$

It should be noticed that standard engineering notation is adopted, so, $\gamma_{\alpha\varsigma}$, $\gamma_{\beta\varsigma}$ and $\gamma_{\alpha\beta}$ are expressed as:

$$\gamma_{ij}^{\ u} = 2\varepsilon_{ij}^{\ u} \tag{1.5}$$

The inverse relation of (1.4) is:

$$\varepsilon_{ij}^{\ \sigma} = S_{ijkl}\sigma_{kl} = (C_{ijkl})^{-1}\sigma_{kl} \tag{1.5a}$$

The superscripts ^{u}, $^\varepsilon$ and $^\sigma$ are used in (1.3) to (1.5) to indicate the origin of slave fields; $\varepsilon_{ij}^{\ u}$ come from kinematics, while $\sigma_{ij}^{\ \varepsilon}$ come from constitutive stress-strains relations, instead $\varepsilon_{ij}^{\ \sigma}$ are obtained from stresses. These distinctions will be used in section 1.5 for variational statements. Tensor notations will be used for all theories of this thesis, for the sake of brevity.

1.4 Solution of governing equations

Structural problems of this thesis will be solved in closed form by using Rayleigh-Ritz method. In-plane variation of d.o.f. is expressed as a truncated series expansion of unknown amplitudes A_{Δ}^{i} and trial functions $\Re^{i}(\alpha,\beta)$ that a priori satisfy the prescribed boundary conditions.

$$\Delta = \sum_{i=1}^{m_{\Delta}} A_{\Delta}^{i}\, \Re^{i}(\alpha,\beta)\,; \tag{1.6}$$

Also mechanical boundary conditions could be satisfied, when it is required, by using Lagrange multiplier method, as described below. As regards simply-supported edges, the following boundary conditions are enforced:

$$\begin{gathered} w^{0}(0,\beta)=0\ ;\ w^{0}(L_{\alpha},\beta)=0;\ w^{0}(0,\beta)_{,\alpha\alpha}=0\ ;\ w^{0}(L_{\alpha},\beta)_{\ ,\alpha\alpha}=0 \\ w^{0}(\alpha,0)=0\,;w^{0}(\alpha,L_{\beta})=0\,;w^{0}(\alpha,0)_{,\beta\beta}=0\,;w^{0}(\alpha,L_{\beta})_{\ ,\beta\beta}=0 \end{gathered} \tag{1.7}$$

So, under conditions (1.7) d.o.f. are expressed:

$$\begin{aligned} u_{\alpha}^{0}(\alpha,\beta) &= \sum_{m=1}^{M}\sum_{n=1}^{N} A_{mn}\cos\left(\frac{m\pi}{L_{\alpha}}\alpha\right)\sin\left(\frac{n\pi}{L_{\beta}}\beta\right) \\ u_{\beta}^{0}(\alpha,\beta) &= \sum_{m=1}^{M}\sum_{n=1}^{N} B_{mn}\sin\left(\frac{m\pi}{L_{\alpha}}\alpha\right)\cos\left(\frac{n\pi}{L_{\beta}}\beta\right) \\ w^{0}(\alpha,\beta) &= \sum_{m=1}^{M}\sum_{n=1}^{N} C_{mn}\sin\left(\frac{m\pi}{L_{\alpha}}\alpha\right)\sin\left(\frac{n\pi}{L_{\beta}}\beta\right) \\ \Gamma_{\alpha}{}^{0}(\alpha,\beta) &= \sum_{m=1}^{M}\sum_{n=1}^{N} D_{mn}\cos\left(\frac{m\pi}{L_{\alpha}}\alpha\right)\sin\left(\frac{n\pi}{L_{\beta}}\beta\right) \\ \Gamma_{\beta}{}^{0}(\alpha,\beta) &= \sum_{m=1}^{M}\sum_{n=1}^{N} D_{mn}\sin\left(\frac{m\pi}{L_{\alpha}}\alpha\right)\cos\left(\frac{n\pi}{L_{\beta}}\beta\right) \end{aligned} \tag{1.8}$$

As regards clamped edges for a cantilever beam, the following boundary conditions are enforced:

$$\begin{gathered} u_{\alpha}{}^{0}(0,0)=0\ ;w^{0}(0,0)=0\,;w^{0}(0,0)_{,\alpha}=0\ ;\Gamma_{\alpha}^{0}(0,0)=0 \\ u_{\alpha}(0,\varsigma)_{,\varsigma}=0\,;u_{\varsigma}(0,\varsigma)_{,\varsigma}=0\,;u_{\varsigma}(0,\varsigma)_{,\alpha\varsigma}=0 \end{gathered} \tag{1.9}$$

While also support conditions $u_{\varsigma}(\overline{\alpha},\varsigma)=0$ is enforced for propped-cantilever beams. In numerical applications, fulfilment of mechanical boundary conditions (1.11) is obtained using Lagrange multipliers method. So, the following series can be used for d.o.f. for cantilever and propped cantilever beams:

$$\Delta = \sum_{i=1}^{I} A_{\Delta}^{i} \left(\frac{\alpha}{L_{\alpha}}\right)^{i} \tag{1.10}$$

In order to increase accuracy, also mechanical boundary conditions on shear force can be enforced for cantilever and propped cantilever beams, e.g.:

$$\int_{-h/2}^{h/2} \sigma_{\alpha\varsigma}(\overline{\alpha},\varsigma)d\varsigma = T_{\overline{\alpha}} \tag{1.11}$$

Fulfilment of (1.11) will be used for clamped edges and imposed by using Lagrange multiplier method. Alternatively, also a higher-order of expansions of displacements across the thickness could be assumed to fulfil mechanical boundary conditions, however, this latter technique will not be adopted.

Once trial functions and order of expansion are chosen, deriving governing functional with respect to unknown amplitudes and equating to zero, an algebraic system is obtained and it can be solved in a few seconds with low computational cost, whose solution are the explicit value of amplitudes. So, displacement, strain and stress fields can be obtained.

For displacement-based theories, Total Potential Energy (TPE) is used as functional, while Hellinger-Reissner (HR) or Hu-Washizu (HW) variational theorems are used for mixed theories. In the next section, HW and HR variational statements will be briefly outlined because they are the basis of mixed theories of the next chapter and of hybrid element [6].

1.5 Mixed HR and HW Variational Statements

Hereafter, HR and HW variational theorems are briefly overviewed. Laminated and sandwich beams and plates are elastic bodies of volume V, whose surface S is split into S_t and S_u. Surface tractions $\tilde{t}_i$ are prescribed on S_t, while surface displacements $\tilde{u}_i$ are prescribed on S_u, so, $S_t \cup S_u \equiv S$. The three unknown internal fields are displacement, strain and stress fields, which are continuous and piecewise differentiable in the whole volume V, because, for the sake of simplicity, no discontinuities in material or geometry are allowed. The body is in static equilibrium under body forces b_i defined in V, that along with $\tilde{u}_i$ and $\tilde{t}_i$ are the three known data. The three unknown volume fields (displacements, strains, stresses) are linked by field equations, which are strain-displacement (1.3), constitutive (1.4) and internal equilibrium equations (1.18), while boundary conditions ($u_i = \tilde{u}_i$ on S_u and $t_i = \sigma_{ij} n_j = \tilde{t}_i$ on S_t, where n_j are components of external unit normal) link volume fields and prescribed surface fields $\tilde{t}_i$ and $\tilde{u}_i$. Field equations and boundary conditions are governing equations of elastostatic.

The strong form of linear elastostatic is reported into Strong Form Tonti diagram (see Figure 1.1) that represents the field equations of a mathematical model in a graphical form.

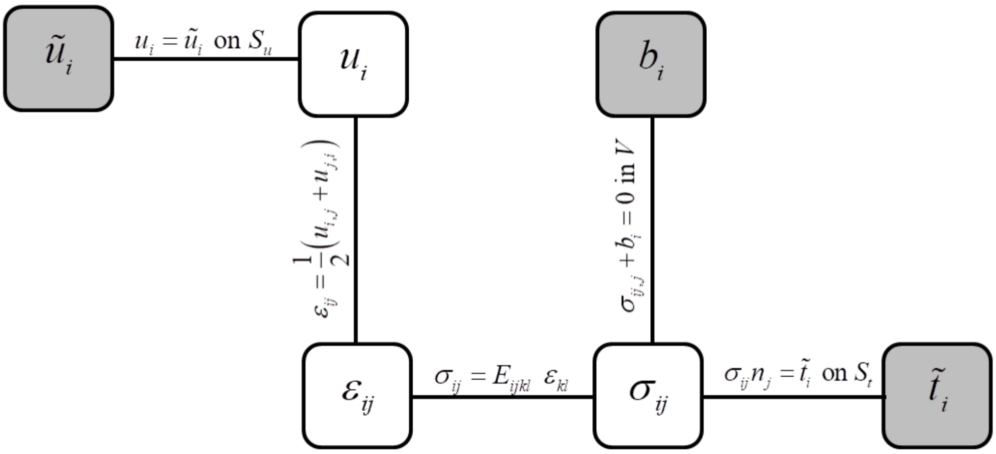

Figure 1.1: Strong Form Tonti diagram

The primary variables in this case are displacements u_i, while strains ε_{ij} and stresses σ_{ij} are the first and the second intermediate variables. Boundary conditions (PBC and TBC) link prescribed displacements $\tilde{u}_i$ and tractions $\tilde{t}_i$ to u_i and σ_{ij}, respectively, while equilibrium equations link b_i to stresses. Strain-displacement and constitutive relations link three unknown fields. It is possible to obtain infinite variational forms from the strong form of Figure 1.1. In order to do this, the following steps have to be followed:

- Choice of mater field(s): one or more internal fields are assumed as masters, that are subjected to variations in variational process. All other fields are called slaves; they are not subjected to variations and are obtained from masters. Depending on the number of master fields, variational principle can be defined as single- or multi-field.
- Weak and strong connections are determined: master fields are linked to other fields through:
    - strong connections that are enforced point to point;
    - weak connections, that are enforced only in integral form.

  It should be noticed that slave fields are obtained from master fields through strong connections.
- Weak connections are enforced in average sense through Lagrange multipliers. In other words, weak connections are multiplied for Lagrange multipliers and integrated.

- Lagrange multipliers are appropriately substituted and the divergence theorem is applied; integration is performed by parts and the first variation of functional is obtained.
- The exact variation of functional respect to master field can be calculated.

In order to get total potential energy, only displacements are assumed as master fields, so, strain and stresses are assumed as slave fields. So, strain-displacement and constitutive equations are strong connections as like as essential boundary conditions $u_i = \tilde{u}_i$ on S_u. On the contrary, natural boundary conditions and equilibrium equations are the weak connections.

$$\begin{aligned} &\text{Strong:} \quad \varepsilon_{ij} = \frac{1}{2}(u_{i,j} + u_{j,i}) \text{ in } V \,; \quad \sigma_{ij} = E_{ijkl}\varepsilon_{kl} \text{ in } V \,; \quad u_i = \hat{u}_i \text{ on } S_u \\ &\text{Weak:} \quad \sigma_{ij,j} + b_i = 0 \text{ in } V \,; \quad \sigma_{ij} n_j = \hat{t}_i \text{ on } S_t \end{aligned} \tag{1.12a}$$

Because of ε_{ij} and σ_{ij} are slave fields and come from master displacements they will be indicated as $\varepsilon_{ij}{}^u$ and $\sigma_{ij}{}^u$ in the following steps. In order to obtain variational principle, equilibrium equation is integrated and multiplied for Lagrange multiplier vector λ_i:

$$\int_V (\sigma_{ij,j}^u + b_i)\lambda_i \; dV = \int_V \sigma_{ij,j}^u \; \lambda_i \; dV + \int_V b_i \lambda_i \; dV = 0 \tag{1.12b}$$

Through divergence theorem, the previous expression can be rewritten, considering a symmetric stress tensor, as:

$$\int_V \sigma_{ij,j}^u \; \lambda_i \; dV = -\int_V \sigma_{ij}^u \frac{1}{2}(\lambda_{i,j} + \lambda_{j,i}) \; dV + \int_S \sigma_{ij}^u \; n_j \; \lambda_i \; dS \tag{1.12c}$$

Assuming Lagrange multiplier vector as the variation of master displacements, the following expression can be obtained:

$$\begin{aligned} \int_V \sigma_{ij,j}^u \; \partial u_i \; dV &= -\int_V \sigma_{ij}^u \frac{1}{2}(\partial u_{i,j} + \partial u_{j,i}) \; dV + \int_S \sigma_{ij}^u \; n_j \; \partial u_i \; dS = \\ &= -\int_V \sigma_{ij}^u \; \partial \varepsilon_{ij}^u \; dV + \int_S \sigma_{ij}^u \; n_j \; \partial u_i \; dS \end{aligned} \tag{1.12d}$$

So, substituting (1.12d) into (1.12b), the following expression is obtained:

$$\int_V \sigma_{ij}^u \; \partial \varepsilon_{ij}^u \; dV + \int_S \sigma_{ij}^u \; n_j \; \partial u_i \; dS - \int_V b_i \; \partial u_i \; dV = 0 \tag{1.12e}$$

It should be noticed that the surface integral can be rewritten as:

$$\int_S \sigma_{ij}^u \; n_j \; \partial u_i \; dS = \int_{S_t} \sigma_{ij}^u \; n_j \; \partial u_i \; dS + \int_{S_u} \sigma_{ij}^u \; n_j \; \partial u_i \; dS \tag{1.12f}$$

∂u_i is null on S_u and the second part of (1.12f) can be rewritten, according to (1.12a), so:

$$\int_{S_t} \sigma_{ij}^u \; n_j \; \partial u_i \; dS = \int_{S_t} \hat{t}_i \; \partial u_i \; dS \tag{1.12g}$$

Substituting the first variation of total potential energy $\partial \Pi_{TPE}$ is obtained:

$$\partial \Pi_{TPE} = \int_V \sigma_{ij}^u \; \partial \varepsilon_{ij}^u \; dV - \int_{S_t} \hat{t}_i \; \partial u_i \; dS - \int_V b_i \; \partial u_i \; dV = 0 \tag{1.12h}$$

From which the exact variation respect master field can be obtained:

$$\Pi_{TPE} = \frac{1}{2} \int_V \sigma_{ij}^u \; \varepsilon_{ij}^u \; dV - \int_{S_t} \hat{t}_i \; u_i \; dS - \int_V b_i \; u_i \; dV \tag{1.12h}$$

Similarly, HW and HR variational principles can be obtained, assuming different master fields. HW variational theorem can be used to create theories whose displacements, strains and stresses can be assumed independently from each other. So, master fields are u_i, ε_{ij} and σ_{ij}. Slave strains that are obtained through displacement-strain relations are indicated as ε_{ij}^u, while slave stresses that are obtained from constitutive relations are indicated as σ_{ij}^e. Similarly to total potential energy, strain-displacement, constitutive equations are the strong connections. Instead, equilibrium equations, essential and natural boundary conditions are the weak links, as well as the compatibility between strains $\varepsilon_{ij}^u - \varepsilon_{ij}$ and stresses $\sigma_{ij}^e - \sigma_{ij}$. So, there are five weak connections:

$$\begin{aligned} \partial \Pi_{HW}^g = & \int_V (\varepsilon_{ij}^u - \varepsilon_{ij}) \partial \sigma_{ij} dV + \int_V (\sigma_{ij}^e - \sigma_{ij}) \partial \varepsilon_{ij} dV - \int_V (\sigma_{ij,j}^u + b_i) \partial u_i \; dV + \\ & + \int_{S_t} (\sigma_{ij} n_j - \hat{t}_i) \partial u_i \; dS - \int_{S_u} [(u_i - \tilde{u}_i) n_j \partial \sigma_{ij}] dS \end{aligned} \tag{1.13a}$$

The divergence theorem is applied:

$$\begin{aligned} -\int_V \sigma_{ij,j} \; \partial u_i \; dV = & +\int_V \sigma_{ij} \; \partial \varepsilon_{ij}^u \; dV - \int_S \sigma_{ij} \; \mathrm{n}_j \; \partial u_i \; dV = \\ & = +\int_V \sigma_{ij} \; \partial \varepsilon_{ij}^u \; dV - \int_{S_t} \sigma_{ij} \; \mathrm{n}_j \; \partial u_i \; dV - \int_{S_u} \sigma_{ij} \; \mathrm{n}_j \; \partial u_i \; dV \end{aligned} \tag{1.13b}$$

Substituting:

$$\begin{aligned} \partial \Pi_{HW}^g = & \int_V (\varepsilon_{ij}^u - \varepsilon_{ij}) \partial \sigma_{ij} dV + \int_V (\sigma_{ij}^e - \sigma_{ij}) \partial \varepsilon_{ij} dV - \int_V b_i \partial u_i \; dV + \\ & + \int_{S_t} (\sigma_{ij} n_j - \hat{t}_i) \partial u_i \; dS - \int_{S_u} (u_i - \tilde{u}_i) n_j \partial \sigma_{ij} dS + \\ & + \int_V \sigma_{ij} \; \partial \varepsilon_{ij}^u \; dV - \int_{S_t} \sigma_{ij} \; \mathrm{n}_j \; \partial u_i \; dV - \int_{S_u} \sigma_{ij} \; \mathrm{n}_j \; \partial u_i \; dV = \end{aligned}$$

$$= \int_V (\varepsilon_{ij}^u - \varepsilon_{ij}) \partial\sigma_{ij}\; dV + \int_V (\sigma_{ij}^e - \sigma_{ij}) \partial\varepsilon_{ij} - \int_V b_i \partial u_i\; dV + \int_V \sigma_{ij}\; \partial\varepsilon_{ij}^u\; dV +$$

$$+ \int_{S_t} (\sigma_{ij} n_j - \hat{t}_i) \partial u_i\; dS - \int_{S_t} \sigma_{ij}\; \mathrm{n}_j\; \partial u_i\; dS + \tag{1.13c}$$

$$+ \int_{S_u} (u_i - \tilde{u}_i) n_j \partial\sigma_{ij} dS - \int_{S_u} \sigma_{ij}\; \mathrm{n}_j\; \partial u_i\; dS$$

(1.13c) can be rewritten in compact form as:

$$\partial\Pi_{HW}^g = \int_V [(\varepsilon_{ij}^u - \varepsilon_{ij}) \partial\sigma_{ij} + (\sigma_{ij}^e - \sigma_{ij}) \partial\varepsilon_{ij} + \sigma_{ij} \partial\varepsilon_{ij}^u - b_i \partial u_i] dV - \int_{S_t} \tilde{t}_i \partial u_i dS +$$
$$- \int_{S_u} [(u_i - \tilde{u}_i) n_j \partial\sigma_{ij} + \sigma_{ij} n_j \partial u_i] dS = 0 \tag{1.13d}$$

Similarly, HR variational theorem is obtained assuming independently displacements and stresses (that are also master fields). So, slave strains that are obtained from displacements are indicated as ε_{ij}^u, while those obtained from stresses are indicated as ε_{ij}^σ. Strain-displacement relations, constitutive equations and boundary conditions on displacements $u_i = \tilde{u}_i$ on S_u are the strong connections. Equilibrium equations, natural boundary conditions and compatibility of strains $\varepsilon_{ij}^u - \varepsilon_{ij}^\sigma$ are weak connections:

$$\partial\Pi_{HR} = \int_V (\varepsilon_{ij}^u - \varepsilon_{ij}^\sigma) \partial\sigma_{ij} dV - \int_V (\sigma_{ij,j}^u + b_i) \partial u_i\; dV + \int_{S_t} (\sigma_{ij} n_j - \hat{t}_i) \partial u_i\; dS \tag{1.13e}$$

Using divergence theorem, the following expression is obtained:

$$-\int_V \sigma_{ij,j}\; \partial u_i\; dV = +\int_V \sigma_{ij}\; \partial\varepsilon_{ij}^u\; dV - \int_S \sigma_{ij}\; \mathrm{n}_j\; \partial u_i\; dV =$$
$$= +\int_V \sigma_{ij}\; \partial\varepsilon_{ij}^u\; dV - \int_{S_t} \sigma_{ij}\; \mathrm{n}_j\; \partial u_i\; dV - \int_{S_u} \sigma_{ij}\; \mathrm{n}_j\; \partial u_i\; dV = \tag{1.13f}$$
$$= +\int_V \sigma_{ij}\; \partial\varepsilon_{ij}^u\; dV - \int_{S_t} \sigma_{ij}\; \mathrm{n}_j\; \partial u_i\; dV$$

It should be noticed that $\int_{S_u} \sigma_{ij}\; \mathrm{n}_j\; \partial u_i\; dV = 0$ because of essential boundary condition. Substituting (1.13f) into (1.13e) and rearranging, the first variation of Hellinger-Reissner variational theorem is obtained:

$$\partial\Pi_{HR} = \int_V (\varepsilon_{ij}^u - \varepsilon_{ij}^\sigma) \partial\sigma_{ij} dV - \int_V b_i \partial u_i\; dV + \int_V \sigma_{ij}\; \partial\varepsilon_{ij}^u\; dV +$$
$$+ \int_{S_t} (\sigma_{ij} n_j - \hat{t}_i) \partial u_i\; dS - \int_{S_t} \sigma_{ij}\; \mathrm{n}_j\; \partial u_i\; dV = \tag{1.13g}$$
$$= \int_V [\; (\varepsilon_{ij}^u - \varepsilon_{ij}^\sigma) \partial\sigma_{ij} + \sigma_{ij}\; \partial\varepsilon_{ij}^u - b_i \partial u_i] dV - \int_{S_t} \hat{t}_i\; \partial u_i\; dS$$

It should be noticed that tractions and body forces are imposed null in numerical applications. A lot of mixed theories based on HR or HW variational statements will be developed and their features, assumption, simplifying hypothesis and accuracy will be discussed in the next chapter.

1.6 Parent Zig-zag Adaptive Theory (ZZA)

ZZA theory is discussed because it is the fundamental theory and basis of research activity, from which all the theories of the following chapters have been generalized. As previously stated, this theory is both displacement-based and physically-based. So, similarly to other DZZ theories, the following physical constraints have to be imposed: compatibility of out-of-plane stresses and displacements, fulfilment of boundary conditions of stresses and local equilibrium equations at different points across the thickness.

<u>Description of displacement field</u>

According to [4], the displacement field of zig-zag adaptive theory (ZZA) in compact form can be subdivided into three contributions:

$$
\begin{aligned}
u_\alpha(\alpha,\beta,\varsigma) &= \left[U^0_{\alpha\_FSDT}(\alpha,\beta,\varsigma)\right] + \left[U^0_{\alpha\_HT}(\alpha,\beta,\varsigma)\right] + \left[U^0_{\alpha\_ZZ}(\alpha,\beta,\varsigma)\right] \\
u_\varsigma(\alpha,\beta,\varsigma) &= \left[U^0_{\varsigma\_FSDT}(\alpha,\beta,\varsigma)\right] + \left[U^0_{\varsigma\_HT}(\alpha,\beta,\varsigma)\right] + \left[U^0_{\varsigma\_ZZ}(\alpha,\beta,\varsigma)\right]
\end{aligned}
\tag{1.14a}
$$

α,β are in-plane coordinates, while ς is the through-the-thickness one. u_α and u_ς are in-plane and transverse displacements, respectively. $U^0_{\alpha\_FSDT}$ and $U^0_{\varsigma\_FSDT}$ contributions are the same of FSDT [53] and contain the only five fixed d.o.f. of this theory, which are middle plane displacements ($u_\alpha{}^0$, w^0) and rotations (Γ^0_α). So, accordingly to [53], $U^0_{\alpha\_FSDT}$ and $U^0_{\varsigma\_FSDT}$ contain a linear and a uniform variation of in-plane and transverse displacements across the thickness, respectively:

$$
\begin{aligned}
U^0_{\alpha\_FSDT}(\alpha,\beta,\varsigma) &= u_\alpha{}^0(\alpha,\beta) + \varsigma(\Gamma^0_\alpha(\alpha,\beta) - w^0(\alpha,\beta)_{,\alpha}) \\
U^0_{\varsigma\_FSDT}(\alpha,\beta,\varsigma) &= w^0(\alpha,\beta)
\end{aligned}
\tag{1.14b}
$$

As like as any zig-zag theory, ZZA is developed adding higher-order and zig-zag contributions to FSDT kinematics. Higher-order contributions are indicated as $U^0_{\alpha\_HT}$ and $U^0_{\varsigma\_HT}$ in (1.14a), whose expression is:

$$
\begin{aligned}
U^0_{\alpha\_HT}(\alpha,\beta,\varsigma) &= \varsigma^2 C^i_\alpha(\alpha,\beta) + \varsigma^3 D^i_\alpha(\alpha,\beta) \\
U^0_{\varsigma\_HT}(\alpha,\beta,\varsigma) &= \varsigma\ b^i(\alpha,\beta) + \varsigma^2 c^i(\alpha,\beta) + \varsigma^3 d^i(\alpha,\beta) + \varsigma^4 e^i(\alpha,\beta)
\end{aligned}
\tag{1.14c}
$$

Higher-order coefficients are indicated as C_α^i, D_α^i, b^i, c^i, d^i, e^i. They are multiplied for global functions, which are used to describe displacements across the thickness. For ZZA and most of its variants they are assumed as truncated power series expansions (cubic for in-plane displacements and quartic for transverse one). Differently to the most zig-zag theories in literature, these terms are recalculated for each layer across the thickness, through the fulfilment of out-of-plane stresses boundary conditions on the top and bottom layers and equilibrium equations at different points across the thickness. So, displacements can adapt themself to strong variations of mechanical properties across the thickness.

Zig-zag contributions are indicated as $U^0_{\alpha\_ZZ}$ and $U^0_{\varsigma\_ZZ}$ in (1.14a) and their expression is:

$$U^0_{\alpha\_ZZ}(\alpha,\beta,\varsigma)=\sum_{k=1}^{n_i}\Phi_\alpha^k(\alpha,\beta)\,Z_1(\varsigma)+\sum_{k=1}^{n_i}{}_\alpha C_u^k(\alpha,\beta)H_k(\varsigma)$$

$$U^0_{\varsigma\_ZZ}(\alpha,\beta,\varsigma)=\sum_{k=1}^{n_i}\Psi^k(\alpha,\beta)\,Z_1(\varsigma)+\sum_{k=1}^{n_i}\Omega^k(\alpha,\beta)\,Z_2(\varsigma)+\sum_{k=1}^{n_i}C_\varsigma^k(\alpha,\beta)H_k(\varsigma) \tag{1.14d}$$

Layerwise coefficients Φ_α^k, Ψ^k, Ω^k, ${}_\alpha C_u^k$, and C_ς^k are calculated by imposing the continuity of transverse shear and normal stresses, of gradient of transverse normal stress and of displacements at interfaces. k is the index of interfaces, where $n_i = i-1$.

Coefficients Φ_α^k and Ψ^k are multiplied for Di Sciuva's zig-zag function [42] (indicated as $Z_1(\varsigma)$) and allow fulfilment of transverse shear and normal stresses continuity, while Ω^k are multiplied for Icardi's parabolic zig-zag function [54] (indicated as $Z_2(\varsigma)$) and are calculated through the compatibility of gradient of transverse normal stress at the interfaces. Explicit expression of zig-zag functions is:

$$Z_1(\varsigma)=(\varsigma-\varsigma_k)H_k(\varsigma)$$

$$Z_2(\varsigma)=(\varsigma-\varsigma_k)^2H_k(\varsigma) \tag{1.14e}$$

$H_k(\varsigma)$ is Heaviside's function, that is null for $\varsigma<\varsigma_k$:

$$H_k(\varsigma)=\begin{cases}1 & \text{if} \quad \varsigma\geq\varsigma_k\\ 0 & \text{if} \quad \varsigma<\varsigma_k\end{cases} \tag{1.14f}$$

ς_k is the thickness coordinate of k-th interface. Coefficients ${}_\alpha C_u^k$, and C_ς^k are calculated by imposing the continuity of in-plane and transverse displacements across the thickness. Also continuity coefficients are redefined for each layer across the thickness; similarly to classical zig-zag theories, they are not included to describe kinematic of the bottom layer because no interfaces are still met.

So, the displacement field of ZZA is:

$$u_\alpha(\alpha,\beta,\varsigma)=u_\alpha{}^0(\alpha,\beta)+\varsigma(\Gamma_\alpha^0(\alpha,\beta)-w^0(\alpha,\beta)_{,\alpha})+\varsigma^2 C_\alpha^i(\alpha,\beta)+\varsigma^3 D_\alpha^i(\alpha,\beta)+$$
$$+\sum_{k=1}^{n_i}\Phi_\alpha^k(\alpha,\beta)\ (\varsigma-\varsigma_k)H_k(\varsigma)+\sum_{k=1}^{n_i}{}_\alpha C_u^k(\alpha,\beta)H_k(\varsigma) \tag{1.14g}$$

$$u_\varsigma(\alpha,\beta,\varsigma)=w^0(\alpha,\beta)+\varsigma\ b^i(\alpha,\beta)+\varsigma^2 c^i(\alpha,\beta)+\varsigma^3 d^i(\alpha,\beta)+\varsigma^4 e^i(\alpha,\beta)+$$
$$+\sum_{k=1}^{n_i}\Psi^k(\alpha,\beta)\ (\varsigma-\varsigma_k)H_k(\varsigma)+\sum_{k=1}^{n_i}\Omega^k(\alpha,\beta)\ (\varsigma-\varsigma_k)^2 H_k(\varsigma)+\sum_{k=1}^{n_i}C_\varsigma^k(\alpha,\beta)H_k(\varsigma)$$

$$H_k(\varsigma)=\begin{cases}1 & \text{if} \quad \varsigma\geq\varsigma_k\\ 0 & \text{if} \quad \varsigma<\varsigma_k\end{cases}$$

<u>Calculation of coefficients</u>

Higher order coefficients C_α^i, D_α^i, b^i, c^i, d^i, e^i are calculated by enforcing the boundary conditions of out-of-plane stresses and of gradient of transverse normal stress at upper and lower faces (equations (1.15) to (1.17)).

$$\sigma_{\alpha\varsigma}\left(\varsigma=\pm\frac{h}{2}\right)=0 \tag{1.15}$$

$$\sigma_{\varsigma\varsigma,\varsigma}\left(\varsigma=\pm\frac{h}{2}\right)=0 \tag{1.16}$$

$$\sigma_{\varsigma\varsigma}\left(\varsigma=\pm\frac{h}{2}\right)=p^{0\pm} \tag{1.17}$$

p^{0+} is the distributed loading on the upper face, while p^{0-} is the loading on the lower one. Thanks to symbolic calculus, in numerical applications, the exact in-plane expression of loading is used for computation of work of external forces, so, no approximations or series expansions are needed.

Since, the number of higher order terms is greater than number of equations (1.15) to (1.17), remaining terms are calculated by imposing the fulfilment of local equilibrium equations at selected points across the thickness:

$$\begin{aligned}\sigma_{\alpha\beta,\beta}+\sigma_{\alpha\varsigma,\varsigma}&=b_\alpha\\ \sigma_{\alpha\varsigma,\alpha}+\sigma_{\varsigma\varsigma,\varsigma}&=b_\varsigma\end{aligned} \tag{1.18}$$

It should be noticed that terms b^i, c^i can be omitted in all layers except the first one from below without loss of accuracy, obtaining a little time saving. Assuming this latter choice, only three equilibrium equations (one point) are needed for the upper and lower bounding faces, while six ones (two points) are used for the inner layers.

Continuity coefficients Φ_α^k, Ψ^k, Ω^k are determined by imposing:

$$\sigma_{\alpha\varsigma}({}^{(k)}\varsigma^+)=\sigma_{\alpha\varsigma}({}^{(k)}\varsigma^-);\sigma_{\varsigma\varsigma}({}^{(k)}\varsigma^+)=\sigma_{\varsigma\varsigma}({}^{(k)}\varsigma^-);\sigma_{\varsigma\varsigma,\varsigma}({}^{(k)}\varsigma^+)=\sigma_{\varsigma\varsigma,\varsigma}({}^{(k)}\varsigma^-) \tag{1.19}$$

respectively, while ${}_\alpha C_u^k$, and C_ς^k are calculated by imposing:

$$u_\alpha({}^{(k)}\varsigma^+)=u_\alpha({}^{(k)}\varsigma^-);u_\varsigma({}^{(k)}\varsigma^+)=u_\varsigma({}^{(k)}\varsigma^-) \tag{1.20}$$

It is also possible to split a physical layer into two or more computational ones, with the intended aim to increase accuracy of theory, for cases with strong layerwise effects, having more equilibrium points across the thickness. This latter strategy will be adopted to analyse functionally-graded sandwiches in numerical applications. For other cases, no computational layers are used, because high accuracy of results is already obtained without any split of physical ones.

It should be noticed that higher order and compatibility coefficients are obtained in a closed form using symbolic calculus tool; all terms are functions of material properties, geometry and of d.o.f. and their derivatives. Because of a lot of derivatives of d.o.f. are involved into displacement field (and as a consequence into strain energy) due to higher-order and continuity terms, finite elements with a high number of nodal d.o.f. can be obtained. However, they cannot be used to analyze very complex structures. Despite this, it is possible to obtain a C° formulation of the ZZA theory using SEUPT technique (see [55] and chapter 8), in order to get simple Lagrangian accurate finite elements starting from this theory.

ZZA requires a lot of time for its building and it's unknown which contributions are important and which are negligible depending on the type of problem. Expression of its displacements is very complex, so, in the next chapter all steps made, to obtain a simpler and still accurate generalization ZZA, are reported.

ZZA

- Displacement-based, pshysically-based zig-zag theory;
- Piecewise cubic in-plane displacements $u_\alpha^{(3)}$ (redefined coefficients);
- Piecewise fourth-order transverse displacement $u_\varsigma^{(4)}$ (redefined coefficients);
- Terms are calculated by imposing the full set of physical constraints.

PROS	**CONS**
Good processing time, comparable with those of ESL;	Its expression is very complex.
High accuracy, still comparable with those of 3-D FEA and exact solutions.	A simplification and a generalization of this theory could be developed.

Table 1.1: Characteristic features of ZZA theory.

1.7 Quick accuracy assessment of ZZA

Accuracy of ZZA has been thoroughly assessed in [11]- [13]. Only some significant results are here reported, that prove its accuracy and efficiency, which justifies the development of the present theories based on it. Further examples will be given in the following chapters, as well as in [20]- [23]. Figures also contain results provided by mixed FEA3-D elements, which will be used as reference solution if exact ones is not available, whose features briefly explained in the next section.

Lay-up, load and boundary conditions, material properties, trial functions and expansion order that will be adopted are reported in Tables 1.2 to 1.5, while results for this two cases are reported in Tables 1.6.1-1.6.2 and Figures 1.1 and 1.2.

Case	Lay-up	Layer thickness	Material	BCS	Load	Lx/h	Ref
1.1	[0/90/0]	$[(h/3)_3]$	$[r_2]$	SS	Sinusoidal	4	[15]
1.2	$[\ 0\ ]_{11}$	$[0.01h/0.025h$ $/0.015h/0.02h$ $/0.03h/0.4h]_S$	$[s1/s2/s3$ $/s1/s3/s4]_S$	SS	Sinusoidal	4	[13]

Table 1.2: Data of cases

Case	Expansion order	Mesh $(x_a \cdot y_b \cdot z_h)^{(+)}$	Trial functions
1.1 [15] 1.2 [13]	1 1	16·2·60 16·2·60	$u_\alpha^0(\alpha,\beta)=\sum_{m=1}^{M} A_m \cos\left(\frac{m\pi\alpha}{L_\alpha}\right)$; $w^0(\alpha,\beta)=\sum_{m=1}^{M} C_m \sin\left(\frac{m\pi\alpha}{L_\alpha}\right)$; $\gamma_x^0(\alpha,\beta)=\sum_{m=1}^{M} D_m \cos\left(\frac{m\pi\alpha}{L_\alpha}\right)$

(+)A uniform mesh is used; x_a and y_b represent the number of elements in α and β directions, respectively, z_h is the number of elements across the thickness;

(-)Number of d.o.f. used; under brackets the number of unknowns used in reference paper by analytical models.

Table 1.3: Expansion order, FEA-3D meshing and trial functions

Material name	r	s1	s2	s3	s4
E1[GPa]	25E2	1	33	25	0.05
E2[GPa]	E2	1	1	1	0.05
E3 [GPa]	E2	1	1	1	0.05
G12 [GPa]	0.5E2	0.2	0.8	0.5	0.0217
G13 [GPa]	0.5E2	0.2	0.8	0.5	0.0217
G23 [GPa]	0.2E2	0.2	0.8	0.5	0.0217
υ12	0.25	0.25	0.25	0.25	0.15
υ13	0.25	0.25	0.25	0.25	0.15
υ23	0.25	0.25	0.25	0.25	0.15

Table 1.4. Mechanical properties.

Load	BCS	Type	Sketch	Formula
Sinusoidal	SS	Beam	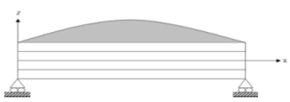	$p^0(\alpha)=p^0{}_u \sin(\pi\alpha/L_\alpha)$ if $0\le\alpha\le L_\alpha$

Table 1.5: Loading and boundary conditions

It should be noticed that case 1.1 is a standard case considered by almost all researchers, while case 1.2 is challenging owing to strong asymmetry of material properties across the thickness. Hereafter, displacement fields of First-Order Shear Deformation Theory (FSDT) [53] and of Higher-order Shear Deformation Theory (HSDT) [56] are reported as comparison results. FSDT assumes the following displacement field truncated at the first order [53]:

$$u_\alpha(\alpha,\beta,\varsigma)=u_\alpha{}^0(\alpha,\beta)+\varsigma(\Gamma_\alpha^0(\alpha,\beta)-w^0(\alpha,\beta)_{,\alpha}) \qquad (1.21)$$
$$u_\varsigma(\alpha,\beta,\varsigma)=w^0(\alpha,\beta)$$

It should be noticed that transverse normal strain is null across the thickness, while transverse shear strain is constant across ς. Thus, transformed reduced stiffness have to be used and transverse shear stresses are not continuous across the thickness. Moreover, there is not the fulfilment of boundaries conditions on stresses. A shear correction factor and post-processing techniques are mandatory, in order to get a realistic representation of σ_{ij} ; anyway this theory get very bad results if layerwise effects are relevant and it is not precise also for some lay-ups (e.g. for soft core sandwich). So, in order to improve accuracy, HSDT was developed [56]:

$$u_\alpha(\alpha,\beta,\varsigma)=u_\alpha{}^0(\alpha,\beta)+\varsigma(\Gamma_\alpha^0(\alpha,\beta)-w^0(\alpha,\beta)_{,\alpha})+\varsigma^2C_\alpha(\alpha,\beta)+\varsigma^3D_\alpha(\alpha,\beta) \qquad (1.22)$$
$$u_\varsigma(\alpha,\beta,\varsigma)=w^0(\alpha,\beta)$$

Terms C_α and D_α are calculated by imposing the fulfilment of (1.15). Similarly to FSDT, transverse normal strain is null across the thickness, so, transformed reduced stiffness have to be still used. Because transverse shear stress is not continuous across the thickness, results have to be post-processed in order to get a realistic representation of out-of-plane stresses. Because of their too simple kinematics this theory cannot obtain good results if layerwise effects relevant.

1.7.1 Results for cases 1.1 and 1.2 by ZZA, FSDT and HSDT

Firstly, a [0/90/0] laminated beam (case 1.1), under a sinusoidal loading is analyzed. All layers are made of the same material and have the same thickness. A length to thickness ratio of 4 is considered. Results (reported in Figure 1.2 and Tables 1.6.1 in tabular form, for the sake of completeness) are compared to exact solution, provided by Pagano [57], except that in-plane stress (not provided in [57]), for which 3-D FEA is used as reference solution. Transverse shear and transverse normal stresses of HSDT and FSDT are obtained by post-processing through integration of local equilibrium equations and a shear correction factor of 5/6 is assumed for FSDT. The following normalizations are used for case 1.1:

$$\overline{u_\alpha} = \frac{E_2 u_\alpha\left(0,\varsigma\right)}{hp^0} \quad \overline{u_\varsigma} = \frac{100E_2 h^3 u_\varsigma\left(\frac{L_\alpha}{2},\varsigma\right)}{L_\alpha^4 p^0} \quad \overline{\sigma_{\alpha\alpha}} = \frac{\sigma_{\alpha\alpha}\left(\frac{L_\alpha}{2},\varsigma\right)}{p^0} \quad \overline{\sigma_{\alpha\varsigma}} = \frac{\sigma_{\alpha\varsigma}\left(0,\varsigma\right)}{p^0} \quad \overline{\sigma_{\varsigma\varsigma}} = \frac{\sigma_{\varsigma\varsigma}\left(\frac{L_\alpha}{2},\varsigma\right)}{p^0} \tag{1.23a}$$

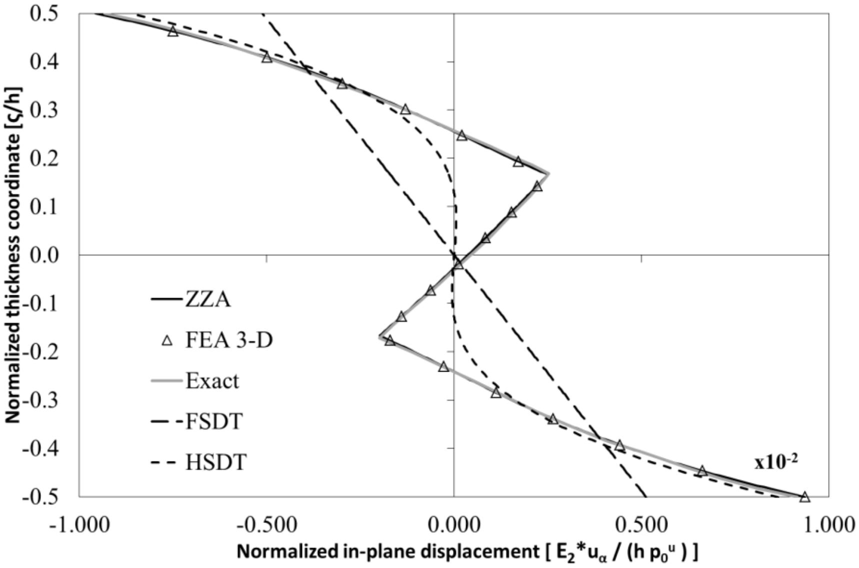

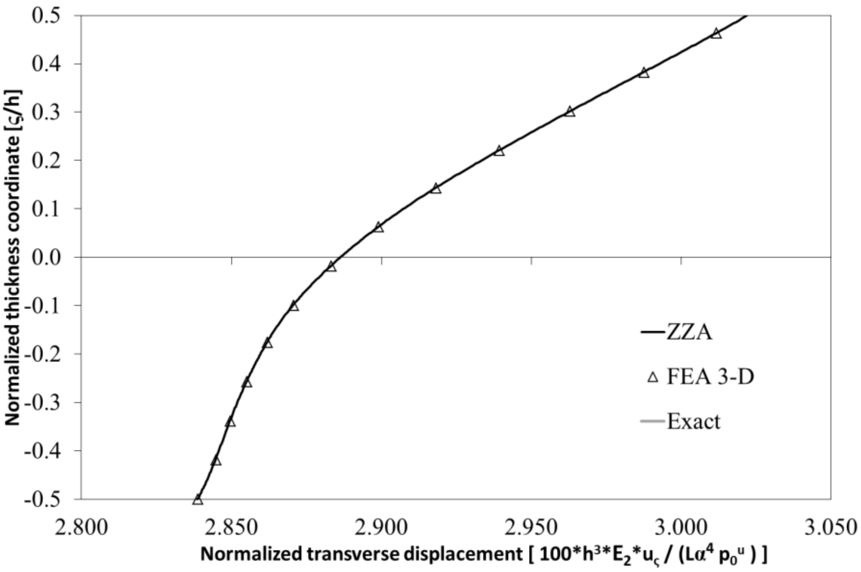

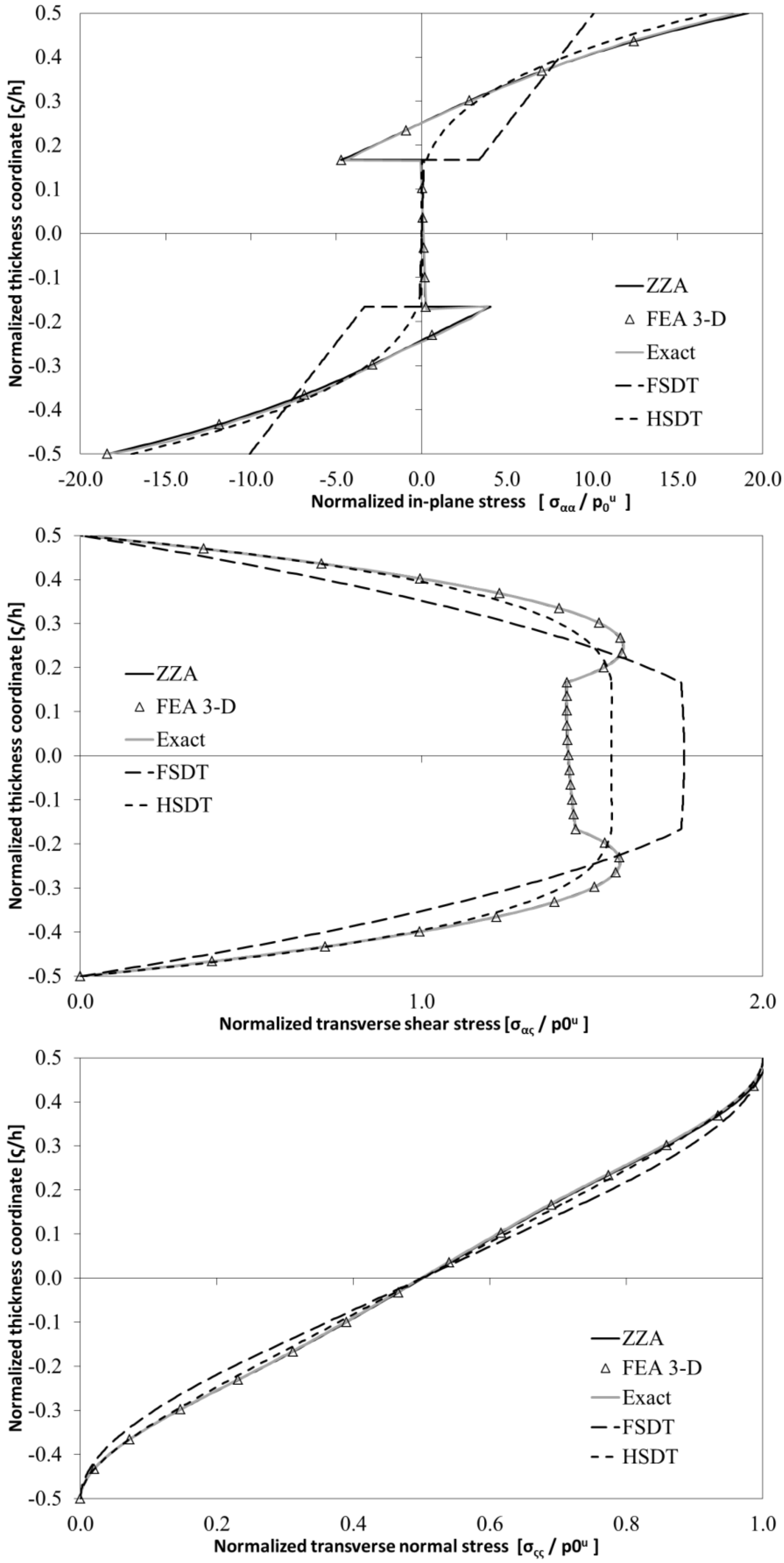

Figure 1.2: Normalized displacements and stresses, case 1.1

It should be noticed that 3-D FEA obtain results that are in a very good agreement with exact solution and also ZZA calculate stresses and displacements very close to reference ones. Instead, FSDT and HSDT theories are not able to reproduce the correct trend of displacements and stresses across the thickness, even if they are post-processed. Transverse displacements provided by these theories are not reported in Figure 1.2 because errors are very high and the curves would not fit within the scales.

Case 1.1	Position	Exact [15]	3-D FEA	ZZA	FSDT	HSDT
	up	0.9352	0.9372	0.9362	0.5123	0.8639
u_α	down	-0.9323	-0.9378	-0.9371	-0.5123	-0.8639
	max	0.9352	0.9372	0.9362	0.5123	0.8639
	min	-0.9323	-0.9378	-0.9371	-0.5123	-0.8639
	up	-	3.0224	3.0220	2.4094	2.6985
u_ς	down	-	2.8390	2.8386	2.4094	2.6985
	max	-	3.0224	3.0220	2.4094	2.6985
	min	-	2.8390	2.8386	2.4094	2.6985
	up	18.7664	18.9669	18.8549	10.0854	17.0063
$\sigma_{\alpha\alpha}$	down	-18.6899	-18.4311	-18.4292	-10.0854	-17.0063
	max	18.7664	18.9669	18.8549	10.0854	17.0063
	min	-18.6899	-18.4311	-18.4292	-10.0854	-17.0063
$\sigma_{\alpha\varsigma}$	max	1.5918	1.5919	1.5902	1.7602	1.5566
	min	0	0	0	0	0
$\sigma_{\varsigma\varsigma}$	up	1.0000	1.0000	1.0000	1.0000	1.0000
	max	1.0000	1.0000	1.0000	1.0000	1.0000

Table 1.6.1: Results in tabular form for case 1.1

As regards case 1.2, it is a simply-supported eleven layers sandwich beam under a sinusoidal loading ($L\alpha/h=4$). The lower face is damaged reducing elastic modulus E_3 by a factor of 100. Each face is a five layer laminate made of different materials (see Tables 1.1 to 1.6). Material s1 has weak properties in both tension, compression and shear, s2 is very stiff, s3 is compliant in shear and stiff in compression and tension, while the core material s4 is weak. This case was previously studied by Icardi [54] and it is very challenging because transverse shear stresses of faces assume an opposite sign. The following normalizations are assumed for this case:

$$\overline{u_\alpha}=\frac{u_\alpha(L_\alpha,\varsigma)}{hp^0}\quad \overline{u_\varsigma}=\frac{u_\varsigma(L_\alpha,\varsigma)}{hp^0}\quad \overline{\sigma_{\alpha\alpha}}=\frac{\sigma_{\alpha\alpha}(L_\alpha,\varsigma)}{p^0(L_\alpha/h)^2}\quad \overline{\sigma_{\alpha\varsigma}}=\frac{\sigma_{\alpha\varsigma}(L_\alpha,\varsigma)}{P^0}\quad \overline{\sigma_{\varsigma\varsigma}}=\frac{\sigma_{\varsigma\varsigma}(L_\alpha,\varsigma)}{p^0} \tag{1.23b}$$

Case 1.2	Position	Exact [13]	3-D FEA	ZZA	FSDT	HSDT
	up	-0.0153	-0.0153	-0.0153	-0.0012	0.0029
u_α	down	-0.0026	-0.0026	-0.0026	0.0012	-0.0029
	max	0.0424	0.0424	0.0426	0.0012	0.0030
	min	-0.0153	-0.0153	-0.0152	-0.0012	-0.0030
	up	0.3861	0.3861	0.3864	0.0202	0.0563
u_ς	down	-0.0875	-0.0875	-0.0872	0.0202	0.0563
	max	0.3861	0.3861	0.3864	0.0202	0.0563
	min	-0.0876	-0.0876	-0.0878	0.0202	0.0563
	up	-	0.8734	0.8732	0.0668	0.1547
$\sigma_{\alpha\alpha}$	down	-	0.1448	0.1453	-0.0668	-0.1547
	max	-	21.4108	21.4011	2.0285	4.0974
	min	-	-16.4857	-16.4760	-2.0285	-4.0974
$\sigma_{\alpha\varsigma}$	max	5.7220	5.7005	5.7337	1.4122	1.3981
	min	-0.6498	-0.6490	-0.6512	0	0
$\sigma_{\varsigma\varsigma}$	up	1.0000	1.0000	1.0000	1.0000	1.0000
	max	1.0000	1.0000	1.0000	1.0000	1.0000
	min	-0.0252	-0.0252	-0.0252	0	0

Table 1.6.2: Results in tabular form for case 1.2

Again, results by ZZA and 3-D FEA are always in a very good agreement with exact solution provided by [54]. Instead, FSDT (shear correction factor of 5/6 is used) and HSDT theories calculate inaccurate displacements and stresses and they are not able to reproduce the distribution of quantities across the thickness, even if post-processing is used.

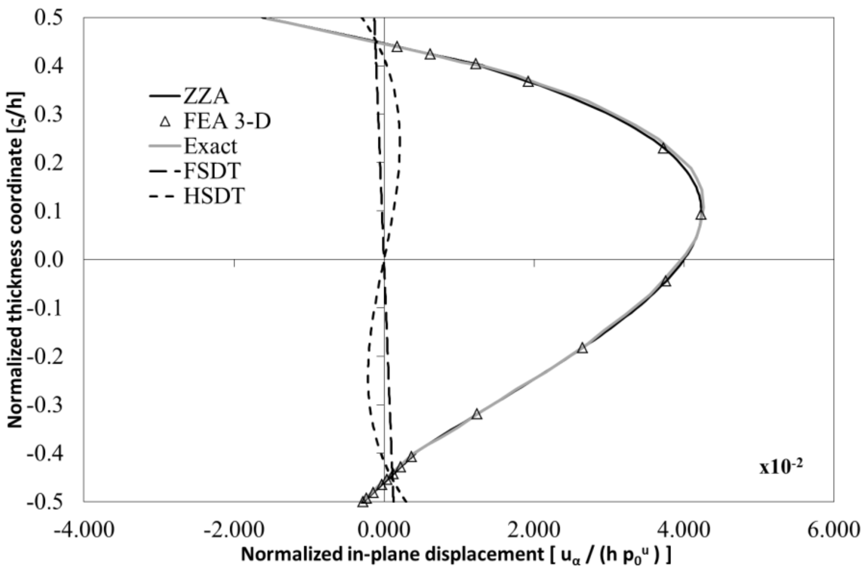

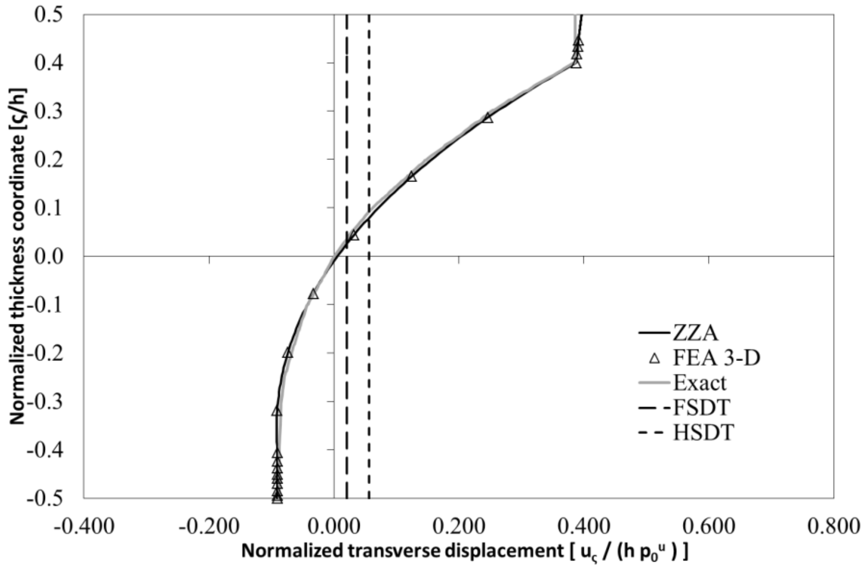
Normalized thickness coordinate [ς/h]
Normalized transverse displacement [$u_ς$ / (h p_0^u)]
ZZA
FEA 3-D
Exact
FSDT
HSDT

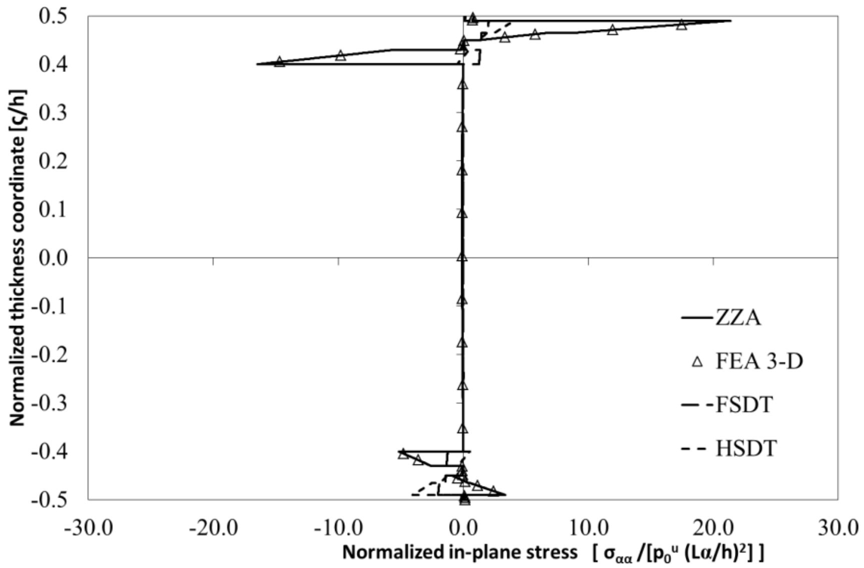
Normalized thickness coordinate [ς/h]
Normalized in-plane stress [$σ_{αα}$ /[p_0^u (Lα/h)^2]]
ZZA
FEA 3-D
FSDT
HSDT

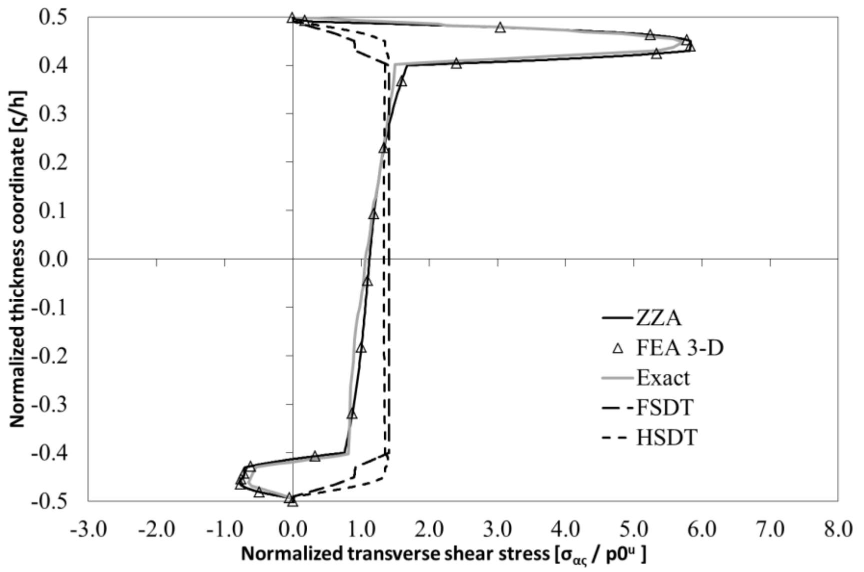
Normalized thickness coordinate [ς/h]
Normalized transverse shear stress [$σ_{ας}$ / p0^u]
ZZA
FEA 3-D
Exact
FSDT
HSDT

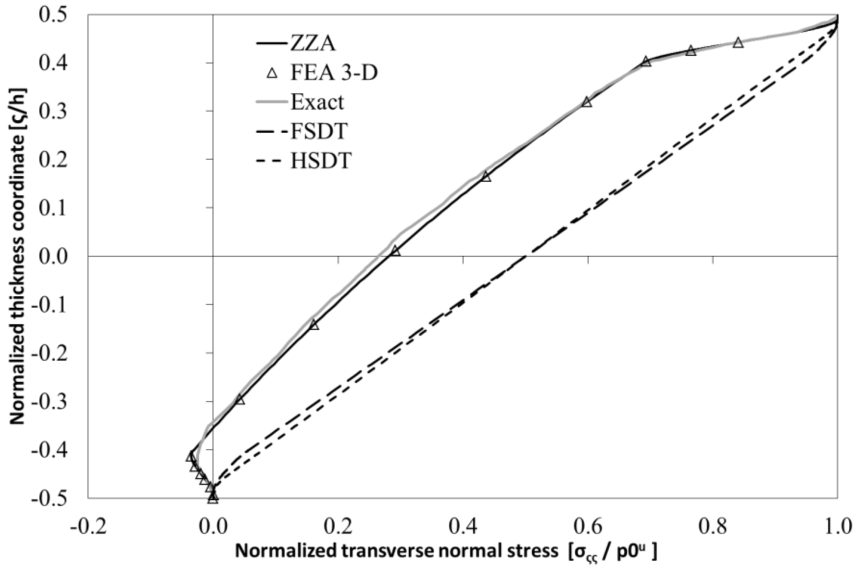

Figure 1.3: Normalized displacements and stresses, case 1.2

These results demonstrate the accuracy of ZZA and of 3-D FEA; this latter theory will be used as reference solution, if exact one is not available. Moreover it is demonstrated that simplified FSDT and HSDT theories cannot achieve the same accuracy of higher-order adaptive theories, even if they are post-processed and they are completely inadequate if there are strong layerwise effects, as for case 1.2. Table 1.6.3 reports processing time of theories of this section. It should be noticed that ZZA has a processing time that is 2 to 3 times larger than ESL theories, but its accuracy is much higher. E.g., maximum percentage error for case 1.2 is about 0.6% for ZZA (see Table 1.6.2) while FSDT and HSDT provide more than 70% of percentage error for all displacements and stresses.

Theory	Case 1.1	Case 1.2
ZZA	4.3157	17.7618
FSDT	1.9507	6.6445
HSDT	2.2694	9.3617

Table 1.6.3: Processing time [s]

1.8 3-D FEA reference solution used in numerical assessments

Exact solutions are used as reference solutions, whenever available. Otherwise, 3-D finite element solutions are used. Such solution have been obtained employing the mixed 3D continuum element by Icardi and Atzori [6], whose features are briefly reminded.

Nodal d.o.f. of this eight-nodes mixed solid element are indicated as $\{q_e\}$ and are displacements and out-of-plane stresses. Also the electric field along ς and the temperature rise are incorporated in nodal d.o.f. vector, with the intended aim to allow analysis of piezoactuated composites including thermal effects. So, the expression of $\{q_e\}$ is:

$$\{q_e\}^T = \{u_i,\, v_i,\, w_i,\, \sigma_{xz,i},\, \sigma_{yz,i},\, \sigma_{zz,i}, T_i, E_{z,i}\} \tag{1.24}$$

where the superscript ^{T} indicate a transposed vector. Anyway, $T_i, E_{z,i}$ will be omitted in applications of this thesis. The following serendipity, linear interpolation functions for every d.o.f. are used:

$$\begin{aligned}
N_1 &= 0.125*(1-\xi_1)(1-\xi_2)(1-\xi_3) & N_5 &= 0.125*(1-\xi_1)(1-\xi_2)(1+\xi_3)\\
N_2 &= 0.125*(1+\xi_1)(1-\xi_2)(1-\xi_3) & N_6 &= 0.125*(1+\xi_1)(1-\xi_2)(1+\xi_3)\\
N_3 &= 0.125*(1+\xi_1)(1+\xi_2)(1-\xi_3) & N_7 &= 0.125*(1+\xi_1)(1+\xi_2)(1+\xi_3)\\
N_4 &= 0.125*(1-\xi_1)(1+\xi_2)(1-\xi_3) & N_8 &= 0.125*(1-\xi_1)(1+\xi_2)(1+\xi_3)
\end{aligned} \tag{1.25}$$

All nodal d.o.f. can be rearranged:

$$\begin{aligned}
\{qu^e\}^T &= \{u_1 \quad u_2 \quad u_3 \quad u_4 \quad u_5 \quad u_6 \quad u_7 \quad u_8\}^e;\\
\{qv^e\}^T &= \{v_1 \quad v_2 \quad v_3 \quad v_4 \quad v_5 \quad v_6 \quad v_7 \quad v_8\}^e;\\
\{qw^e\}^T &= \{w_1 \quad w_2 \quad w_3 \quad w_4 \quad w_5 \quad w_6 \quad w_7 \quad w_8\}^e;\\
\{q\sigma^e_{xz}\}^T &= \{\sigma_{xz1} \quad \sigma_{xz2} \quad \sigma_{xz3} \quad \sigma_{xz4} \quad \sigma_{xz5} \quad \sigma_{xz6} \quad \sigma_{xz7} \quad \sigma_{xz8}\}^e;\\
\{q\sigma^e_{yz}\}^T &= \{\sigma_{yz1} \quad \sigma_{yz2} \quad \sigma_{yz3} \quad \sigma_{yz4} \quad \sigma_{yz5} \quad \sigma_{yz6} \quad \sigma_{yz7} \quad \sigma_{yz8}\}^e;\\
\{q\sigma^e_{zz}\}^T &= \{\sigma_{zz1} \quad \sigma_{zz2} \quad \sigma_{zz3} \quad \sigma_{zz4} \quad \sigma_{zz5} \quad \sigma_{zz6} \quad \sigma_{zz7} \quad \sigma_{zz8}\}^e;\\
\{qT^e\}^T &= \{T_1 \quad T_2 \quad T_3 \quad T_4 \quad T_5 \quad T_6 \quad T_7 \quad T_8\}^e;\\
\{qE^e\}^T &= \{E_1 \quad E_2 \quad E_3 \quad E_4 \quad E_5 \quad E_6 \quad E_7 \quad E_8\}^e;
\end{aligned} \tag{1.26}$$

So, the eight independent components can be expressed as:

$$\begin{aligned}
&u^e = \mathbf{N}\{qu^e\} \quad v^e = \mathbf{N}\{qv^e\} \quad w^e = \mathbf{N}\{qw^e\}\\
&\sigma^e_{xz} = \mathbf{N}\{q\sigma^e_{xz}\} \quad \sigma^e_{yz} = \mathbf{N}\{q\sigma^e_{yz}\} \quad \sigma^e_{zz} = \mathbf{N}\{q\sigma^e_{zz}\}\\
&T^e = \mathbf{N}\{qT^e\} \quad E^e = \mathbf{N}\{qE^e\}
\end{aligned} \tag{1.27}$$

The topological transformation from physical (x_1, x_2, x_3) to natural volume (ξ_1, ξ_2, ξ_3) is used, in order to simplify and harmonize calculus of integrals of strain energy, so:

$$x_i = \mathbf{N}\{x^e\} \tag{1.28}$$

As regards derivative, the following relations apply:

$$\begin{Bmatrix} \dfrac{\partial}{\partial \xi_1} \\ \dfrac{\partial}{\partial \xi_2} \\ \dfrac{\partial}{\partial \xi_3} \end{Bmatrix} = [J] \begin{Bmatrix} \dfrac{\partial}{\partial \alpha} \\ \dfrac{\partial}{\partial \beta} \\ \dfrac{\partial}{\partial \varsigma} \end{Bmatrix} \quad ; \quad \begin{Bmatrix} \dfrac{\partial}{\partial \alpha} \\ \dfrac{\partial}{\partial \beta} \\ \dfrac{\partial}{\partial \varsigma} \end{Bmatrix} = [J]^{-1} \begin{Bmatrix} \dfrac{\partial}{\partial \xi_1} \\ \dfrac{\partial}{\partial \xi_2} \\ \dfrac{\partial}{\partial \xi_3} \end{Bmatrix} \tag{1.29}$$

where $[J]$ is Jacobian matrix and $[J]^{-1}$ its inverse

$$[J] = \begin{bmatrix} \dfrac{\partial \alpha}{\partial \xi_1} & \dfrac{\partial \beta}{\partial \xi_1} & \dfrac{\partial \varsigma}{\partial \xi_1} \\ \dfrac{\partial \alpha}{\partial \xi_2} & \dfrac{\partial \beta}{\partial \xi_2} & \dfrac{\partial \varsigma}{\partial \xi_2} \\ \dfrac{\partial \alpha}{\partial \xi_3} & \dfrac{\partial \beta}{\partial \xi_3} & \dfrac{\partial \varsigma}{\partial \xi_3} \end{bmatrix} \longrightarrow [J]^{-1} = \frac{1}{|J|} \begin{bmatrix} \dfrac{\partial \varsigma}{\partial \xi_3} & -\dfrac{\partial \varsigma}{\partial \xi_2} & -\dfrac{\partial \varsigma}{\partial \xi_1} \\ -\dfrac{\partial \beta}{\partial \xi_3} & \dfrac{\partial \beta}{\partial \xi_2} & -\dfrac{\partial \beta}{\partial \xi_1} \\ -\dfrac{\partial \alpha}{\partial \xi_3} & -\dfrac{\partial \alpha}{\partial \xi_2} & \dfrac{\partial \alpha}{\partial \xi_1} \end{bmatrix} \tag{1.30}$$

So, the following expressions of strains, obtained by strain-displacement relations are obtained:

$$\begin{aligned}
\varepsilon_{xx}^{u} &= \frac{\partial \mathbf{N} qu^e}{\partial x} = \left(\frac{\partial \mathbf{N}}{\partial \xi_1}\frac{\partial \xi_1}{\partial \alpha} + \frac{\partial \mathbf{N}}{\partial \xi_2}\frac{\partial \xi_2}{\partial \alpha} + \frac{\partial \mathbf{N}}{\partial \xi_3}\frac{\partial \xi_3}{\partial \alpha} \right)\{qu^e\} \\
\varepsilon_{yy}^{u} &= \frac{\partial \mathbf{N} qv^e}{\partial y} = \left(\frac{\partial \mathbf{N}}{\partial \xi_1}\frac{\partial \xi_1}{\partial \beta} + \frac{\partial \mathbf{N}}{\partial \xi_2}\frac{\partial \xi_2}{\partial \beta} + \frac{\partial \mathbf{N}}{\partial \xi_3}\frac{\partial \xi_3}{\partial \beta} \right)\{qv^e\} \\
\varepsilon_{zz}^{u} &= \frac{\partial \mathbf{N} qu^e}{\partial z} = \left(\frac{\partial \mathbf{N}}{\partial \xi_1}\frac{\partial \xi_1}{\partial \varsigma} + \frac{\partial \mathbf{N}}{\partial \xi_2}\frac{\partial \xi_2}{\partial \varsigma} + \frac{\partial \mathbf{N}}{\partial \xi_3}\frac{\partial \xi_3}{\partial \varsigma} \right)\{qw^e\} \\
\varepsilon_{xy}^{u} &= \left(\frac{\partial \mathbf{N}}{\partial \xi_1}\frac{\partial \xi_1}{\partial \beta} + \frac{\partial \mathbf{N}}{\partial \xi_2}\frac{\partial \xi_2}{\partial \beta} + \frac{\partial \mathbf{N}}{\partial \xi_3}\frac{\partial \xi_3}{\partial \beta} \right)\{qu^e\} + \left(\frac{\partial \mathbf{N}}{\partial \xi_1}\frac{\partial \xi_1}{\partial \alpha} + \frac{\partial \mathbf{N}}{\partial \xi_2}\frac{\partial \xi_2}{\partial \alpha} + \frac{\partial \mathbf{N}}{\partial \xi_3}\frac{\partial \xi_3}{\partial \alpha} \right)\{qv^e\} \\
\varepsilon_{xz}^{u} &= \left(\frac{\partial \mathbf{N}}{\partial \xi_1}\frac{\partial \xi_1}{\partial \varsigma} + \frac{\partial \mathbf{N}}{\partial \xi_2}\frac{\partial \xi_2}{\partial \varsigma} + \frac{\partial \mathbf{N}}{\partial \xi_3}\frac{\partial \xi_3}{\partial \varsigma} \right)\{qu^e\} + \left(\frac{\partial \mathbf{N}}{\partial \xi_1}\frac{\partial \xi_1}{\partial \alpha} + \frac{\partial \mathbf{N}}{\partial \xi_2}\frac{\partial \xi_2}{\partial \alpha} + \frac{\partial \mathbf{N}}{\partial \xi_3}\frac{\partial \xi_3}{\partial \alpha} \right)\{qw^e\} \\
\varepsilon_{yz}^{u} &= \left(\frac{\partial \mathbf{N}}{\partial \xi_1}\frac{\partial \xi_1}{\partial \beta} + \frac{\partial \mathbf{N}}{\partial \xi_2}\frac{\partial \xi_2}{\partial \beta} + \frac{\partial \mathbf{N}}{\partial \xi_3}\frac{\partial \xi_3}{\partial \beta} \right)\{qw^e\} + \left(\frac{\partial \mathbf{N}}{\partial \xi_1}\frac{\partial \xi_1}{\partial \varsigma} + \frac{\partial \mathbf{N}}{\partial \xi_2}\frac{\partial \xi_2}{\partial \varsigma} + \frac{\partial \mathbf{N}}{\partial \xi_3}\frac{\partial \xi_3}{\partial \varsigma} \right)\{qv^e\}
\end{aligned} \tag{1.31}$$

Considering the effect of thermal expansion on strains:

$$\begin{aligned}
\varepsilon_{xx}^{T} &= \alpha_1 \Delta T \\
\varepsilon_{yy}^{T} &= \alpha_2 \Delta T \\
\varepsilon_{zz}^{T} &= \alpha_3 \Delta T
\end{aligned} \tag{1.32}$$

and piezoelectric constitutive equations:

$$\begin{aligned}
\varepsilon_{ij} &= C_{ijkl}\sigma_{kl} + \overline{d_{kij}} E_k \\
D_i &= \overline{d_{kij}}\sigma_{kl} + p_{ij} E_j
\end{aligned} \tag{1.33}$$

the following expressions of in-plane stresses can be obtained:

$$\begin{matrix}\{\varepsilon^u\}=[B]\{q^e\} \\ \{\varepsilon^\sigma\}=[C]\{\sigma\}\end{matrix} \longrightarrow \begin{Bmatrix}\sigma_{11} \\ \sigma_{12} \\ \sigma_{22}\end{Bmatrix}=\left([S^*][B^*]-[P]\right)\{q^e\} \tag{1.34}$$

where $[S^*]$ is the submatrix of stiffness matrix (obtained removing the last three rows), $[B^*]$ is the submatrix of $[B]$ (obtained removing the last two columns) and $[P]$ is:

$$[P]=\begin{bmatrix} & \bar{\Lambda}_{11}\{N\} & e_{31}\{N\} \\ [0] & \bar{\Lambda}_{12}\{N\} & e_{32}\{N\} \\ & \bar{\Lambda}_{22}\{N\} & e_{33}\{N\}\end{bmatrix}$$

(1.43)

where $\bar{\Lambda}_{ij}$ and e_{3i} are thermal expansion and piezoelectric stress coefficients. So, vector of stresses can be expressed as:

$$\{\sigma\}=\begin{bmatrix} & & & [S^*][B^*]-[P] & & & \\ 0 & 0 & 0 & \mathbf{N} & 0 & 0 & 0 \\ 0 & 0 & 0 & 0 & \mathbf{N} & 0 & 0 \\ 0 & 0 & 0 & 0 & 0 & \mathbf{N} & 0\end{bmatrix}\{q^e\}=\left[\hat{S}\right]\{q^e\} \tag{1.35}$$

Strains and stresses can be substituted into HR functional (1.13g), whose expression (1.36) is obtained considering only mechanical d.o.f.:

$$\Pi=\{q^e\}^T\left[\int_V\left(\left[\hat{S}\right]^T[B]-\frac{1}{2}\left[\hat{S}\right]^T[B]\left[\hat{S}\right]\right)dV\right]\{q^e\} \tag{1.36}$$

Deriving the expression of Π for each $\{q_e\}$, the element stiffness matrix $[K_e]$ can be obtained; using standard techniques it is also possible to obtain element mass matrix $[M_e]$ and vector of nodal forces $\{F_e\}$.

Chapter 2 – Mixed theories derived from ZZA

The main goal of this thesis is development of general and efficient version of ZZA. In this chapter, only mixed variants of the parent theory are presented, while theories with a growing degree of generalization are developed and discussed in the next chapter. The most advanced theories have similar features to HT, axiomatic/asymptotic approaches and CUF particularizations, but because of their low computational costs, that are always comparable to ESL ones and require very low number of unknowns, they can be used as alternatives than more expensive formulations widespread in literature [14], irrespective lay-up, loading and boundary conditions considered.

Features of currently available zigzag theories are overviewed in the next section, since their characteristics are retaken in the subsequent theories of this study.

2.1 Discussion of layerwise functions

As stated in the previous chapter, nowadays composite and sandwich structures are widespread in a lot of fields of engineering and their use could further increase in the next years. However, their modelling is very challenging and a lot of structural models to describe their behaviour have been proposing during the years. ESL are not used in this thesis because they can't get accurate results if strong layerwise effects are present, for some lay-ups (e.g. for soft-core sandwiches [39]) and certain loading and boundary condition. Even though they require post-processing techniques and a shear correction factor (that is strong case-dependent [38]), they often are not able to get also global quantities. Instead, DL are very accurate but the number of unknowns depends on the number of layers, so, they cannot be used to analyse structures of industrial interest.

Indeed, as deeply explained in section 1.1, the main focus of this thesis are zig-zag theories, which guarantee the right balance between accuracy and cost saving. They are developed by adding layerwise and higher-order contributions to ESL, as displacement-based or mixed theories (if displacement, strain and stress fields are assumed separately one to another or not) and as kinematic-based/Murakami's like or physically-based/Di Sciuva's like (depending on zig-zag functions that are incorporated and conditions that are imposed).

As regard Di Sciuva's like zig-zag theories, zig-zag contributions are calculated by enforcing the continuity of out-of-plane stresses and of the gradient of transverse normal stress across the thickness (see section 1.6). Some remarkable examples of these kind of theories can be found in papers by Li and

Liu [58], by Zhen and Wanji [59] (global-local theories), by Kim and Cho [60], by Tessler et al. [61] (that developed RZT theory), by Iurlaro et al. [62] (RZT with cubic transverse displacement), by Icardi [54] (physically-based theory with a second-order zig-zag function), by Icardi and Sola [4] (ZZA theory), by Shariyat [63] and by Icardi and Urraci [15] to [23] (various mixed and displacement-based physically-based theories).

Instead, as regard Murakami's like zig-zag theories, a periodic change of slope of displacements across the thickness is imposed; usually, these theories are developed in mixed form, assuming stresses apart through Hellinger-Reissner variational theorem. Some important examples of these theories can be found in papers by Zhen and Wanji [64] (mixed kinematic-based HW theory), Brischetto et al. [51], Demasi [65], Rodrigues et al. [66], Carrera and coworkers [30], [67] and [68] (these latter theories are particularization of Carrera's Unified Formulation (CUF) [14]).

In recent papers, Gherlone [44] and Groh and Weaver [45] demonstrate that physically-based zig-zag theories are more accurate than Murakami's like ones (with the same degree of representation) but Zhen and Wanji [64] affirm the opposite. Anyway, results by [15] to [23] confirm findings by [44] and [45] for a great number of challenging benchmarks. A lot of results that will show the behaviour of various models, both displacements-based and mixed ones, both physically- and kinematic-based ones, will be reported in chapters 4 and 5 for static and dynamic relevant cases.

So, according to [44] and [45], physically-based zig-zag theories are chosen as the main topic of this work. Particularly, the starting point of research is ZZA by Icardi and Sola [4], because it demonstrates its superiority and accuracy for a lot of challenging cases, requiring only 5 d.o.f. (see section 1.6). An accurate description of transverse displacement and the imposition of continuity of gradient of transverse normal stress are characteristic features of ZZA (and of theories obtained from it in [15] to [23]). It should be noticed that an accurate modelling of transverse deformation is mandatory, in order to get accurate results under localized loading (Carrera and Ciuffreda [69]), for damaged sandwiches (Icardi [54]), for high frequency vibrations and transient response analyses (Rekatsinas et al. [70]), to calculate pumping modes (Icardi and Urraci [17]) and to get accurate stresses for clamped and propped-cantilever sandwich beam under uniform static loading (Mattei and Bardella [71]). Regarding cantilever and propped-cantilever beams, it should be noticed that their modelling is challenging, because, according to Carrera et al. [72] and Tessler et al. [61] transverse shear stresses is null at clamped edges for traditional plate models. Anyway, recent refined zig-zag theories ([4], [15] to [23], [61], [72]) are able to overcome this issue.

As explained in section 1.1, CUF permits user to choice the order of expansion of displacements (and consequently the number of unknowns that depend directly from it) as an input, obtaining arbitrary mixed kinematic based zig-zag, equivalent single layer, layerwise and hierarchical structural models as its particularizations (see [46]- [49]). Regarding hierarchical theories, the variation of displacement field across the thickness is postulated a priori, by choosing a hierarchical set of locally defined polynomials, without layerwise functions and no physical or kinematic constraints are imposed. No post-processing techniques are needed, as long as an appropriate expansion order of displacements across the thickness (so, an appropriate number of unknowns) is chosen.

Regarding the representation of displacements across the thickness, Taylor's series, trigonometric and exponential functions, a combination of both and radial basis functions were used by many researchers; a lot of important findings can be found in papers [62], [73], [74], [75], [76], [77], [78] and [79]. Recently, Candiotti et al. [50] investigated non polynomial through-thickness representations (exponential, sinusoidal and hyperbolic expansions) of variables using an axiomatic/asymptotic method combined with CUF (thanks to arbitrariness regarding choice of displacements), concluding that a sinusoidal expansion of displacements across the thickness was the best option among the considered models.

However, it should be noticed that recent refined higher-order physically-based zig-zag theories [18]- [23], which are obtained by redefining coefficients across the thickness and calculating them by imposing the full set of physical constraints of ZZA (compatibility of out-of-plane stresses, gradient of transverse normal stress and displacements across the thickness, boundary conditions on stresses, fulfilment of local equilibrium equations across the thickness, see section 1.6), can get accurate results, indistinguishable from exact ones, irrespective zig-zag functions chosen, which can be also omitted without any loss of accuracy. Moreover, for these higher-order theories different functions than power series (e.g. trigonometric or exponential expansions) can be chosen differently for each displacements and from point to point across the thickness. Differently to [50], indistinguishable results are obtained, as long as coefficients are redefined and calculated on a physical basis. On the contrary, if coefficients are not redefined across the thickness or only a few of physical constraints of ZZA are imposed, results by Candiotti et al. [50] are confirmed and they strongly depend from representation chosen.

So, theories [18]- [23] have a great degree of generalizations (similar to those provided by hierarchical and axiomatic/asymptotic theories) and are much more efficient than HT, MZZ or particularizations of [14], because only five fixed d.o.f. are needed. As a consequence, the most general theory, ZZA_GEN [23], here retaken in section 3.5.3 (where its new particularizations are proposed and assessed), can compete with formulations widespread in literature, such as [14], resulting very interesting by virtue of its very low computational burden.

The progressive refinement of ZZA is reported in chapters 2 and 3, as well as theories that will be used for calculations for elastostatic (chapter 4), dynamic (chapter 5) and impact damage applications (chapter 6). In this chapter, mixed formulations obtained from ZZA are discussed, while in the next one, many variants of the parent theory are reported or developed. Each of theories of chapters 2 and 3 have peculiar features, which are useful to demonstrate when the choices of zig-zag or representation functions are critical or otherwise when they can be changed. Symbolic calculus is used to develop and assess all theories of this thesis. For this reason, the symbolic procedure that is general and valid for all physically-based zig-zag theories, is reported in Appendix 3.

In order to preserve accuracy and efficiency of ZZA, while keeping only essential contributions within displacement strain and stress fields, the first group of theories that was developed concerns mixed HR and HW theories.

2.2 Multilayered mixed theories so far developed

As shown in the previous section, ZZA has an accuracy degree comparable with those of DL, anyway, its displacement fields is very complex and it requires a lot of time for its building, despite its time calculation is similar to FSDT. So, the intended aim is to develop a refined and (possibly) generalized version of ZZA, which must keep the same accuracy of the parent theory but a simpler expression of displacement field. In order to do this, a lot studies are required with the purpose to understand which contributions of ZZA are important and which can be eventually omitted.

So far, a lot of mixed theories have been proposed in Literature, usually developed through HR variational theorem, whose stresses are assumed apart from displacements of a simplified kinematics. A remarkable example is the mixed EFSDTM theory, developed by Kim and Cho [60] by using HR variational theorem, whose kinematics is the same of FSDT while stresses are obtained from a higher-order zig-zag theory (EHOPT). Another interesting HR mixed physically-based theory is RZT, developed by Tessler et al. [61] and refined by Iurlaro et al. [62]. Cubic piecewise in-plane displacements and a uniform transverse one across the thickness are assumed, while stresses are obtained by integrating local equilibrium equations.

EDZN theory by Brischetto et al. [51] is cited as a notable example of mixed HR kinematic-based theory. This theory is obtained as a particularization of CUF [14] whose displacements include Murakami's zig-zag function and are expanded to N-order across the thickness (N is chosen by user). Differently to EFSDTM and RZT, transverse displacement is not assumed uniform across the thickness, so, EDZN is able to obtain stresses that are in well agreement with exact solutions also for thick sandwich with quite-strong layerwise effects. Anyway, an expansion order across the thickness of N=7 (thus 27 d.o.f.) is required to obtain better results, but despite this, displacements are quite wrong.

As an example of mixed HW theory, GHZTM theory developed by Zhen and Wanji [64] is mentioned. This theory is developed in kinematic-based form, whose displacements (transverse displacement is uniform across the thickness), strains and stresses are assumed apart each other, with the intended aim to create an efficient and accurate C0 finite element (it should be noticed that elements with these features were previously developed in [6] and [55] using different techniques). An interesting findings of [64] affirms that physically-based theories are less accurate than kinematic-based ones, while results of previous papers by Gherlone [44] and Groh and Weaver [45] affirm the opposite.

With the purpose to decrease computational burden of ZZA and also to settle this dispute, different theories both in physically- and kinematic-based forms are developed, through the use of HR and HW variational theorems. Their features are similar to those of theories previously cited (and of other remarkable theories here not cited for sake of brevity). Moreover, another purpose of these theories is to better understand if an accurate description of transverse displacement and deformability is always required to obtain accurate results, as affirmed by Mattei and Bardella [71] and by [17]. It should be noticed that all theories developed by author in this thesis or in [15], [18]- [22], [24] assume the same number of d.o.f. and the same in-plane expansion order of trial functions, in order to test their performance under the same conditions. Figure 2.1 reports genealogy of models of this chapter.

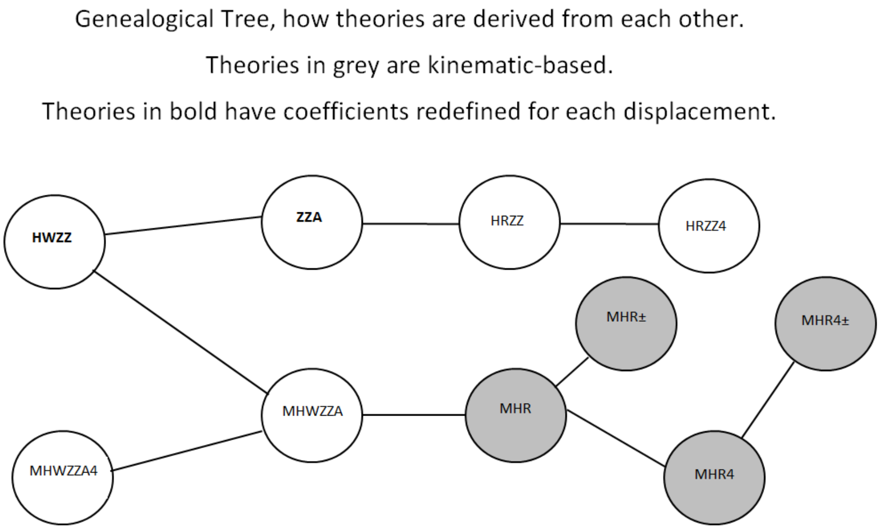

Figure 2.1: Genealogy of theories of section 2.2

2.3 Mixed HR zig-zag theories of this study

For each theory of chapters 2 and 3, a qualitative description is reported, where tables summarize their main characteristics. Their specifics, along with their displacement, strain and stress fields are reported in specific subsections.

Firstly, HRZZ theory, retaken from [15], is cited. It is a mixed HR physically-based model, whose coefficients of in-plane displacements are redefined layer-by-layer across the thickness, while transverse displacement is uniform across the thickness, similarly to [60], [62], [64]. Transverse normal stress is the same of ZZA, while transverse shear stresses are assumed by integrating local equilibrium equations. Nevertheless this theory usually obtains good results, inaccurate description of displacements and stresses are provided when laminates have strong layerwise effects, confirming that an accurate description of transverse displacement and deformability is required for these cases, according to [71] and [17].

Theory	**Main features**
HRZZ	• Mixed HR physically-based zig-zag theory; • Piecewise in-plane displacements $u_\alpha^{(3)}$ (redefined coefficient); • Uniform transverse displacement $u_\varsigma^{(0)}$; • Transverse normal stress from ZZA; • Transverse shear stresses apart, by integrating local equilibrium equations.

PROS	**CONS**
Better results than ESL;	Inaccurate results for strong layerwise effects;
Good results for mid layerwise effects;	Inaccurate results for high natural frequencies;
More accurate than other simplified theories, like MHR and MHR4 (see 2.4)	Poor results when an accurate description of transverse displacement is required.
	Processing time are similar to those of ZZA

$^{(n)}$ indicates the order of expansion of in-plane and transverse displacements

Table 2.1a: Characteristic features of HRZZ and HRZZ4 theories.

HRZZ4 [15] constitutes a variation of HRZZ, whose in-plane displacements are the same of its counterpart but a fourth-order polynomial transverse displacement is assumed. Results obtained by this theory are similar to those of HRZZ, confirming that only a piecewise description of displacements (obtained by redefining coefficients layer-by-layer across the thickness) allows to get the maximal accuracy [17]. It should be also noticed that use of theories with a simplified kinematics (like HRZZ and HRZZ4) is discouraged also to get high natural frequencies or for dynamic problems that require an accurate description of transverse displacement (e.g. pumping modes of sandwich structures see [17], [19] and chapter 5). The processing time of HRZZ and HRZZ4 is similar to that of ZZA, so, use of these theories is neither advantageous, from the point of view of accuracy, nor for computational cost savings.

HRZZ4	• Mixed HR physically-based zig-zag theory; • Piecewise in-plane displacements $u_\alpha^{(3)}$ (redefined coefficients); • Fourth-order polynomial transverse displacement $u_\varsigma^{(4)}$ (not redefined coefficients); • Transverse normal stress from ZZA; • Transverse shear stresses apart, by integrating local equilibrium equations.

PROS	CONS
Better results than ESL;	Inaccurate results for strong layerwise effects;
Good results for mid layerwise effects; More accurate than other simplified theories, like MHR and MHR4 (see 2.4)	Inaccurate results for high natural frequencies; Poor results when an accurate description of transverse displacement is required. Processing time are similar to those of ZZA

$^{(n)}$ indicates the order of expansion of in-plane and transverse displacements

Table 2.1b: Characteristic features of HRZZ and HRZZ4 theories.

2.3.1 Mixed HRZZ and HRZZ4 theories

In this section, HRZZ and HRZZ4 developed under HR variational theorem (1.13g) in physically-based form are reported (they are retaken from [15]). Their qualitative features are described in previous section.

Regarding HRZZ, it is a physically-based zig-zag theory, whose transverse displacement is uniform across the thickness and in-plane ones are piecewise cubic:

$$\begin{aligned} u_\alpha(\alpha,\beta,\varsigma) &= [\ u_\alpha{}^0(\alpha,\beta)+\varsigma(\Gamma_\alpha^0(\alpha,\beta)-w^0(\alpha,\beta)_{,\alpha})\ ]_0 + [\ C_\alpha^i(\alpha,\beta)\varsigma^2 + D_\alpha^i(\alpha,\beta)\varsigma^3\ ]_i + \\ &\quad [\ \sum_{k=1}^{n_i}\Phi_\alpha^k(\alpha,\beta)(\varsigma-\varsigma_k)H_k(\varsigma) + \sum_{k=1}^{\Im}{}_\alpha C_u^k(\alpha,\beta)H_k(\varsigma)\ ]_c \\ u_\varsigma(\alpha,\beta,\varsigma) &= w^0(\alpha,\beta) \end{aligned} \quad (2.1)$$

It should be noticed that symbols already defined for ZZA in (1.14g) are not explained also in this section (e.g. symbols of in-plane and thickness coordinates). For their meaning refer to section 1.6. Due to this choice, transverse normal strain $\varepsilon_{\varsigma\varsigma}$ obtained by stress-strain relations is null. So, transformed, reduced stiffness properties are assumed. Transverse shear stresses are obtained apart from displacements by integrating in-plane stresses, while, with the intended aim to include a more correct transverse deformability, transverse normal one $\sigma_{\varsigma\varsigma}$ is the same of ZZA. Coefficients C_α^i and D_α^i are calculated by imposing boundary conditions on transverse shear stresses (1.15) and the first equilibrium equation (1.18) at different points across the thickness. Φ_α^k are obtained by imposing the compatibility of transverse shear stresses (1.19), while ${}_\alpha C_u^k$ restore the continuity of in-plane displacements (1.20). So, the full, set of physical constraints of ZZA is not imposed. Nevertheless coefficients of in-plane displacements are redefined for each layer, results of this theory are less accurate than ZZA, HWZZ and other higher-order theories, because of u_ς is too simple. Particularly, this theory provide very inaccurate results when there are strong layerwise effects, when an accurate transverse displacement is required or for dynamic problems, demonstrating that only an accurate description of transverse deformability and the imposition of full set of physical constraints (and coefficients of displacements redefined for each layer) prevent loss of accuracy.

With the intended aim to increase accuracy of HRZZ, HRZZ4 is developed. Transverse displacement is a fourth-order polynomial, but, differently to in-plane ones, its coefficients are not redefined across the thickness:

$$\begin{aligned} u_\alpha(\alpha,\beta,\varsigma) &= [\ u_\alpha{}^0(\alpha,\beta)+\varsigma(\Gamma^0_\alpha(\alpha,\beta)-w^0(\alpha,\beta)_{,\alpha})\ ]_0+[\ C^i_\alpha(\alpha,\beta)\varsigma^2+D^i_\alpha(\alpha,\beta)\varsigma^3\ ]_i+ \\ &\quad [\ \sum_{k=1}^{n_i}\Phi^k_\alpha(\alpha,\beta)(\varsigma-\varsigma_k)H_k(\varsigma)+\sum_{k=1}^{3}{}_\alpha C^k_u(\alpha,\beta)H_k(\varsigma)\ ]_c \\ u_\varsigma(\alpha,\beta,\varsigma) &= [\ w^0(\alpha,\beta)\ ]_0+[\ b\ (\alpha,\beta)\varsigma+c\ (\alpha,\beta)\varsigma^2+d\ (\alpha,\beta)\varsigma^3+e\ (\alpha,\beta)\varsigma^4\ ]_i \end{aligned} \tag{2.2}$$

Because of the transverse displacement is not uniform across the thickness, reduced stiffness properties are not necessary. Again, transverse normal stress is the same of ZZA, while transverse shear stresses are obtained by integrating local equilibrium equations. Coefficients C^i_α, D^i_α, Φ^k_α and ${}_\alpha C^k_u$ are calculated like HRZZ, while b, c, d and e are calculated by imposing boundary conditions on transverse normal stress and its gradient (1.16) and (1.17). Again, the whole set of physical constraint of ZZA is not imposed, being coefficients of u_ς not redefined layer-by-layer across the thickness. Nevertheless $\sigma_{\varsigma\varsigma}$ is retaken from ZZA, the description of transverse deformability is too poor and the same defects of HRZZ still apply. Results demonstrate that only theories whose coefficients are redefined layer-by-layer across the thickness for each displacement and calculated by imposing the full set of physical constraints of ZZA are always accurate, irrespective the lay-up, material properties, loading and boundary conditions of examined cases.

2.4 Mixed HWZZ zig-zag theory of this study

With the intended aim to overcome issues of HRZZ and HRZZ4, a mixed HW physically-based theory, called HWZZ is developed [15], whose displacements, strains and stresses are assumed apart each-other preserving only essential contributions for each field and decreasing computational burden of ZZA. Particularly, master displacement field is retaken from ZZA, whose second-order zig-zag contributions are omitted, but coefficients are still redefined layer-by-layer across the thickness and no subdivision into mathematical layers is allowed. This decomposition is restored for out-of-plane master strains, that are also used to calculate in-plane stresses, while out-of-plane ones are obtained by integrating local equilibrium equations. Results of static and dynamic analyses provided by this theory, for which all physical constraints are imposed and coefficients of displacements are redefined layer-by-layer across the thickness, are very close to those provided by ZZA, also for structures whose layerwise effects are strong, confirming that only a redefinition of coefficients across the thickness and imposition of all physical constraints (1.15)-(1.20) prevents loss of accuracy.

Computational burden of this theory is lower than ZZA, because only essential contributions are present for each field, but cost saving is only 10% of the overall processing time of the parent theory. Indeed, HW variational principle introduces additional contributions into energy, that undermine the beneficial effects of simplifications. Thus, cheaper but still accurate variants of HWZZ and ZZA are developed (and explained) in following sections.

HWZZ

- Mixed HW pshysically-based zig-zag theory;
- Piecewise in-plane displacements $u_\alpha^{(3)}$ (redefined coefficients);
- Piecewise transverse displacement $u_\varsigma^{(4)}$ (redefined coefficients);
- Second order zig-zag omitted for master transverse displacement, no decomposition into mathematical layers allowed;
- Subdivision into mathematical layers admitted for out-of-plain master strains;
- Master out-of-plane stresses obtained by integrating local equilibrium equations;

PROS	CONS
Results very close to ZZA ones, also when when are strong layerwise effects, irrespective loading and boundary conditions. Processing time is lower than ZZA one.	Time saving is only about 10% of processing time of ZZA.

$^{(n)}$ indicates the order of expansion of in-plane and transverse displacements

Table 2.2: Characteristic features of HWZZ theory.

2.4.1 Displacement, strain and stress fields of HWZZ

This theory is developed through HW variational theorem (1.13d) and was previously presented in [15]. The purpose of this theory is to decrease the computational burden of ZZA (whose time calculation is still comparable with those of equivalent single layer theories), keeping only essential contributions for displacement, strain and stress fields and maintaining the same accuracy of parent theory.

Master displacement field is obtained from that of ZZA neglecting second-order zig-zag contributions (Ω^k). No decomposition into mathematical layer is allowed for displacement field, so, terms ${}_\alpha C_u^j$ and C_ς^j (that impose continuity of displacements at mathematical layer interfaces) are omitted:

$$\begin{aligned} u_\alpha(\alpha,\beta,\varsigma) &= \left[\ u_\alpha{}^0(\alpha,\beta)+\varsigma(\Gamma_\alpha^0(\alpha,\beta)-w^0(\alpha,\beta)_{,\alpha})\ \right]_0+\left[\ C_\alpha^i(\alpha,\beta)\varsigma^2+D_\alpha^i(\alpha,\beta)\varsigma^3\ \right]_i+ \\ &\left[\ \sum_{k=1}^{n_i}\Phi_\alpha^k(\alpha,\beta)(\varsigma-\varsigma_k)H_k(\varsigma)\ \right]_c \\ u_\varsigma(\alpha,\beta,\varsigma) &= \left[\ w^0(\alpha,\beta)\ \right]_0+\left[\ b^i(\alpha,\beta)\varsigma+c^i(\alpha,\beta)\varsigma^2+d^i(\alpha,\beta)\varsigma^3+e^i(\alpha,\beta)\varsigma^4\ \right]_i+ \\ &\left[\ \sum_{k=1}^{n_i}\Psi^k(\alpha,\beta)(\varsigma-\varsigma_k)H_k(\varsigma)\ \right]_c \end{aligned} \tag{2.3}$$

Coefficients are still redefined for each layer and C_α^i, D_α^i, b^i, c^i, d^i, e^i are calculated by imposing boundary conditions on out-of-plane stresses (1.15)-(1.16) and equilibrium at different points across the thickness (1.18). Again, Φ_α^k and Ψ^k restore the continuity of transverse shear and normal stresses (1.19).

As regard master strain field, they are obtained using strain-displacements relations (1.1) assuming the following displacement field, where the decomposition into mathematical layer is again allowed, so, ${}_\alpha C_u^j$ and C_ς^j are reintroduced:

$$\begin{aligned} u_\alpha(\alpha,\beta,\varsigma) &= [\ u_\alpha{}^0(\alpha,\beta)+\varsigma(\Gamma_\alpha^0(\alpha,\beta)-w^0(\alpha,\beta)_{,\alpha})\ ]_0+[\ C_\alpha^i(\alpha,\beta)\varsigma^2+D_\alpha^i(\alpha,\beta)\varsigma^3\ ]_i+ \\ &\quad [\ \sum_{k=1}^{n_i}\Phi_\alpha^k(\alpha,\beta)(\varsigma-\varsigma_k)H_k(\varsigma)+\sum_{j=1}^{3}{}_\alpha C_u^j(\alpha,\beta)H_j(\varsigma)\ ]_c \\ w_\varsigma(\alpha,\beta,\varsigma) &= [\ w^0(\alpha,\beta)\ ]_0+[\ b^i(\alpha,\beta)\varsigma+c^i(\alpha,\beta)\varsigma^2+d^i(\alpha,\beta)\varsigma^3+e^i(\alpha,\beta)\varsigma^4\ ]_i+ \\ &\quad [\ \sum_{k=1}^{n_i}\Psi^k(\alpha,\beta)(\varsigma-\varsigma_k)H_k(\varsigma)+\sum_{j=1}^{3}C_\varsigma^j(\alpha,\beta)H_j(\varsigma)\ ]_c \end{aligned} \tag{2.4}$$

Again, C_α^i, D_α^i, b^i, c^i, d^i, e^i, Φ_α^k and Ψ^k enable the fulfilment of boundary conditions, equilibrium equations, equilibrium equations and compatibility of stresses at interfaces (1.15)-(1.16), (1.18), (1.19), while ${}_\alpha C_u^j$ and C_ς^j are calculated by imposing the continuity of displacements between mathematical layers (1.20). So, strains assume the following expressions:

$$\begin{aligned} \varepsilon_{\alpha\alpha}(\alpha,\beta,\varsigma) &= \breve{\tilde{U}}(\alpha,\beta,\varsigma)_{,\alpha}+\sum_{k=1}^{s}\Phi_{\alpha,\alpha}^k(\alpha,\beta)(\varsigma-\varsigma_k)H_k(\varsigma) \\ \varepsilon_{\beta\beta}(\alpha,\beta,\varsigma) &= \breve{\tilde{V}}(\alpha,\beta,\varsigma)_{,\beta}+\sum_{k=1}^{s}\Phi_{\beta,\beta}^k(\alpha,\beta)(\varsigma-\varsigma_k)H_k(\varsigma) \\ \varepsilon_{\varsigma\varsigma}(\alpha,\beta,\varsigma) &= \breve{\tilde{W}}(\alpha,\beta,\varsigma)_{,\varsigma}+\sum_{k=1}^{s}\Psi^k(\alpha,\beta)H_k(\varsigma) \\ \gamma_{\alpha\varsigma}(\alpha,\beta,\varsigma) &= [\breve{\tilde{U}}(\alpha,\beta,\varsigma)_{,\varsigma}+\sum_{k=1}^{s}\Phi_\alpha^k(\alpha,\beta)H_k(\varsigma)+\breve{\tilde{W}}(\alpha,\beta,\varsigma)_{,\alpha}+\sum_{k=1}^{s}\Psi_{,\alpha}^k(\alpha,\beta)(\varsigma-\varsigma_k)H_k(\varsigma)] \\ \gamma_{\beta\varsigma}(\alpha,\beta,\varsigma) &= [\breve{\tilde{V}}(\alpha,\beta,\varsigma)_{,\varsigma}+\sum_{k=1}^{s}\Phi_\beta^k(\alpha,\beta)H_k(\varsigma)+\breve{\tilde{W}}(\alpha,\beta,\varsigma)_{,\beta}+\sum_{k=1}^{s}\Psi_{,\beta}^k(\alpha,\beta)(\varsigma-\varsigma_k)H_k(\varsigma)] \\ \gamma_{\alpha\beta}(\alpha,\beta,\varsigma) &= [\breve{\tilde{U}}(\alpha,\beta,\varsigma)_{,\beta}+\sum_{k=1}^{s}\Phi_{\alpha,y}^k(\alpha,\beta)(\varsigma-\varsigma_k)H_k(\varsigma)+\breve{\tilde{V}}(\alpha,\beta,\varsigma)_{,\alpha}+\sum_{k=1}^{s}\Phi_{\beta,\alpha}^k(\varsigma-\varsigma_k)H_k(\varsigma)] \end{aligned} \tag{2.5}$$

where the symbols $\breve{\tilde{U}}$, $\breve{\tilde{V}}$ and $\breve{\tilde{W}}$ are:

$$\begin{aligned} \breve{\tilde{U}}(\alpha,\beta,\varsigma) &= u_\alpha{}^0(\alpha,\beta)+\varsigma(\Gamma_\alpha^0(\alpha,\beta)-w^0(\alpha,\beta)_{,\alpha})+C_\alpha^i(\alpha,\beta)\varsigma^2+D_\alpha^i(\alpha,\beta)\varsigma^3+\sum_{j=1}^{3}{}_\alpha C_u^j(\alpha,\beta)H_j(\varsigma) \\ \breve{\tilde{V}}(\alpha,\beta,\varsigma) &= u_\beta{}^0(\alpha,\beta)+\varsigma(\Gamma_\beta^0(\alpha,\beta)-w^0(\alpha,\beta)_{,\beta})+C_\beta^i(\alpha,\beta)\varsigma^2+D_\beta^i(\alpha,\beta)\varsigma^3+\sum_{j=1}^{3}{}_\beta C_u^j(\alpha,\beta)H_j(\varsigma) \\ \breve{\tilde{W}}(\alpha,\beta,\varsigma) &= w^0(\alpha,\beta)+b^i(\alpha,\beta)\varsigma+c^i(\alpha,\beta)\varsigma^2+d^i(\alpha,\beta)\varsigma^3+e^i(\alpha,\beta)\varsigma^4+\sum_{j=1}^{3}C_\varsigma^j(\alpha,\beta)H_j(\varsigma) \end{aligned} \tag{2.6}$$

As regard master stress field, in-plane stresses ($\sigma_{\alpha\alpha}$, $\sigma_{\beta\beta}$, $\sigma_{\alpha\beta}$) are obtained using stress-strain relations (1.2), while out-of-plane ones are obtained by integrating local equilibrium equations (1.18). As a consequence, also the continuity of gradient of transverse normal stress across the thickness is guaranteed (1.19), overcoming all simplifications made, and so imposing the full set of physical constraints:

$$\sigma_{\alpha\varsigma} = \int_{-h/2}^{h/2} (b_\alpha - \sigma_{\alpha\alpha,\alpha} - \sigma_{\alpha\beta,\beta}) d\varsigma$$
$$\sigma_{\beta\varsigma} = \int_{-h/2}^{h/2} (b_\beta - \sigma_{\alpha\beta,\alpha} - \sigma_{\beta\beta,\beta}) d\varsigma \tag{2.7}$$
$$\sigma_{\varsigma\varsigma} = \int_{-h/2}^{h/2} (b_\varsigma - \sigma_{\alpha\varsigma,\alpha} - \sigma_{\beta\varsigma,\beta}) d\varsigma =$$
$$\int_{-h/2}^{h/2} \left[b_\varsigma - \int_{-h/2}^{h/2} (b_{\alpha,\alpha} - \sigma_{\alpha\alpha,\alpha\alpha} - \sigma_{\alpha\beta,\alpha\beta}) dz - \int_{-h/2}^{h/2} (b_{\beta,\beta} - \sigma_{\alpha\beta,\alpha\beta} - \sigma_{\beta\beta,\beta\beta}) d\varsigma \right] d\varsigma$$

Because of simplifications on (2.3), displacements have to be post-processed and amplitudes A_Δ^i obtained by Rayleigh-Ritz method (see section 1.4) are substituted into displacement field of ZZA (1.10). Because of coefficients of displacement, strain and stress fields are redefined layer-by-later across the thickness and the whole set of physical constraints is imposed, very accurate results, indistinguishable than those obtained by ZZA, are obtained with a lower processing time, demonstrating that HW variational theorem can be used to create accurate and simple theories. Anyway the cost saving obtained by HWZZ is only about 10%, so, other theories are developed, with the intended aim to create a more general and a more simple version of ZZA (see chapter 3).

2.5 Mixed kinematic-based zig-zag theories of this study

Unlike physically-based theories such as HRZZ, HRZZ4, HWZZA, where amplitudes of zig-zag functions are determined by imposing the fulfilment of interfacial stress compatibility conditions, a reverse of the slope of displacements is imposed at each interface for kinematic-based theories.

Two mixed HR kinematic-based theories, called MHR and MHR4, were developed [15] and assessed. The first one has similar characteristics of other theories of Literature, whose in-plane displacements are piecewise cubic and include Murakami's layerwise function, while transverse one is a fourth-order polynomial and out-of-plane stresses are calculated separately by integrating local equilibrium equations. Thus, nevertheless coefficients of displacement field are not redefined (and are obtained by imposing the BCS of stresses (1.15)-(1.17)), a periodic change of the slope of in-plane displacement is imposed at each interface, regardless lay-up and material properties. Because of this latter feature, this theory cannot provide good results when Murakami's rule is not respected and also for structures whose layerwise effects are too strong, being its kinematics too simple.

MHR

- Mixed HR kinematic-based zig-zag theory;
- Piecewise in-plane displacements $u_\alpha^{(3)}$ (not redefined coefficient) with Murakami's zig-zag function;

- Fourth-order polynomial transverse displacement $u_\varsigma^{(4)}$ (not redefined coefficient);
- Out-of-plane stresses by integrating local equilibrium equations;

PROS	CONS
Better results than ESL;	Inaccurate results for strong layerwise effects;
Good results if Murakami's rule is respected;	Inaccurate results if Murakami's rule is not respceted;
Very low processing time.	Inaccurate results for high natural frequencies;
	Poor results when an accurate description of transverse displacement is required.

$^{(n)}$ indicates the order of expansion of in-plane and transverse displacements

Table 2.3a: Characteristic features of MHR theory.

Even the inclusion of Murakami's zig-zag functions into transverse displacement, like for MHR4 theory, cannot increase accuracy of this theory. So, similar results of MHR are obtained and similar considerations apply for both theories. Processing time of these theories is very low and their development is very easy, but their usage is discouraged unless Murakami's rule is respected and strong layerwise effects are absent. These statements still apply also for dynamic problems (e.g. high natural frequencies or pumping modes, that require a proper description of displacement field). Indeed, very high expansion order of displacements across the thickness are required to get quite accurate results [51]. So, results by Gherlone [44] and Groh and Weaver [45] about the superiority of physically-based theories over kinematic-based ones, if the same expansion order is assumed, are confirmed.

MHR4

- Mixed HR kinematic-based zig-zag theory;
- Piecewise in-plane displacements $u_\alpha^{(3)}$ (not redefined coefficient) with Murakami's zig-zag function;
- Piecewise transverse displacement $u_\varsigma^{(0)}$ (not redefined coefficient) with Murakami's zig-zag function;
- Out-of-plane stresses by integrating local equilibrium equations;

PROS	CONS
Better results than ESL;	Inaccurate results for strong layerwise effects;
Good results if Murakami's rule is respected;	Inaccurate results if Murakami's rule is not respceted;
Very low processing time.	Inaccurate results for high natural frequencies;
	Poor results when an accurate description of transverse displacement is required;
	Nevertheless Murakami's zig-zag function is also included

into transverse displacement, similar results than MHR are obtained.

$^{(n)}$ indicates the order of expansion of in-plane and transverse displacements

Table 2.3b: Characteristic features of MHR4 theory.

2.5.1 MHR and MHR4

As previously stated, MHR and MHR4 are developed under HR variational theorem (1.13g) in kinematic-based form (they are retaken from [15]). Their qualitative features are described in previous section, while their specifics are reported here.

Regarding MHR, this is a kinematic-based zig-zag theory, whose features are similar to other models of Literature and the following displacement field is assumed:

$$\begin{aligned} u_\alpha(\alpha,\beta,\varsigma) &= \left[\; u_\alpha{}^0(\alpha,\beta)+\varsigma(\Gamma^0_\alpha(\alpha,\beta)-w^0(\alpha,\beta)_{,\alpha})\;\right]_0 + \left[\; C_\alpha(\alpha,\beta)\varsigma^2 + D_\alpha(\alpha,\beta)\varsigma^3\;\right]_i + \\ &\quad + u_{\alpha z}(\alpha,\beta)M^k(\varsigma) \end{aligned} \tag{2.8}$$

$$u_\varsigma(\alpha,\beta,\varsigma) = \left[\; w^0(\alpha,\beta)\;\right]_0 + \left[\; a\;(\alpha,\beta)\varsigma + b\;(\alpha,\beta)\varsigma^2 + c\;(\alpha,\beta)\varsigma^3 + d\;(\alpha,\beta)\varsigma^4\;\right]_i$$

Transverse displacement is a fourth-order polynomial, while in-plane displacements are piecewise cubic and include Murakami's zig-zag function, which provides a periodic change of slope of displacements at each layer interface, irrespective lay-up and material properties:

$$M^k(\varsigma) = (-1)^k \zeta^k \tag{2.9}$$

where ζ^k, whose superscript ^{k} is the layer number, is expressed as:

$$\zeta^k = a^k\varsigma - b^k, \quad a^k = \frac{2}{\varsigma_{k+1}-\varsigma_k}, \quad b^k = \frac{\varsigma_{k+1}+\varsigma_k}{\varsigma_{k+1}-\varsigma_k} \tag{2.10}$$

Coefficients of displacements are not redefined across the thickness and C_α, D_α are calculated by imposing boundary conditions on transverse shear stresses (1.15), a, b, c and d by imposing (1.16) and (1.17). With the intended aim to test all theories under the same conditions, MHR must have the same number of d.o.f. than other theories. To do this, an additional equation is imposed, so, $u_{\alpha z}$ are calculated by imposing the fulfilment of first and second equilibrium equations (1.18) at a point near the reference plane. It should be noticed that this latter choice is peculiar of MHR and usually in Literature also $u_{\alpha z}$ is an additional degree of freedom. Despite this, results obtained by MHR are similar to others obtained by kinematic-based models in Literature (see results of chapters 4 and 5). Because of its too simple kinematics, this theory is not adequate for strong layerwise effects, for dynamic calculations and to analyse structures when Murakami's rule is not respected. Because of HRZZ and HRZZ4 obtain better results than this theory, it is demonstrated the superiority of physically-based theories on kinematic-based ones, when the same expansion order across the thickness is assumed, confirming results of [44] and [45]. Moreover, it is also demonstrated that only theories whose coefficients are redefined for each layer across the thickness and that impose the full set of physical constraints (1.15)-(1.20) are always precise. Similar findings still apply also for MHR4 theory, whose in-plane displacements are the same of MHR, while transverse one contain Murakami's zig-zag function, so, a periodic change of slope is imposed also for u_ς:

$$\begin{aligned} u_\alpha(\alpha,\beta,\varsigma) &= [\ u_\alpha{}^0(\alpha,\beta)+\varsigma(\Gamma_\alpha^0(\alpha,\beta)-w^0(\alpha,\beta)_{,\alpha})\ ]_0+[\ C_\alpha(\alpha,\beta)\varsigma^2+D_\alpha(\alpha,\beta)\varsigma^3\ ]_i+ \\ &\quad +u_{\alpha z}(\alpha,\beta)M^k(\varsigma) \\ u_\varsigma(\alpha,\beta,\varsigma) &= [\ w^0(\alpha,\beta)\ ]_0+[\ a\ (\alpha,\beta)\varsigma+b\ (\alpha,\beta)\varsigma^2+c\ (\alpha,\beta)\varsigma^3+d\ (\alpha,\beta)\varsigma^4\ ]_i+ \\ &\quad +w_z(\alpha,\beta)M^k(\varsigma) \end{aligned} \tag{2.11}$$

Nevertheless transverse displacement is piecewise polynomial, again, kinematics of this theory is too poor, so, it cannot provide accurate results for cases with strong layerwise effects, for dynamic calculations and when Murakami's rule is not respected. The same findings about superiority of physically-based theories, which provide better results assuming the same expansion order across the thickness, are still valid. C_α, D_α, a, b, c, d and $u_{\alpha z}$ are calculated like MHR theory, while w_z is obtained by imposing the third equilibrium equation at a point near middle surface.

Despite their low accuracy, MHR and MHR4 are very interesting, thanks to their processing time that is very low. So, four variants are developed, with the intended aim to increase their accuracy and possibly to overcome some of their deficiency, so, MHR±, MHR4±, MHWZZA, MHWZZA4 theories are obtained and explained in the next subsection.

2.6 MZZ with slope defined on a physical basis and with improved fields

With the intended aim to increase accuracy of MHR and MHR4, four theories called MHWZZA, MHWZZA4 [15], MHR± e MHR4± [17] are developed. MHWZZA is a mixed HW theory, whose displacement field is the same of MHR, while strain and stress fields come from HWZZ. Incorporation of strains and stresses from a physically-based model strongly increase accuracy of this theory for elastostatic benchmarks, confirming previous statements about superiority of physically-based theories. However, the accuracy of HWZZ and ZZA cannot be reached, because kinematics is too poor. Particularly, very inaccurate results are provided for dynamic studies (see [17]), being the accuracy depending also on displacements. Similar findings still apply also including transverse displacement of ZZA into displacement field of MHWZZA4, confirming that only theories whose coefficients are redefined layer-by-layer across the thickness for each displacements and calculated by imposing the full set of physical constraints (1.15)-(1.20) can achieve maximal accuracy.

MHWZZA

- Mixed HW zig-zag theory;
- Displacements from MHR;
- Strains and stresses from HWZZ;

PROS	CONS
Better results than MHR and MHR4; Good results for mid layerwise effects; Lower processing time than ZZA.	Inaccurate results for strong layerwise effects; Very inaccurate results for dynamic studies; Poor results when an accurate description of transverse displacement is required.

MHWZZA4

- Mixed HW zig-zag theory;
- In-plane displacements from MHR, transverse one from ZZA;
- Strains and stresses from HWZZ;

PROS	CONS
Better results than MHR and MHR4; Good results for mid layerwise effects; Lower processing time than ZZA.	Inaccurate results for strong layerwise effects; Very inaccurate results for dynamic studies; Poor results when an accurate description of transverse displacement is required.

Table 2.4: Characteristic features of MHWZZA and MHWZZA4 theories.

Similar findings also apply for MHR± and MHR4± theories. They are similar to their counterparts MHR and MHR4, but the inversion of slope of displacements at interfaces is determined on a physical basis (see [17] for details), improving their accuracy also for lay-ups that don't respect Murakami's rule and preserving very low processing time. Anyway MHR± and MHR4± (whose coefficients of displacement field are not redefined) cannot achieve the same accuracy of ZZA and HWZZ for lay-ups that have strong layerwise effects or for dynamic studies, because their too poor kinematics.

MHR±

- Mixed HR kinematic-based zig-zag theory;
- Displacement field from MHR;
- Right sign of Murakami's zig-zag function for each layer is determined on a physical basis;
- Out-of-plane stresses by integrating local equilibrium equations;

PROS	CONS
Better results than MHR;	Inaccurate results for strong layerwise effects;
Good results also if Murakami's rule is not respected thanks to calculation of sign of Murakami's zig-zag function on a physical basis;	Inaccurate results for high natural frequencies;
Very low processing time.	Poor results when an accurate description of transverse displacement is required.

MHR4±

- Mixed HR kinematic-based zig-zag theory;
- Displacement field from MHR4;
- Right sign of Murakami's zig-zag function for each layer is determined on a physical basis;
- Out-of-plane stresses by integrating local equilibrium equations;

PROS	CONS
Better results than MHR4;	Inaccurate results for strong layerwise effects;
Good results also if Murakami's rule is not respected thanks to calculation of sign of Murakami's zig-zag function on a physical basis;	Inaccurate results for high natural frequencies;
Very low processing time.	Poor results when an accurate description of transverse displacement is required.

Table 2.5: Characteristic features of MHR± and MHR4± theories.

2.6.1 MHR±, MHR4±, MHWZZA, MHWZZA4 theories

MHR± is obtained from MHR assuming the same displacement field. Coefficients are still calculated in the same way, but now a periodic change of in-plane displacements is not imposed at each interface, but determined on a physical basis, choosing for any interface which sign of (2.9) produce the minimum residual force norm from (1.18) (it should be noticed that processing time is almost the same, because the operations described are very cheap). In the same way theory MHR4± can be obtained from MHR4. It should be noticed that differently to MHR and MHR4, $u_{\alpha z}$ and w_z are calculated for each layer, in order to determine their sign on a physical basis. Results will show that this choice has beneficial effects on accuracy, indeed good predictions are also obtained for lay-ups that do not fulfil Murakami's rule. Anyway, being their kinematics too poor they cannot be used when layerwise effects are too strong, despite having very low processing time.

With the intended aim to improve MHR performance, MHWZZA was developed. Its displacement field is the same of MHR (2.8), while strains and stresses are the same of HWZZ (see section 2.4), so, this theory is developed by using HW variational theorem. In detail, starting from displacement field (2.4), strains are obtained and in-plane stresses are calculated using stress-strains relations (1.4), while out-of-plane ones are obtained by integrating local equilibrium equations (1.18). Thanks to incorporation of strains and stresses that come from physically-based models, results of this theory are better than MHR and MHR4 ones, but their accuracy is lower if cases with very strong layerwise effects are analysed [15]. Moreover, natural frequencies and modal displacements and stresses are very bad predicted, demonstrating that this theory cannot be used for dynamic calculations, nevertheless its processing time is lower than ZZA. Findings of this theory demonstrate that only theories whose coefficients are redefined for each displacements and that impose the full set of physical constraints can always get displacements and stresses without any loss of accuracy. The same conclusions still apply also for MHWZZA4, where transverse displacement of ZZA is assumed (1.14g), while in-plane displacements, strains and stresses are the same of MHWZZA.

2.7 Remarks about mixed theories

Various mixed theories are developed and reported in this chapter, in order to test if mixed formulations are a viable option to keep kinematics simple and obtain accurate results and to settle dispute of superior accuracy of kinematic- or physically-based theories.

A lot of lower-order theories are created, whose features are similar to ones of literature and whose displacements assume simplified expressions, both in physically- and kinematic-based forms. Results (see chapters 4 and 5) confirm superior accuracy of physically-based theories on kinematic-based ones. However, all mixed lower-order theories that do not take into account an accurate description of transverse normal deformability cannot reach the same accuracy of higher-order theories and their cost saving is not very high. So, mixed theories with only a partial fulfilment of physical constraints are no advantageous from the standpoint of results and processing time.

Only HWZZ, higher-order mixed version of ZZA whose fields contain only essential contributions and that impose the full set of physical constraints of parent theory demonstrates its great accuracy, with a cost saving of 10%. Anyway, because of cost saving obtained by HWZZ is rather limited, different formulations must be further considered in order to attempt to achieve the objectives to obtain more efficient generalized theories.

Chapter 3 – Theories that generalize ZZA

As shown in previous chapter, lower-order mixed theories are useless, unless the full set of physical constraints of parent theory is imposed, as HWZZ. Anyway, cost saving obtained is rather limited, so, different formulations must be considered in order to achieve the objectives to obtain more efficient generalized theories. Particularly, it is needed to check if accuracy depends from the choices of zig-zag and representation functions, if the full set of physical constraints of ZZA is imposed in a pointwise sense.

3.1 Effects of the choice of zig-zag functions

As shown in previous chapter, mixed formulations allow development of theories with lower computational burden. The best model reported in 2.2.1 is HWZZ, whose accuracy is the same of its parent theory (ZZA) but its computational burden is 10% less than ZZA one. Anyway, cost saving obtained by HWZZ is rather limited, because processing time it is mainly determined by integration of strain energy (see Figure 3.1):

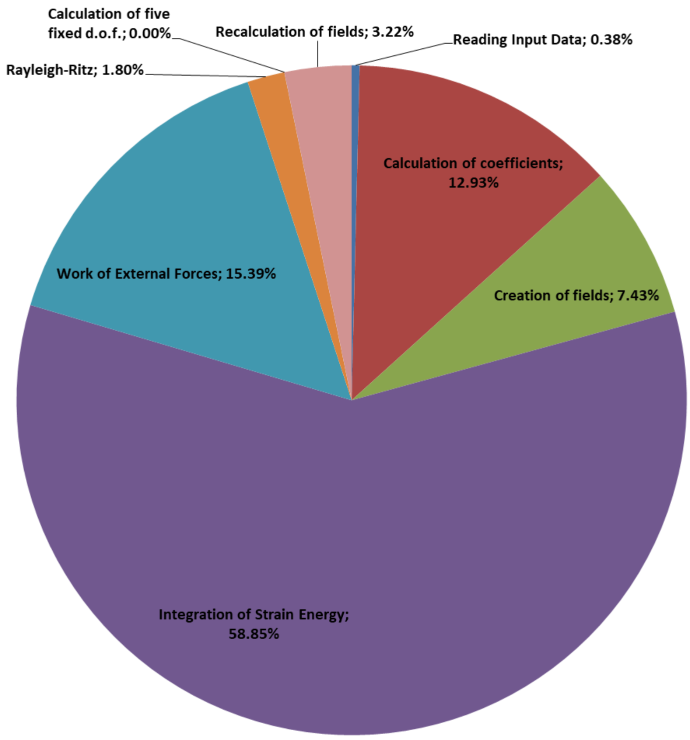

Figure 3.1: Detailed description of computational effort of HWZZ

The computational burden of integration of strain energy strongly depends by complexity of fields of theory and of zig-zag functions expressions, whose summations increase processing time of integration of upper layers. As a consequence, computational effort strongly rises if the number of layers is high. Instead, kinematic-based theories MHR and MHR4, which include Murakami's zig-zag function, show lower cost than physically-based ones, also thanks to particularly simple expression of their layerwise function, but their results are very inaccurate, making them useless.

3.1.1 Different assumptions of zig-zag functions

So, with the intended aim to lower computational effort of strain energy integration, a new theory called ZZM is developed. The same expression of displacements of ZZA is assumed but Di Sciuva's (see [42]) and Icardi's (see [54]) zig-zag functions are substituted with Murakami's (see [43]) and M2ZZ (see [17] and (2.11)) ones. Nevertheless the inclusion of Murakami's zig-zag function, ZZM is a physically-based zig-zag adaptive theory, because zig-zag amplitudes are redefined layer-by-layer across thickness and recalculated by imposing the continuity of transverse shear stresses, of transverse normal stress and its gradient at each interface. As a consequence, a periodic change of slope at each interface is not imposed, differently to kinematic-based models and, similarly to ZZA, redefinition of coefficients allows ZZM to adapt itself to variation of solution.

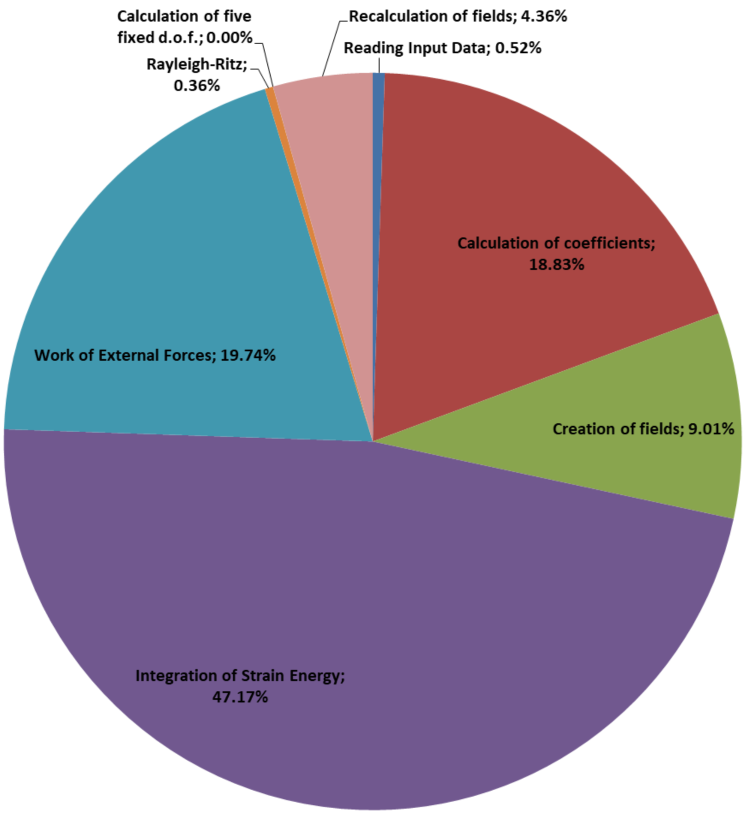

Figure 3.2: Detailed description of computational effort of ZZM

Surprisingly, results provided by this theory are indistinguishable to ZZA ones. So, the conclusion is that the choice of zig-zag functions is immaterial for this type of theories (physically-based adaptive). Indeed, they can be substituted with other functions (e.g. Murakami's one) without any loss of accuracy, provided that coefficients are redefined layer-by-layer across the thickness and calculated by imposing the full-set of physical constraints (1.15)-(1.20). On the contrary, if these latter conditions are not fully satisfied, accuracy of models heavily depends by assumptions, consistently with results previously obtained by MHR and MHR4. Moreover, ZZM has a cost saving at least of 25% than ZZA and HWZZ, thanks to more simple expressions of layerwise functions (which also don't contain any summations) that decrease computational effort of strain energy integration (Figure 3.2). Similarly to previous section, Table 3.1 reports only a qualitative description of ZZM, while its specific features and expression of displacement, strain and stress fields are in section 3.1.3.

ZZM

- Displacement-based, physically-based zig-zag theory;
- Piecewise in-plane displacements $u_\alpha^{(3)}$ (redefined coefficients);
- Piecewise transverse displacement $u_\varsigma^{(4)}$ (redefined coefficients);
- Same displacement field of ZZA but different zig-zag functions are assumed.
- Murakami's zig-zag function and M2ZZ one are included in displacement field.

PROS	CONS
Results always indistinguishable to ZZA ones. Cost saving is betond 25%.	Its expression could be more simplified.

$^{(n)}$ indicates the order of expansion of in-plane and transverse displacements

Table 3.1: Characteristic features of ZZM theory.

3.1.2 Theories with redefined coefficients without zig-zag functions

Since adaptive theories redefine coefficients across the thickness, the fulfilment of interfacial stress compatibility conditions (1.19) could be achieved by calculating some coefficients through them, also without the use of zigzag functions. Because this implies a greater efficiency, it is interesting to verify this hypothesis. So, another physically-based theory, called ZZA* [17] is developed, whose displacement field is the same of ZZA but Di Sciuvsa's and Icardi's layerwise functions are omitted and substituted with power series of transverse coordinate (ς and ς^2). So, this theory does not contain any zig-zag function but similarly to parent theory ZZA coefficients are redefined for each layer across the thickness and obtained by imposing (1.15)-(1.20). Again, results obtained are indistinguishable to ZZA and ZZM ones, confirming that the choice of zig-zag functions is immaterial and they can freely omitted or changed for adaptive theories, without any loss of accuracy, as coefficients are redefined across the thickness and all physical constraints are enforced. Computational burden obtained by this theory is similar to that of ZZM and lower to ZZA one, thanks to the simpler expression of zig-zag function.

ZZA*	• Displacement-based, physically-based zig-zag theory; • Piecewise in-plane displacements $u_{\alpha}^{(3)}$ (redefined coefficients); • Piecewise transverse displacement $u_{\varsigma}^{(4)}$ (redefined coefficients); • Same displacement field of ZZA but power series are used instead of zig-zag functions • Zig-zag functions are omitted.	
	PROS	**CONS**
	Results always indistinguishable to ZZA ones. Cost saving is beyond 25%.	Its expression could be more simplified.

$^{(n)}$ indicates the order of expansion of in-plane and transverse displacements

Table 3.2: Characteristic features of ZZA* theory.

It should be noticed that HW mixed formulations of ZZM and ZZA* can be obtained, following exactly the same steps previously described in section 2.4 for HWZZ from ZZA. These two theories, called HWZZM and HWZZM* [17] respectively obtain indistinguishable results than HWZZ and a very little cost saving than ZZM and ZZA*. Nevertheless these theories obtain very good results, their expressions are still too complex, so further studies are needed with the intended aim to create simpler and generalized variants. Figure 3.3 report genealogical tree of theories of this section:

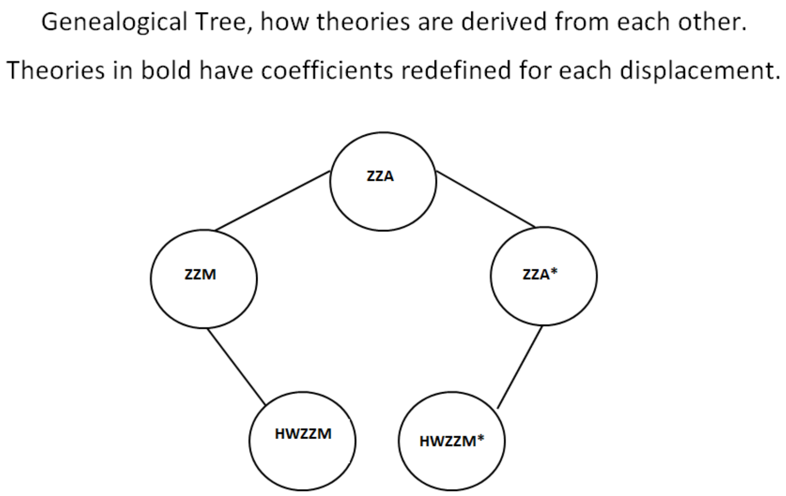

Figure 3.3: Genealogy of theories with different zig-zag functions

3.1.3 ZZM and HWZZM

ZZM is a displacement-based Di Sciuva's like adaptive theory (coefficients are recomputed for each layer); Di Sciuva's zig-zag function $(\varsigma-\varsigma_k)H_k(\varsigma)$ is substituted with Murakami's one (2.9) and second-order zig-zag function $(\varsigma-\varsigma_k)^2 H_k(\varsigma)$ is substituted with a second-order layerwise function, firstly presented in [17] and called M2ZZ in this thesis, whose expression is the following:

$$M_{2ZZ}^k(\varsigma)=\frac{(2\varsigma)^2}{\varsigma_{k+1}-\varsigma_k} \tag{3.1}$$

So, the displacement field is:

$$\begin{aligned} u_\alpha(\alpha,\beta,\varsigma)=&\left[\ u_\alpha{}^0(\alpha,\beta)+\varsigma(\Gamma_\alpha^0(\alpha,\beta)-w^0(\alpha,\beta)_{,\alpha})\ \right]_0+\left[\ C_\alpha^i(\alpha,\beta)\varsigma^2+D_\alpha^i(\alpha,\beta)\varsigma^3\ \right]_i+\\ &\left[\ A_k^{u_\alpha}(\alpha,\beta)\left[\frac{2\varsigma}{\varsigma_{k+1}-\varsigma_k}-\frac{\varsigma_{k+1}+\varsigma_k}{\varsigma_{k+1}-\varsigma_k}\ \right]+{}_\alpha C_u^k(\alpha,\beta)\right]_c\\ u_\varsigma(\alpha,\beta,\varsigma)=&\left[\ w^0(\alpha,\beta)\ \right]_0+\left[\ b^i(\alpha,\beta)\varsigma+c^i(\alpha,\beta)\varsigma^2+d^i(\alpha,\beta)\varsigma^3+e^i(\alpha,\beta)\varsigma^4\ \right]_i+\\ &\left[A_k^{u_\varsigma}(\alpha,\beta)\left[\frac{2\varsigma}{\varsigma_{k+1}-\varsigma_k}-\frac{\varsigma_{k+1}+\varsigma_k}{\varsigma_{k+1}-\varsigma_k}\right]+B_k^{u_\varsigma}(\alpha,\beta)\left[\frac{(2\varsigma)^2}{\varsigma_{k+1}-\varsigma_k}\right]+C_\varsigma^k(\alpha,\beta)\right]_c \end{aligned} \tag{3.2}$$

Nevertheless this theory contains Murakami's zig-zag function, ZZM is physically-based, because amplitudes $A_k^{u_\alpha}$, $A_k^{u_\varsigma}$ and $B_k^{u_\varsigma}$ are obtained by enforcing the continuity of transverse shear and normal stresses and of gradient of transverse normal stress at the interfaces between two layers. Terms ${}_\alpha C_u^k$ and C_ς^k are still obtained by imposing the continuity of displacements across the thickness. The remaining coefficients, C_α^i, D_α^i, b^i, c^i, d^i and e^i are obtained by enforcing the fulfilment of stress boundary conditions and of local equilibrium equations at different points across the thickness (1.18). Numerical results will show that displacements and stresses obtained by ZZM are indistinguishable from those obtained by ZZA, that incorporates different zig-zag functions. Moreover, time calculations will show that this theory is cheaper than ZZA and HWZZ, because the expression of zig-zag functions is simpler.

From this theory, a HW mixed counterpart can be obtained, following the same steps previously described in section 2.4. This theory is called HWZZM and was developed in [17]. So, master displacement field is:

$$\begin{aligned} u_\alpha(\alpha,\beta,\varsigma)=&\,u_\alpha{}^0(\alpha,\beta)+\varsigma(\Gamma_\alpha^0(\alpha,\beta)-w^0(\alpha,\beta)_{,\alpha})+C_\alpha^i(\alpha,\beta)\varsigma^2+D_\alpha^i(\alpha,\beta)\varsigma^3+\\ &+A_k^{u_\alpha}(x,y)\left[\frac{2\varsigma}{\varsigma_{k+1}-\varsigma_k}-\frac{\varsigma_{k+1}+\varsigma_k}{\varsigma_{k+1}-\varsigma_k}\ \right]\\ u_\varsigma(\alpha,\beta,\varsigma)=&\,w^0(\alpha,\beta)+b^i(\alpha,\beta)\varsigma+c^i(\alpha,\beta)\varsigma^2+d^i(\alpha,\beta)\varsigma^3+e^i(\alpha,\beta)\varsigma^4+\\ &+A_k^{u_\varsigma}(\alpha,\beta)\left[\frac{2\varsigma}{\varsigma_{k+1}-\varsigma_k}-\frac{\varsigma_{k+1}+\varsigma_k}{\varsigma_{k+1}-\varsigma_k}\right] \end{aligned} \tag{3.3}$$

Master strain field is obtained by using strain-displacement relations on the following slave displacement field:

$$u_\alpha(\alpha,\beta,\varsigma)=[\ u_\alpha{}^0(\alpha,\beta)+\varsigma(\Gamma_\alpha^0(\alpha,\beta)-w^0(\alpha,\beta)_{,\alpha})\ ]_0+[\ C_\alpha^i(\alpha,\beta)\varsigma^2+D_\alpha^i(\alpha,\beta)\varsigma^3\ ]_i+$$
$$[\ A_k^{u_\alpha}(\alpha,\beta)[\frac{2\varsigma}{\varsigma_{k+1}-\varsigma_k}-\frac{\varsigma_{k+1}+\varsigma_k}{\varsigma_{k+1}-\varsigma_k}\ ]+{}_\alpha C_u^k(\alpha,\beta)]_c \tag{3.4}$$
$$u_\varsigma(\alpha,\beta,\varsigma)=[\ w^0(\alpha,\beta)\ ]_0+[\ b^i(\alpha,\beta)\varsigma+c^i(\alpha,\beta)\varsigma^2+d^i(\alpha,\beta)\varsigma^3+e^i(\alpha,\beta)\varsigma^4\ ]_i+$$
$$[A_k^{u_\varsigma}(\alpha,\beta)[\frac{2\varsigma}{\varsigma_{k+1}-\varsigma_k}-\frac{\varsigma_{k+1}+\varsigma_k}{\varsigma_{k+1}-\varsigma_k}]+C_\varsigma^k(\alpha,\beta)]_c$$

so, ε_{ij} expressions are:

$$\begin{aligned}
&\varepsilon_{\alpha\alpha}(\alpha,\beta,\varsigma)=\breve{\tilde{U}}(\alpha,\beta,\varsigma)_{,\alpha}+A_{k,\alpha}^{u_\alpha}(\alpha,\beta)M^k(\varsigma)\\
&\varepsilon_{\beta\beta}(\alpha,\beta,\varsigma)=\breve{\tilde{V}}(\alpha,\beta,\varsigma)_{,\beta}+A_{k,\beta}^{u_\beta}(\alpha,\beta)M^k(\varsigma)\\
&\varepsilon_{\varsigma\varsigma}(\alpha,\beta,\varsigma)=\breve{\tilde{W}}(\alpha,\beta,\varsigma)_{,\varsigma}+A_k^{u_\varsigma}(\alpha,\beta)M_{,\varsigma}^k(\varsigma)\\
&\gamma_{\alpha\varsigma}(\alpha,\beta,\varsigma)=[\breve{\tilde{U}}(\alpha,\beta,\varsigma)_{,\varsigma}+A_k^{u_\alpha}(\alpha,\beta)M_{,\varsigma}^k(\varsigma)+\breve{\tilde{W}}(\alpha,\beta,\varsigma)_{,\alpha}+A_{k,\alpha}^{u_\varsigma}(\alpha,\beta)M^k(\varsigma)]\\
&\gamma_{\beta\varsigma}(\alpha,\beta,\varsigma)=[\breve{\tilde{V}}(\alpha,\beta,\varsigma)_{,\varsigma}+A_k^{u_\beta}(\alpha,\beta)M_{,\varsigma}^k(\varsigma)+\breve{\tilde{W}}(\alpha,\beta,\varsigma)_{,\beta}+A_{k,\beta}^{u_\varsigma}(\alpha,\beta)M^k(\varsigma)]\\
&\gamma_{\alpha\beta}(\alpha,\beta,\varsigma)=[\breve{\tilde{U}}(\alpha,\beta,\varsigma)_{,\beta}+A_{k,\beta}^{u_\alpha}(\alpha,\beta)M^k(\varsigma)+\breve{\tilde{V}}(\alpha,\beta,\varsigma)_{,\alpha}+A_{k,\alpha}^{u_\beta}(\alpha,\beta)M^k(\varsigma)]
\end{aligned} \tag{3.5}$$

where $\breve{\tilde{U}}$, $\breve{\tilde{V}}$ and $\breve{\tilde{W}}$ are:

$$\begin{aligned}
&\breve{\tilde{U}}(\alpha,\beta,\varsigma)=u_\alpha{}^0(\alpha,\beta)+\varsigma(\Gamma_\alpha^0(\alpha,\beta)-w^0(\alpha,\beta)_{,\alpha})+C_\alpha^i(\alpha,\beta)\varsigma^2+D_\alpha^i(\alpha,\beta)\varsigma^3+{}_\alpha C_u^i(\alpha,\beta)\\
&\breve{\tilde{V}}(\alpha,\beta,\varsigma)=u_\beta{}^0(\alpha,\beta)+\varsigma(\Gamma_\beta^0(\alpha,\beta)-w^0(\alpha,\beta)_{,\beta})+C_\beta^i(\alpha,\beta)\varsigma^2+D_\beta^i(\alpha,\beta)\varsigma^3+{}_\beta C_u^i(\alpha,\beta)\\
&\breve{\tilde{W}}(\alpha,\beta,\varsigma)=w^0(\alpha,\beta)+b^i(\alpha,\beta)\varsigma+c^i(\alpha,\beta)\varsigma^2+d^i(\alpha,\beta)\varsigma^3+e^i(\alpha,\beta)\varsigma^4+C_\varsigma^i(\alpha,\beta)
\end{aligned} \tag{3.6}$$

Finally, master in-plane stresses ($\sigma_{\alpha\alpha}$, $\sigma_{\beta\beta}$, $\sigma_{\alpha\beta}$) are obtained using stress-strain relations (1.2), while out-of-plane ones are obtained by integrating local equilibrium equations (1.18), so their expressions are the same of (2.7). Again, this theory obtains results that are indistinguishable from those of ZZA, HWZZ and ZZM and with lower processing time than latter theories (whose time calculation are still comparable to those of ESL) demonstrating that HW can be used in order to create mixed cheaper and accurate theories. Moreover, because ZZM and HWZZM obtain same results of ZZA and HWZZ, it is demonstrated that the choice of zig-zag functions is immaterial and they can be changed without any loss of accuracy, according to [17]. It should be noticed that this latter statement applies only for physically-based adaptive theories, whose coefficients are recomputed for each layer and calculated by imposing all physical constraints of ZZA (1.15)-(1.20), otherwise the accuracy is strongly dependent by this choice (as shown in the previous chapter).

3.1.4 ZZA* and HWZZM*

Another physically-based adaptive theory, called ZZA*, was previously developed in [17], in order to verify if zig-zag functions can be omitted without any loss of accuracy, since ZZM and HWZZM theories demonstrate that they can be changed obtaining the same results of ZZA and HWZZ. For this reason, contributions of first and second order zig-zag functions of ZZA are substituted with ς and ς^2, respectively. So, the displacement field is:

$$
\begin{aligned}
u_\alpha(\alpha,\beta,\varsigma) &= [\ u_\alpha{}^0(\alpha,\beta)+\varsigma(\Gamma_\alpha^0(\alpha,\beta)-w^0(\alpha,\beta)_{,\alpha})\ ]_0+\{\ \sum_{k=1}^{n_i}\ {}_k\tilde{B}_\alpha^i(\alpha,\beta)\varsigma\ + \\
&\quad +[C_\alpha^i(\alpha,\beta)\varsigma^2]+[D_\alpha^i(\alpha,\beta)\varsigma^3]+\sum_{k=1}^{n_i}\ {}_k\tilde{C}_\alpha^i(\alpha,\beta)\ \}_{i+c} \\
u_\varsigma(\alpha,\beta,\varsigma) &= [\ w^0(\alpha,\beta)\ ]_0+\{\ [b^i(\alpha,\beta)\varsigma+\sum_{k=1}^{n_i}\ {}_k\tilde{b}^i(\alpha,\beta)\varsigma]+[c^i(\alpha,\beta)\varsigma^2+ \\
&\quad +\sum_{k=1}^{n_i}\ {}_k\tilde{c}^i(\alpha,\beta)\varsigma^2]+[d^i(\alpha,\beta)\varsigma^3]+e^i(\alpha,\beta)\varsigma^4+\sum_{k=1}^{n_i}\ {}_k\tilde{d}^i(\alpha,\beta)\ \}_{i+c}
\end{aligned}
\tag{3.7}
$$

Terms ${}_k\tilde{B}_\alpha^i$, ${}_k\tilde{b}^i$ and ${}_k\tilde{c}^i$ are obtained by imposing the continuity of transverse shear and normal stresses and its gradient at the interfaces between two layers (1.19), while ${}_k\tilde{C}_\alpha^i$ and ${}_k\tilde{d}^i$ enable the fulfilment of continuity of displacements (1.20) across the thickness. The remaining coefficients, C_α^i, D_α^i, b^i, c^i, d^i and e^i are obtained by enforcing the fulfilment of stress boundary conditions and of local equilibrium equations at different points across the thickness (1.15)-(1.18). It should be noticed that terms b^i and c^i could be omitted, without any loss of accuracy, for all layers above the first one ($i>1$), slightly reducing computational burden of this theory.

Furthermore, results obtained by ZZA* are indistinguishable from those of ZZA, demonstrating that zig-zag functions can be changed (see section 3.1.1) or also omitted for higher-order zig-zag adaptive theories, without any loss of accuracy; moreover, processing time of ZZA* is lower than ZZA, ZZM, HWZZ and HWZZM. In the following section other physically-based adaptive theories will be presented in order to test the latter statements deeply.

Similarly to HWZZ and HWZZM, another adaptive mixed theory, called HWZZM*, can be obtained from ZZA*, following the same steps of section 2.4. So, master displacement field is:

$$
\begin{aligned}
u_\alpha(\alpha,\beta,\varsigma) &= [\ u_\alpha{}^0(\alpha,\beta)+\varsigma(\Gamma_\alpha^0(\alpha,\beta)-w^0(\alpha,\beta)_{,\alpha})\ ]_0+\{\ \sum_{k=1}^{n_i}\ {}_k\tilde{B}_\alpha^i(\alpha,\beta)\varsigma\ + \\
&\quad +[C_\alpha^i(\alpha,\beta)\varsigma^2]+[D_\alpha^i(x,y)\varsigma^3]\ \}_{i+c} \\
u_\varsigma(\alpha,\beta,\varsigma) &= [\ w^0(\alpha,\beta)\ ]_0+\{\ [b^i(\alpha,\beta)\varsigma+\sum_{k=1}^{n_i}\ {}_k\tilde{b}^i(\alpha,\beta)\varsigma]+[c^i(\alpha,\beta)\varsigma^2]+ \\
&\quad +[d^i(\alpha,\beta)\varsigma^3]+e^i(\alpha,\beta)\varsigma^4\ \}_{i+c}
\end{aligned}
\tag{3.8}
$$

Master strain field is obtained by the following slave displacement field:

$$
\begin{aligned}
u_\alpha(\alpha,\beta,\varsigma) &= [\ u_\alpha{}^0(\alpha,\beta)+\varsigma(\Gamma_\alpha^0(\alpha,\beta)-w^0(\alpha,\beta)_{,\alpha})\ ]_0+\{\ \sum_{k=1}^{n_i}\ {}_k\tilde{B}_\alpha^i(\alpha,\beta)\varsigma\ + \\
&\quad +[C_\alpha^i(\alpha,\beta)\varsigma^2]+[D_\alpha^i(\alpha,\beta)\varsigma^3]+\sum_{k=1}^{n_i}\ {}_k\tilde{C}_\alpha^i(\alpha,\beta)\ \}_{i+c} \\
u_\varsigma(\alpha,\beta,\varsigma) &= [\ w^0(\alpha,\beta)\ ]_0+\{\ [b^i(\alpha,\beta)\varsigma+\sum_{k=1}^{n_i}\ {}_k\tilde{b}^i(\alpha,\beta)\varsigma]+[c^i(\alpha,\beta)\varsigma^2]+ \\
&\quad +[d^i(\alpha,\beta)\varsigma^3]+e^i(\alpha,\beta)\varsigma^4+\sum_{k=1}^{n_i}\ {}_k\tilde{d}^i(\alpha,\beta)\ \}_{i+c}
\end{aligned}
\tag{3.9}
$$

so, the following ε_{ij} are obtained:

$$\begin{aligned}
&\varepsilon_{\alpha\alpha}(\alpha,\beta,\varsigma)=\breve{\tilde{U}}(\alpha,\beta,\varsigma)_{,\alpha}+\sum_{k=1}^{n_i}{}_k\tilde{B}^i_{\alpha,\alpha}(\alpha,\beta)\varsigma\\
&\varepsilon_{\beta\beta}(\alpha,\beta,\varsigma)=\breve{\tilde{V}}(\alpha,\beta,\varsigma)_{,\beta}+\sum_{k=1}^{n_i}{}_k\tilde{B}^i_{\beta,\beta}(\alpha,\beta)\varsigma\\
&\varepsilon_{\varsigma\varsigma}(\alpha,\beta,\varsigma)=\breve{\tilde{W}}(\alpha,\beta,\varsigma)_{,\varsigma}+\sum_{k=1}^{n_i}{}_k\tilde{b}^i(\alpha,\beta)\\
&\gamma_{\alpha\varsigma}(\alpha,\beta,\varsigma)=[\breve{\tilde{U}}(\alpha,\beta,\varsigma)_{,\varsigma}+\sum_{k=1}^{n_i}{}_k\tilde{B}^i_{\alpha}(\alpha,\beta)+\breve{\tilde{W}}(\alpha,\beta,\varsigma)_{,\alpha}+\sum_{k=1}^{n_i}{}_k\tilde{b}^i_{,\alpha}(\alpha,\beta)\varsigma]\\
&\gamma_{\beta\varsigma}(\alpha,\beta,\varsigma)=[\breve{\tilde{V}}(\alpha,\beta,\varsigma)_{,\varsigma}+\sum_{k=1}^{n_i}{}_k\tilde{B}^i_{\beta}(\alpha,\beta)+\breve{\tilde{W}}(\alpha,\beta,\varsigma)_{,\beta}+\sum_{k=1}^{n_i}{}_k\tilde{b}^i_{,\beta}(\alpha,\beta)\varsigma]\\
&\gamma_{\alpha\beta}(\alpha,\beta,\varsigma)=[\breve{\tilde{U}}(\alpha,\beta,\varsigma)_{,\beta}+\sum_{k=1}^{n_i}{}_k\tilde{B}^i_{\alpha,\beta}(\alpha,\beta)\varsigma+\breve{\tilde{V}}(\alpha,\beta,\varsigma)_{,\alpha}+\sum_{k=1}^{n_i}{}_k\tilde{B}^i_{\beta,\alpha}(\alpha,\beta)\varsigma]
\end{aligned} \tag{3.10}$$

where $\breve{\tilde{U}}$, $\breve{\tilde{V}}$ and $\breve{\tilde{W}}$ are:

$$\begin{aligned}
&\breve{\tilde{U}}(\alpha,\beta,\varsigma)=u_\alpha{}^0(\alpha,\beta)+\varsigma(\Gamma^0_\alpha(\alpha,\beta)-w^0(\alpha,\beta)_{,\alpha})+C^i_\alpha(\alpha,\beta)\varsigma^2+D^i_\alpha(\alpha,\beta)\varsigma^3+{}_\alpha C^i_u(\alpha,\beta)\\
&\breve{\tilde{V}}(\alpha,\beta,\varsigma)=u_\beta{}^0(\alpha,\beta)+\varsigma(\Gamma^0_\beta(\alpha,\beta)-w^0(\alpha,\beta)_{,\beta})+C^i_\beta(\alpha,\beta)\varsigma^2+D^i_\beta(\alpha,\beta)\varsigma^3+{}_\beta C^i_u(\alpha,\beta)\\
&\breve{\tilde{W}}(\alpha,\beta,\varsigma)=w^0(\alpha,\beta)+b^i(\alpha,\beta)\varsigma+c^i(\alpha,\beta)\varsigma^2+d^i(\alpha,\beta)\varsigma^3+e^i(\alpha,\beta)\varsigma^4+C^i_\varsigma(\alpha,\beta)
\end{aligned} \tag{3.11}$$

Finally, master in-plane stresses ($\sigma_{\alpha\alpha}$, $\sigma_{\beta\beta}$, $\sigma_{\alpha\beta}$) are obtained using stress-strain relations (1.2), while out-of-plane ones are calculated by integrating local equilibrium equations (1.18), so their expressions are the same of (2.7). Once again, this theory obtains the same results of ZZA, ZZM, ZZA*, HWZZ and HWZZM with lower processing time.

3.2 Choice of number of equilibrium points

As ZZA* and ZZM theories calculate indistinguishable results from ZZA (also with lower computational burden), it was concluded that the choice of zig-zag functions is immaterial and that such functions can be changed or omitted without any loss of accuracy. These statements are valid only if coefficients are redefined for each layer across the thickness and calculated by imposing the full set of physical constraints of ZZA (1.15)-(1.20):

- boundary conditions on out-of-plane stresses;
- continuity of displacements, of transverse shear, transverse normal stresses and its gradient across the thickness;
- fulfillment of local equilibrium equations at different points across the thickness.

About the latter conditions, at least one equilibrium point (three equations) are needed for the outer layers and at least two of them (six equations) for the inner ones to obtain maximal accuracy. More equilibrium equations could be imposed, including additional higher-order terms into displacement field, but this technique won't be used in numerical applications.

With the intended aim to determine the minimum number of equilibrium points necessary to obtain maximal accuracy, three different theories are developed as refined variants of HSDT. These three models, called HSDT_32, HSDT_33 and HSDT_34, are three physically-based zig-zag adaptive theories, whose coefficients are redefined layer-by-layer across the thickness. Similarly to ZZA* zig-zag functions are omitted and substituted with power of thickness coordinate ς of first and second order, but also summations (that were still included in ZZA*) are omitted. Coefficients of HSDT_32, HSDT_33 and HSDT_34 are calculated by imposing boundary conditions (1.15)-(1.17) and continuity of out-of-plane stresses (1.19), but the number of equilibrium points that is imposed is different for each theory.

All these theories are displacement-based, so, strains and stresses are calculated by constitutive equations and $\sigma_{\alpha\varsigma}$, $\sigma_{\beta\varsigma}$ and $\sigma_{\varsigma\varsigma}$ are eventually post-processed by integrating local equilibrium equations to increase their accuracy. A brief description of these theories is reported in the following section.

3.2.1 Equilibrium points for lower-order theories

HSDT_32 has piecewise cubic in-plane displacements and a piecewise parabolic transverse one, so, only three equilibrium equations are needed for a three-layers beam. Results of this theory are very inaccurate, also when there are mild layerwise effects, especially for dynamic calculations, because its kinematics is too simple. For this reason, results provided by HSDT_32 will not be reported for the most challenging cases. Bad findings of this theory confirm that a model, whose kinematics is too simple, cannot work properly, unless a mixed formulation is adopted and stresses are assumed apart from displacements. Moreover, it is confirmed that if the full set of physical constraints of ZZA is not imposed, like for HSDT_32, there is a loss of accuracy, regardless coefficients are redefined or not.

HSDT_32

- Displacement-based, physically-based zig-zag theory;
- Piecewise in-plane displacements $u_\alpha^{(3)}$ (redefined coefficients);
- Piecewise parabolic transverse displacement $u_\varsigma^{(2)}$ (redefined coefficients);
- Zig-zag functions are omitted.

PROS	CONS
Processing time lower than ZZA one,	Very inaccurate results also for mid layerwise effects. Very inaccurate results for dynamic case

Table 3.3: Characteristic features of HSDT_32 theory.

HSDT_33 theory, instead, have both in-plane and transverse displacements piecewise cubic, so, five equilibrium equations are needed for a three-layers beam. As a consequence, a greater accuracy than HSDT_32 is obtained. HSDT_33 provides quite precise results also if there are fairly strong layerwise effects, anyway, accuracy of ZZA, ZZA* and ZZM cannot be reached because the full set of physical constraints of ZZA is not imposed.

HSDT_33

- Displacement-based, physically-based zig-zag theory;
- Piecewise in-plane displacements $u_\alpha^{(3)}$ (redefined coefficients);
- Piecewise cubic transverse displacement $u_\varsigma^{(3)}$ (redefined coefficients);
- Zig-zag functions are omitted.

PROS	CONS
Processing time lower than ZZA one; Better results than HSDT_32; Good accuracy also for quite strong layerwise effects	Accuracy is slightly lower than ZZA one.

Table 3.4: Characteristic features of HSDT_33 theory.

3.2.2 Minimum number of required equilibrium points

Finally, HSDT_34 theory is developed, whose transverse displacement is a fourth-order piecewise polynomial across the thickness. Expansion order is the same of ZZA and the same number of equilibrium equations is imposed. Results demonstrate previous findings: this theory, whose coefficients are redefined layer-by-layer across the thickness and calculated by imposing the full set of physical constraints of ZZA (thus also the same number of equilibrium points) obtains indistinguishable results than ZZA (and other higher-order theories obtained from it), irrespective of zig-zag assumed, which can be also omitted (along with their summations) without any loss of accuracy.

HSDT_34

- Displacement-based, physically-based zig-zag theory;
- Piecewise in-plane displacements $u_\alpha^{(3)}$ (redefined coefficients);
- Piecewise fourth-order transverse displacement $u_\varsigma^{(4)}$ (redefined coefficients);
- Zig-zag functions are omitted.

PROS	CONS
Processing time lower than ZZA one; Better results than HSDT_32 and HSDT_33; Indistinguishable results than ZZA, ZZM, ZZA* and mixed theories obtained from them.	Its expression could be more simplified.

Table 3.5: Characteristic features of HSDT_34 theory.

Results obtained by HSDT_32, HSDT_33 and HSDT_34, demonstrate that at least a piecewise cubic and a piecewise fourth-order polynomial expansion order are required to get accurate results.

3.2.3 HSDT_32, HSDT_33, HSDT_34 theories

Three physically-based adaptive theories are developed, which do not contain any zig-zag function, being their choice immaterial if coefficients are redefined for each layer across the thickness (according to section 3.1.2) and calculated on a physical basis by imposing (1.15)-(1.20). Three different expansion orders are chosen for these theories, which assume piecewise cubic in-plane displacements and a piecewise parabolic, cubic and fourth-order polynomial transverse one, with the intended aim to understand which is the minimum number of equilibrium equations needed to obtain accurate results. Being displacement-based models, strains and stresses of these theories are obtained by constitutive equations.

Regarding HSDT_32, it has piecewise cubic in-plane displacements and a piecewise parabolic transverse one:

$$\begin{aligned} u_\alpha(\alpha,\beta,\varsigma) &= [u^0(\alpha,\beta)+\varsigma(\Gamma_\alpha^0(\alpha,\beta)-w^0(\alpha,\beta)_{,\alpha})]_0 + B_\alpha^i(\alpha,\beta)\varsigma + C_\alpha^i(\alpha,\beta)\varsigma^2 + \\ &\quad + D_\alpha^i(\alpha,\beta)\varsigma^3 + A_\alpha^i(\alpha,\beta) \\ u_\varsigma(\alpha,\beta,\varsigma) &= [w^0(\alpha,\beta)]_0 + b^i(\alpha,\beta)\varsigma + c^i(\alpha,\beta)\varsigma^2 + a^i(\alpha,\beta) \end{aligned} \tag{3.12}$$

$B_\alpha^{i=1}$, $A_\alpha^{i=1}$ and $a^{i=1}$ are assumed null for the first layer from below. A_α^i and a^i are calculated by imposing the continuity of displacements (1.20), while B_α^i, C_α^i, D_α^i, b^i and c^i enable the fulfilment of (1.15)-(1.17), (1.19) and of local equilibrium equation (1.18). For this theory, only three equilibrium equations are needed for a three-layers beam. Because its kinematics is too poor, very inaccurate results are obtained, especially for dynamic calculations. So, it is confirmed that a model cannot work properly if its kinematics is too simple, unless a mixed formulation (with stresses apart from displacements) is adopted. Moreover, it is reiterated that if the full set of physical constraints of ZZA is not imposed, inaccurate results could be predicted.

Instead, a cubic piecewise transverse displacement is assumed for HSDT_33:

$$u_\alpha(\alpha,\beta,\varsigma)=[u^0(\alpha,\beta)+\varsigma(\Gamma^0_\alpha(\alpha,\beta)-w^0(\alpha,\beta)_{,\alpha})]_0+B^i_\alpha(\alpha,\beta)\varsigma+C^i_\alpha(\alpha,\beta)\varsigma^2+ \\ +D^i_\alpha(\alpha,\beta)\varsigma^3+A^i_\alpha(\alpha,\beta) \\ u_\varsigma(\alpha,\beta,\varsigma)=[w^0(\alpha,\beta)]_0+b^i(\alpha,\beta)\varsigma+c^i(\alpha,\beta)\varsigma^2+d^i(\alpha,\beta)\varsigma^3+a^i(\alpha,\beta) \tag{3.13}$$

Similarly to HSDT_32, A^i_α and a^i are calculated by imposing (1.20), while B^i_α, C^i_α, D^i_α, b^i and c^i by imposing (1.15)-(1.17),(1.19) and (1.18). For this theory, five equilibrium equations are needed for a three-layers beam. HSDT_33 is more accurate than HSDT_32, thanks to its more complex displacement field. As a consequence, this theory can also give good prediction also for laminations with quite strong layerwise effects, but the precision of ZZA cannot be obtained, because the full set of physical constraints of ZZA is not imposed. Newly, $B^{i=1}_\alpha$, $A^{i=1}_\alpha$ and $a^{i=1}$ are assumed null for the first layer from below.

Regarding HSDT_34, a piecewise fourth-order polynomial transverse displacement is assumed:

$$u_\alpha(\alpha,\beta,\varsigma)=[u^0(\alpha,\beta)+\varsigma(\Gamma^0_\alpha(\alpha,\beta)-w^0(\alpha,\beta)_{,\alpha})]_0+B^i_\alpha(\alpha,\beta)\varsigma+C^i_\alpha(\alpha,\beta)\varsigma^2+ \\ +D^i_\alpha(\alpha,\beta)\varsigma^3+A^i_\alpha(\alpha,\beta) \\ u_\varsigma(\alpha,\beta,\varsigma)=[w^0(\alpha,\beta)]_0+b^i(\alpha,\beta)\varsigma+c^i(\alpha,\beta)\varsigma^2+d^i(\alpha,\beta)\varsigma^3+e^i(\alpha,\beta)\varsigma^3+a^i(\alpha,\beta) \tag{3.14}$$

Again, $B^{i=1}_\alpha$, $A^{i=1}_\alpha$ and $a^{i=1}$ are null for the first layer from below, A^i_α and a^i are obtained by imposing (1.20), while B^i_α, C^i_α, D^i_α, b^i, c^i and d^i by imposing (1.15)-(1.17), (1.19) and (1.18). Because of expansion order is the same of ZZA and the same number of equilibrium points is assumed, the full set of physical constraints of ZZA (1.15)-(1.20) is imposed. As a consequence, the same results of ZZA are provided by HSDT_34, demonstrating that zig-zag functions can be changed or omitted without any loss of accuracy.

Summarizing, results of this section demonstrate that at least the same number of conditions of ZZA have to be imposed to get the maximal accuracy. In the next section, two other aspects about the role of coefficients and the representation of displacements across the thickness are deeply explored, in order to simplify and generalize ZZA.

3.3 Theories with no prefixed role of coefficients

Coefficients of ZZA and other theories obtained from it (ZZM, ZZA*, HWZZ, HWZZM, HWZZM*) are calculated by imposing the full set of physical constraints (1.15)-(1.20). Each coefficient of displacement field has a fixed role, as deeply explained in section 1.6. For example, zig-zag amplitudes Φ^k_α, Ψ^k, Ω^k that multiply Di Sciuva's and Icardi's zig-zag functions (1.14g), are calculated by imposing the continuity of transverse shear stresses, transverse normal one and its gradient at the interfaces. Instead, higher-order coefficients C^i_α, D^i_α, b^i, c^i, d^i, and e^i impose the fulfillment of boundary conditions and equilibrium equations (section 1.6). Anyway, more investigations are necessary, with the intended aim to understand if the role of coefficients can be changed or not.

So, ZZA_RDF [19] is developed, whose coefficients assume different roles respect to ZZA. E.g., Φ_{α}^{k} are calculated by imposing the fulfilment of first equilibrium equation, while C_{α}^{i} impose the continuity of transverse shear stresses. Results obtained by ZZA and ZZA_RDF are indistinguishable from each other, demonstrating that role of coefficients can be freely exchanged, so it is not necessary to assign them in advance, as long as coefficients are redefined layer-by-layer across the thickness and calculated by imposing the full set of physical constraints. A detailed description of this theory can be found in following section, along with reference frame adopted to prevent numerical errors. The same identical features of ZZA still apply also for ZZA_RDF. In a similar way, HWZZ_RDF can be obtained, assigning different roles to coefficients of HWZZ.

ZZA_RDF	
	• Displacement-based, physically-based zig-zag theory; • Piecewise in-plane displacements $u_{\alpha}^{(3)}$ (redefined coefficients); • Piecewise fourth-order transverse displacement $u_{\varsigma}^{(4)}$ (redefined coefficients); • Role of coefficients is switched than ZZA.
	PROS: Same results and features than ZZA. — **CONS**: Same cons of ZZA still apply.

Table 3.6: Characteristic features of ZZA_RDF theory.

3.3.1 ZZA_RDF theory

This theory is developed in order to test the effect of switch the role of coefficients. For example, Φ_{α}^{k}, Ψ^{k}, Ω^{k} of ZZA theory are calculated by imposing (1.19), while C_{α}^{i}, D_{α}^{i}, b^{i}, c^{i}, d^{i}, and e^{i} enforce the fulfilment of (1.15)-(1.18). Regarding ZZA_RDF, the displacement field is the same of ZZA (1.14g), but role of coefficients is different than the parent theory: Φ_{α}^{k} enable the fulfilment of first equilibrium equation, while C_{α}^{i} impose the continuity of transverse shear stresses. Because of results obtained by ZZA_RDF and ZZA are the same, it is demonstrated that the role of coefficients can be exchanged, without any loss of accuracy, if coefficients are redefined for each layer and the full set of physical constraints is imposed. Anyway, it should be noticed that for some lay-ups one interface can coincide with middle reference plane (thickness coordinate is ς=0) and apparently not any term could be used to impose the continuity conditions. For example, coefficients c^{i}, that multiply ς^{2} within transverse shear stress expression, doesn't seem able to impose its continuity if $\varsigma_k = 0$, because their product vanish for $\varsigma = \varsigma_k$. Anyway, this issue can be solved by assuming a difference reference frame than ZZA, whose distance is $h_d > h / 2$ from the bottom face:

$$
\begin{aligned}
u_\alpha(\alpha,\beta,\varsigma) &= [u_\alpha{}^0(\alpha,\beta) + (\varsigma - h_d + h/2)(\Gamma_\alpha^0(\alpha,\beta) - w^0(\alpha,\beta)_{,\alpha})]_0 + \\
&+ [C_\alpha^i(\alpha,\beta)\varsigma^2 + D_\alpha^i(\alpha,\beta)\varsigma^3]_i + [\sum_{k=1}^{n_i} \Phi_\alpha^k(\alpha,\beta)(\varsigma - \varsigma_k)H_k(\varsigma) + \sum_{k=1}^{n_\Im} {}_\alpha C_u^k(\alpha,\beta)H_k(\varsigma)]_c \\
u_\varsigma(\alpha,\beta,\varsigma) &= [w^0(\alpha,\beta)]_0 + [b^i(\alpha,\beta)\varsigma + c^i(\alpha,\beta)\varsigma^2 + d^i(\alpha,\beta)\varsigma^3 + e^i(\alpha,\beta)\varsigma^4]_i + \\
&+ [\sum_{k=1}^{n_i} \Psi^k(\alpha,\beta)(\varsigma - \varsigma_k)H_k(z) + \sum_{k=1}^{n_i} \Omega^k(\alpha,\beta)(\varsigma - \varsigma_k)^2 H_k(z) + \sum_{k=1}^{n_\Im} C_\varsigma^k(\alpha,\beta)H_k(\varsigma)]_c \\
&(h_d \le \varsigma \le h_d + h)
\end{aligned}
\tag{3.15}
$$

Because of the same results are obtained, results confirm that role of coefficients can be changed and a different reference frame can be assumed, without any loss of accuracy, if the full set of physical constraints is imposed and coefficients are redefined for each layer across the thickness. Moreover, a mixed HW version of this theory can be obtained, called HWZZ_RDF, assuming the same simplifications of section 2.4. the same results of HWZZ are obtained by HWZZ_RDF.

3.4 Effects of the choice of global representation functions

Before proceeding with generalization of ZZA, it is necessary to study the effects to assume different functions to represent variation of displacements across the thickness for physically-based adaptive theories. A deeply study about this topic was faced by Mantari et al. [79], where trigonometric, exponential and hyperbolic functions were used to represent variation of displacements across the thickness of theories obtained like particularization of CUF. Results of theories demonstrate a strong dependence from the chosen representation and that only a sinusoidal representation allow to get an accuracy similar to polynomial one.

With the intended aim to investigate if this dependence still exists also for adaptive physically-based zig-zag theories, ZZA**** was developed [16], whose qualitative description is here reported, while details, fields and characteristic features are described in following section. In-plane displacements contain a sinusoidal representation across the thickness, while a combination of sinusoidal, exponential and power of thickness coordinate ς is assumed for transverse displacement. Obviously, terms are redefined layer-by-layer across the thickness and all physical constraints of ZZA are imposed and zig-zag functions are omitted. Results obtained by this theory are surprisingly very close to ZZA ones (difference between them is lower than 0.1%), demonstrating that for physically-based adaptive theories, also functions that describe the representation of displacements across the thickness can be changed without any loss of accuracy. Obviously, the representation function chosen must be able to describe for each layer a cubic and a fourth-order polynomial for in-plane and transverse displacements respectively. Processing time of ZZA**** is similar to those of ZZA* and ZZM, resulting more efficient than parent theory ZZA.

ZZA****	
	• Displacement-based, physically-based zig-zag theory; • Piecewise in-plane displacements $u_\alpha^{(3)}$ with sinusoidal representation (redefined coefficients); • Piecewise transverse displacement $u_\varsigma^{(4)}$, where a combination of sinusoidal, exponential and power functions represent variation across the thickness (redefined coefficients);

PROS	CONS
Results very close to ZZA; High accuracy, also for strong layerwise effects; Very good processing time, lower than those of ZZA.	Its expression could be more simplified and generalized.

Table 3.7: Characteristic features of ZZA_RDF theory.

3.4.1 ZZA**** theory

ZZA**** displacement-based zig-zag theory was created in [16] with the purpose to investigate the effect of choice of functions used to describe transverse representation of displacements. This theory contains the same zig-zag functions of ZZA but different global functions than power series are used to represent variations of displacement across the thickness. So, the displacement field is:

$$
\begin{aligned}
u_\alpha(\alpha,\beta,\varsigma) &= [\; u_\alpha{}^0(\alpha,\beta)+\varsigma(\Gamma_\alpha^0(\alpha,\beta)-w^0(\alpha,\beta)_{,\alpha}) \;]_0 + [\; C_\alpha^i(\alpha,\beta)\cos(\varsigma/h)+D_\alpha^i(\alpha,\beta)\sin(\varsigma/h) \;]_i + \\
&\quad [\; \sum_{k=1}^{n_i}\Phi_\alpha^k(\alpha,\beta)(\varsigma-\varsigma_k)H_k(\varsigma)+\sum_{j=1}^{n_\Im}{}_\alpha C_u^j(\alpha,\beta)H_j(\varsigma) \;]_c \\
u_\varsigma(\alpha,\beta,\varsigma) &= [\; w^0(\alpha,\beta) \;]_0 + [\; b^i(\alpha,\beta)(\varsigma/h)+c^i(\alpha,\beta)e^{(\varsigma/h)}+d^i(\alpha,\beta)\cos(\varsigma/h)+e^i(\alpha,\beta)\sin(\varsigma/h) \;]_i + \\
&\quad +[\; \sum_{k=1}^{n_i}\Psi^k(\alpha,\beta)(\varsigma-\varsigma_k)H_k(\varsigma)+\sum_{k=1}^{n_i}\Omega^k(\alpha,\beta)(\varsigma-\varsigma_k)^2H_k(\varsigma)+\sum_{j=1}^{n_\Im}C_\varsigma^j(\alpha,\beta)H_j(\varsigma) \;]_c
\end{aligned}
\tag{3.16}
$$

Coefficients are calculated similarly to ZZA, so, Φ_α^i , Ψ^k, Ω^k, ${}_\alpha C_u^i$ and C_ς^j impose the continuity of out-of-plane stresses and displacements at layer interfaces, while the remaining terms, C_α^i, D_α^i, b^i, c^i, d^i and e^i are obtained by enforcing the fulfilment of stress boundary conditions at outer layers and of local equilibrium equations at different points across the thickness (1.18). It should be noticed that any other role can be assigned to coefficients, according to results of section 3.3.

Numerical results of this theory are practically the same of ZZA (differences lower than 0.1%) and other higher-order adaptive theories; so, it is again demonstrated that for theories with these features, not only zig-zag functions can be changed or omitted, but also global functions, that are used to represent variation of displacements across the thickness can be assumed differently, without any loss of accuracy. In next two sections, different theories, called ZZA_X, are presented as generalizations of ZZA, based on findings described in previous sections.

3.5 Generalization of physically-based zig-zag theories

In this section, DZZ theories with a high degree of generalization are developed on the basis of the previous results. Results obtained by theories from 3.1 to 3.4 affirm that if coefficients are redefined for each layer across the thickness and all physical constraints are imposed:

- Choice of zig-zag function is immaterial, they can be changed or omitted without any loss of accuracy;
- Functions that are used to describe the representation of displacements across the thickness can be changed, without any loss of accuracy (they only must be able to describe for each layer a cubic and a fourth-order polynomial for in-plane and transverse displacements, respectively). So, exponential, sinusoidal or polynomial representations can be assumed (also a combination of them).
- There is no need to assign a specific role to coefficients;

On the contrary, accuracy of theories is strongly dependent on zig-zag and representation functions if terms are not redefined for each layer or the full set of physical constraints is not satisfied. So, new generalized version of ZZA can be developed.

3.5.1 ZZA_X theory

Thanks to previous results a new physically-based zig-zag theory is developed, that is a refined and generalized version of ZZA, called ZZA_X. As a consequence, ZZA and all other theories previously described can be obtained as its particularizations (section 3.5.2 reports a deeply description of displacements fields and other characteristic features of this theory). Displacement field is expressed as a truncated series of products of unknown coefficients and a set of functions of thickness coordinate. These functions have to be linearly independent and their combination must be able to represent at least a cubic and a fourth-order polynomial for in-plane and transverse displacements, respectively. So, exponential, sinusoidal and power series functions or their combination can be assumed. The number of terms can be chosen by user for each displacement (at least three terms are necessary for in-plane and four for transverse one, accordingly to sections 3.2 and 3.2.2).

The distinctive feature of ZZA_X is the possibility to choose a different representation not only for each displacements, but also differently for any region across the thickness (e.g. using a sinusoidal representation for some layers and a polynomial one for the others, see section 3.5.2 for details). So, user can choose an appropriate and proper representation for each region of each displacements and choose the more suited functions depending on the problem, with the intended aim to ensure the maximal efficiency, because these decisions can provide numerical advantages. For these reasons, the level of generalization of ZZA_X is very high and it is able to compete with more famous and used examples in Literature, such as [14]. Moreover, processing time of this theory is very low (using the same order of expansion of ZZA), demonstrating also a high degree of efficiency, because the number of unknown d.o.f. is not increased compared to the parent theory. Different expansion orders (thus a different number of terms) could be assumed, but a higher number of terms is unnecessary and a lower one can cause loss of accuracy for challenging benchmarks.

Nevertheless this theory offers a high degree of generalization, it still contains the same linear contribution of FSDT. So, another general model is created in section 3.5.3, where this latter limiting assumption is omitted, with the intended aim to test if it is important to get accurate results.

ZZA_X	• Displacement-based, physically-based zig-zag theory; • Piecewise in-plane displacements $u_{\alpha}^{(3)}$ (redefined coefficients); • Piecewise transverse displacement $u_{\varsigma}^{(4)}$ (redefined coefficients); • The number of terms for each displacements can be chosen by user as an input; • The functions that are used for representation can be freely chosen; • Different representations can be assumed for each displacements and for each region across then thickness	
	PROS	**CONS**
	Generalized and refined version of ZZA; All theories of previous sections can be obtained from ZZA_X as particularizations; If the same number of terms of ZZA is chosen, similar results are always achieved; Very low processing time (high efficiency).	It still contains linear contribution by FSDT. Bounded only by the limits of the imagination.

$^{(n)}$ indicates the order of expansion of in-plane and transverse displacements

Table 3.8: Characteristic features of ZZA_X theory.

3.5.2 Displacement field of ZZA_X

This theory was developed in [18], with the intended aim to create a generalized version of ZZA. This theory is adaptive, so, its coefficients are redefined for each layer across the thickness. Moreover, it does not contain any layerwise function and a general representation of variables is assumed across the thickness. Thus, the displacement field is expressed as a truncated series of products of general functions of ς, indicated as $F^{\alpha}{}_{k}$ and G_k, which must be linearly independent, and unknown amplitudes:

$$
\begin{aligned}
&u_{\alpha}(\alpha,\beta,\varsigma)=[\ u_{\alpha}{}^{0}(\alpha,\beta)+\varsigma(\Gamma_{\alpha}^{0}(\alpha,\beta)-w^{0}(\alpha,\beta)_{,\alpha})\ ]_{0}+[\ \sum_{k=1}^{n_{\alpha}}C_{k\_\alpha}^{i}(\alpha,\beta)\ {}^{i}F^{\alpha}{}_{k}(\varsigma)\ +C_{\alpha}^{i}(\alpha,\beta)\ ]_{i+c}\\
&u_{\varsigma}(\alpha,\beta,\varsigma)=[\ w^{0}(\alpha,\beta)\ ]_{0}+[\ \sum_{k=1}^{n_{\varsigma}}D_{k}^{i}(\alpha,\beta)\ {}^{i}G_{k}(\varsigma)\ +C_{\varsigma}^{i}(\alpha,\beta)\ ]_{i+c}\\
&C_{1-\alpha}^{i=1}=C_{\alpha}^{i=1}=C_{\varsigma}^{i=1}=0
\end{aligned}
\tag{3.17}
$$

It should be noticed that this theory is still zig-zag adaptive, like ZZA and other theories of this chapter. $[...]_0$ is the same of FSDT and contains the same d.o.f. (middle plane displacements $u_{\alpha}{}^{0}$, w^0 and shear rotations Γ_{α}^{0}, see section 1.7 and (1.21)). Superscript i indicates the layer, while the superscript k indicates the k-th term of summation. So, n_{α} and n_{ς} represent the number of components of transverse representation of in-plane and transverse displacements respectively, which are chosen as an input by user; it should be noticed that they coincide with the degree of polynomial if power series ς^k are assumed. If $n_{\alpha}=3$ and $n_{\varsigma}=4$ the same number of conditions of ZZA can be imposed, so, indistinguishable results are obtained, irrespective the chosen functions for ${}^{i}F^{\alpha}{}_{k}$ and ${}^{i}G_k$.

Unknown amplitudes $C_{k-\alpha}^{i}$ and D_k^i are obtained by enforcing the fulfilment of stress boundary conditions, of local equilibrium equations at different points across the thickness and of continuity of out-of-plane stresses and of the gradient of transverse normal stress at the interfaces between two layers (1.15)-(1.19). Finally, coefficients C_{α}^{i} and C_{ζ}^{i} enable the continuity of displacements (1.20). A specific role is not assigned to any coefficients, because it is demonstrated that it is not necessary (see section 3.3). So, all physical constraints are enforced in strong form and an algebraic system is obtained, whose solutions are explicit expressions of $C_{k-\alpha}^{i}$, D_k^i, C_{α}^{i}, C_{ζ}^{i}. Use of this theory is very advantageous, because it allows to test different functions to represent global transverse variation of quantities. Furthermore, it is also possible to assume different representations for each variables and from region to region across the thickness. Moreover, time calculation decreases, because computational time for integration of strain energy is lower.

As previously explained, to be comparable to ZZA and theories obtained from it, k will vary from 1 to 3 and from 1 to 4 for in-plane and transverse displacements, respectively, unless otherwise stated. In accordance of choice of global functions $F^{\alpha}{}_{k}$ and G_k, ZZA_X assumes different names; in Table 3.9 particularizations retaken from [18] are reported:

Theory name	Function
ZZA_PP34 $n_\alpha = 3$, $n_\varsigma = 4$	$^{i}F^{\alpha}{}_{k}(\varsigma) = {}^{i}G_{k}(\varsigma) = (\varsigma)^{k}$
ZZA_PT34 $n_\alpha = 3$, $n_\varsigma = 4$	$^{i}F^{\alpha}{}_{k}(\varsigma) = {}^{i}G_{k}(\varsigma) = \begin{cases} \sin((k+1)\pi\varsigma/2h) & \text{if } k \text{ is odd} \\ \cos(k\pi\varsigma/2h) & \text{if } k \text{ is even} \end{cases}$
ZZA_PM34 $n_\alpha = 3$, $n_\varsigma = 4$	$^{i}F^{\alpha}{}_{k}(\varsigma) = {}^{i}G_{k}(\varsigma) = \begin{cases} \varsigma & \text{if } k = 1 \\ \exp(\varsigma/h) & \text{if } k = 2 \\ \sin(\pi\varsigma/2h) & \text{if } k \text{ is odd} \\ \cos(\pi\varsigma/2h) & \text{if } k \text{ is even} \end{cases}$
ZZA_PMTP34 $n_\alpha = 3$, $n_\varsigma = 4$	$^{i}F^{\alpha}{}_{k}(\varsigma) = \begin{cases} \varsigma & \text{if } k = 1 \\ \exp(\varsigma/h) & \text{if } k = 2 \\ \sin(\pi\varsigma/2h) & \text{if } k \text{ is odd} \\ \cos(\pi\varsigma/2h) & \text{if } k \text{ is even} \end{cases}$ $^{i}F^{\beta}{}_{k}(\varsigma) = \begin{cases} \sin((k+1)\pi\varsigma/2h) & \text{if } k \text{ is odd} \\ \cos(k\pi\varsigma/2h) & \text{if } k \text{ is even} \end{cases}$ $^{i}G_{k}(\varsigma) = (\varsigma)^{k}$

Table 3.9. Particularizations of ZZA_X theory retaken from [18].

Results obtained by these theories are indistinguishable from those of ZZA and other adaptive higher-order theories obtained from it, confirming that zig-zag functions can be changed or omitted without any loss of accuracy and also the representation functions can be changed and assumed differently for each displacement (see ZZA_PMTP34). Moreover, there is no need to assign a specific role to coefficients, for this kind of theories, whose coefficients are redefined layer by layer and obtained by imposing the full set of physical constraints (1.15)-(1.20). Processing time of ZZA_X theories is lower than ZZA, ZZM, ZZA****, HWZZ, HWZZM and HWZZM*, resulting the most efficient theories here presented. Moreover, the following new nine further particularizations are developed:

Theory name	Function	
ZZA_XN1 $n_\alpha = 3$, $n_\varsigma = 4$	$^{i}F^{\alpha}{}_{k}(\varsigma) = {}^{i}G_{k}(\varsigma) = (\varsigma)^{k}$	if $i \le 3$
	$^{i}F^{\alpha}{}_{k}(\varsigma) = {}^{i}G_{k}(\varsigma) = \begin{cases} \sin((k+1)\pi\varsigma/2h) & \text{if } k \text{ is odd} \\ \cos(k\pi\varsigma/2h) & \text{if } k \text{ is even} \end{cases}$	if $i > 3$
ZZA_XN2 $n_\alpha = 3$, $n_\varsigma = 4$	$^{i}F^{\alpha}{}_{k}(\varsigma) = {}^{i}G_{k}(\varsigma) = \begin{cases} \sin((k+1)\pi\varsigma/2h) & \text{if } k \text{ is odd} \\ \cos(k\pi\varsigma/2h) & \text{if } k \text{ is even} \end{cases}$	if $i \le 2$
	$^{i}F^{\alpha}{}_{k}(\varsigma) = {}^{i}G_{k}(\varsigma) = (\varsigma)^{k}$	if $i > 2$

ZZA_XN3 $n_\alpha = 3$, $n_\varsigma = 4$	${}^iF^\alpha{}_k(\varsigma) = {}^iG_k(\varsigma) = (\varsigma)^k$	if $i \le 4$
	${}^iF^\alpha{}_k(\varsigma) = {}^iG_k(\varsigma) = \begin{cases} \sin((k+1)\pi\varsigma/2h) & \text{if } k \text{ is odd} \\ \cos(k\pi\varsigma/2h) & \text{if } k \text{ is even} \end{cases}$	if $4 < i < 6$
	${}^iF^\alpha{}_k(\varsigma) = {}^iG_k(\varsigma) = \begin{cases} \varsigma & \text{if } k = 1 \\ \exp(\varsigma/h) & \text{if } k = 2 \\ \sin(\pi\varsigma/2h) & \text{if } k \text{ is odd} \\ \cos(\pi\varsigma/2h) & \text{if } k \text{ is even} \end{cases}$	if $i \ge 6$
ZZA_XN4 $n_\alpha = 3$, $n_\varsigma = 4$	${}^iF^\alpha{}_k(\varsigma) = {}^iG_k(\varsigma) = (\varsigma)^k$	if $i \le 3$
	${}^iF^\alpha{}_k(\varsigma) = {}^iG_k(\varsigma) = \begin{cases} \varsigma & \text{if } k = 1 \\ \exp(\varsigma/h) & \text{if } k = 2 \\ \sin(\pi\varsigma/2h) & \text{if } k \text{ is odd} \\ \cos(\pi\varsigma/2h) & \text{if } k \text{ is even} \end{cases}$	if $3 < i < 6$
	${}^iF^\alpha{}_k(\varsigma) = {}^iG_k(\varsigma) = \begin{cases} \sin((k+1)\pi\varsigma/2h) & \text{if } k \text{ is odd} \\ \cos(k\pi\varsigma/2h) & \text{if } k \text{ is even} \end{cases}$	if $i \ge 6$
ZZA_XN5 $n_\alpha = 3$, $n_\varsigma = 4$	${}^iF^\alpha{}_k(\varsigma) = {}^iG_k(\varsigma) = \begin{cases} \varsigma & \text{if } k = 1 \\ \exp(\varsigma/h) & \text{if } k = 2 \\ \sin(\pi\varsigma/2h) & \text{if } k \text{ is odd} \\ \cos(\pi\varsigma/2h) & \text{if } k \text{ is even} \end{cases}$	if $i \le 2$
	${}^iF^\alpha{}_k(\varsigma) = {}^iG_k(\varsigma) = (\varsigma)^k$	if $2 < i < 5$
	${}^iF^\alpha{}_k(\varsigma) = {}^iG_k(\varsigma) = \begin{cases} \sin((k+1)\pi\varsigma/2h) & \text{if } k \text{ is odd} \\ \cos(k\pi\varsigma/2h) & \text{if } k \text{ is even} \end{cases}$	if $i \ge 5$

ZZA_XN6

$n_{\alpha} = 3$, $n_{\varsigma} = 4$

$$
{}^{i}F^{\alpha}{}_{k}(\varsigma) = \begin{cases} \begin{cases} \varsigma & \text{if } k = 1 \\ \exp(\varsigma / h) & \text{if } k = 2 \\ \sin(\pi\varsigma / 2h) & \text{if } k \text{ is odd} \\ \cos(\pi\varsigma / 2h) & \text{if } k \text{ is even} \end{cases} & \text{if} \quad i \leq 3 \\ \varsigma^{k} & \text{if} \quad i > 3 \end{cases}
$$

$$
{}^{i}F^{\beta}{}_{k}(\varsigma) = \begin{cases} \varsigma^{k} & \text{if} \quad i > 3 \\ \begin{cases} \varsigma & \text{if } k = 1 \\ \exp(\varsigma / h) & \text{if } k = 2 \\ \sin(\pi\varsigma / 2h) & \text{if } k \text{ is odd} \\ \cos(\pi\varsigma / 2h) & \text{if } k \text{ is even} \end{cases} & \text{if} \quad i \leq 3 \end{cases}
$$

$$
{}^{i}G_{k}(\varsigma) = \begin{cases} \varsigma^{k} & \text{if} \quad i > 3 \\ \begin{cases} \sin((k+1)\pi\varsigma / 2h) & \text{if } k \text{ is odd} \\ \cos(k\pi\varsigma / 2h) & \text{if } k \text{ is even} \end{cases} & \text{if} \quad i \geq 3 \end{cases}
$$

	${}^{i}F^{\alpha}{}_{k}(\varsigma)=\begin{cases}\begin{cases}\varsigma & \text{if } k=1\\ \exp(\varsigma/h) & \text{if } k=2\\ \sin(\pi\varsigma/2h) & \text{if } k \text{ is odd}\\ \cos(\pi\varsigma/2h) & \text{if } k \text{ is even}\end{cases} & \text{if } \quad i\le 3\\ \varsigma^{k} & \text{if } \quad 3<i<6\\ \begin{cases}\sin((k+1)\pi\varsigma/2h) & \text{if } k \text{ is odd}\\ \cos(k\pi\varsigma/2h) & \text{if } k \text{ is even}\end{cases} & \text{if } \quad i\ge 6\end{cases}$
ZZA_XN7 $n_{\alpha}=3$, $n_{\varsigma}=4$	${}^{i}F^{\beta}{}_{k}(\varsigma)=\begin{cases}\varsigma^{k} & \text{if } \quad i>3\\ \begin{cases}\varsigma & \text{if } k=1\\ \exp(\varsigma/h) & \text{if } k=2\\ \sin(\pi\varsigma/2h) & \text{if } k \text{ is odd}\\ \cos(\pi\varsigma/2h) & \text{if } k \text{ is even}\end{cases} & \text{if } \quad 3<i<6\\ \begin{cases}\sin((k+1)\pi\varsigma/2h) & \text{if } k \text{ is odd}\\ \cos(k\pi\varsigma/2h) & \text{if } k \text{ is even}\end{cases} & \text{if } \quad i\ge 6\end{cases}$
	${}^{i}G_{k}(\varsigma)=\begin{cases}\varsigma^{k} & \text{if } \quad i>3\\ \begin{cases}\varsigma & \text{if } k=1\\ \exp(\varsigma/h) & \text{if } k=2\\ \sin(\pi\varsigma/2h) & \text{if } k \text{ is odd}\\ \cos(\pi\varsigma/2h) & \text{if } k \text{ is even}\end{cases} & \text{if } \quad i\ge 3\end{cases}$

ZZA_XN8 $n_\alpha = 3$, $n_\varsigma = 4$	$^iF^{\alpha}{}_k(\varsigma)=\begin{cases}\begin{cases}\varsigma & \text{if } k=1\\ \exp(\varsigma/h) & \text{if } k=2\\ \sin(\pi\varsigma/2h) & \text{if } k \text{ is odd}\\ \cos(\pi\varsigma/2h) & \text{if } k \text{ is even}\end{cases} & \text{if} \quad i\le 3\\ \varsigma^k & \text{if} \quad 3<i<5\\ \begin{cases}\varsigma & \text{if } k=1\\ \exp(\varsigma/h) & \text{if } k=2\\ \sin(\pi\varsigma/2h) & \text{if } k \text{ is odd}\\ \cos(\pi\varsigma/2h) & \text{if } k \text{ is even}\end{cases} & \text{if} \quad i\ge 5\end{cases}$ $^iF^{\beta}{}_k(\varsigma)=\begin{cases}\varsigma^k & \text{if} \quad i>3\\ \begin{cases}\varsigma & \text{if } k=1\\ \exp(\varsigma/h) & \text{if } k=2\\ \sin(\pi\varsigma/2h) & \text{if } k \text{ is odd}\\ \cos(\pi\varsigma/2h) & \text{if } k \text{ is even}\end{cases} & \text{if} \quad 3<i<6\\ \varsigma^k & \text{if} \quad i\ge 6\end{cases}$ $^iG_k(\varsigma)=\varsigma^k$ for each i
ZZA_XN9 $n_\alpha = 3$, $n_\varsigma = 4$	$^iF^{\alpha}{}_k(\varsigma)=\varsigma^k$ for each i $^iF^{\beta}{}_k(\varsigma)=\begin{cases}\varsigma^k & \text{if} \quad i>1\\ \begin{cases}\varsigma & \text{if } k=1\\ \exp(\varsigma/h) & \text{if } k=2\\ \sin(\pi\varsigma/2h) & \text{if } k \text{ is odd}\\ \cos(\pi\varsigma/2h) & \text{if } k \text{ is even}\end{cases} & \text{if} \quad 1<i<nl\\ \varsigma^k & \text{if} \quad i=nl\end{cases}$ nl is the number of layer $^iG_k(\varsigma)=\varsigma^k$ for each i

Table 3.10. New particularizations of ZZA_X theory.

Also results of new theories ZZA_XN1 to ZZA_XN9 are indistinguishable from those of ZZA, confirming that the representation can be assumed differently for each displacements and for each region from point to point, without any loss of accuracy, if coefficients are redefined across the thickness for each layer and the full set of physical constraints of ZZA (1.15)-(1.20) is imposed. Another new theory, called ZZA_XN10 is reported in Table 3.11:

Theory name	Function	
ZZA_XN10 $n_\alpha = 4$, $n_\varsigma = 3$	${}^{i}F^{\alpha}{}_{k}(\varsigma) = {}^{i}G_{k}(\varsigma) = (\varsigma)^{k}$	for each i

Table 3.11. ZZA_XN10 theory.

This particularization is different because, differently to ZZA, the number of terms of in-plane displacements is four, while the number of transverse one is three. Again, because of coefficients are redefined for each layer across the thickness and at least the same number of physical constraints is imposed, this theory obtains results very close to ZZA and other theories obtained from it. It should be noticed that the position across the thickness of equilibrium points is more important than the previous theories and in particular, more accurate findings are obtained if they are assumed near the interfaces, instead of within them.

As shown by accurate theories here developed (see chapters 4 and 5 for results), the level of generalization of ZZA_X is very high, because it is possible to choose a different representation not only for each displacements, but also different for any region across the thickness, with the chance of assuming an opportune and a proper representation for each region of displacement field depending on problem, thus ensuring efficiency (processing time are very low) and accuracy, as long as the same number of physical constraints is imposed and coefficients are redefined for each layer. For these reasons, this model is able to compete with more famous and used examples in Literature, such as [14]. In the next section another general theory is reported, called ZZA_GEN. Differently to ZZA_X, it does not contain linear contribution by FSDT.

3.5.3 ZZA_GEN theory

As previously stated, this theory is created as a generalized version of ZZA_X omitting linear contribution across the thickness retaken from FSDT. So, expression of ZZA_GEN across the thickness is obtained as a truncated series of functions of ς and unknown coefficients.

Similarly to ZZA_X, coefficients are redefined for each layer across the thickness and user can choose the expression of functions and the expansion order. In order to test performance of ZZA_GEN under the same conditions of ZZA, expansion order is fixed to four for in-plane displacements and five for transverse one. Five coefficients of the first layer from below (two for in-plane displacements and one for transverse one, similarly to ZZA theory) are chosen as new d.o.f of this theory, which assume a similar role of $u_\alpha{}^0$, w^0, Γ^0_α. All other coefficients are calculated by imposing the full set of physical constraints of ZZA

(1.15)-(1.20). It should be noticed that no zig-zag functions are included into displacement field, because this choice does not affect results, being coefficients redefined for each layer across the thickness and calculated on a physical basis.

Similarly to ZZA_X, the distinctive feature of ZZA_GEN is the possibility to choose a different representation not only for each displacements, but also differently for any region across the thickness (e.g. using a sinusoidal representation for some layers and a polynomial one for the others, see section 3.5.4 for details). Because of numerical applications will show that very accurate and indistinguishable results are provided, it is confirmed that this choice is immaterial if coefficients are recomputed across the thickness and calculated by imposing the full set of physical constraints. It should be noticed that the only substantial difference between ZZA_GEN and ZZA_X is the omission of linear contribution of FSDT; moreover, d.o.f. are explicitly present only in the first layer

For these reasons, the degree of generalization of ZZA_GEN is higher than ZZA_X. Results obtained by particularizations of ZZA_GEN are very close to ones provided by ZZA and other higher-order theories, demonstrating that the accuracy of ZZA_X does not even depend by assumption of linear contribution of FSDT into displacement field. Similarly to previous findings, previous statement is only valid under considered conditions (higher order adaptive theories with coefficients redefined for each layer across the thickness and calculated by imposing the full set of physical constraints).

ZZA_GEN

- Displacement-based, physically-based zig-zag theory;
- Piecewise in-plane displacements $u_\alpha^{(3)}$ (redefined coefficients);
- Piecewise transverse displacement $u_\varsigma^{(4)}$ (redefined coefficients);
- The number of terms for each displacements can be chosen by user as an input;
- The functions that are used for representation can be freely chosen;
- Different representations can be assumed for each displacements and for each region across then thickness;
- No linear contribution of FSDT is included into displacement field.

PROS	CONS
Generalized and refined version of ZZA; All theories of previous sections can be obtained from ZZA_GEN as particularizations; Similar features than ZZA_X Very low processing time (high efficiency).	Bounded only by the limits of the imagination.

$^{(n)}$ indicates the order of expansion of in-plane and transverse displacements

Table 3.12: Characteristic features of ZZA_GEN theory.

3.5.4 Displacement field of ZZA_GEN

This theory was developed in a paper that is currently under review as a generalized version of DZZ and ZZA_X. This theory is adaptive, so, its coefficients are redefined for each layer across the thickness. Being a general version of ZZA_X, it has similar features than parent theory, so, this theory does not contain any layerwise function and a general representation of variables is assumed across the thickness. Indeed, because its coefficients are redefined for each layer and calculated by imposing the full set of physical constraints (1.15)-(1.20), then:

- The choice of zig-zag functions is immaterial and they can be changed or omitted without any loss of accuracy;
- Functions that are used to describe the representation of displacements across the thickness can be changed, without any loss of accuracy, as long as they are able to describe for each layer a cubic and a fourth-order polynomial for in-plane and transverse displacements; under these conditions exponential, sinusoidal or polynomial representations can be assumed and also a combination of them;
- There is no need to assign a specific role to coefficients;

Moreover, linear contribution of FSDT (that is included into ZZA and all theories derived from it up to section 3.5.2) is omitted for ZZA_GEN and its particularizations, with the intended aim to test if it is essential to get accuracy. Anyway, results obtained by ZZA_GEN are indistinguishable from those obtained by ZZA_X1 to ZZA_X10, demonstrating that under these same conditions also linear contribution of FSDT can be omitted. So, the displacement field is:

$$\begin{aligned} u_\alpha{}^j(\alpha,\beta,\varsigma) &= \sum_{i=0}^{n_\alpha=3} \left[{}^jC_\alpha^i(\alpha,\beta) F^i(\varsigma) \right] \\ u_\varsigma{}^j(\alpha,\beta,\varsigma) &= \sum_{i=0}^{n_\varsigma=4} \left[{}^jC_\varsigma^i(\alpha,\beta) G^i(\varsigma) \right] \end{aligned} \tag{3.18}$$

Displacements are product of unknown amplitudes (${}^jC_\alpha^i$ and ${}^jC_\varsigma^i$) and generic functions of the thickness coordinate $F^i(\varsigma)$ and $G^i(\varsigma)$), whose expressions will be explained in the following part of this section, where j is the layer index. These five coefficients of the first layer ${}^1C_\alpha^0$, ${}^1C_\alpha^1$ and ${}^1C_\varsigma^0$ are assumed as the only five degrees of freedom of this theory, instead of u_α^0, Γ_α^0 and w^0 of ZZA and its variants. n_α and n_ς are fixed to three and four for in-plane and transverse displacements, respectively, with the intended aim to test this theory under the same conditions of ZZA and other models of this chapter. Remaining coefficients ${}^{j}C_{\alpha}^{i}$ and ${}^{j}C_{\varsigma}^{i}$ for i or $j>1$ are calculated by imposing the full set of physical constraints (1.15)-(1.20). Particularly, two equilibrium points are chosen for the inner layers (six equations), while only one (three equations) is necessary for the outer ones. Eight boundary conditions are enforced (1.15)-(1.18) (four equations for each outer layers), while four continuity of out-of-plane stresses and of gradient of transverse normal stress and three compatibility conditions of displacements are imposed at each interfaces. So, the expressions of $13N-5$ coefficients can be determined. It should be noticed that they depend only from geometry, material properties, five d.o.f. ${}^{1}C_{\alpha}^{0}$, ${}^{1}C_{\alpha}^{1}$, ${}^{1}C_{\varsigma}^{0}$ and their derivatives. The expression of d.o.f. are calculated by using Rayleigh-Ritz, similarly to ZZA and theories obtained from it.

Regarding numerical applications, two different particularizations will be used. The first one is called ZZA_GEN1 and it is retaken from [20]:

$$F^{i}(\varsigma)=G^{i}(\varsigma)=\varsigma^{i} \tag{3.19}$$

The second one is called ZZA_GEN2* and it is new:

$$F^{i}(\varsigma)=G^{i}(\varsigma)=\left\{\begin{array}{ll}1 & \text{for } i=0\\ \varsigma & \text{for } i=1\\ \sin(\pi\varsigma/h) & \text{for } i=2\\ e^{\varsigma/h} & \text{for } i=3\\ \cos(\pi\varsigma/h) & \text{for } i=4\end{array}\right\} \qquad \text{for} \quad j=even$$

$$F^{i}(\varsigma)=G^{i}(\varsigma)=\varsigma^{i} \qquad \text{for} \quad j=odd \tag{3.20}$$

As previously stated, results obtained by these theories are very accurate, indistinguishable from those of other higher-order theories, and they demonstrate that also linear contribution by FSDT is not necessary to obtain precise displacements and stresses. Moreover, similarly to ZZA_X these theories are very general, efficient, able to compete with more famous and used examples in Literature [14] and very interesting, because they require only five d.o.f.

Figure 3.4 shows the genealogical tree of all theories of chapters 2 and 3 (all particularizations of theories are not expressly reported in Figure, for the sake of clarity, being their number very high), while Figure 3.5 contains the flow-chart that summarizes all steps performed in chapters 2 and 3.

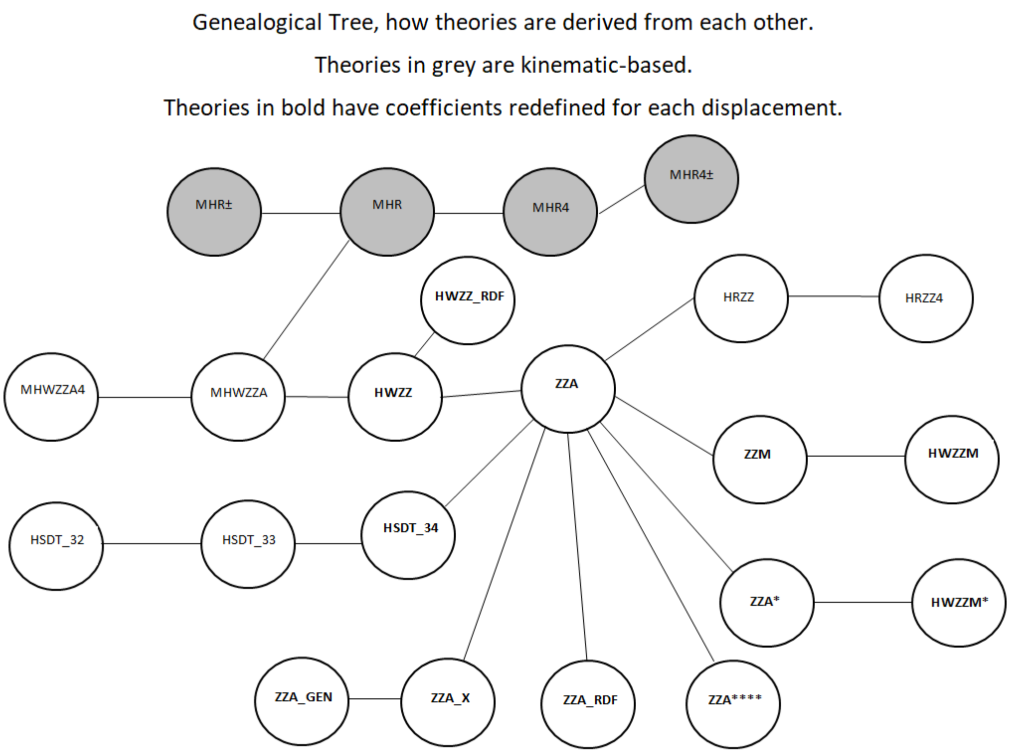

Figure 3.4: Genealogy of all theories of chapters 2 and 3

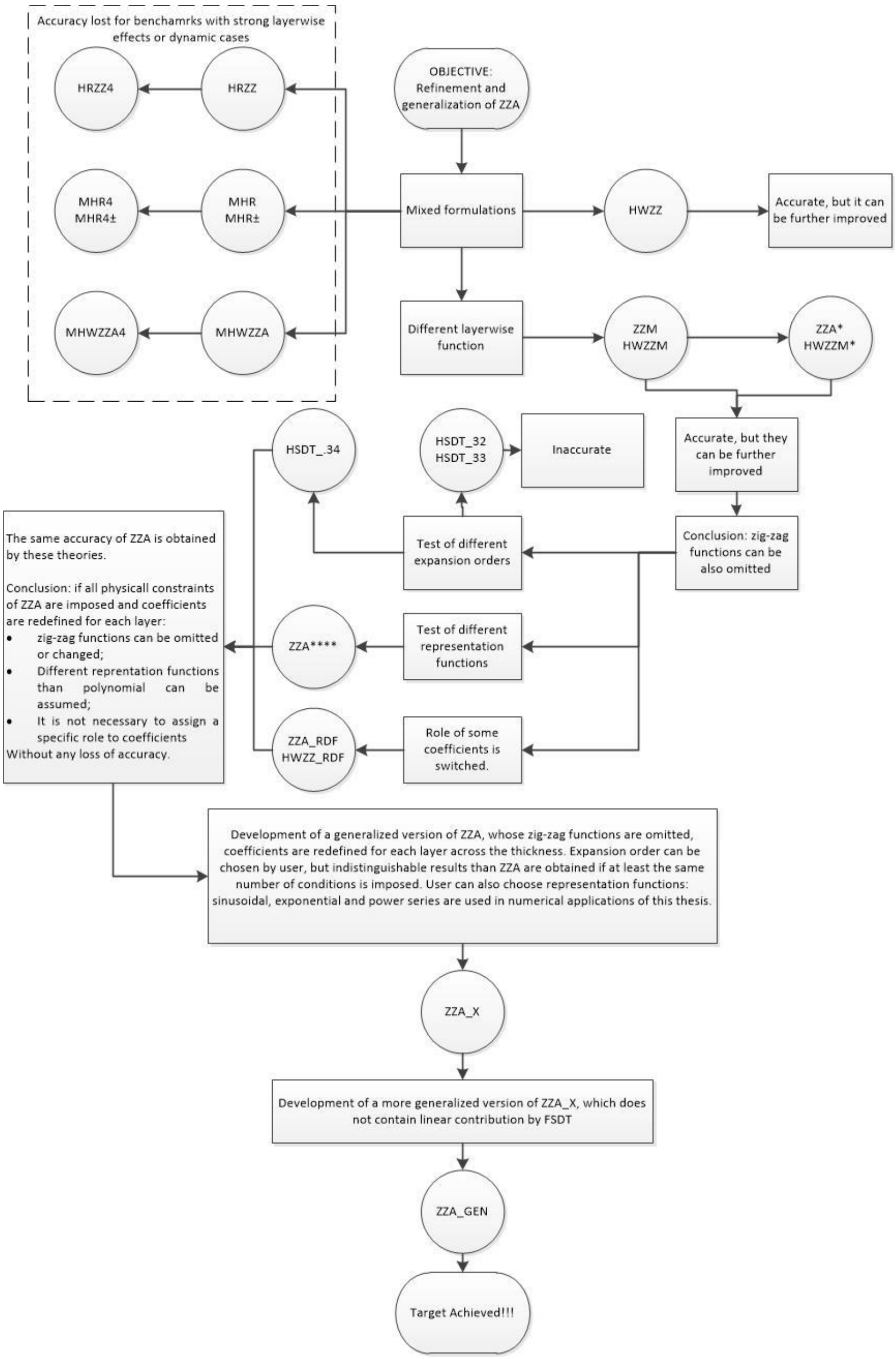

Figure 3.5: Flow-chart of all steps needed to develop ZZA_X

In the next chapters, theories are assessed considering challenging elastostatic and dynamic benchmarks retaken from literature. Tables 3.13a to 3.15i report material properties, lay-up and processing time of all elastostatic and dynamic cases considered in papers produced during PhD activity. Grey highlighted benchmarks are analyzed also into this thesis. Obviously, the same tables are valid for natural frequencies benchmarks, but there are no applied loads.

Material name	c1 [iso]	c2 [iso]	Foam	Gr-Ep	hh	i1	i2	m	mc	n [iso]	p
E1[GPa]	-	-	0.035	132.38	$250x10^{-3}$	6.89	0.1	$32.57x10^{3}$	0.1	-	172.4
E2[GPa]	-	-	0.035	10.76	$250x10^{-3}$	6.89	0.1	$1x10^{3}$	0.1	-	6.89
E3 [GPa]	M1	M2	0.035	1.076	$2500x10^{-3}$	6.89	0.1	$1x10^{3}$	0.1	M3	6.89
G12 [GPa]	-	-	0.0123	5.65	$1x10^{-3}$	2.59	0.037	$6.5x10^{2}$	0.04	-	3.45
G13 [GPa]	-	-	0.0123	5.65	$875x10^{-3}$	2.59	0.037	$8.21x10^{3}$	0.04	-	3.45
G23 [GPa]	-	-	0.0123	3.61	$1750x10^{-3}$	2.59	0.037	$3.28x10^{3}$	0.04	-	1.378
υ12	0.34	0.34	0.4	0.24	0.9	0.33	0.33	0.25	0.25	0.33	0.25
υ13	0.34	0.34	0.4	0.24	$3x10^{-5}$	0.33	0.33	0.25	0.25	0.33	0.25
υ23	0.34	0.34	0.4	0.49	$3x10^{-5}$	0.33	0.33	0.25	0.25	0.33	0.25

M1 E_l/E_u=5/4, E_l/E_c=10^5 M2 E_l/E_u=5/4, E_l/E_c=10^4 M3 E_u/E_l=1.6, E_u/E_c=$166.6\cdot 10^5$

[iso]=isotropic E_1=E_2=E_3 G_1=G_2=G_3

Table 3.13a: Material properties; part 1.

Material name	pf	pvc	q	r	s1	s2	s3	s4
E1[GPa]	25x103	25x101	0.273	25E2	1	33	25	0.05
E2[GPa]	1x103	25x101	0.273	E2	1	1	1	0.05
E3 [GPa]	1x103	25x101	0.273	E2	1	1	1	0.05
G12 [GPa]	5x102	9.62x101	0.1102	0.5E2	0.2	0.8	0.5	0.0217
G13 [GPa]	5x102	9.62x101	0.413	0.5E2	0.2	0.8	0.5	0.0217
G23 [GPa]	2x102	9.62x101	0.413	0.2E2	0.2	0.8	0.5	0.0217
υ12	0.25	0.3	0.25	0.25	0.25	0.25	0.25	0.15
υ13	0.25	0.3	0.25	0.25	0.25	0.25	0.25	0.15
υ23	0.25	0.3	0.25	0.25	0.25	0.25	0.25	0.15

Table 3.13b: Material properties; part 2.

Material name	da	db	dc	dd	de	df	dg	dh	dl1	dl2	dm1	dm2	dm3	dmc
E1[GPa]	M1	30E2	25E2	181	40E2	131	$6.89\cdot10^{-3}$	25E2	33.5	139	1	33	0.05	0.1
E2[GPa]	-	-	-	10.3	-	10.34	$6.89\cdot10^{-3}$	-	8	3.475	1	1	0.05	0.1
E3 [GPa]	E2	E2	E2	10.3	E2	10.34	$6.89\cdot10^{-3}$	E2	8	3.475	1	1	0.02	0.1
G12 [GPa]	0.6E2	0.6E2	0.5E2	7.17	0.6E2	6.205	$3.45\cdot10^{-3}$	0.5E2	2.26	1.7375	0.02	8	0.0217	0.04
G13 [GPa]	0.6E2	0.6E2	0.5E2	7.17	0.6E2	6.895	$3.45\cdot10^{-3}$	0.2E2	2.26	1.7375	0.02	8	0.0217	0.04
G23 [GPa]	0.5E2	0.5E2	0.2E2	2.87	0.5E2	6.895	$3.45\cdot10^{-3}$	0.2E2	3	0.695	0.02	8	0.0217	0.04
υ_{12}	0.25	0.25	0.25	0.25	0.25	0.22	0	0.25	0.35	0.25	0.25	0.25	0.15	0.25
υ_{13}	0.25	0.25	0.25	0.25	0.25	0.22	0	0.25	0.35	0.25	0.25	0.25	0.15	0.25
υ_{23}	0.25	0.25	0.25	0.33	0.25	0.49	0	0.25	0.33	0.25	0.25	0.25	0.15	0.25
ρ	ρ	ρ	ρ	1587	ρ	1627	97	ρ	1627	1627	1558.35	1558.35	16.3136	ρ

Table 3.13c: Material properties; part 3.

Material name	dm *	do1	do2	do3	dp	dq	dr1	dr2	ds	dt	du1	du2	dv	dw	dz
E1[GPa]	E1	206.84	0.138	0.0138	172.4	132.4	33.5	139	6.89	0.035	36.23	190	0.036	0.070	0.020
E2[GPa]	E2	5.171	0.138	0.0138	6.89	10.8	8	3.475	6.89	0.035	10.62	7.7	0.036	0.070	0.020
E3 [GPa]	E2	5.171	0. 138	0. 0138	6.89	10.8	8	3.475	6.89	0.035	7.21	7.7	0.036	0.070	0.020
G12 [GPa]	0.5E2	2.551	0.1027	0.01027	3.45	5.6	2.26	1.7375	3.45	0.0123	5.6	4.2	0.013	0.019	0.012
G13 [GPa]	0.5E2	2.551	0.1027	0.01027	3.45	5.6	2.26	1.7375	3.45	0.0123	5.68	4.2	0.013	0.019	0.012
G23 [GPa]	0.2E2	2.551	0.06205	0.006205	1.378	5.6	3	0.695	3.45	0.0123	3.46	2.96	0.013	0.019	0.012
υ_{12}	0.25	0.25	0.35	0.35	0.25	0.24	0.35	0.25	0	0.4	0.26	0.3	0.38	0.3	0.3
υ_{13}	0.25	0.25	0.35	0.35	0.25	0.24	0.35	0.25	0	0.4	0.33	0.3	0.38	0.3	0.3
υ_{23}	0.25	0.25	0.02	0.02	0.25	0.24	0.35	0.25	0	0.4	0.48	0.3	0.38	0.3	0.3
ρ	1558.35	1558.35	16.3136	16.3136	1558.35	1443	1627	1627	97	32	1800	1600	32	52.1	39.7

* E1/E2=3,25,40 for case b

Table 3.13d: Material properties; part 4.

BCS	Sketch	Loading
Simply Supported beams under sinusoidal loading	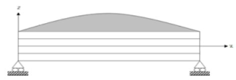	$p^0(x) = p^0{}_u \sin(\pi x / L_x) \;\text{ if }\; 0 \le x \le L_x$

$$u^0(x,y) = \sum_{m=1}^{M} A_m \cos\left(\frac{m\pi x}{L_x}\right); \quad w^0(x,y) = \sum_{m=1}^{M} C_m \sin\left(\frac{m\pi x}{L_x}\right); \quad \Gamma_x^0(x,y) = \sum_{m=1}^{M} D_m \cos\left(\frac{m\pi x}{L_x}\right)$$

For case f [17]:

$$u_\alpha{}^0(x,y) = \sum_{j=1}^{J}\sum_{i=1}^{I} A_{\alpha i}\left(\frac{x}{L_x}\right)^i\left(\frac{y}{L_y}\right)^j; \Gamma_\alpha^0(x,y) = \sum_{j=1}^{J}\sum_{i=1}^{I} D_{\alpha i}\left(\frac{x}{L_x}\right)^i\left(\frac{y}{L_y}\right)^j;$$

Case	Lay-up	Layer thickness	Material	Lx/h	Ly/Lx	Expansion Order
a [15] d [16] a [20]	[0/-90/0/-90]	[0.25h]4	$[p]_4$	4	-	1
b [15] d [18]	$[90/0_5/90]$	$[0.1h_2/0.2h_3/0.1h_2]$	$[pf_2/pvc/hh]_S$	8	-	1
c [15]	$[0/90/0_2/90]$	[0.3h/0.2h/0.15h/ 0.25h/0.1h]	$[pf_3/m/pf]$	8	-	1
d [15]	$[\pm45/\mp45/0/90_2/$ $0/\mp45/\pm45]$	$[\ h/12\ ]_{12}$	$[pf_{12}]$	8	-	1
n* [15]	$[0/90/0_4/90]$	$[0.1h_2/0.2h_3/$ $0.15h/0.05h]$	$[pf_2/pvc/hh]_S$	8	-	1
a [16]	$[0/90/0/0/0/90]_S$	$[((0.0333h)_3/$ $0.35h)_2/$ $(0.0333h)_3]$	$[(p_3/q)_2/\ p_3]$	5	-	1
b [16]	[90/0]	[0.5h/0.5h]	$[r_2]$	4	-	1
c* [16] i* [18]	$[\ 0\ ]_{11}$	[0.01h/0.025h/ 0.015h/0.02h/ $0.03h/0.4h]_S$	[s1/s2/s3/s1/ $s3/s4]_S$	4	-	1
a [18]	[90/0]	[0.5h/0.5h]	$[r_2]$	4	-	1
b [18]	[0/90/0]	$[\ (h/3)_3\ ]$	$[p_3]$	4	-	1
c [18]	$[0/90/0_3/90]_S$	$[((0.0333h)_3/$ $0.35h)_2/$ $(0.0333h)_3]$	$[(p_3/q)_2/\ p_3]$	5	-	1
b [22]	[0/90/0]	$[\ (h/3)_3\ ]$	$[p_3]$	4	-	1
b1 [17]	[0/90/0]	$[(h/3)]_3$	$[dp]_3$	10	-	1
b2 [17]	[0/90/0/90]	$[(h/4)]_4$	$[dp]_4$	10	-	1
b3 [17]	$[0]_3$	[0.1h/0.8h/0.1h]	[dp/dmc/dp]	4,10,20	-	1
e1 [17]	[0/90/0]	[0.25h/0.5h/0.25h]	$[dd]_3$	5,10,20	-	5
f [17]	[0/90]	$[(h/2)]_2$	$[dh]_2$	10	0.1	6
g [17]	$[0_8]$	[0.025h/0.05h/ $0.125h/0.3h]_S$	$[dm2/dm1/dm2/dm3]_S$	5	-	3
a [19]	[0/90/0]	$[(h/3)]_3$	$[dp]_3$	4,10,20	-	5
b (section 5.2)	[0/90/0]	$[(h/3)]_3$	$[dm]_3$	4	-	5
* Damaged; in grey cases retaken also in this thesis.						

Table 3.14a: List of cases (simply-supported beams)

BCS	Sketch	Loading
Simply Supported plates under bi-sinusoidal loading	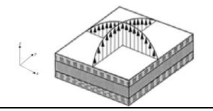	$p^0(x,y) = p^0{}_u \sin(\pi x / L_x)\sin(\pi y / L_y)$ if $0 \le x \le L_x$ and $0 \le y \le L_y$

$$u^0(x,y) = \sum_{m=1}^{M}\sum_{n=1}^{N} A_{mn} \cos\left(\frac{m\pi}{L_x}x\right)\sin\left(\frac{n\pi}{L_y}y\right); \quad v^0(x,y) = \sum_{m=1}^{M}\sum_{n=1}^{N} B_{mn} \sin\left(\frac{m\pi}{L_x}x\right)\cos\left(\frac{n\pi}{L_y}y\right);$$

$$w^0(x,y) = \sum_{m=1}^{M}\sum_{n=1}^{N} C_{mn} \sin\left(\frac{m\pi}{L_x}x\right)\sin\left(\frac{n\pi}{L_y}y\right);$$

$$\Gamma_x{}^0(x,y) = \sum_{m=1}^{M}\sum_{n=1}^{N} D_{mn} \cos\left(\frac{m\pi}{L_x}x\right)\sin\left(\frac{n\pi}{L_y}y\right); \quad \Gamma_y{}^0(x,y) = \sum_{m=1}^{M}\sum_{n=1}^{N} E_{mn} \sin\left(\frac{m\pi}{L_x}x\right)\cos\left(\frac{n\pi}{L_y}y\right);$$

Case	Lay-up	Layer thickness	Material	Lx/h	Ly/Lx	Expansion Order
e [15]	$[0/0]_S$	$[0.1h/0.4h]_S$	$[\text{Gr-Ep/Foam}]_S$	10	1	1
f [15] e [16] e [18] c [22]	[0/0/0]	[0.2h/0.7h/0.1h]	[c1/c1/c1]	4	3	1
g [15] j [16] b [23]	[0/0/0]	$[0.1h/0.4h]_S$	[p/mc/p]	4	1	1
l* [15] i* [16] f* [18] b [20] f [22]	[0/0/0]	[0.2h/0.7h/0.1h]	[c2/c2/c2]	4	3	1
q* [15] j* [18] c* [20]	[0/0/0]	[0.05h/0.85h/0.10h]	[p/mc/p]	4	1	1
c [23]	[0/90/0]	$[(h/3)_3]$	$[p_3]$	4	1	1
c1 [17]	[0/90/0/90]	$[(h/4)]_4$	$[da]_4$	5	1	1
c2 [17]	[90/0/90/0]	$[(h/4)]_4$	$[db]_4$	10/3	1	1
d1 [17]	[0/90/0]	$[(h/3)]_3$	$[dc]_3$	4,10,20, 30,50,100	1	1
d2 [17]	[0/90/0]	$[(h/3)]_3$	$[dp]_3$	10	1	4
e3 [17]	[0/90/0/0/90]	$[(h/24)2 / (5h/12)]_S$	$[df_2/dg]_S$	10	1	6
h [17] c [19]	[0/90/0/0/90]	$[(h/24)2 / (5h/12)]_S$	[dr1/dr2/ds/dr1/dr2]	5	1	10
i1 [17]	$[(45/\text{-}45)_2/45/0]_S$	$[(0.381mm)_5/(12.7mm)]_S$	$[do1_5/do2]_S$	20.8696	1	11
i2 [17]	[0/90/0]	[0.25h/0.5h/0.25h]	$[dq]_3$	14.941	1	11
i3 [17]	$[(0/90)_2/0_2]_S$	$[(0.381mm)_5 /(12.7mm)]_S$	$[do1_5/do2/do3/do1_5]$	10	1	11
b [19]	[0]	[h]	♣	10	1	10
d [19]	[0/90/0/0/90]	$[(h/24)_2 / (5h/12)]_S$	[dr1/dr2/dt/dr1/dr2]	5	1	10
e [19]	$[0_5]$	$[(h/24)_2 / (5h/12)]_S$	[du1/du2/dv/du1/du2]	4	1	15
f [19]	$[0_5]$	$[(h/24)_2 / (5h/12)]_S$	[du1/du2/dw/du1/du2]	4	1	15
g [19]	$[0_6]$	$[(h/24)_2$ / (30h/48) / (10h/48) / $(h/24)_2]$	[du1/du2/dv/dz/du1/du2]	4	1	15
* Damaged; in grey cases retaken also in this thesis. ♣ material properties are specified in text (section 5.3)						

Table 3.14b: Table 3b. List of cases (simply-supported plates)

BCS	Sketch	Loading
Propped-cantilever beam under a uniform loading	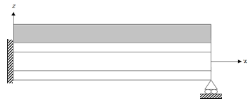	$p^0(x) = p^0{}_u$ if $0 \le x \le L_x$
$u^0(x,y)=\sum_{i=1}^{I} A_i \left(\frac{x}{L_x}\right)^i; \ w^0(x,y)=\sum_{i=1}^{I} C_i \left(\frac{x}{L_x}\right)^i; \ \Gamma_x^0(x,y)=\sum_{i=1}^{I} D_i \left(\frac{x}{L_x}\right)^i$		

Case	Lay-up	Layer thickness	Material	Lx/h	Expansion Order
h [15] f [16] m [18] e [21] a [23]	[0/0/0]	[(2h/7)/(4h/7)/(h/7)]	[n/n/n]	5.714	9
t [15] d [21] a [22]	[0/0/0]	[(2h/7)/(4h/7)/(h/7)]	[n/n/n]	14.286	9
u [15] g [16] g [18] f [20]	[0/0/0]	[(2h/7)/(4h/7)/(h/7)]	[n/n/n]	20	9
v [15]	[0/0/0]	[(2h/7)/(4h/7)/(h/7)]	[n/n/n]	50	9
y* [15]	[0/0/0]	[(2h/7)/(4h/7)/(h/7)]	[n/n/n]	5.714	9
* Damaged; in grey cases retaken also in this thesis.					

Table 3.14c: List of cases (propped-cantilever beams)

BCS	Sketch	Loading
Simply-supported beams under a sinusoidal loading (2 halfwaves)	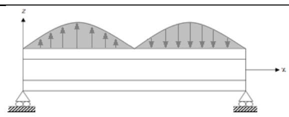	$p^0(x) = p^0{}_u \sin(2\pi x / L_x)$ if $0 \le x \le L_x$
$u^0(x,y)=\sum_{m=1}^{M} A_m \cos\left(\frac{2m\pi x}{L_x}\right); \ w^0(x,y)=\sum_{m=1}^{M} C_m \sin\left(\frac{2m\pi x}{L_x}\right); \ \Gamma_x^0(x,y)=\sum_{m=1}^{M} D_m \cos\left(\frac{2m\pi x}{L_x}\right)$		

Case	Lay-up	Layer thickness	Material	Lx/h	Expansion Order
i [15] a [21] d [22]	$[0/0]_S$	$[0.1h/0.4h]_S$	$[\text{Gr-Ep/Foam}]_S$	10	1
j* [15] b* [21]	$[0/0]_S$	$[0.1h/0.4h]_S$	$[\text{Gr-Ep/Foam}]_S$	10	1
* Damaged; in grey cases retaken also in this thesis.					

Table 3.14d: List of cases (simply-supported beams under sinusoidal loading - 2 halfwaves)

BCS	Sketch	Loading
Simply-supported beams under step loadings	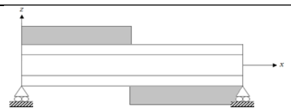	$p^0(x)=\begin{cases} p^0_u & \text{if } 0 \le x \le L_x/2 \\ -p^0_u & \text{if } L_x/2 \le x \le L_x \end{cases}$
$u^0(x,y)=\sum_{m=1}^{M} A_m \cos\left(\frac{2m\pi x}{L_x}\right);\ w^0(x,y)=\sum_{m=1}^{M} C_m \sin\left(\frac{2m\pi x}{L_x}\right);\ \Gamma_x^0(x,y)=\sum_{m=1}^{M} D_m \cos\left(\frac{2m\pi x}{L_x}\right)$		

Case	Lay-up	Layer thickness	Material	Lx/h	Expansion Order
k [15] c [21]	$[0/0]_S$	$[0.1h/0.4h]_S$	$[\text{Gr-Ep/Foam}]_S$	10	1
o [15] d [20]	$[90/0_5/90]$	$[0.1h_2/0.2h_3/0.1h_2]$	$[pf_2/pvc/hh]_S$	8	1
p* [15]	$[90/0_5/90]$	$[0.1h_2/0.2h_3/0.1h_2]$	$[pf_2/pvc/hh]_S$	8	1
r [15] k [18] e [20] e [22] e [23]	$[0]_{11}$	[0.01h/0.025h/ 0.015h/0.02h/ 0.03h/0.4h]s	$[s1/s2/s3/s1/$ $s3/s4]_S$	4	1
s* [15]	$[0]_{11}$	[0.01h/0.025h/ 0.015h/0.02h/ 0.03h/0.4h]s	$[s1/s2/s3/s1/$ $s3/s4]_S$	4	1
* Damaged; in grey cases retaken also in this thesis.					

Table 3.14e: List of cases (simply-supported beams under step loadings)

BCS	Sketch	Loading
Simply-supported plates under uniform localized step loadings	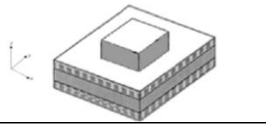	$p^0(x,y)=p^0_u$ if $\begin{cases} L_x/4 \le x \le 3L_x/4 \\ L_y/4 \le y \le 3L_y/4 \end{cases}$

$$u^0(x,y)=\sum_{m=1}^{M}\sum_{n=1}^{N} A_{mn}\cos\left(\frac{m\pi}{L_x}x\right)\sin\left(\frac{n\pi}{L_y}y\right);\quad v^0(x,y)=\sum_{m=1}^{M}\sum_{n=1}^{N} B_{mn}\sin\left(\frac{m\pi}{L_x}x\right)\cos\left(\frac{n\pi}{L_y}y\right);$$

$$w^0(x,y)=\sum_{m=1}^{M}\sum_{n=1}^{N} C_{mn}\sin\left(\frac{m\pi}{L_x}x\right)\sin\left(\frac{n\pi}{L_y}y\right);$$

$$\Gamma_x{}^0(x,y)=\sum_{m=1}^{M}\sum_{n=1}^{N} D_{mn}\cos\left(\frac{m\pi}{L_x}x\right)\sin\left(\frac{n\pi}{L_y}y\right);\quad \Gamma_y{}^0(x,y)=\sum_{m=1}^{M}\sum_{n=1}^{N} E_{mn}\sin\left(\frac{m\pi}{L_x}x\right)\cos\left(\frac{n\pi}{L_y}y\right);$$

Case	Lay-up	Layer thickness	Material	Lx/h	Ly/Lx	Expansion Order
m [15] k [16] h [18] d [23]	[0/0/0]	[0.05h/0.9h/0.05h]	[i1/i2/i1]	5	1	20

Table 3.14f: List of cases (simply-supported plates under localized step loading)

BCS	Sketch	Loading
Simply-supported beams under step loadings (2 steps)	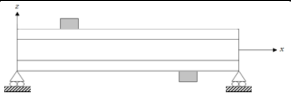	$p^0(x)=\begin{cases} p^0{}_u & \text{if} \quad L_x/8 \le x \le 3L_x/8 \\ -p^0{}_u & \text{if} \quad 5L_x/8 \le x \le 7L_x/8 \end{cases}$

$$u^0(x,y)=\sum_{m=1}^{M} A_m \cos\left(\frac{2m\pi x}{L_x}\right);\; w^0(x,y)=\sum_{m=1}^{M} C_m \sin\left(\frac{2m\pi x}{L_x}\right);\; \Gamma_x^0(x,y)=\sum_{m=1}^{M} D_m \cos\left(\frac{2m\pi x}{L_x}\right)$$

Case	Lay-up	Layer thickness	Material	Lx/h	Expansion Order
w* [15] f* [23]	[0/0/0]	[(2h/7)/(4h/7) /(h/7)]	[n/n/n]	5.714	1
x* [15] l* [18]	[0/0/0]	[(2h/7)/(4h/7) /(h/7)]	[n/n/n]	25	1
* Damaged; in grey cases retaken also in this thesis.					

Table 3.14g: List of cases (simply-supported beams under localized step loadings)

BCS	Sketch	Loading
Propped-cantilever beam under a uniform loading	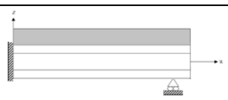 support at α=0.9Lα	$p^0(\alpha)=p^0{}_u$ if $0 \le \alpha \le L_\alpha$

$$u^0(x,y)=\sum_{i=1}^{I} A_i\left(\frac{x}{L_x}\right)^i;\; w^0(x,y)=\sum_{i=1}^{I} C_i\left(\frac{x}{L_x}\right)^i;\; \Gamma_x^0(x,y)=\sum_{i=1}^{I} D_i\left(\frac{x}{L_x}\right)^i$$

Case	Lay-up	Layer thickness	Material	Lx/h	Expansion Order
h [16]	[0/0/0]	[(2h/7)/(4h/7) /(h/7)]	[n/n/n]	5.714	9
* Damaged; in grey cases retaken also in this thesis.					

Table 3.14h: List of cases (propped-cantilever beam with support at 0.9Lα)

BCS	
Clamped plates	

$$u_\alpha{}^0(x,y)=\sum_{j=1}^{J}\sum_{i=1}^{I} A_{\alpha i}\left(\frac{x}{L_x}\right)^i\left(\frac{y}{L_y}\right)^j;\; \Gamma^0_\alpha(x,y)=\sum_{j=1}^{J}\sum_{i=1}^{I} D_{\alpha i}\left(\frac{x}{L_x}\right)^i\left(\frac{y}{L_y}\right)^j;$$

Case	Lay-up	Layer thickness	Material	BCS	Lx/h	Ly/Lx	Expansion Order
d2 [17]	[0/90/0]	$[(h/3)]_3$	$[p]_3$	CCCC	10	1	4
e2 [17]	[0/90/0]	$[(h/3)]_3$	$[e]_3$	CCCC	10	1	10

Table 3.14i: List of cases (clamped plates used in the study of natural frequencies).

BCS	
Clamped-supported plates	
$u_{\alpha}^{0}(x,y)=\sum_{j=1}^{J}\sum_{i=1}^{I}A_{\alpha i}\left(\frac{x}{L_x}\right)^{i}\left(\frac{y}{L_y}\right)^{j};\ \Gamma_{\alpha}^{0}(x,y)=\sum_{j=1}^{J}\sum_{i=1}^{I}D_{\alpha i}\left(\frac{x}{L_x}\right)^{i}\left(\frac{y}{L_y}\right)^{j};$	

Case	Lay-up	Layer thickness	Material	BCS	Lx/h	Ly/Lx	Expansion Order
d2 [17]	[0/90/0]	$[(h/3)]_3$	$[p]_3$	CSCS	10	1	4

Table 3.14j: List of cases (clamped-supported plates).

Processing time of theories

Preliminarily, Tables 4a to 4c show time calculations for elastostatic and dynamic cases, in order to demonstrate that the most advanced, general and significant theories show processing time very close to FSDT ones (but with a superior accuracy). So, it is demonstrated a major efficiency than HT, MZZ and CUF particularizations because they require a high expansion order of variables across the thickness. It should be noticed that processing time is reported in [s] and includes symbolic computations. A laptop computer with quad-core CPU @ 2.60GHz, 64-bit operating system and 8.00 GB RAM was used. A graphical, condensed comparison of computing times is added for each Table from 3.15a to 3.15l in Figures 3.6a to 3.6l (processing times are reported normalized to ZZA ones).

Case	a	b	c	d	e	f	g	h	i	j	k	l	m
	[14]	[14]	[14]	[14]	[14]	[14]	[14]	[14]	[14]	[14]	[14]	[14]	[14]
ZZA	13.5620	19.9740	16.3883	40.8100	10.5768	10.6297	10.6768	15.0671	4.9770	4.9120	5.6127	10.5392	10.9591
HRZZ	14.9182	20.9727	17.2077	44.8910	12.1633	11.6926	11.1786	18.2312	5.3990	5.5423	7.4582	11.5234	12.5887
HRZZ4	14.7821	20.9727	17.5078	44.8801	12.9170	11.6649	11.4805	18.2237	5.4094	5.2737	11.0258	11.8083	12.5681
HWZZ	12.0193	18.4149	14.5241	32.8215	6.6664	6.6997	6.7164	12.4271	4.4949	4.5726	5.2894	6.4675	6.7755
MHR	8.1514	11.7768	8.6557	22.2391	6.5138	6.5659	6.5879	6.9574	4.3663	4.5619	4.8186	6.7454	6.6732
MHR4	8.6564	11.7603	8.9334	22.2916	6.8826	6.4724	6.2271	6.4946	4.3310	4.3291	4.9692	6.5908	6.5056
MHWZZA	10.7396	16.8825	13.3830	30.0784	8.5096	8.2006	8.1997	7.2359	4.4726	4.6131	5.1828	8.2660	8.6730
MHWZZA4	10.2451	16.7948	13.9403	30.7918	8.1205	8.6045	8.9273	7.8365	4.6211	4.7301	5.2798	8.5094	8.9862
FSDT	2.7860	4.2943	3.2548	5.3116	5.4858	4.9372	4.8155	7.3303	2.3014	2.3045	2.4700	4.1470	4.0778

Case	n	o	p	q	r	s	t	u	v	w	x	y
	[14]	[14]	[14]	[14]	[14]	[14]	[14]	[14]	[14]	[14]	[14]	[14]
ZZA	19.7816	19.6433	19.7018	10.3465	17.5977	17.7618	15.0929	15.9719	15.5691	5.1241	5.0712	15.8988
HRZZ	20.7518	20.2183	20.5618	11.6618	20.9194	20.9960	18.4274	18.2261	18.0730	7.5249	7.9113	18.2287
HRZZ4	20.6340	20.6428	20.6898	11.4963	21.1942	21.6093	18.9174	18.4891	18.2253	11.8633	11.5603	18.4489
HWZZ	18.0556	18.4597	18.5196	6.5745	15.1594	15.8755	12.0471	12.8490	12.4573	5.6470	5.1993	12.3960
MHR	11.3941	11.4933	11.4818	6.8583	12.0285	11.9971	6.7118	6.6258	6.9350	4.1371	4.5774	6.9651
MHR4	11.2161	11.4761	11.3615	6.2430	12.5987	12.4183	6.1582	6.9702	6.2895	4.1968	4.6969	6.4367
MHWZZA	16.7661	16.9729	16.1719	8.3921	14.1698	14.3591	7.2626	7.6952	7.2143	5.9613	5.3375	7.9157
MHWZZA4	16.1256	16.7753	16.4800	8.0087	14.2118	14.8513	7.1210	7.5861	7.6056	5.8986	5.8352	7.8126
FSDT	6,1726	6,2168	6,1601	5,0712	6,5481	6,6445	5,9211	4,0522	6,1263	1,9067	2.3261	6.1245

Table 3.15a: Processing time of theories from [14]

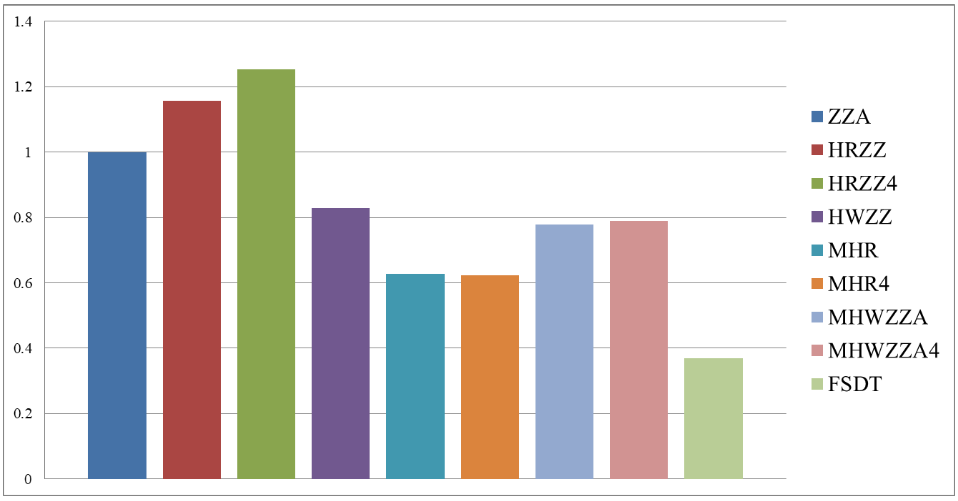

Figure 3.6a: Graphical, condensed comparison of computing times of theories of Table 3.15a. Results are normalized to processing time of ZZA.

Case	a1	a2	b1	b2	b3	c1	c2	d1	d2	e1	e2	e3	f
	[15]	[15]	[15]	[15]	[15]	[15]	[15]	[15]	[15]	[15]	[15]	[15]	[15]
ZZA	15.0671	15.9719	5.3866	6.8790	5.1194	29.6992	30.6735	26.4457	27.3202	15.2146	49.8998	52.3788	20.9916
HRZZ	18.2312	18.2261	4.6117	6.1888	4.8988	27.7977	28.4370	24.2019	25.0022	13.9237	45.6660	57.0334	19.2106
HRZZ4	18.2237	18.4891	5.0138	5.0387	5.0302	34.1087	36.4426	26.3526	27.2240	15.1610	49.7241	53.0857	20.9177
HWZZ	12.4271	12.8490	4.9640	6.2761	4.8679	27.3591	28.5739	24.5286	25.3396	14.1116	46.2823	37.5954	19.4698
MHR	6.9574	6.6258	2.8107	4.8288	2.7918	22.1087	23.6429	17.3712	17.9456	9.9939	32.7772	38.6301	13.7886
MHR4	6.4946	6.9702	2.9093	5.1452	2.6853	23.0599	24.0987	17.8493	18.4395	10.2689	33.6793	44.4327	14.1681
MHWZZA	7.2359	7.6952	3.7606	5.2613	3.6640	25.6959	25.6960	20.5304	21.2093	11.8114	38.7383	44.4865	16.2963
MHWZZA4	7.8365	7.5861	3.7602	5.2608	3.6636	25.7012	25.8412	20.5553	21.2350	11.8257	38.7852	47.7931	16.3160
HWZZM	11.5344	11.7059	4.1887	5.5954	4.0014	27.2368	27.1604	22.0831	22.8133	12.7047	41.6680	46.8301	17.5287
HWZZMA	11.5265	11.6018	4.1595	5.4061	3.9401	26.7922	26.4161	21.6381	22.3536	12.4487	40.8284	47.2328	17.1755
HWZZMB	11.5307	11.6289	4.1817	5.5216	3.9819	26.5349	26.8692	21.8242	22.5459	12.5558	41.1795	47.2427	17.3232
HWZZMC	11.5314	11.6457	4.1869	5.5926	3.9198	26.5605	26.8951	21.8288	22.5506	12.5584	41.1881	47.2981	17.3269
HWZZMB2	11.5310	11.6389	4.1659	5.5490	3.9905	26.5797	26.9146	21.8544	22.5770	12.5731	41.2365	47.2202	17.3472
HWZZMC2	11.5317	11.6401	4.1849	5.5951	3.8996	26.5905	26.9255	21.8184	22.5399	12.5524	41.1686	46.4436	17.3186
HWZZM0	11.4287	11.5912	4.1554	5.5079	3.7994	26.2617	26.3411	21.4596	22.1692	12.3460	40.4915	37.7979	17.0338
MHR±	6.9574	6.6258	3.0388	4.8770	2.8197	22.1087	23.6429	17.4648	18.0423	10.0477	32.9538	38.8376	13.8629
MHR4±	6.4946	6.9702	3.0384	5.1967	2.7122	23.0599	24.0987	17.9451	18.5385	10.3241	33.8602	47.7931	14.2442
ZZA*	11.4951	11.6125	3.8722	5.1722	3.8378	25.3302	25.2592	20.7581	21.6727	12.0695	38.7513	44.4886	16.4770
HWZZM*	10.9577	11.0035	3.9374	5.3156	3.8013	24.0637	24.5123	19.5104	20.3723	11.2246	37.2096	41.8193	15.4866
FSDT	-	-	3.0397	3.8151	2.6100	8.7624	8.8968	11.7092	12.0963	6.7364	22.0938	25.3415	-
HSDT	-	-	3.2507	4.1839	2.6134	11.5608	11.6764	13.1811	13.6169	7.5832	24.8711	28.5271	-

Case	g	h	i1	i2	i3
	[15]	[15]	[15]	[15]	[15]
ZZA	20.4415	57.4363	147.6859	76.1909	143.1814
HRZZ	18.7072	52.5631	135.1555	69.7264	130.4250
HRZZ4	20.3696	57.2341	147.1661	75.9227	150.2565
HWZZ	18.9596	53.2725	136.9795	70.6674	138.1438
MHR	13.4273	37.7277	97.0092	50.0468	93.0318
MHR4	13.7968	38.7660	99.6791	51.4242	100.9251
MHWZZA	15.8692	44.5891	114.6519	59.1487	117.1169
MHWZZA4	15.8884	44.6430	114.7906	59.2202	116.9716
HWZZM	17.0694	47.9613	123.3228	63.6220	119.6847
HWZZMA	16.7254	46.9949	120.8379	62.3400	117.8773
HWZZMB	16.8693	47.3990	121.8770	62.8761	122.6692
HWZZMC	16.8728	47.4089	121.9025	62.8892	121.4148
HWZZMB2	16.8926	47.4645	122.0455	62.9630	125.2797
HWZZMC2	16.8648	47.3864	121.8446	62.8594	125.6217
HWZZM0	16.5874	46.6071	119.8407	61.8256	114.0284
MHR±	13.4996	37.9309	97.5317	50.3164	93.58166
MHR4±	13.8709	38.9742	100.2145	51.7004	98.46074
ZZA*	16.2159	44.6040	114.6902	59.8047	112.7978
HWZZM*	14.7633	42.3786	106.6619	56.2164	106.5141
FSDT	9.0508	25.4307	65.3900	33.7345	64.1452
HSDT	10.1885	28.6275	73.6099	37.9752	75.5128

Table 3.15b: Processing time of theories from [15]

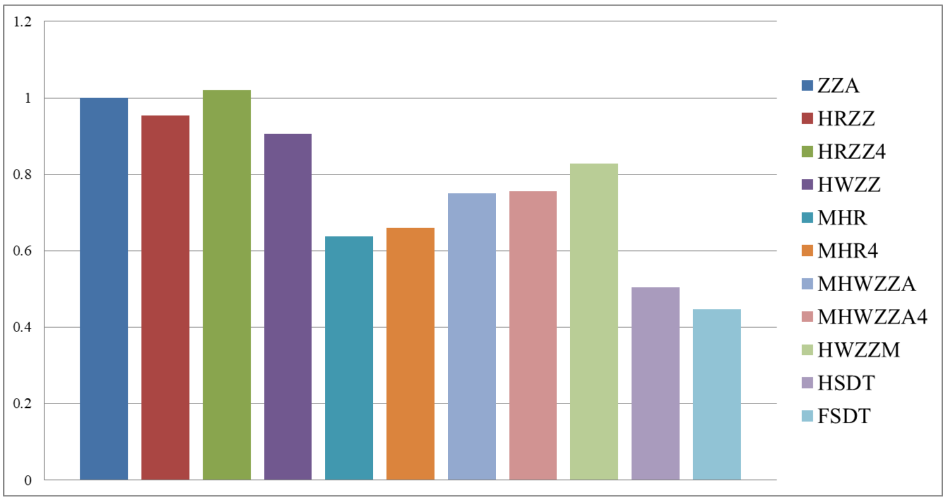

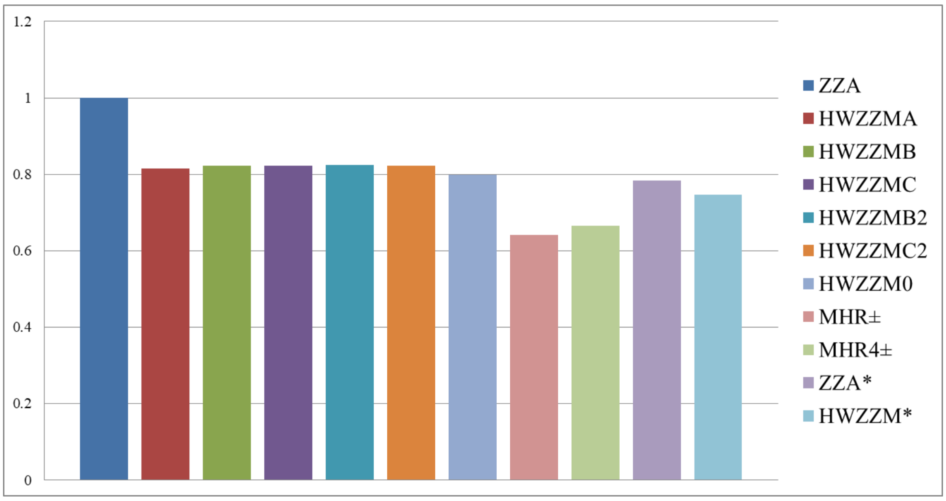

Figure 3.6b: Graphical, condensed comparison of computing times of theories of Table 3.15b. Results are normalized to processing time of ZZA.

Case	d	e	f	g	h	i	h	k
	[16]	[16]	[16]	[16]	[16]	[16]	[16]	[16]
ZZA	13.5620	10.6297	15.0671	15.9719	15.0671	10.5392	10.3465	10.9591
ZZA1	10.9875	6.0213	10.4752	10.8763	10.6351	5.5423	5.9752	5.9741
ZZA2	10.9742	6.0317	10.4875	10.8564	10.6241	5.6574	5.8741	6.0244
ZZA3	10.9657	6.0417	10.4784	10.7419	10.5934	5.5479	5.5369	5.7465
HWZZ	12.0193	6.6997	12.4271	12.8490	12.4271	6.4675	6.5745	6.7755
HWZZM	11.0702	6.1781	11.5344	11.7059	11.5359	5.9675	6.1899	6.2402
HRZZ	14.9182	11.6926	18.2312	18.2261	18.2312	11.5234	11.6618	12.5887
HRZZ4	14.7821	11.6649	18.2237	18.4891	18.2237	11.8083	11.4963	12.5681
MHR	8.1514	6.5659	6.9574	6.6258	6.9574	6.7454	6.8583	6.6732
MHR4	8.6564	6.4724	6.4946	6.9702	6.4946	6.5908	6.2430	6.5056
MHWZZA	10.7396	8.2006	7.2359	7.6952	7.2359	8.2660	8.3921	8.6730
MHWZZA4	10.2451	8.6045	7.8365	7.5861	7.8365	8.5094	8.0087	8.9862
HWZZMA	10.9925	6.1642	11.5265	11.6018	11.5267	5.9249	6.0498	6.0951
HWZZMB	11.0215	6.1737	11.5307	11.6289	11.5317	5.9423	6.1003	6.1143
HWZZMC	11.0498	6.1772	11.5314	11.6457	11.5326	5.9543	6.1240	6.1597
HWZZMB2	11.0314	6.1737	11.5310	11.6389	11.5301	5.9472	6.1157	6.1142
HWZZMC2	11.0492	6.1772	11.5317	11.6401	11.5334	5.9498	6.1291	6.1457
HWZZM0	10.9611	6.0856	11.4287	11.5912	11.4873	5.8752	6.0327	6.0475

Table 3.15c: Processing time of theories from [16]

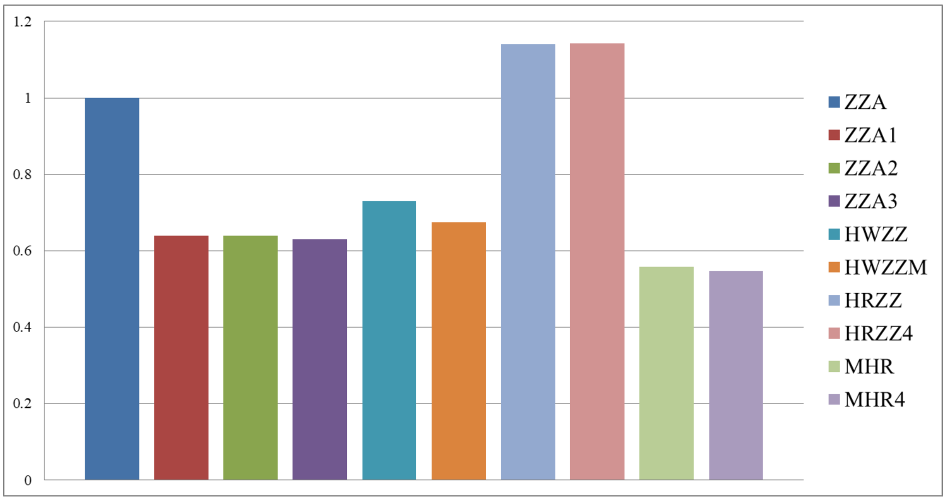

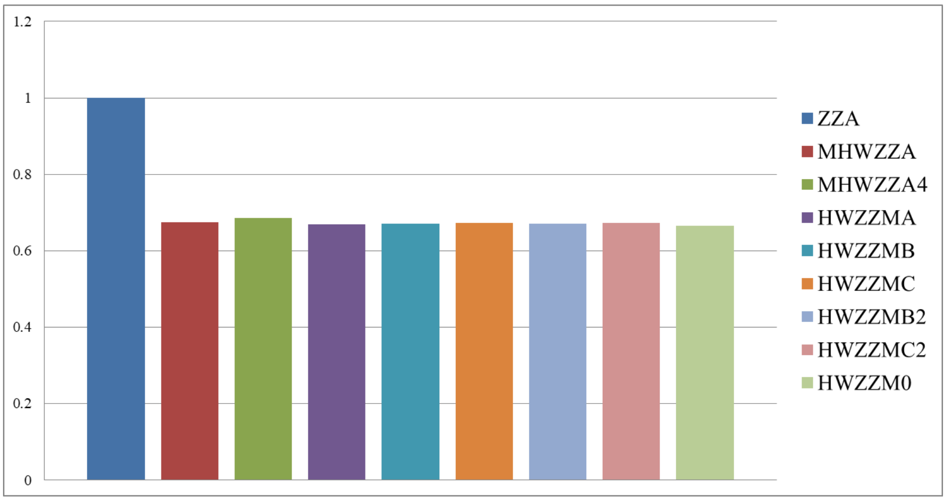

Figure 3.6c: Graphical, condensed comparison of computing times of theories of Table 3.15c. Results are normalized to processing time of ZZA.

Case	a	b	c	d	e	f	g	h	i	j	k	l	m
	[17]	[17]	[17]	[17]	[17]	[17]	[17]	[17]	[17]	[17]	[17]	[17]	[17]
ZZA	3.3140	4.3157	13.9569	16.3883	10.6297	10.5392	15.9719	10.9591	17.7618	10.3465	17.5977	5.0712	15.0671
AT-3D	6.2185	8.5624	27.9147	30.2778	21.5874	20.8736	32.6942	22.3982	34.0219	20.5874	35.6241	9.9517	31.2756
NOZZG	3.1841	3.6358	11.7996	13.8372	8.9871	8.9160	13.4737	9.3003	14.8997	6.6795	15.1430	4.4821	12.7127
ZZA_PT34	2.8537	3.3276	10.7164	12.6027	8.1752	8.1083	12.2958	8.4470	13.7159	7.8975	13.5123	3.8861	11.4931
ZZA_PM34	2.9225	3.4173	11.0321	12.9873	8.3588	8.2848	12.6349	8.6652	13.9970	5.9863	14.7423	5.0158	11.5457
ZZA_PMTP34	3.4455	3.9915	12.9249	15.1781	9.8828	9.8298	14.8378	10.1431	16.3952	5.5894	16.3230	4.6891	13.9214
ZZA_PPM34	3.4014	3.9750	12.8176	15.1030	9.8035	9.7254	14.7325	10.0894	16.3853	5.5478	16.1002	4.6682	13.8047
ZZA_PP34	2.9621	3.4482	11.1867	13.0586	8.5029	8.4040	12.8162	8.7773	13.6458	8.2779	14.5861	4.0354	12.2354
PP23	3.0645	3.8846	8.2573	9.8624	6.3526	6.2106	9.5893	6.4017	10.9514	4.7226	10.6062	4.5327	10.2339
ZS1	2.1342	2.7811	9.3182	10.8485	6.8137	7.0037	10.2210	7.3050	10.5897	6.8947	11.9177	3.2592	9.6038
ZS1_1	1.9396	2.5422	8.0878	9.8260	6.2477	6.0597	9.3034	6.4614	8.9847	6.1258	11.2197	2.9826	8.7055
ZS1_2	2.2610	2.9537	9.5402	11.2410	7.3884	7.3232	10.9019	7.5649	11.0958	7.1060	12.6351	3.4898	10.1534
ZS1_3	2.4760	3.3231	10.5969	12.3715	7.9341	8.1695	12.2374	8.3562	11.4867	7.9118	14.7966	3.7896	11.4258
ZS1_4	2.3205	3.0203	9.5380	11.2525	7.3912	7.3788	11.0865	7.6077	10.9212	7.1585	13.0382	3.4846	10.2185
ZS2	1.2799	1.6089	5.3337	6.2695	4.0342	4.1021	6.2347	4.1427	6.2634	3.9151	6.9072	1.9100	5.8877
ZS3	1.5054	1.9549	6.2391	7.3521	4.7385	4.6719	7.1381	5.0099	7.6527	4.6373	7.8870	2.2805	6.9498
ZS3_1	1.7543	2.3105	7.3627	8.8802	5.6168	5.6890	8.5198	5.8125	8.9873	5.4082	9.4766	2.6976	7.9565
ZS3_2	3.0435	3.8258	12.5779	15.0670	9.3962	9.5709	14.1009	9.9447	17.4143	9.4686	13.8120	4.6254	13.6422
ZZAS1	1.7568	2.3206	7.6841	8.8724	5.8794	5.6498	8.6052	5.8420	8.9926	5.5809	9.6497	2.7667	8.1453
ZZAS2	1.9329	2.4742	7.9767	9.5070	6.0207	6.1254	8.9058	6.2003	9.7453	6.0016	9.9650	2.8867	8.5223
ZZAS3	2.0550	2.6146	8.8262	10.1530	6.7139	6.4991	9.6984	6.8624	10.3285	6.5148	11.0327	3.1558	9.1218
ZZAS4	2.7662	3.7225	11.9672	14.3280	9.2482	9.0977	13.6707	9.2956	14.0969	7.5691	14.1913	5.1216	12.4721
FSDT	1.4502	1.9507	6.1935	3.2548	4.9372	4.1470	4.0522	4.0778	6.6445	5.0712	6.5481	2.3261	7.3303

Table 3.15d: Processing time of theories from [17]

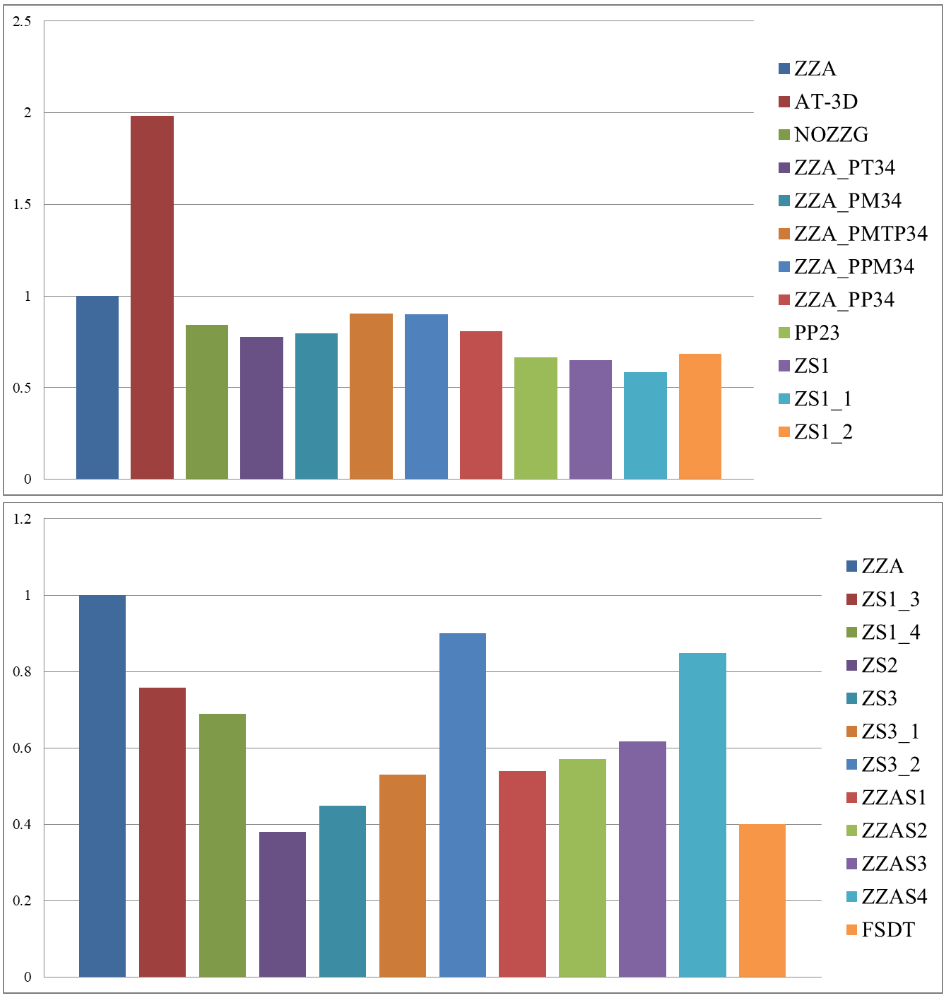

Figure 3.6d: Graphical, condensed comparison of computing times of theories of Table 3.15d. Results are normalized to processing time of ZZA.

Case	h	a	b	d	e	f	g
	[15]	[18]	[18]	[18]	[18]	[18]	[18]
ZZA	57.4363	5.3866	7.0182	46.4055	43.3751	45.7840	54.5138
HRZZ	52.5631	4.6117	6.2076	41.0461	38.3657	40.4964	48.2179
HRZZ4	57.2341	5.0138	6.7541	44.6591	41.7428	44.0610	52.4623
HWZZ	53.2725	4.9640	6.4877	42.8977	40.0964	42.3232	50.3931
MHR	37.7277	2.8107	4.1177	27.2271	25.4491	26.8625	31.9844
MHR4	38.7660	2.9093	4.2454	28.0714	26.2383	27.6955	32.9763
MHWZZA	44.5891	3.7606	5.1634	34.1415	31.9120	33.6843	40.1070
MHWZZA4	44.6430	3.7602	5.1663	34.1607	31.9299	33.7032	40.1295
HWZZM	47.9613	4.1887	5.6511	37.3664	34.9263	36.8660	43.8954
HWZZMA	46.9949	4.1595	5.5746	36.8605	34.4534	36.3669	43.3010
HWZZMB	47.3990	4.1817	5.6134	37.1167	34.6929	36.6197	43.6020
HWZZMC	47.4089	4.1659	5.6065	37.0715	34.6507	36.5750	43.5489
HWZZMB2	47.4645	4.1869	5.6175	37.1439	34.7183	36.6464	43.6339
HWZZMC2	47.3864	4.1849	5.6148	37.1262	34.7018	36.6290	43.6131
HWZZM0	46.6071	4.1554	5.5491	36.6915	34.2955	36.2002	43.1026
MHR±	37.9309	3.0388	4.2840	28.3264	26.4767	27.9471	33.2758
MHR4±	38.9742	3.0384	4.3450	28.7299	26.8538	28.3451	33.7498
ZZA*	44.6040	3.8722	5.2398	34.6466	32.3841	34.1826	40.7003
HWZZM*	42.3786	3.9374	5.1532	34.0740	31.8489	33.6177	40.0277
FSDT	25.4307	3.0397	3.5504	23.4756	21.9426	23.1613	27.5775
HSDT	28.6275	3.2507	3.8809	25.6612	23.9855	25.3175	30.1449
ZZ	36.4137	3.7072	5.0165	33.1702	31.0041	32.7259	38.9659
PP23	28.2542	2.8765	3.8924	25.7375	24.0568	25.3928	30.2345
ZZA_RDF	48.3134	4.9187	6.6559	44.0099	41.1360	43.4205	51.6997
ZZA*_43	38.0547	3.8743	5.2426	34.6650	32.4013	34.2008	40.7219
HWZZ_RDF	44.5274	4.5332	6.1343	40.5611	37.9124	40.0179	47.6483
HSDT_32	31.3042	3.1870	4.3126	28.5158	26.6537	28.1339	33.4983

HSDT_33	33.5957	3.4203	4.6283	30.6032	28.6047	30.1933	35.9504
HSDT_34	37.9586	3.8645	5.2293	34.5775	32.3195	34.1144	40.6191

ZZA_X1	38.3226	3.9015	5.2795	34.9090	32.6294	34.4415	41.0086
ZZA_X2	39.3223	4.0033	5.4172	35.8197	33.4806	35.3400	42.0784
ZZA_X3	39.8173	4.0537	5.4854	36.2706	33.9020	35.7848	42.6081
ZZA_X4	39.7974	4.0517	5.4827	36.2525	33.8851	35.7670	42.5868
ZZA-XX	96.3194	9.8060	13.2694	87.7398	82.0102	86.5648	103.0703
ZZA-XX'	93.6760	9.5369	12.9052	85.3319	79.7595	84.1891	100.2417

Table 3.15e: Processing time of theories from [18]

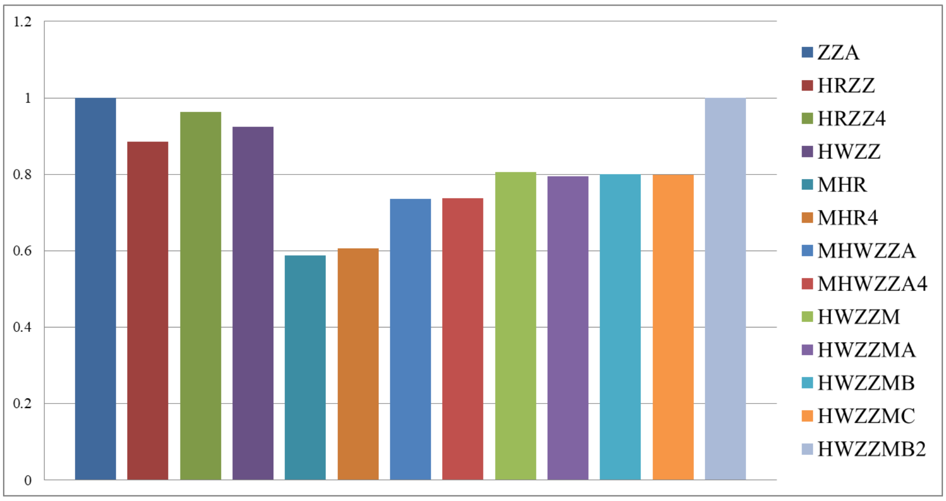

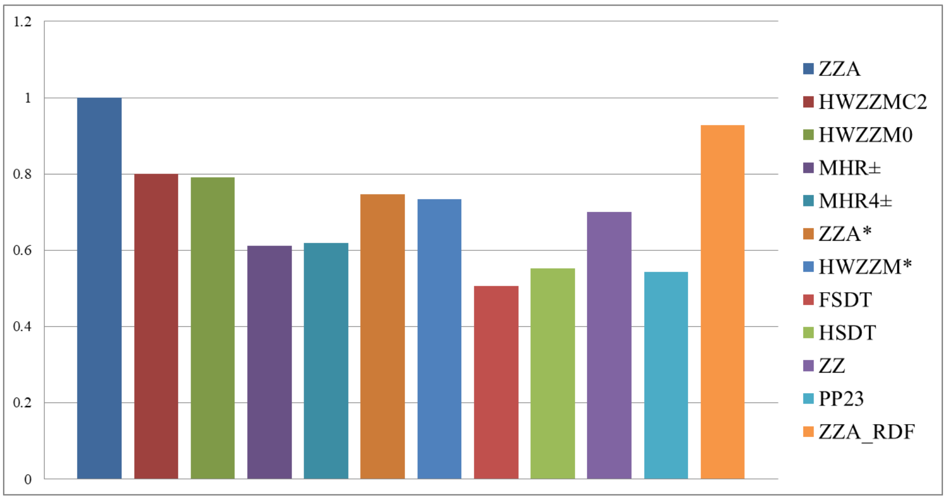

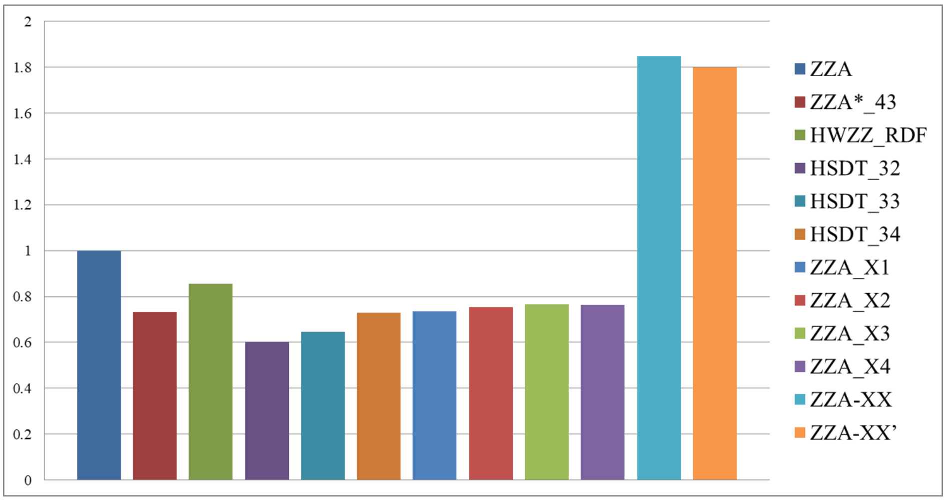

Figure 3.6e: Graphical, condensed comparison of computing times of theories of Table 3.15e. Results are normalized to processing time of ZZA.

Case	a	b	c	d	e	f
	[19]	[19]	[19]	[19]	[19]	[19]
FSDT	2.7860	4.1470	5.0712	6.2168	6.5481	4,0522
ZZA_X_1	10.2237	7.9699	7.7923	14.8450	13.2839	12.0660
ZZA_X_2	10.4743	8.1551	8.0180	15.2373	13.6303	12.4211
ZZA_X_3	10.6675	8.3169	8.1517	15.4161	13.8690	12.5162
ZZA_X_4	10.6481	8.2816	8.1362	15.4323	13.8039	12.6003
HRZZ	14.9182	11.5234	11.6618	20.2183	20.9194	18.2261
HRZZ4	14.7821	11.8083	11.4963	20.6428	21.1942	18.4891
MHR	8.1514	6.7454	6.8583	11.4933	12.0285	6.6258
MHR±	8.6016	6.7688	6.9558	12.5430	12.3437	6.7160
MHR4	8.6564	6.5908	6.2430	11.4761	12.5987	6.9702
MHR4±	9.2370	6.7213	6.3437	12.5583	12.8111	7.0373
HWZZ	12.0193	6.4675	6.5745	18.4597	15.1594	12.8490
HWZZ_RDFX	11.8948	9.2171	9.0704	17.2278	15.5294	14.0459
HWZZM*	10.0139	7.7776	7.6312	14.5394	12.9410	11.7302
HWZZM	10.9757	8.5366	8.3743	15.9133	14.2983	12.8841
MHWZZA	10.7396	8.2660	8.3921	16.9729	14.1698	7.6952
MHWZZA4	10.2451	8.5094	8.0087	16.7753	14.2118	7.5861
ZZA	13.5620	10.5392	10.3465	19.6433	17.5977	15.9719
ZZA_RDFX	12.9947	10.0199	9.9030	18.7144	16.7491	15.2775
ZZA*	10.2076	7.8824	7.7516	14.7835	13.1858	12.0055
HSDT_34X	10.1359	7.9003	7.7450	14.7167	13.1257	12.0035
ZZA*_43X	10.2219	7.9368	7.7749	14.6905	13.1698	11.9624
ZZA-XX	25.7514	20.0141	19.5885	37.1933	33.3160	30.2455
ZZA-XX'	25.0131	19.4123	19.2121	36.2402	32.5449	29.5543

Table 3.15f: Processing time of theories from [19]

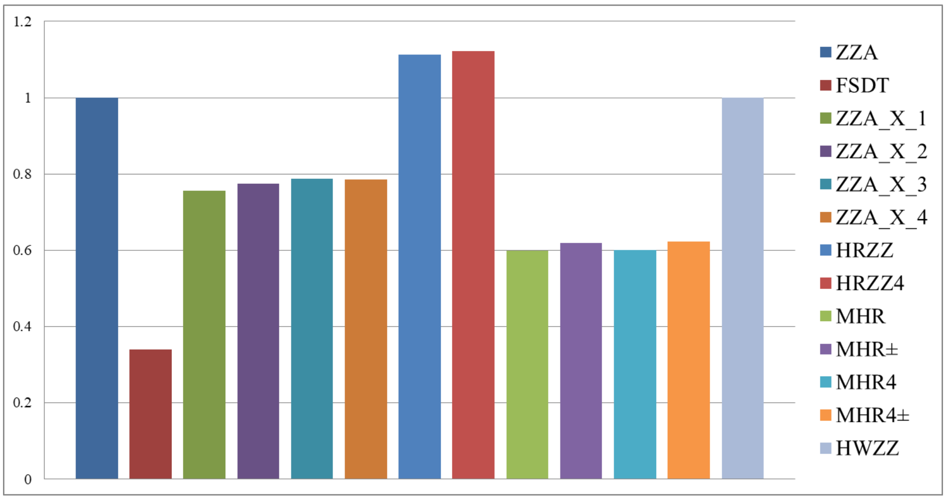

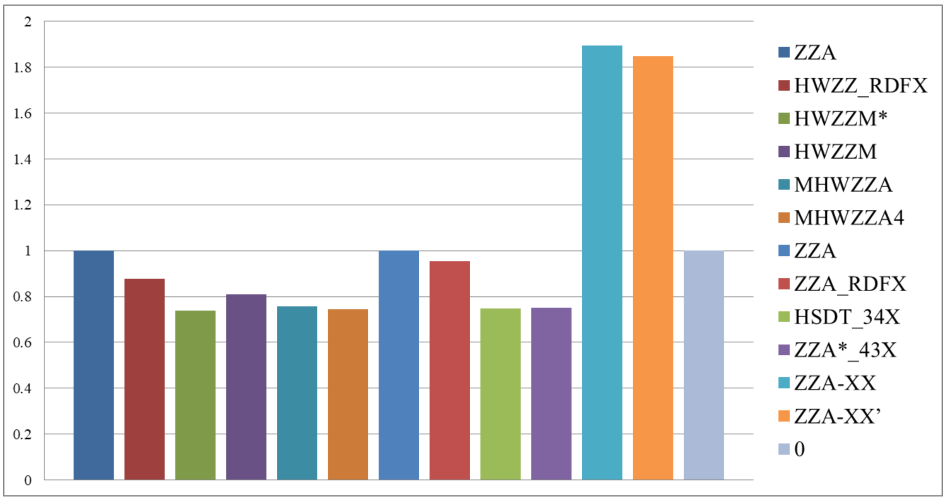

Figure 3.6f: Graphical, condensed comparison of computing times of theories of Table 3.15f. Results are normalized to processing time of ZZA.

Case	a	b	c	d	e
	[20]	[20]	[20]	[20]	[20]
FSDT	2.3014	2.3045	2.4710	5.9211	6.1245
ZZA_X1*	3.7673	3.7015	4.2532	11.4310	12.0417
ZZA_X2*	3.8680	3.8254	4.3774	11.7316	12.3256
ZZA_X3*	3.9032	3.8444	4.3979	11.9151	12.5217
ZZA_X4*	3.8969	3.8535	4.4288	11.8392	12.4289
HRZZ	5.3990	5.5423	7.4582	18.4274	18.2287
HRZZ4	5.4094	5.2737	11.0258	18.9174	18.4489
MHR	4.3663	4.5619	4.8186	6.7118	6.9651
MHR4	4.3310	4.3291	4.9692	6.1582	6.4367
HWZZ	4.4949	4.5726	5.2894	12.0471	12.3960
HWZZ_RDF	4.3621	4.2988	4.9147	13.2034	13.9751
HWZZM*	3.6891	3.6223	4.1572	11.1507	11.7533
HWZZM	4.0107	3.9760	4.5548	12.1959	12.8123
MHWZZA	4.4726	4.6131	5.1828	7.2626	7.9157
MHWZZA4	4.6211	4.7301	5.2798	7.1210	7.8126
ZZA	4.9770	4.9120	5.6127	15.0929	15.8988
ZZA_RDF	4.7548	4.6900	5.3309	14.4480	15.1919
ZZA*	3.7181	3.6988	4.2332	11.3110	11.9627
HSDT_34	3.7371	3.6694	4.2077	11.3441	11.9652
ZZA*_43	3.7393	3.7005	4.2142	11.3391	11.8843
ZZA*_43PRM	3.7438	3.6955	4.2329	11.3713	11.9072
ZZA_X1	3.7705	3.7064	4.2545	11.4102	12.0588
ZZA_X2	3.8508	3.7999	4.3686	11.6656	12.3498
ZZA_X3	3.9127	3.8502	4.3945	11.9047	12.4688
ZZA_X4	3.9074	3.8509	4.4108	11.9031	12.4591
ZZA-XX	9.4659	9.3495	10.6582	28.5583	30.1960
ZZA-XX’	9.2262	9.1041	10.3746	28.0411	29.4950

Table 3.15g: Processing time of theories from [20]

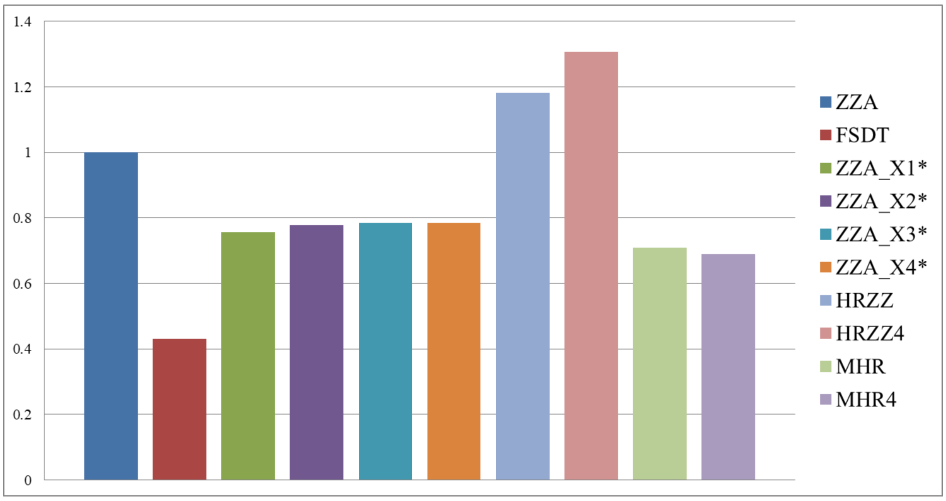

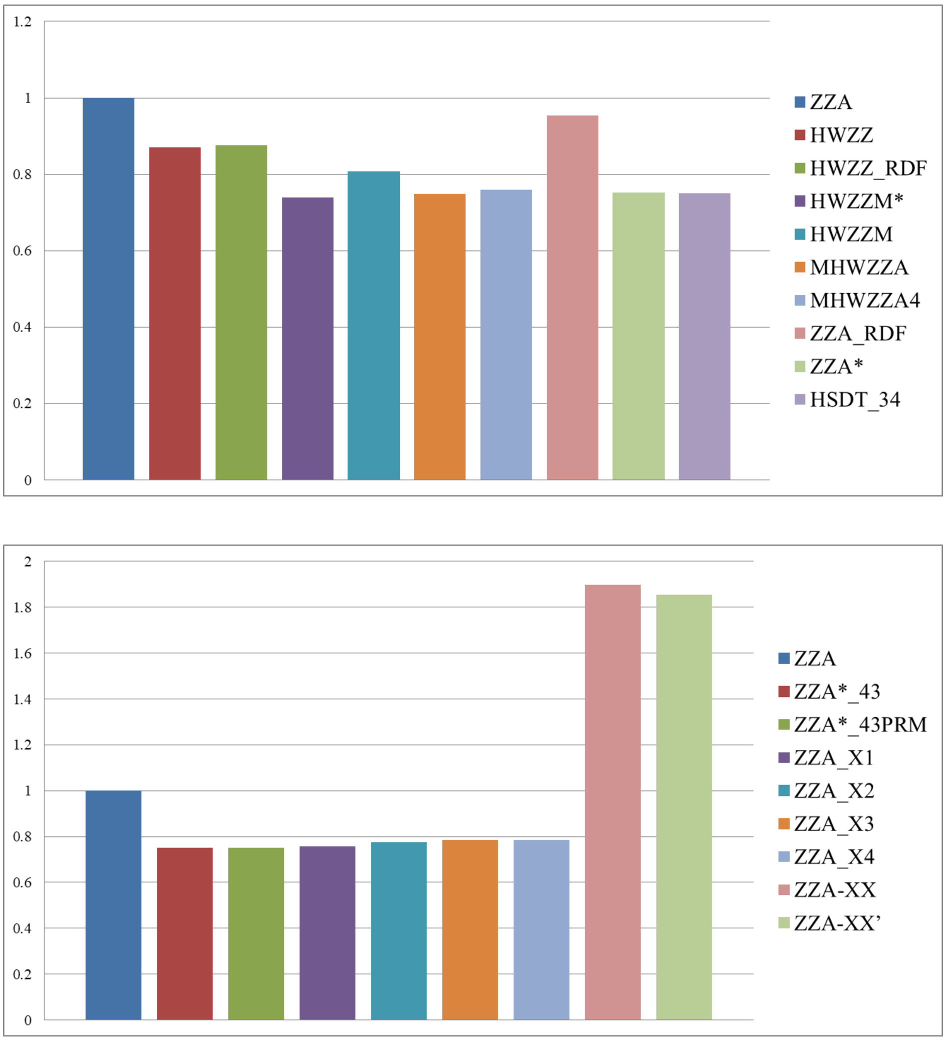

Figure 3.6g: Graphical, condensed comparison of computing times of theories of Table 3.15g. Results are normalized to processing time of ZZA.

Case	a	b	c	d	e	f
	[21]	[21]	[21]	[21]	[21]	[21]
FSDT	4.0338	2.2857	4.0928	1.8971	7.2570	4.0293
Present theory [21]	13.1075	4.1127	8.6521	4.2235	16.2312	9.0803
ZZA_X1	11.9180	3.7531	7.9473	3.8206	14.7913	8.1602
ZZA_X2	12.2758	3.8442	8.0691	3.9522	15.1387	8.4179
ZZA_X3	12.3912	3.8573	8.2443	4.0019	15.4243	8.5103
ZZA_X4	12.5271	3.8553	8.1855	3.9869	15.3804	8.4476
HWZZ	12.7078	4.4355	6.4151	5.1020	15.3278	6.6966
HWZZM	12.7083	3.9657	8.4218	4.0728	15.7581	8.7583
ZZA	15.7617	4.9446	10.4055	5.0946	19.4522	10.8600
ZZA*	11.8971	3.6656	7.7602	3.7789	14.6491	8.1071

Table 3.15h: Processing time of theories from [21]

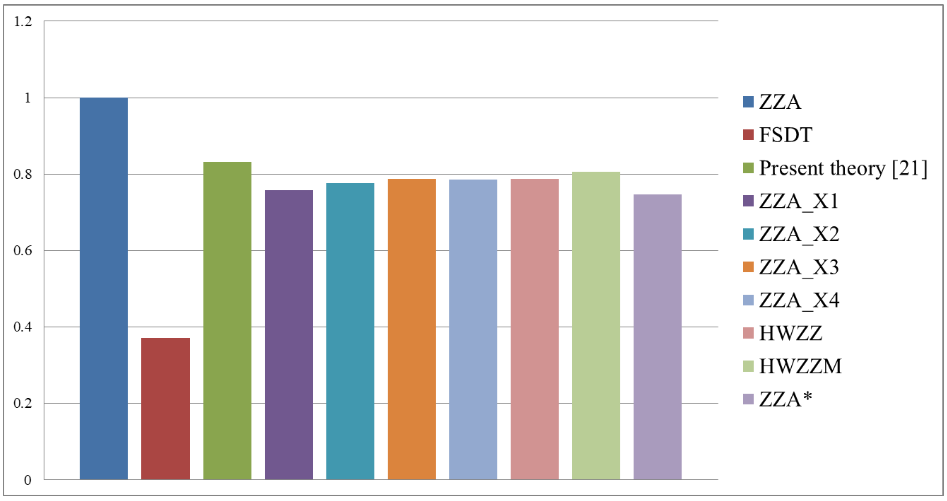

Figure 3.6h: Graphical, condensed comparison of computing times of theories of Table 3.15h. Results are normalized to processing time of ZZA.

Case	a	b	c	d	e	f
	[22]	[22]	[22]	[22]	[22]	[22]
FSDT	4.0464	4.1461	4.1076	4.0520	6.5354	1.9019
ZZA_GEN0	13.1722	8.7215	8.6962	9.1277	14.6543	4.2907
ZZA_GEN1	11.9659	8.0067	7.9544	8.2013	13.2670	3.8517
ZZA_GEN2	11.9921	8.0527	7.9972	8.2408	13.3645	3.8852
ZZA_GEN3	13.1008	8.7057	8.6441	9.0754	14.6530	4.2603
ZZA_X_1	12.3557	8.2010	8.1477	8.4441	13.6177	3.9697
ZZA_X2*	12.4625	8.3430	8.3111	8.5587	13.7859	4.0229
HWZZ	12.7824	6.4927	6.4554	6.7243	15.0879	5.1318
HWZZM	12.8223	8.4773	8.4569	8.8433	14.2111	4.1131
ZZA*	11.9532	7.8892	7.8201	8.1319	13.1593	3.8098
ZZA	15.8358	10.4631	10.4555	10.9519	17.5553	5.1144

Table 3.15i: Processing time of theories from [22]

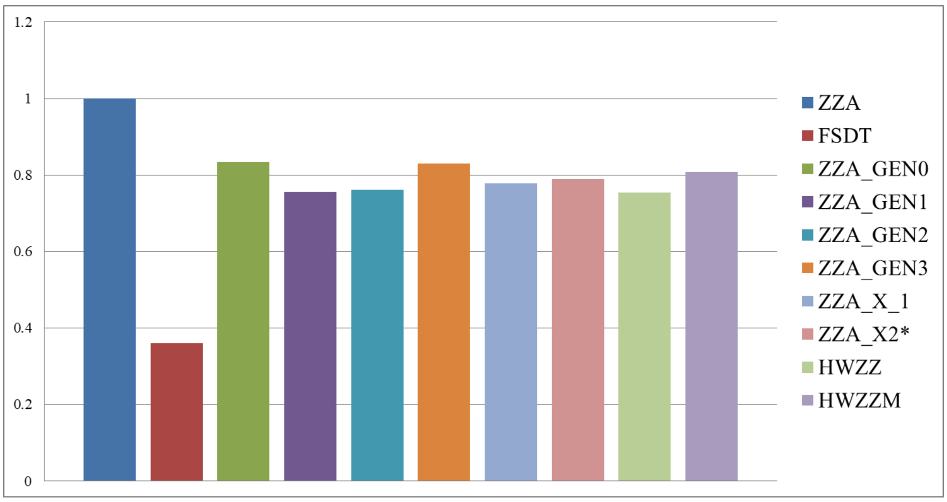

Figure 3.6i: Graphical, condensed comparison of computing times of theories of Table 3.15i. Results are normalized to processing time of ZZA.

Chapter 4 – Elastostatic assessment of theories

In this chapter, results provided by theories of chapters 2 and 3 are presented. Examined cases represent elastostatic benchmarks, retaken from Literature, where both simply-supported and clamped edges are assumed as boundary conditions of beams and plates under sinusoidal, bisinusoidal or uniform loading. Table 4.1 collects all data of benchmarks, while Table 4.2 contains trial functions used for each case and damage properties, while Table 4.3 shows material properties for all cases:

Case	Lay-up	Layer thickness	Material	Sketch	Loading	Lα/h	Lβ/Lα
a (*)	[0/-90/0/-90]	[0.25h]4	$[p]_4$	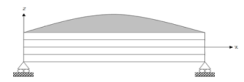	$p^0(\alpha)=p^0{}_u\sin(\pi\alpha/L_\alpha)$ if $0\le\alpha\le L_\alpha$	4	-
b (*)	$[90/0_5/90]$	$[0.1h_2/0.2h_3/0.1h_2]$	$[pf_2/pvc/hh]_S$			8	-
c (§)	[0/0/0]	[0.2h/0.7h/0.1h]	[c1/c1/c1]	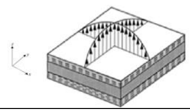	$p^0(\alpha,\beta)=p^0{}_u\sin(\pi\alpha/L_\alpha)\sin(\pi\beta/L_\beta)$ if $0\le\alpha\le L_\alpha$ and $0\le\beta\le L_\beta$	4	3
d (§)	$[0/0]_S$	$[0.1h/0.4h]_S$	$[\text{Gr-Ep/Foam}]_S$			10	1
e (*§)	[0/0/0]	[(2h/7)/(4h/7)/(h/7)]	[n/n/n]	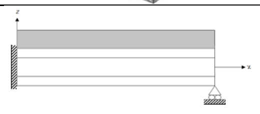	$p^0(\alpha)=p^0{}_u$ if $0\le\alpha\le L_\alpha$	5.714	-
f (*⸸§)	[0/0/0]	[0.05h/0.85h/0.10h]	[p/mc/p]	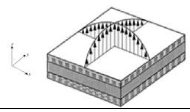	$p^0(\alpha,\beta)=p^0{}_u\sin(\pi\alpha/L_\alpha)\sin(\pi\beta/L_\beta)$ if $0\le\alpha\le L_\alpha$ and $0\le\beta\le L_\beta$	4	1
g (§)	$[0/0]_S$	$[0.1h/0.4h]_S$	$[\text{Gr-Ep/Foam}]_S$	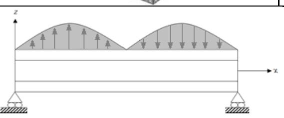	$p^0(\alpha)=p^0{}_u\sin(2\pi\alpha/L_\alpha)$ if $0\le\alpha\le L_\alpha$	10	1
h (*§)	$[0]_{11}$	[0.01h / 0.025h / 0.015h / 0.02h / 0.03h / 0.4h]s	[1/2/3/1/3/4]s	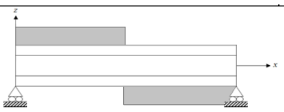	$p^0(\alpha)=\begin{cases}p^0{}_u & \text{if } 0\le\alpha\le L_\alpha/2\\ -p^0{}_u & \text{if } L_\alpha/2\le\alpha\le L_\alpha\end{cases}$	4	-
i (*§)	[0/0/0]	[(2h/7)/(4h/7)/(h/7)]	[n/n/n]	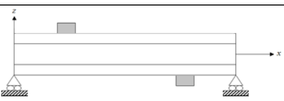	$p^0(\alpha)=\begin{cases}p^0{}_u & \text{if } L_\alpha/8\le\alpha\le 3L_\alpha/8\\ -p^0{}_u & \text{if } 5L_\alpha/8\le\alpha\le 7L_\alpha/8\end{cases}$	5.714	-
j (*⸸§)	[0/0/0]	[0.05h/0.9h/0.05h]	[i1/i2/i1]	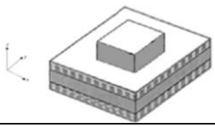	$p^0(\alpha,\beta)=p^0{}_u$ if $\begin{cases}L_\alpha/4\le\alpha\le 3L_\alpha/4\\ L_\beta/4\le\beta\le 3L_\beta/4\end{cases}$	5	1
k (*§)	[0/0/0]	[(2h/7)/(4h/7)/(h/7)]	[n/n/n]	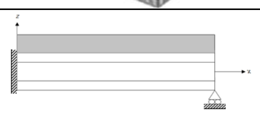	$p^0(\alpha)=p^0{}_u$ if $0\le\alpha\le L_\alpha$	20	-
l	[0/0/0]	[0.1h/0.8h/0.1h]	[qiso/♣/ qiso]	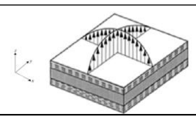	$p^0(\alpha,\beta)=p^0{}_u\sin(\pi\alpha/L_\alpha)\sin(\pi\beta/L_\beta)$ if $0\le\alpha\le L_\alpha$ and $0\le\beta\le L_\beta$	3	1

♣ Functionally graded core (properties in section 4.9)

Whether Murakami's function assumption is not satisfied by u_α (*), u_β (⸸) and u_ς (§)

Table 4.1. List of elastostatic cases.

Case	Trial Functions	Expansion Order
a b	$u_\alpha^0(\alpha)=\sum_{m=1}^{M} A_m \cos\left(\frac{m\pi\alpha}{L_\alpha}\right);\quad w^0(\alpha)=\sum_{m=1}^{M} C_m \sin\left(\frac{m\pi\alpha}{L_\alpha}\right);\quad \Gamma_\alpha^0(\alpha)=\sum_{m=1}^{M} D_m \cos\left(\frac{m\pi\alpha}{L_\alpha}\right)$	1 1
c d f j l	$u_\alpha^0(\alpha,\beta)=\sum_{m=1}^{M}\sum_{n=1}^{N} A_{mn} \cos\left(\frac{m\pi}{L_\alpha}\alpha\right)\sin\left(\frac{n\pi}{L_\beta}\beta\right);\quad u_\beta^0(\alpha,\beta)=\sum_{m=1}^{M}\sum_{n=1}^{N} B_{mn} \sin\left(\frac{m\pi}{L_\alpha}\alpha\right)\cos\left(\frac{n\pi}{L_\beta}\beta\right);$ $w^0(\alpha,\beta)=\sum_{m=1}^{M}\sum_{n=1}^{N} C_{mn} \sin\left(\frac{m\pi}{L_\alpha}\alpha\right)\sin\left(\frac{n\pi}{L_\beta}\beta\right);$ $\Gamma_\alpha{}^0(\alpha,\beta)=\sum_{m=1}^{M}\sum_{n=1}^{N} D_{mn} \cos\left(\frac{m\pi}{L_\alpha}\alpha\right)\sin\left(\frac{n\pi}{L_\beta}\beta\right);\quad \Gamma_\beta{}^0(\alpha,\beta)=\sum_{m=1}^{M}\sum_{n=1}^{N} E_{mn} \sin\left(\frac{m\pi}{L_\alpha}\alpha\right)\cos\left(\frac{n\pi}{L_\beta}\beta\right);$	1 1 1 20 1
e k	$u_\alpha^0(\alpha)=\sum_{i=1}^{I} A_i\left(\frac{\alpha}{L_\alpha}\right)^i;\ w^0(\alpha)=\sum_{i=1}^{I} C_i\left(\frac{\alpha}{L_\alpha}\right)^i;\ \Gamma_\alpha^0(\alpha)=\sum_{i=1}^{I} D_i\left(\frac{\alpha}{L_\alpha}\right)^i$	9 9
g h i	$u_\alpha^0(\alpha)=\sum_{m=1}^{M} A_m \cos\left(\frac{2m\pi\alpha}{L_\alpha}\right);\quad w^0(\alpha)=\sum_{m=1}^{M} C_m \sin\left(\frac{2m\pi\alpha}{L_\alpha}\right);\quad \Gamma_\alpha^0(\alpha)=\sum_{m=1}^{M} D_m \cos\left(\frac{2m\pi\alpha}{L_\alpha}\right)$	1 1

Table 4.2. Trial functions and expansion order.

Material name	1	2	3	4	c1 [iso]	Foam	Gr-Ep	hh	i1	i2	n [iso]	p	pf	pvc	qiso
E1[GPa]	1	33	25	0.05	-	0.035	132.38	$250 x10^{-3}$	6.89	0.1	-	172.4	$25 x10^3$	250	70
E2[GPa]	1	1	1	0.05	-	0.035	10.76	$250 x10^{-3}$	6.89	0.1	-	6.89	$1 x10^3$	250	70
E3 [GPa]	1	1	1	0.05	M1	0.035	10.76	$2500 x10^{-3}$	6.89	0.1	M2	6.89	$1 x10^3$	250	70
G12 [GPa]	0.2	0.8	0.5	0.0217	-	0.0123	5.65	$1 x10^{-3}$	2.59	0.037	-	3.45	$5 x10^2$	96.2	26.92
G13 [GPa]	0.2	0.8	0.5	0.0217	-	0.0123	5.65	$875 x10^{-3}$	2.59	0.037	-	3.45	$5 x10^2$	96.2	26.92
G23 [GPa]	0.2	0.8	0.5	0.0217	-	0.0123	3.61	$1750 x10^{-3}$	2.59	0.037	-	1.378	$2 x10^2$	96.2	26.92
υ12	0.25	0.25	0.25	0.15	0.34	0.4	0.24	0.9	0.33	0.33	0.33	0.25	0.25	0.3	0.3
υ13	0.25	0.25	0.25	0.15	0.34	0.4	0.24	$3 x10^{-5}$	0.33	0.33	0.33	0.25	0.25	0.3	0.3
υ23	0.25	0.25	0.25	0.15	0.34	0.4	0.49	$3 x10^{-5}$	0.33	0.33	0.33	0.25	0.25	0.3	0.3
M1 El/Eu=5/4, El/Ec=10^5					M3 Eu/El=1.6, Eu/Ec=$166.6\cdot10^5$					[iso]=isotropic E1=E2=E3 G1=G2=G3					

Table 4.3. Material properties.

Results will demonstrate what previously stated, that if coefficients are redefined for each layer across the thickness and the full set of physical constraints (1.15)-(1.20) is imposed:

- zig-zag functions can be changed or omitted without any loss of accuracy;
- functions that describe variation of displacements across the thickness can be changed, so, exponential, power series and sinusoidal functions, or a combination of them, can be assumed differently for each displacement and from point to point across the thickness, without any loss of accuracy;
- the role of coefficients can be freely switched;
- linear contribution by FSDT are not necessary to obtain precise displacements and stresses

On the contrary, accuracy becomes strongly dependent by assumptions made and results will also show the superiority of physically-based models than kinematic-based ones, when the same expansion order is assumed.

In order to confirm the previous statements, twelve challenging benchmarks (both multi-layered and sandwich structures) will be analysed and both symmetrical and strongly asymmetrical lay-ups will be considered. Regarding this latter statement, it is very important that theories are able to accurately describe also asymmetric displacements and stresses across the thickness, because this condition could occur during life-service of a structure as a consequence of a damage.

For all cases, only the most significant results will be reported, while the remaining ones will be collected in Appendix 1. With the intended aim to contain this thesis length, results are not reported in tabular form. Normalizations and positions where through-the-thickness quantities are plotted are explicitly reported in text for each case. For cases a to e the accuracy of all theories of chapters 2 and 3 is assessed, while only results provided by the most significant adaptive ones will be reported for cases f to l.

4.1 Case a

This case is a simply-supported laminated composite [0/90/0/90] beam under a sinusoidal loading, whose layers are made of the same material and have the same thickness. This case is interesting because nevertheless the orientation of layers changes at each interface, there is no change of the slope of displacements in the first interface from above, contrarily to what postulated by Murakami's rule, so 3-D effects rise. Anyway, all theories of chapters 2 and 3 quite accurately predict displacements and stresses across the thickness, as shown in Figure 4.1 (in-plane and transverse normal stresses are reported in Appendix 1, being accurately obtained by all theories). The following normalizations are used:

$$\overline{u_\alpha} = \frac{E_2 u_\alpha(0,\varsigma)}{hp^0} \quad \overline{u_\varsigma} = \frac{u_\varsigma\left(\frac{L_\alpha}{2},\varsigma\right)}{hp^0} \quad \overline{\sigma_{\alpha\varsigma}} = \frac{\sigma_{\alpha\varsigma}(0,\varsigma)}{p^0} \tag{4.1}$$

In-plane displacement is not correctly predicted by MHR, MHR4, MHWZZA and MHWZZA4 in the first interface from above, because there is no a change of the slope of this displacement between the third and the fourth-layer. So, this case demonstrate the superiority of physically-based theories, that better predict results than Murakami's ones, if the same expansion order across the thickness is assumed.

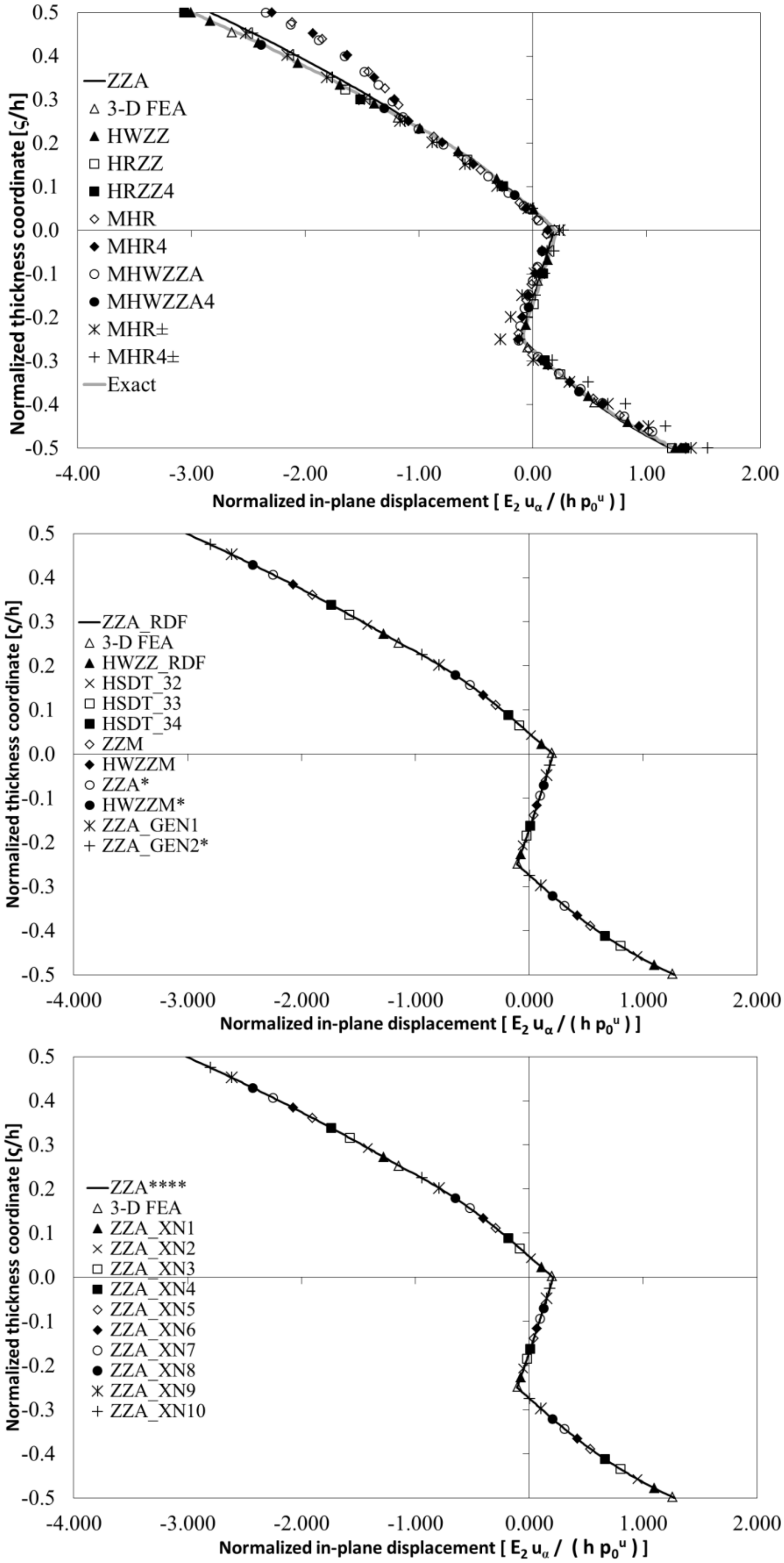

Figure 4.1a: In-plane displacement

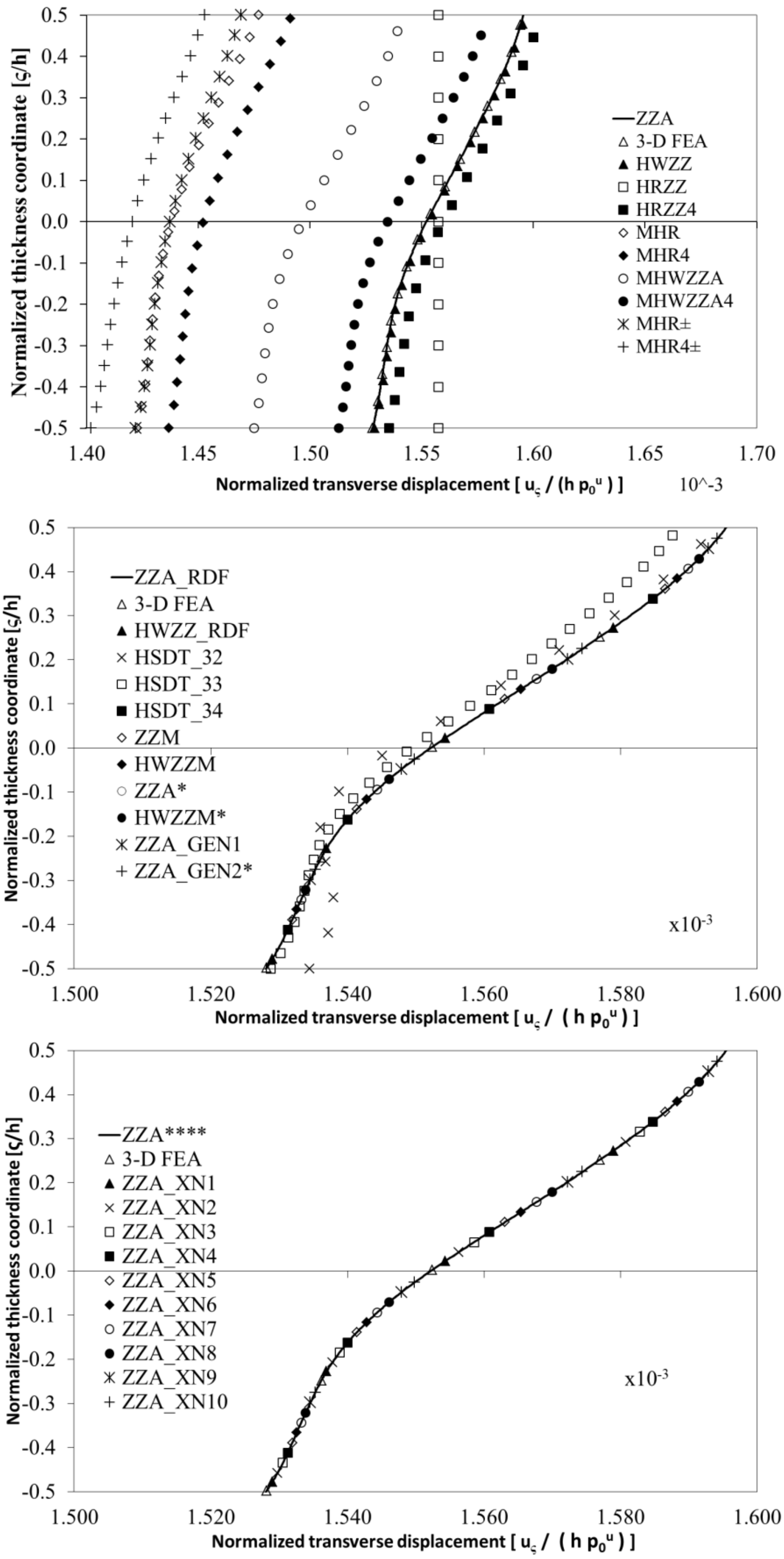

Figure 4.1b: Transverse displacement

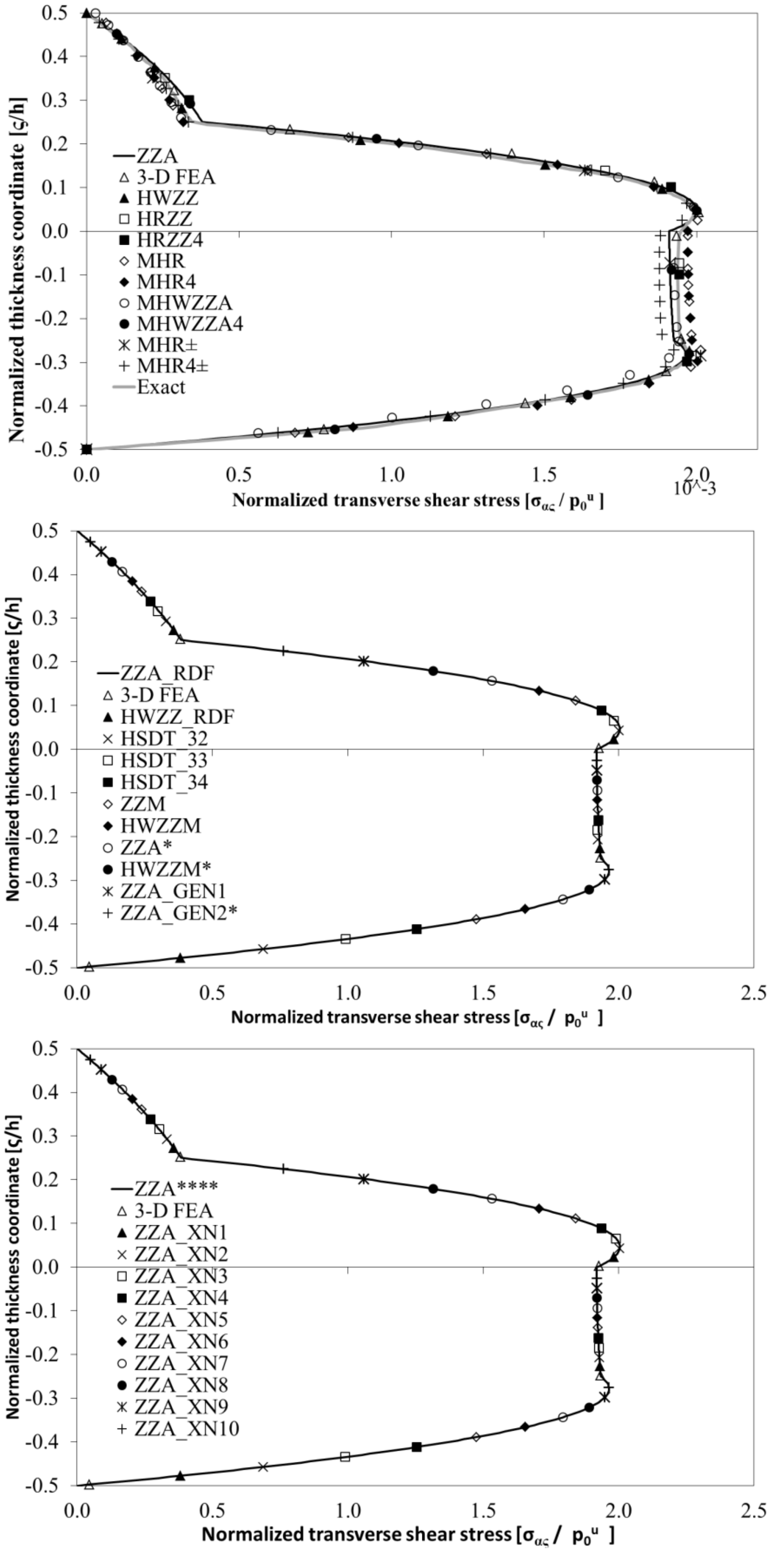

Figure 4.1c: Transverse shear stress

A greater dispersion of results is shown for transverse displacement and all lower order theories make error (both physically and kinematic-based ones, such as MHR, MHR4, MHR±, MHR4±, MHWZZA, MHWZZA4, HRZZ, HRZZ4, HSDT_32 and HSDT_33). Despite this, all theories of chapters 2 and 3 are able to predict accurate stresses, as shown in Figure 4.1c.

Results of 3-D FEA are very close to exact solution, so, it is demonstrated that it can be used as reference if it is not available. Moreover, it is confirmed that all theories of chapters 2 and 3, whose coefficients are redefined for each layer across the thickness and that impose the full set of physical constraints of ZZA (1.15)-(1.20) always provide precise results (very close to reference solutions). These are also indistinguishable from each other (differences are lower than 0.5%), regardless zig-zag or representation functions used (zig-zag functions can be also omitted). Anyway, more benchmarks have to be analysed because this case is not probative about accuracy of models, because layerwise effects are not too strong.

4.2 Case b

A simply-supported laminated beam under a sinusoidal loading, previously studied by Groh and Weaver [45] is analysed, whose length-to-thickness ratio is 8. This case is interesting, because, nevertheless it is not extremely thick, Murakami's rule is not respected, because slope of displacements does not reverse at each interfaces. So, differently to the previous case, MHR and MHR4 appear very inaccurate. Figure 4.2 reports the through-the-thickness variation of displacements and transverse shear stress, for which the following normalizations are assumed:

$$\overline{u_\alpha} = \frac{u_\alpha(0,\varsigma)}{hp^0} \quad \overline{u_\varsigma} = \frac{u_\varsigma\left(\frac{L_\alpha}{2},\varsigma\right)}{hp^0} \quad \overline{\sigma_{\alpha\varsigma}} = \frac{\sigma_{\alpha\varsigma}(L_\alpha,\varsigma)}{p^0} \tag{4.2}$$

while in-plane ad transverse normal stresses are reported in Appendix 1. For this case HSDT_32 is not reported because it provides very inaccurate results.

Regarding in-plane displacement (Figure 4.2a), all theories with the only exception of MHR and MHR4 are able to reproduce it with very low percentage errors. Anyway, results of MHR± and MHR4±, which calculate Murakami's sign on physical basis appear accurate and also MHWZZA and MHWZZA4, which assume strains and displacements of HWZZ and whose results are post-processed using ZZA, appear adequate. So, results by [45] are confirmed. Similar findings also apply to transverse displacement (Figure 4.2b), where results by MHR and MHR4 are not reported being too wrong. Regarding this latter quantity, percentage errors made by HRZZ, HRZZ4, MHWZZA, MHR±, MHR4± and HSDT_32 are greater than those provided by other quantities. However, all theories are able to get an accurate description of transverse shear stress (Figure 4.2c). Anyway, an accurate description of transverse deformability is mandatory to get precise results if there are strong layerwise effects (see case e), otherwise inaccurate results are obtained.

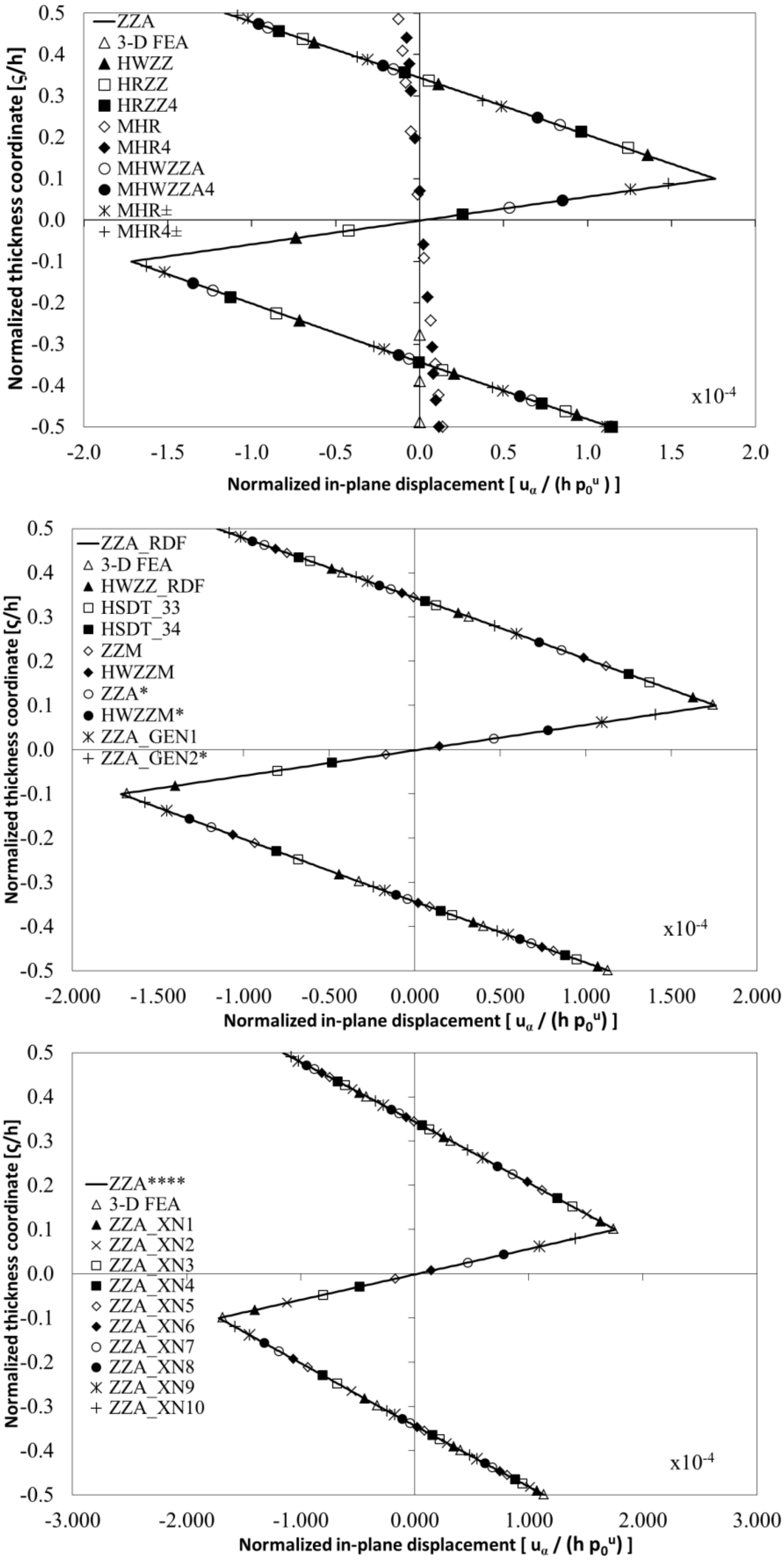

Figure 4.2a: In-plane displacement

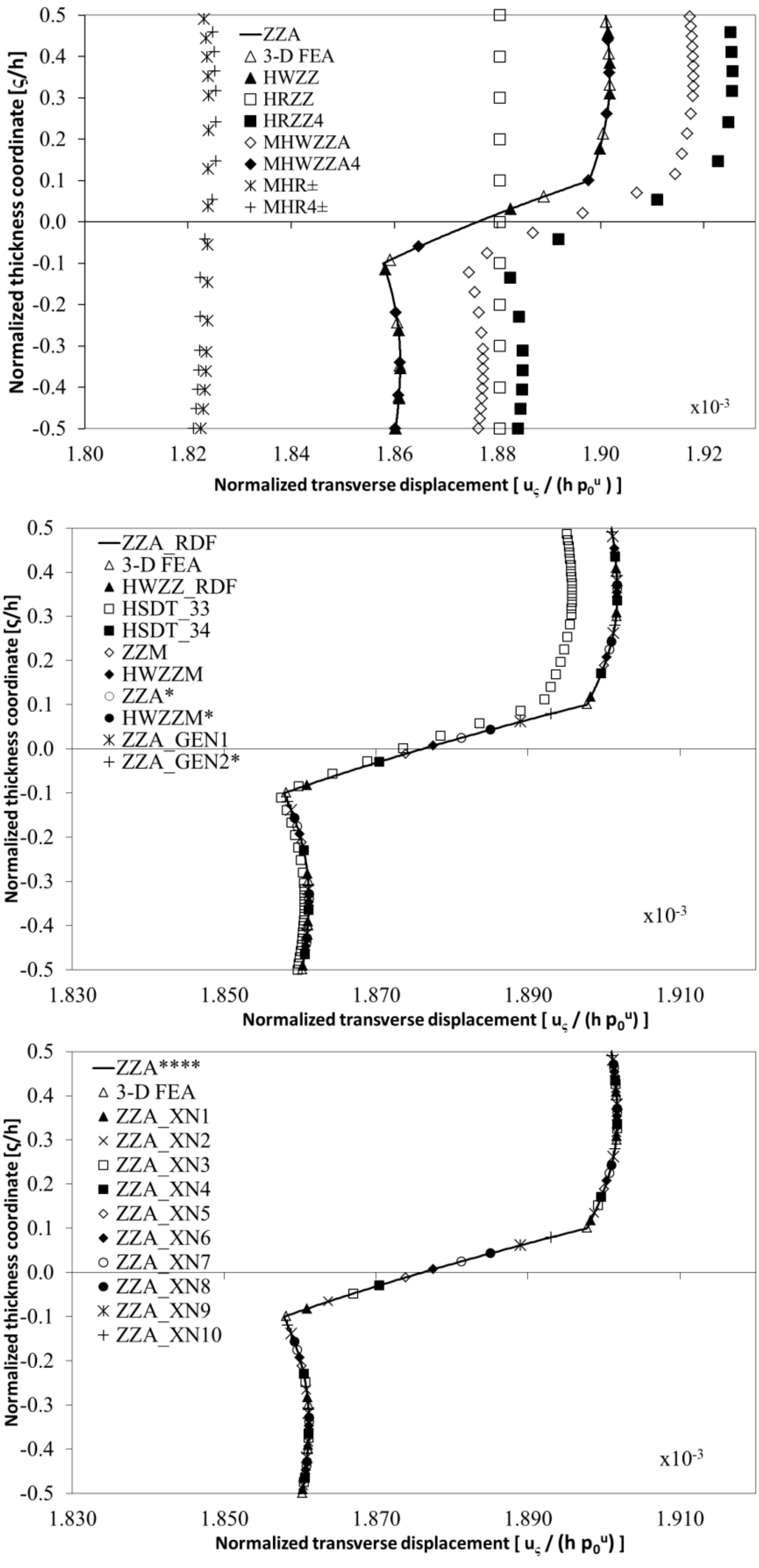

Figure 4.2b: Transverse displacement

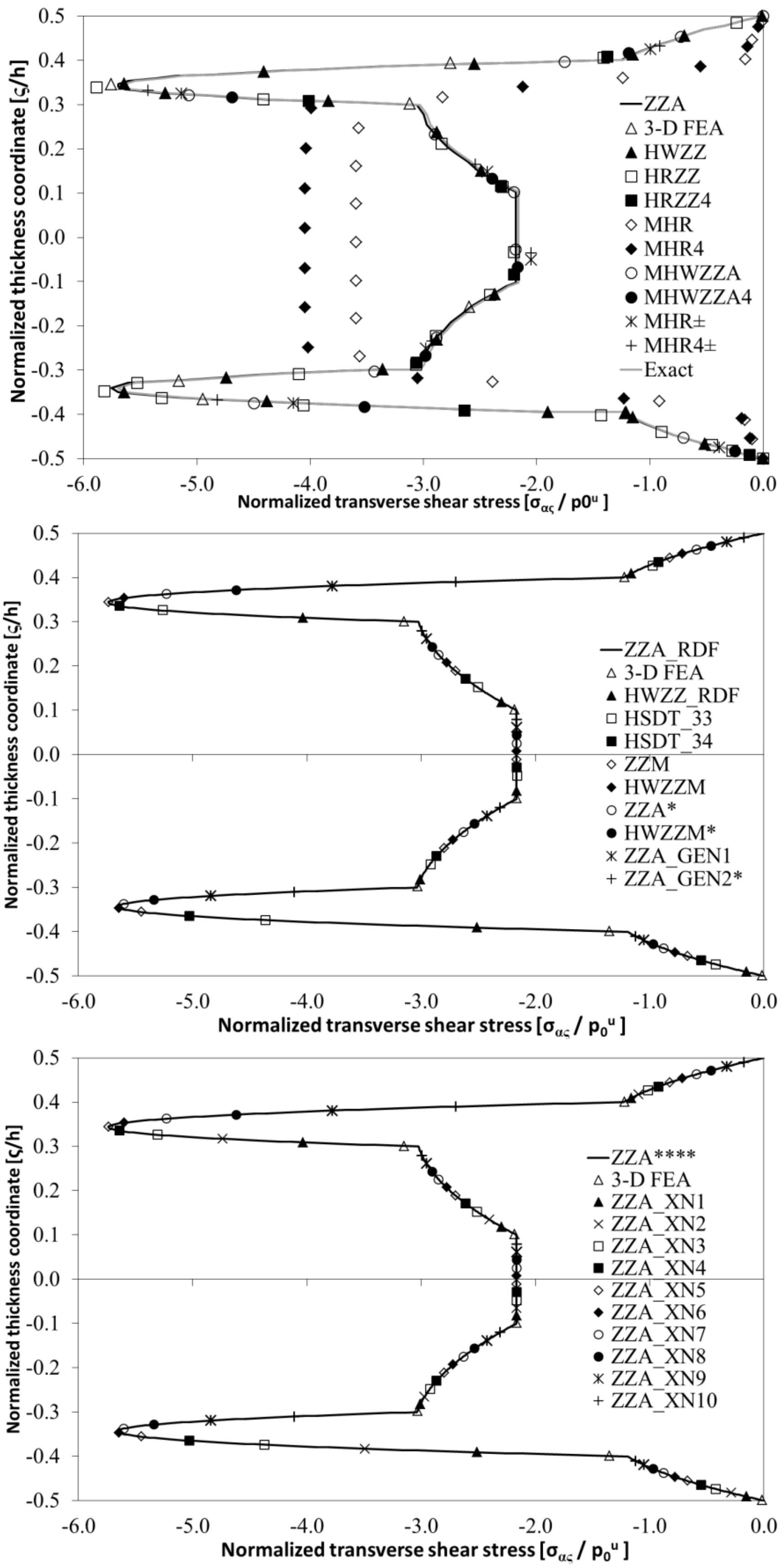

Figure 4.2c: Transverse shear stress

Again it is confirmed the high accuracy of adaptive theories obtained starting from ZZA, whose coefficients are redefined for each layer across the thickness and that impose the full set of physical constraints of ZZA (1.15)-(1.20), confirming that zig-zag functions and ones used to describe variation of displacements across the thickness can be changed without any loss of accuracy. Moreover, the role of coefficients can be freely switched and linear contribution by FSDT can be omitted, always obtaining accurate results (differences between higher-order adaptive theories are lower than 0.5%). In the next two sections two simply-supported sandwich plates will be analyzed, which have mild-layerwise effects.

4.3 Case c

A simply-supported rectangular soft-core sandwich plate (length-to-thickness and length-to-side ratios are 4 and 3 respectively) under a bi-sinusoidal loading is analysed. This case is retaken from [80] where u_α, u_ς, $\sigma_{\alpha\alpha}$ and out-of-plane stresses are reported in Figures 4.3 using the following normalizations:

$$\overline{u_\alpha} = \frac{E_{1\_core}\, h^2\, u_\alpha\left(0,\dfrac{L_\beta}{2},\varsigma\right)}{L_x^3\, p^0} \quad \overline{u_\varsigma} = \frac{u_\varsigma\left(\dfrac{L_\alpha}{2},\dfrac{L_\beta}{2},\varsigma\right)}{hp^0} \quad \overline{\sigma_{\alpha\alpha}} = \frac{\sigma_{\alpha\alpha}\left(\dfrac{L_\alpha}{2},\dfrac{L_\beta}{2},\varsigma\right)}{\left(L_\alpha / h\right)^2 p^0} \tag{4.3}$$

$$\overline{\sigma_{\alpha\varsigma}} = \frac{\sigma_{\alpha\varsigma}\left(0,\dfrac{L_\beta}{2},\varsigma\right)}{\left(L_\alpha / h\right) p^0} \quad \overline{\sigma_{\beta\varsigma}} = \frac{\sigma_{\beta\varsigma}\left(\dfrac{L_\alpha}{2},0,\varsigma\right)}{p^0} \quad \overline{\sigma_{\varsigma\varsigma}} = \frac{\sigma_{\varsigma\varsigma}\left(\dfrac{L_\alpha}{2},\dfrac{L_\beta}{2},\varsigma\right)}{p^0}$$

Other quantities are reported in Appendix 1. The bottom face has a lower thickness and it is made of stiffer material than the upper ones; as a consequence of these geometrical and material asymmetries, layerwise effects rise, so a greater dispersion of results is shown in Figures 4.3 than previous cases. Regarding in-plane displacement reported in Figure 4.3a (Murakami's rule is not respected), all lower-order theories expect MHWZZA4 cannot achieve the accuracy of higher-order adaptive models (ZZA, HWZZ, ZZA_RDF, HWZZ_RDF, HSDT_34, ZZM, HWZZM, ZZA*, HWZZM*, ZZA_GEN1, ZZA_GEN2*, ZZA****, ZZA_XN1 to ZZA_XN10). These latter theories predict results that are always in a very good agreement (discrepancies are lower than 0.5%) and always very close to 3-D FEA and exact solutions, irrespective the representation and zig-zag functions assumed (the latter can be also omitted), moreover, it is also unnecessary to assign a specific role to coefficients. So, findings of previous chapters are confirmed, whenever coefficients are redefined for each layer across the thickness and calculated by imposing the full set of physical constraints (1.15)-(1.20), otherwise results are strongly dependent by assumptions made. These findings about higher-order adaptive theories still apply for each displacements and stresses, so, they won't be repeated in this section.

A greater dispersion of results is also shown for transverse displacement (Figure 4.3b) and also MHWZZA4 is not very accurate; similar findings also apply to in-plane stress (Figure 4.3c), where high errors are provided regarding lower face. Because of this, transverse shear stresses (Figures 4.3d and 4.3e) are quite accurately predicted by all lower-order theories at upper face (with the only exception of HSDT_33), while lower-order theories are not very precise at bottom face. Nevertheless percentage errors are not very high in this case, it is confirmed what widespread in Literature that a precise description of transverse deformability is mandatory to get accurate stresses. Lower percentage errors are provided for transverse normal stress (Figure 4.3e).

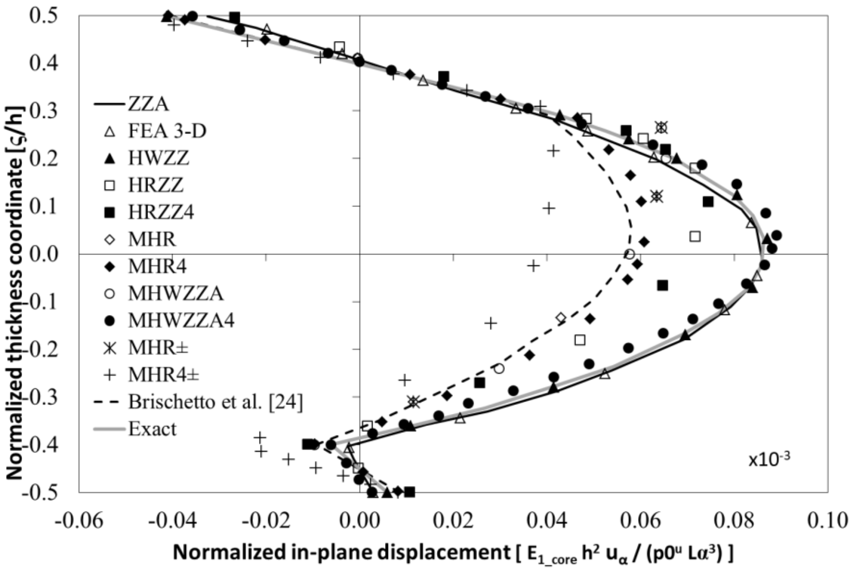

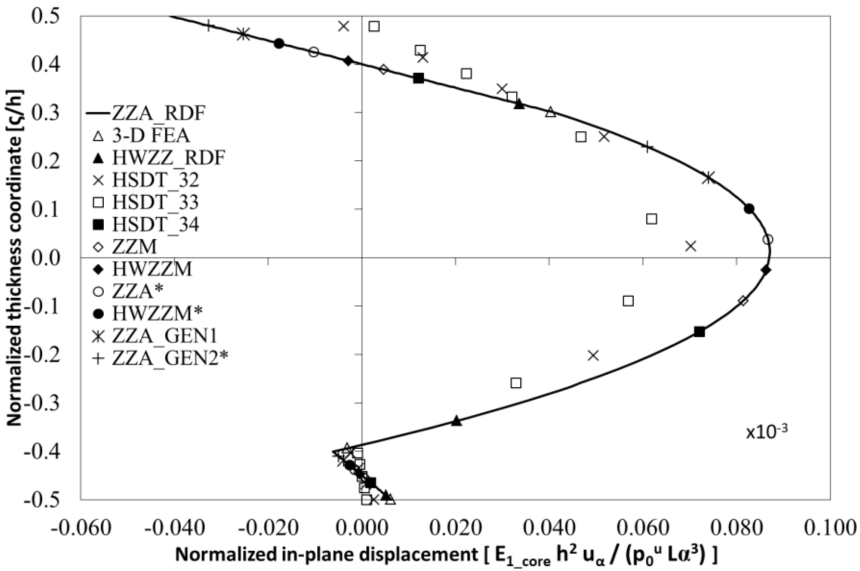

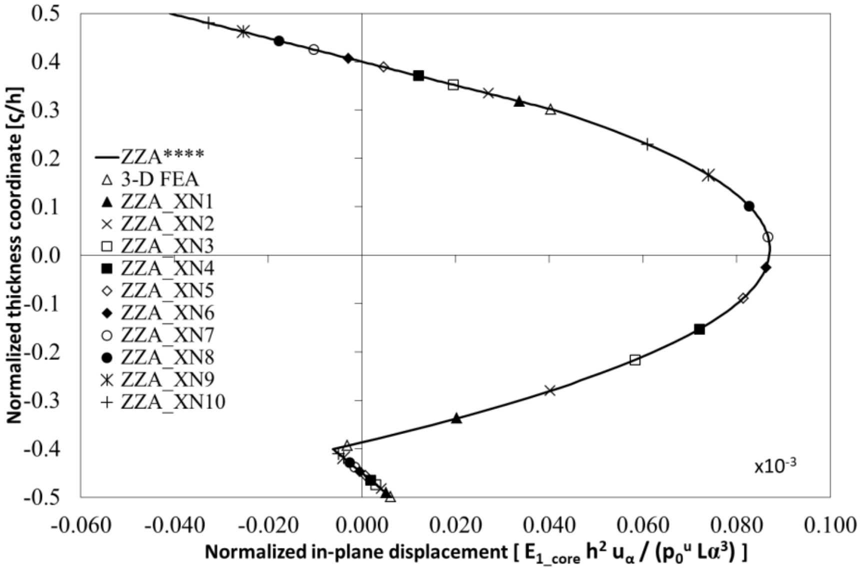

Figure 4.3a: In-plane displacement

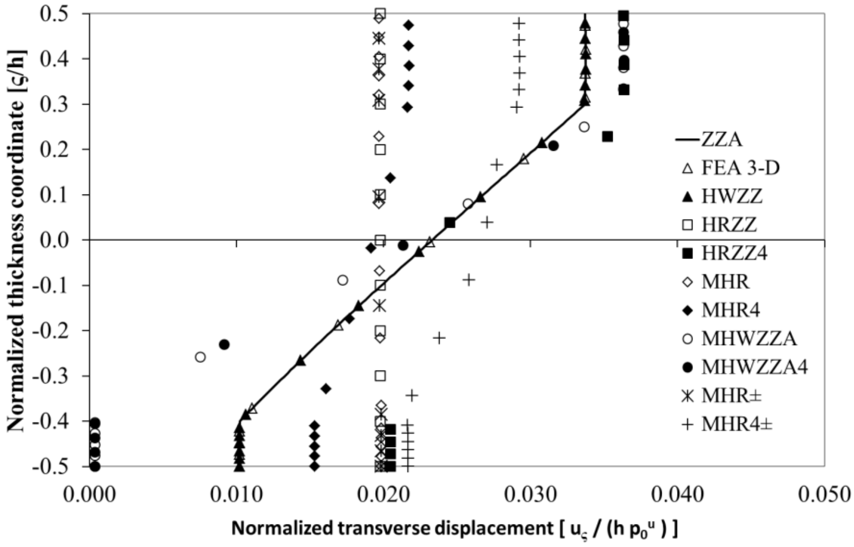

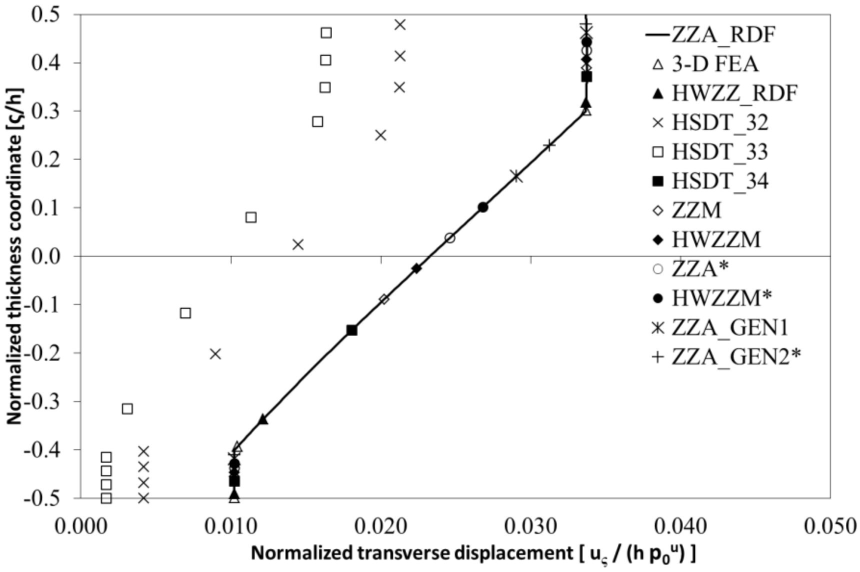

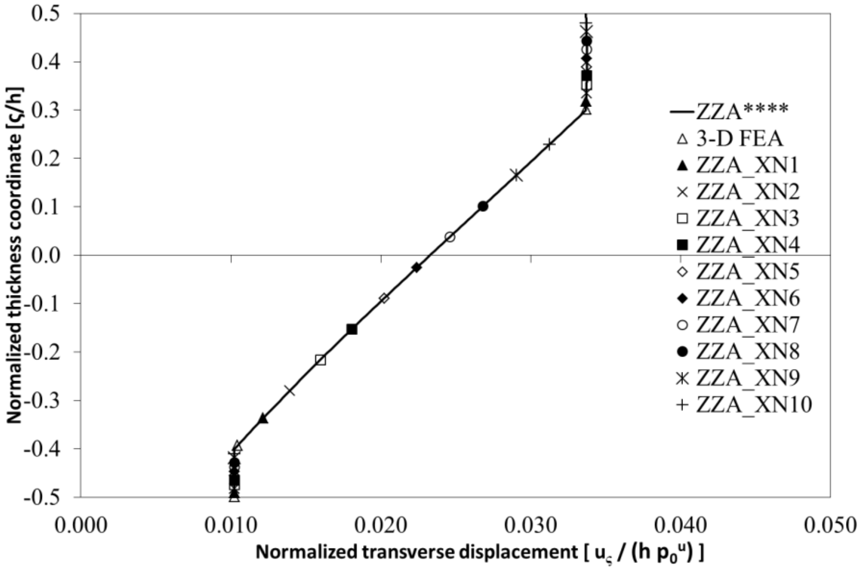

Figure 4.3b: Transverse displacement

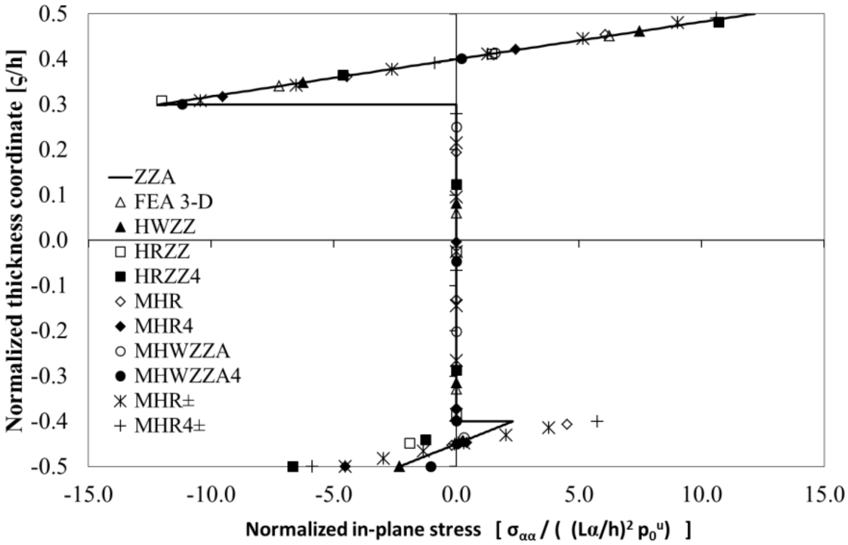

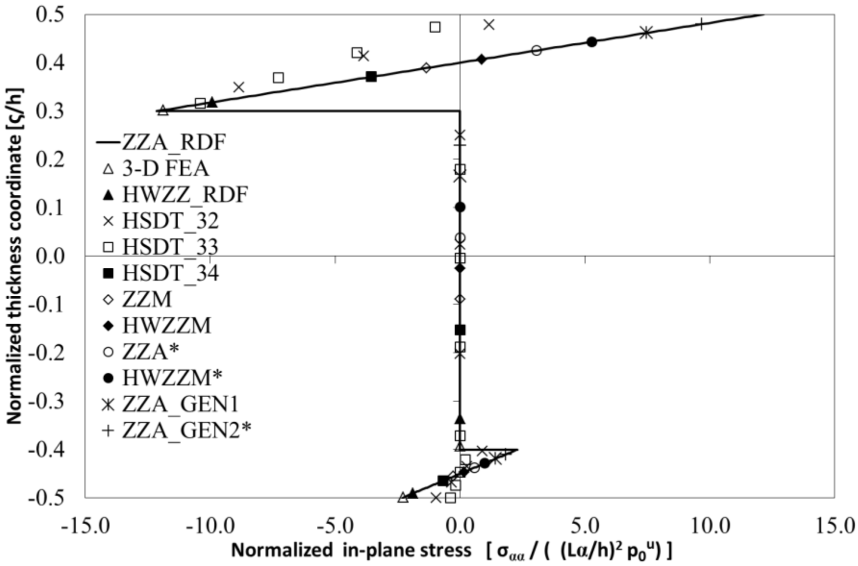

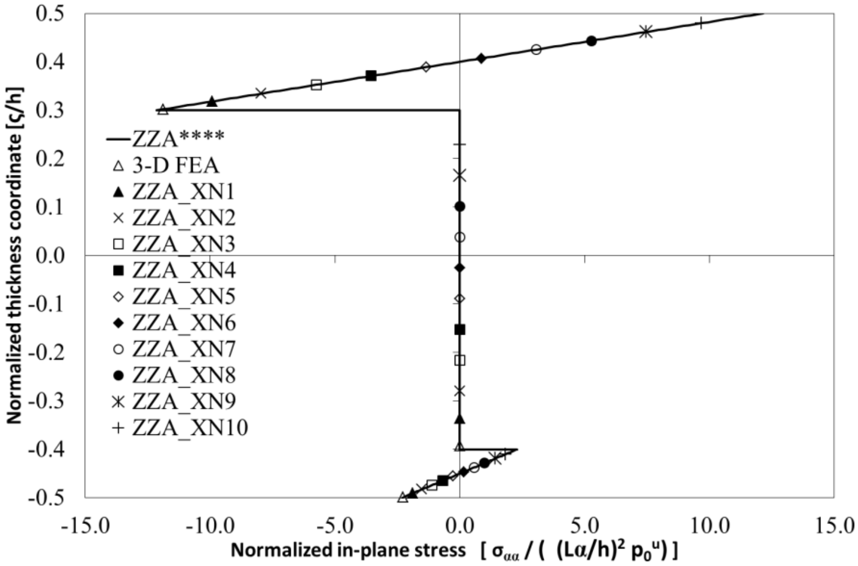

Figure 4.3c: In-plane stress

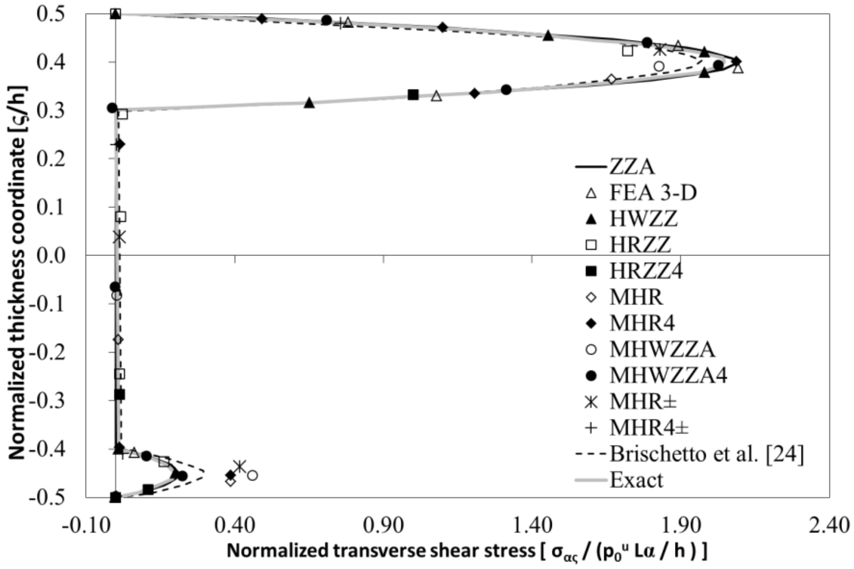

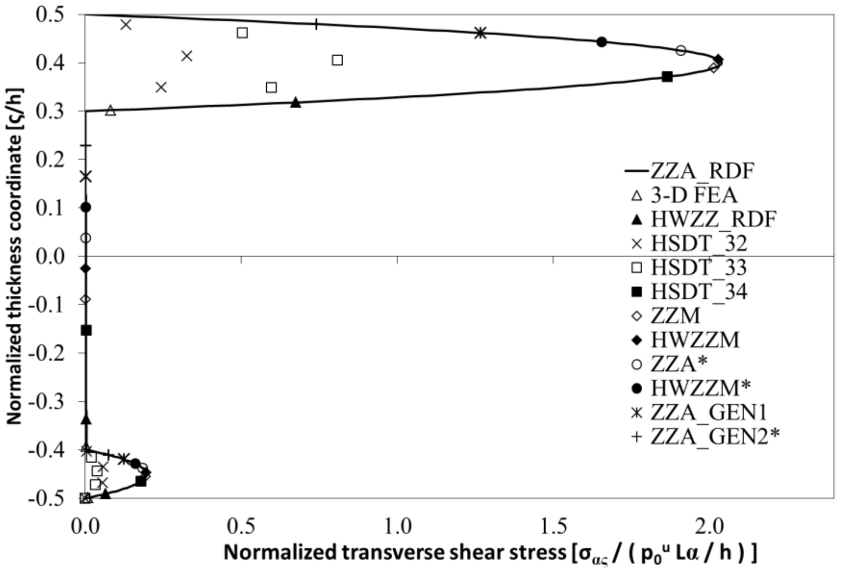

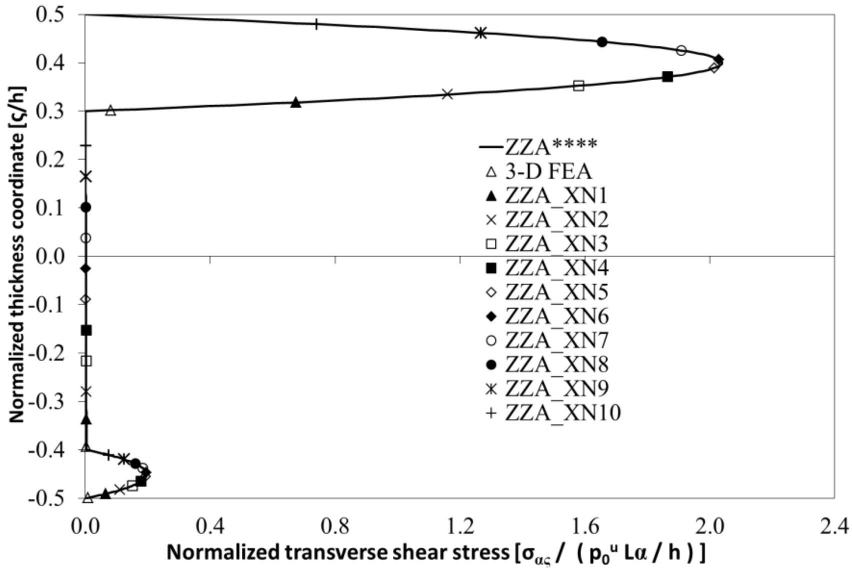

Figure 4.3d: Transverse shear stress

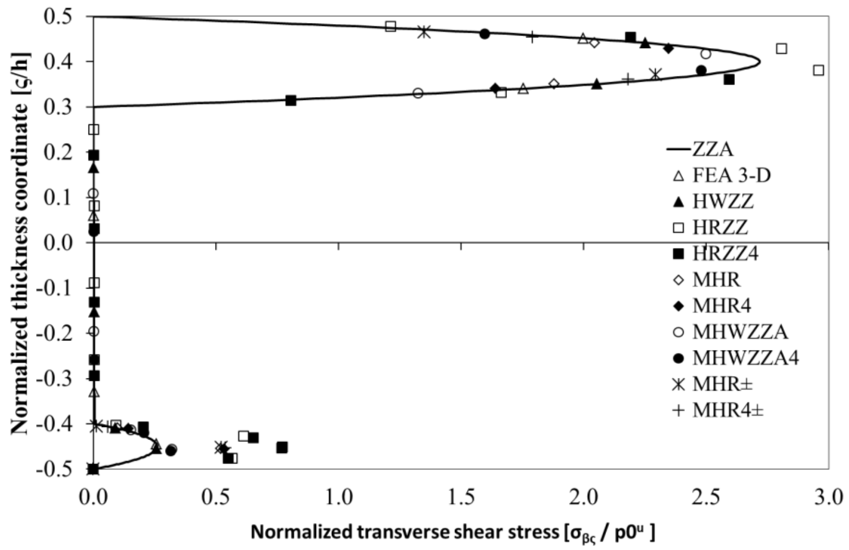

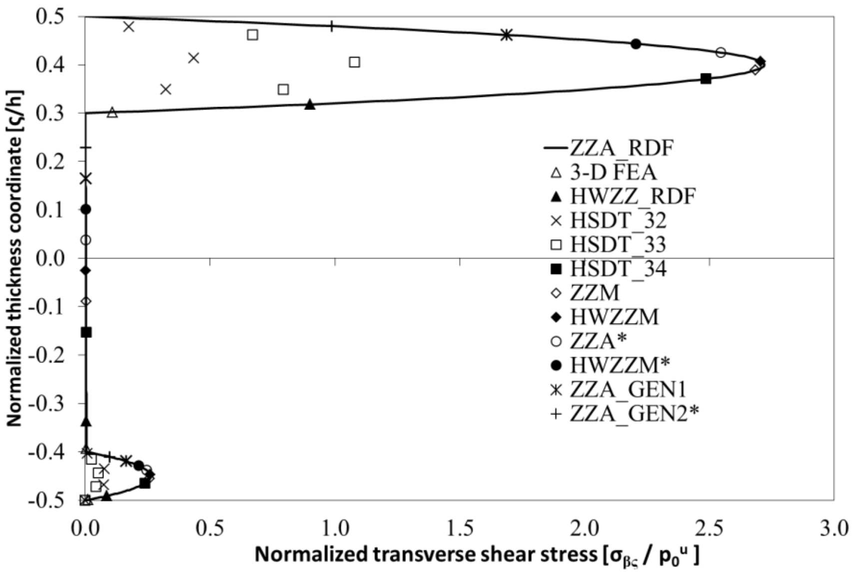

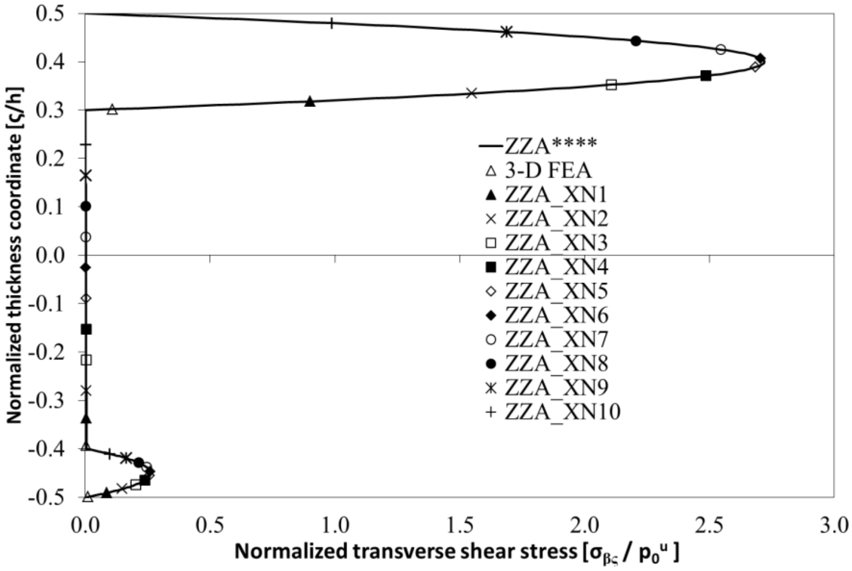

Figure 4.3e: Transverse shear stress

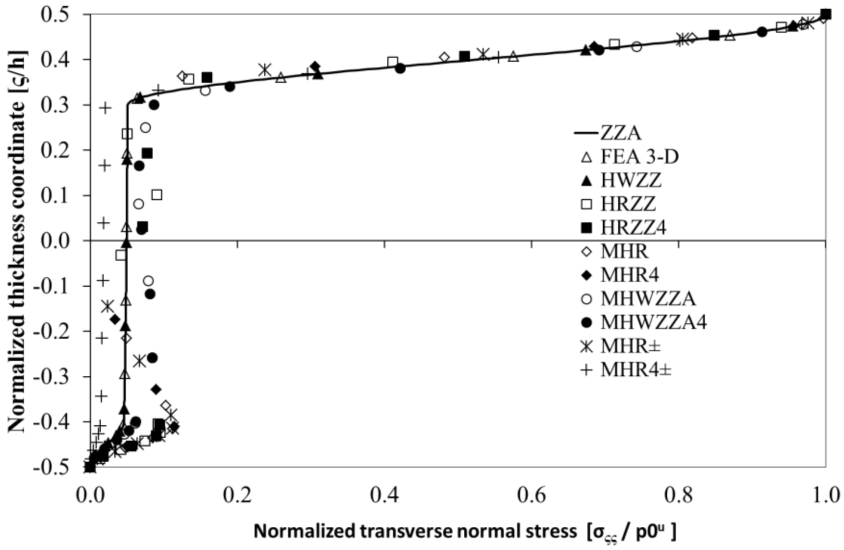

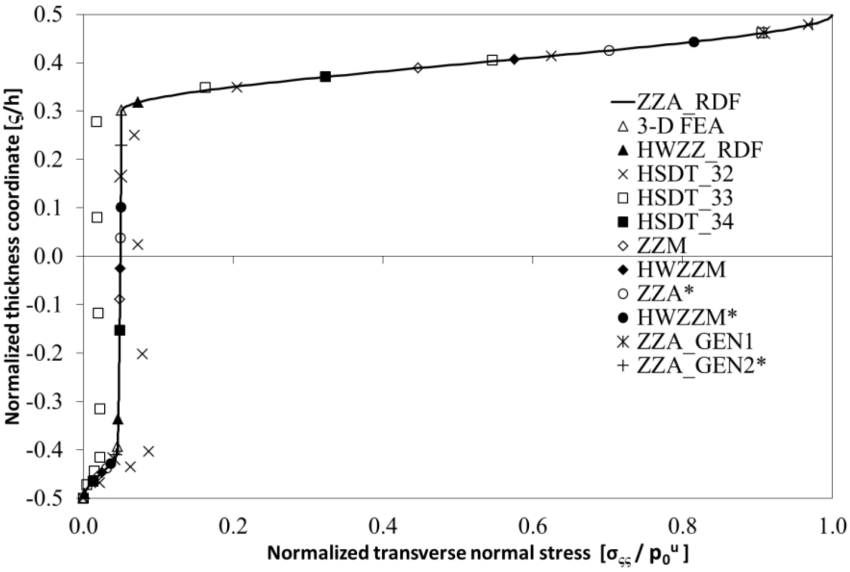

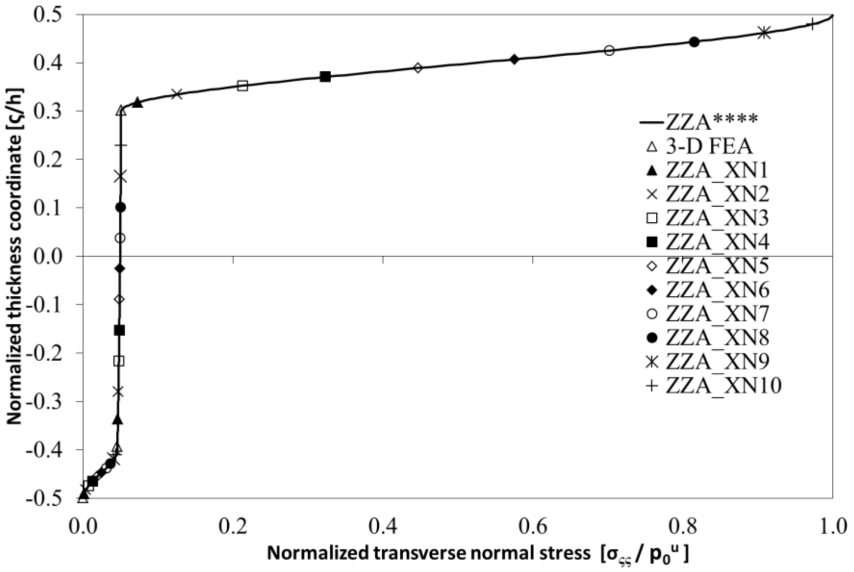

Figure 4.3f: Transverse normal stress

4.4 Case d

This case is a simply-supported square sandwich plate under a bi-sinusoidal loading and it is retaken from [81]. Length-to-thickness ratio is 10, faces are made of Graphite/Epoxy, while the soft core is made of foam. Results provided by theories of u_α, u_ς, $\sigma_{\alpha\varsigma}$ are reported in Figures 4.4 assuming the following normalizations (u_α and $\sigma_{\alpha\varsigma}$ are reported in *m* and *kPa* respectively).

$$\overline{u_\alpha} = u_\alpha\left(0, \frac{L_\beta}{2}, \varsigma\right) \quad \overline{u_\varsigma} = \frac{u_\varsigma\left(\frac{L_\alpha}{2}, \frac{L_\beta}{2}, \varsigma\right)}{hp^0} \quad \overline{\sigma_{\alpha\varsigma}} = \sigma_{\alpha\varsigma}\left(0, \frac{L_\beta}{2}, \varsigma\right) \tag{4.4}$$

Other quantities are reported in Appendix 1. This case is interesting because, nevertheless it is not extremely thick, through-the-thickness displacements and stresses cannot be obtained by simplified ESL theories. Results provided by theories are compared to LLT solution provided by [81].

In plane displacement (Figure 4.4a) is accurately predicted by all theories of this thesis (low percentage errors are provided by lower-order theories at the core), while a greater dispersion of results is obtained for transverse displacement (Figure 4.4b). Anyway, errors are not very high and as a consequence transverse shear stress (Figure 4.4c) is accurately obtained by all theories (higher percentage errors are in the core layer).

Again, higher-order adaptive theories (ZZA, HWZZ, ZZA_RDF, HWZZ_RDF, HSDT_34, ZZM, HWZZM, ZZA*, HWZZM*, ZZA_GEN1, ZZA_GEN2*, ZZA****, ZZA_XN1 to ZZA_XN10) are able to get results in a very good agreement with 3-D FEA and reference solution (LLT), so, all findings about the choice of functions that represent variation of displacements across the thickness and layerwise functions still apply. Anyway, this case is not particularly probative because 3-D effects are not very strong.

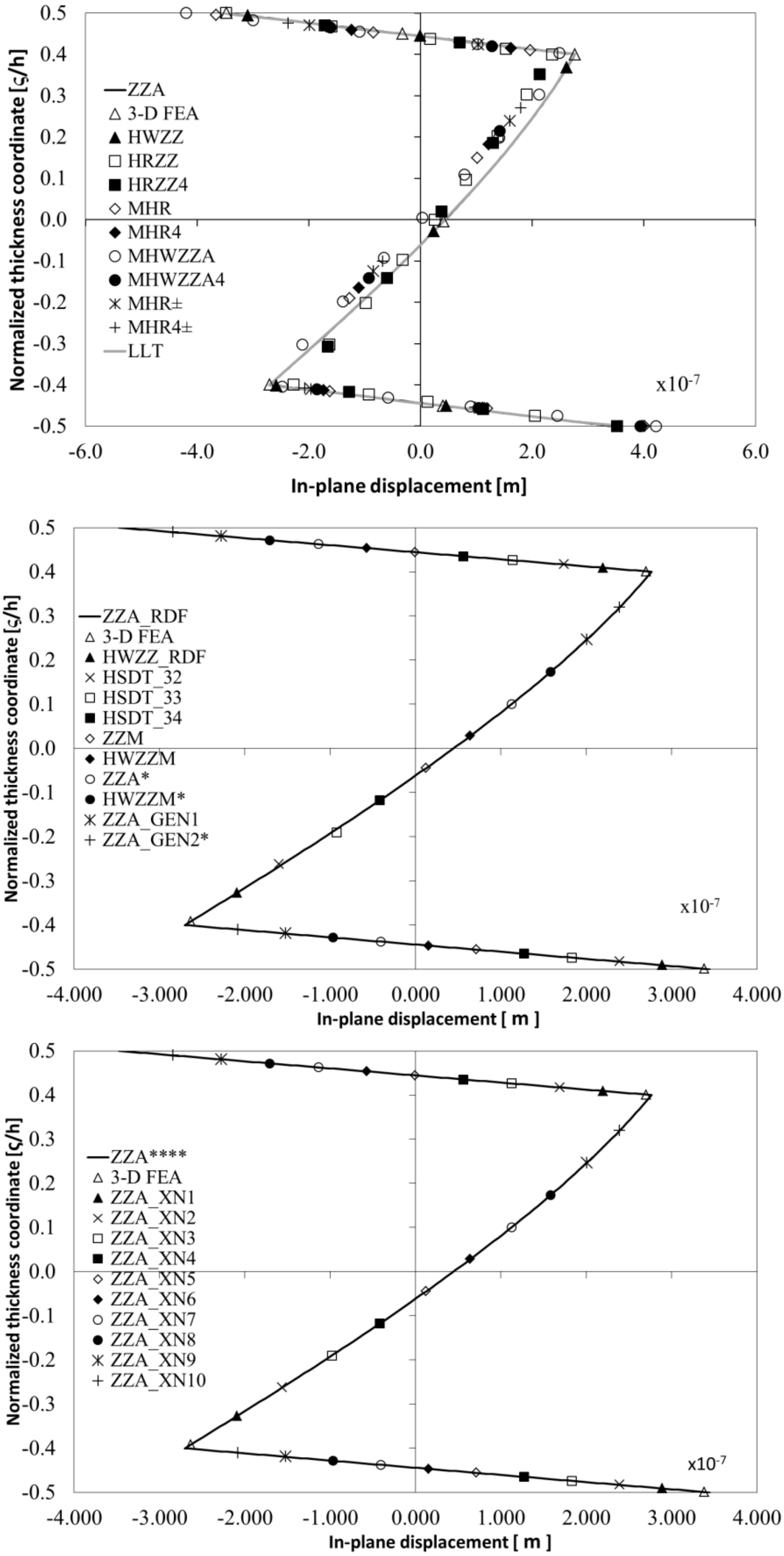

Figure 4.4a: In-plane displacement

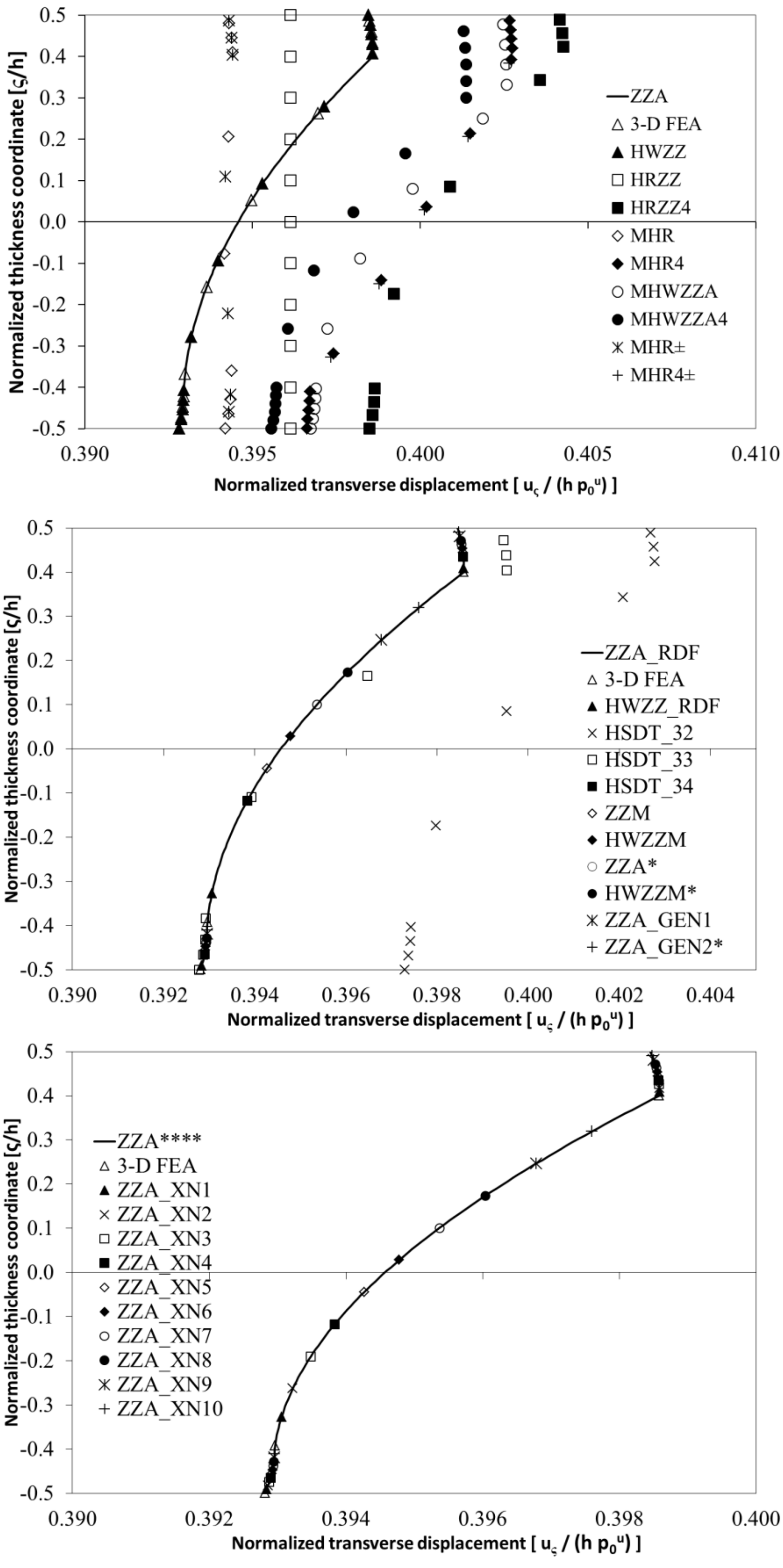

Figure 4.4b: Transverse displacement

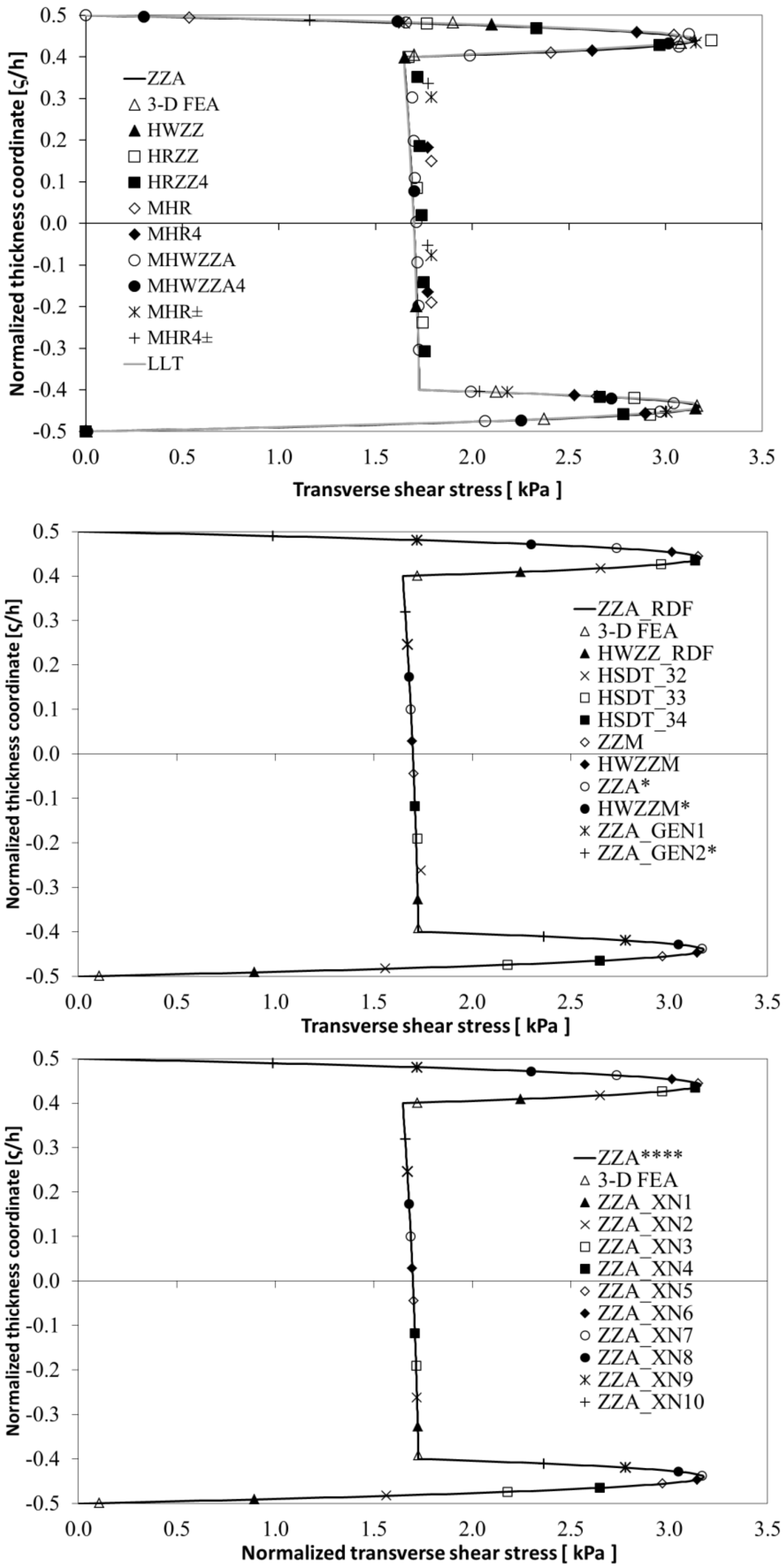

Figure 4.4c: Transverse shear stress

4.5 Cases e

A propped cantilever soft-core sandwich beam under a uniform loading, previously studied by Mattei and Bardella [71] is analyzed. Length-to-thickness ratio is assumed to be 5.714 and upper face has a thickness that is half the bottom one and it is made of a stiffer material. Beam is clamped at $\alpha = 0$, while it is restrained at $\alpha = L_\alpha$. For this case, results are compared to 3-D FEA solution and transverse displacement and transverse shear stress are reported using the following normalizations [71]:

$$\overline{u_\varsigma} = \frac{u_\varsigma(L_\alpha, \varsigma)}{hp^0} \quad \overline{\sigma_{\alpha\varsigma}} = \frac{A\sigma_{\alpha\varsigma}(L_\alpha, \varsigma)}{L_\alpha p^0} \tag{4.5}$$

Like previous benchmarks, other quantities are reported in Appendix 1. Differently to previous cases, additional mechanical boundary conditions have to be imposed regarding shear force at support and also $u_\varsigma(L_\alpha, -h/2) = 0$ have to be enforced using Lagrange multiplier method (see section 1.4). It is not necessary to impose conditions on bending moment, even if they could be enforced without any difficulty. This case is very interesting because geometrical asymmetries, uniform loading and the great differences between mechanical properties of constituent materials act jointly, strongly increasing layerwise effects. Particularly, transverse shear stress assumes different sign for each face. This latter features was noticed also for simply-supported damaged sandwiches [54], [15] and it is difficult to be captured by theories. Indeed, all lower-order theories calculate displacements and stresses with high percentage errors and HSDT_32 is not reported being too inaccurate.

Particularly, transverse displacement is inaccurately reproduced by all lower-order theories and it is underestimated by HRZZ4, MHWZZA and MHWZZA4, it is overestimated by MHR, MHR4, MHR± and MHR4±, while HSDT_33 describe a wrong trend across the core. Moreover, HRZZ, which assumes a uniform transverse displacement across the thickness, obtains the worst results, calculating a wrong null uniform u_ς. Only higher-order adaptive theories (ZZA, HWZZ, ZZA_RDF, HWZZ_RDF, HSDT_34, ZZM, HWZZM, ZZA*, HWZZM*, ZZA_GEN1, ZZA_GEN2*, ZZA****, ZZA_XN1 to ZZA_XN10) are in well agreement with 3-D FEA. A greater dispersion of results is shown also for transverse shear stress, where again lower-order theories cannot achieve the precision of higher-order ones. It should be noticed that MHR± and MHR4±, that calculate sign of Murakami's zig-zag functions on a physical basis, are not able to improve the accuracy of their counterparts (MHR and MHR4) and obtain bad results because their kinematic is too simple. HRZZ, HRZZ4, MHWZZA, MHWZZA4 and HSDT_33 calculate this quantity with lower errors but cannot achieve the same accuracy of higher-order adaptive theories (ZZA, HWZZ, ZZA_RDF, HWZZ_RDF, HSDT_34, ZZM, HWZZM, ZZA*, HWZZM*, ZZA_GEN1, ZZA_GEN2*, ZZA****, ZZA_XN1 to ZZA_XN10). This case confirms what widespread in Literature, that an accurate description of transverse deformability, like those of higher-order theories, is mandatory to get accurate results if there are strong layerwise effects.

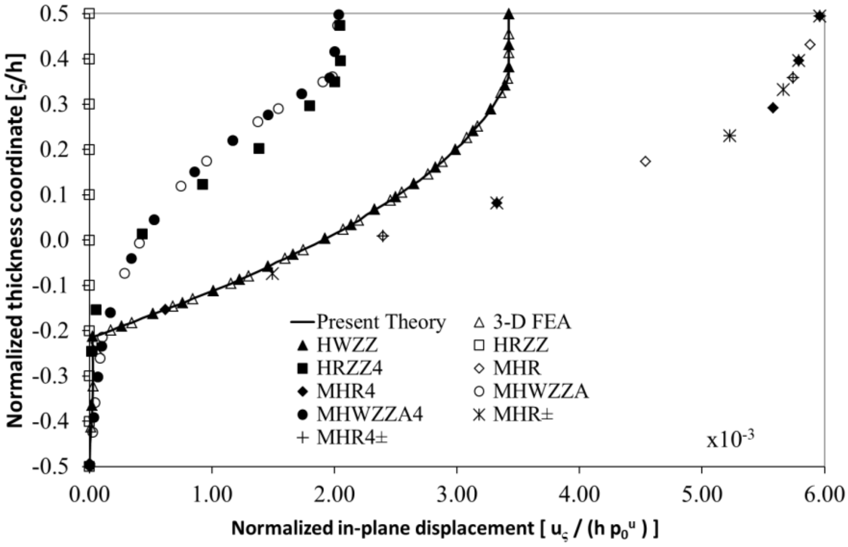

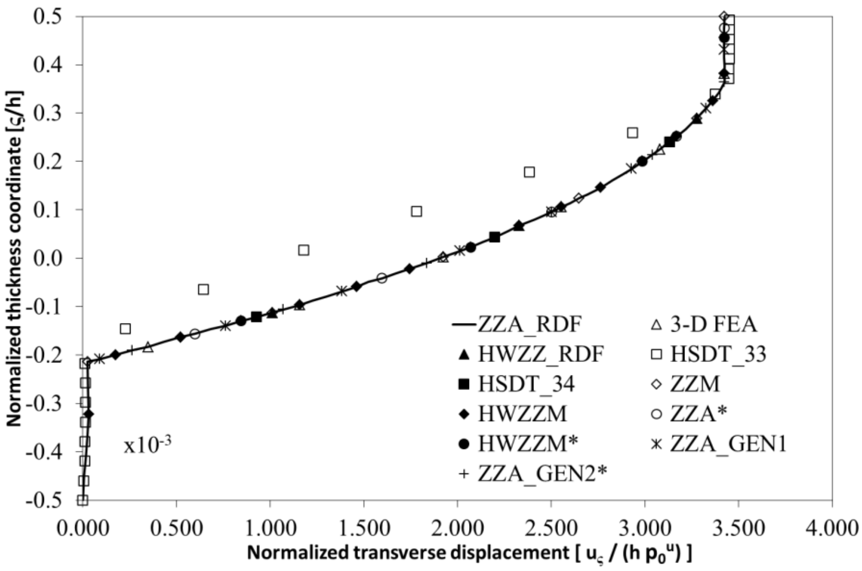

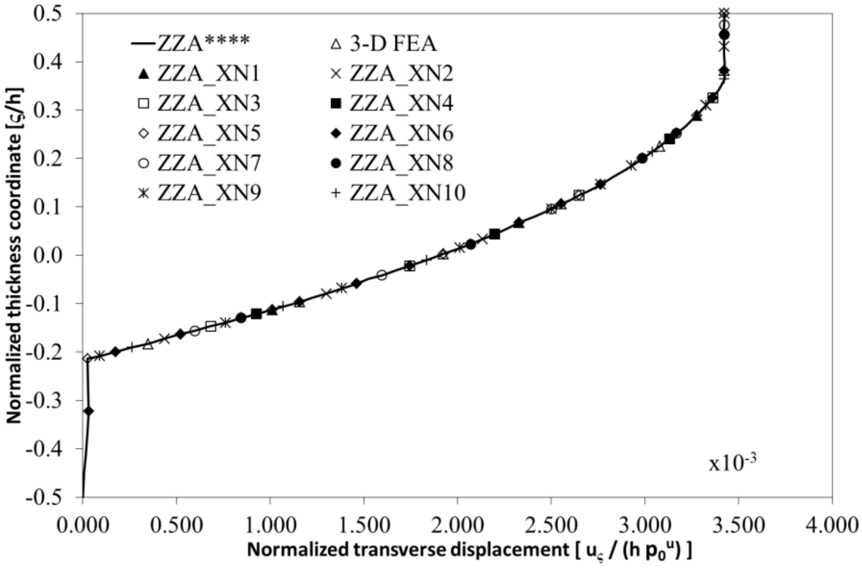

Figure 4.5a: Transverse displacement

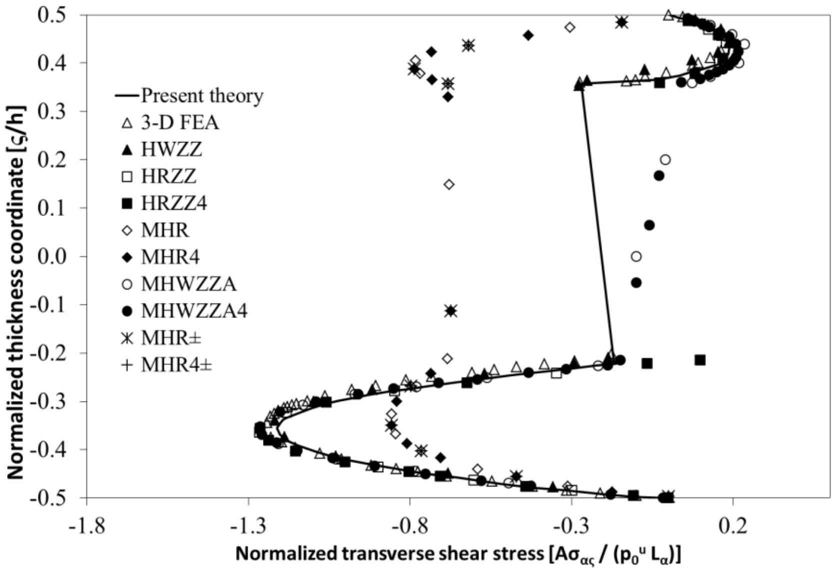

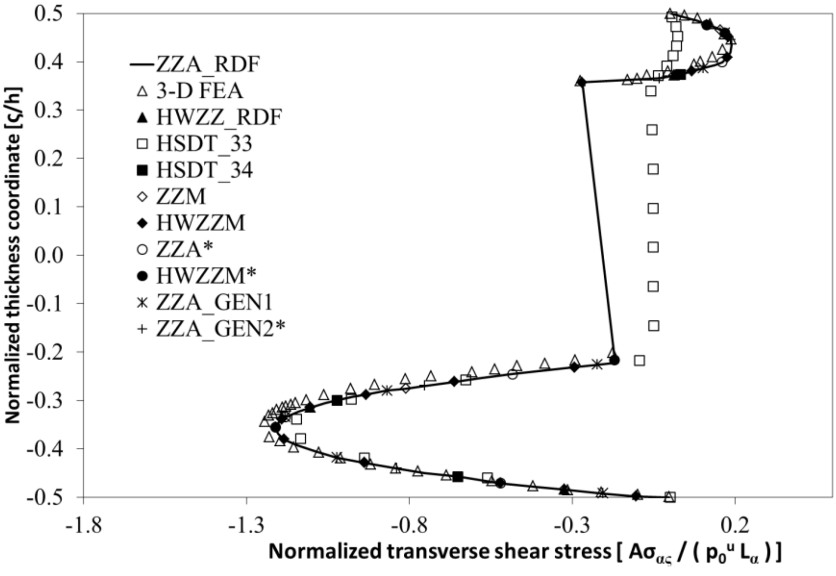

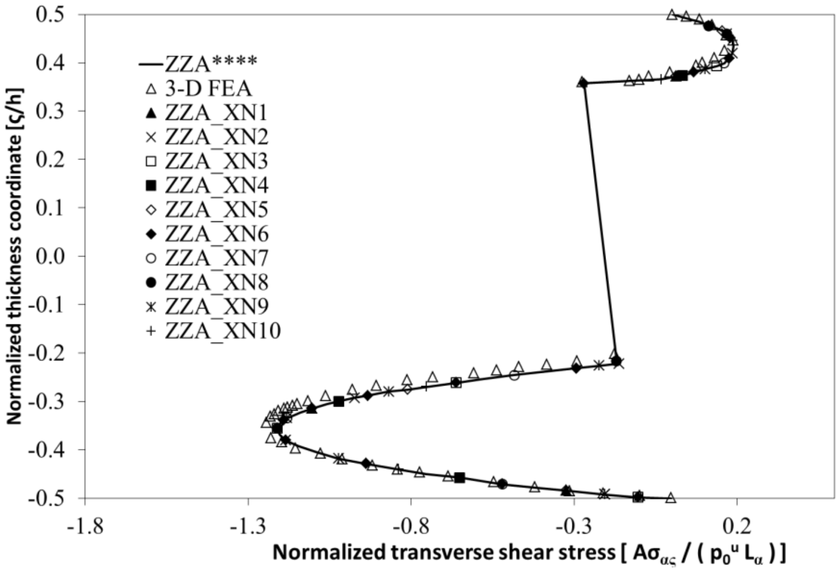

Figure 4.5b: Transverse shear stress

Lower-order theories have proven to be inaccurate for cases with strong layerwise effects and they will not be reported for the following cases.

Instead, higher-order adaptive ones, that have coefficients redefined for each layer across the thickness, that are calculated by imposing the full set of physical constraints (1.15)-(1.20) are always precise and in very good agreement with 3-D FEA or exact solutions. So, it is confirmed that:

- zig-zag functions can be changed or omitted without any loss of accuracy;
- functions that describe variation of displacements across the thickness can be changed, so, exponential, power series and sinusoidal functions, or a combination of them, can be assumed differently for each displacement and from point to point across the thickness, without any loss of accuracy;
- the role of coefficients can be freely switched;
- linear contribution by FSDT are not necessary to obtain precise displacements and stresses

Because of these theories have demonstrated their superiority and provide practically indistinguishable results, only ZZA_GEN1 and ZZA_GEN2* zig-zag theories will be reported in the following cases.

4.6 Case f

A simply-supported sandwich square plate under a bi-sinusoidal loading is analyzed and it is retaken from [15], whose the length-to-thickness ratio is 4. The bottom face has a lower thickness than the upper one and it is damaged (E_{1111} E_{1122} E_{2222} E_{1212} reduced by $1{\cdot}10^{-2}$), while soft core is partially damaged up to 0.15h from below (E_{1122} E_{2222} E_{1212} E_{1313} E_{2323} are reduced by $2{\cdot}10^{-1}$). The following normalizations are used for transverse shear stresses, while other quantities are reported in Appendix 1.

$$\overline{\sigma_{\alpha\varsigma}} = \frac{\sigma_{\alpha\varsigma}\left(0, \frac{L_\beta}{2}, \varsigma\right)}{p^o} \quad \overline{\sigma_{\beta\varsigma}} = \frac{\sigma_{\beta\varsigma}\left(\frac{L_\alpha}{2}, 0, \varsigma\right)}{p^o} \tag{4.6}$$

Because of damage and geometrical asymmetries, strong 3-D effects rise and an opposite sign of stresses is assumed at each face. As a result, lower-order theories cannot achieve the same accuracy of higher-order adaptive ones [15] whose coefficients are redefined for each layer across the thickness and calculated by imposing the full set of physical constraints by ZZA. These theories are always able to reproduce displacements and stresses with very high precision (see [15] and Figure 4.6a) irrespective the lay-up, loading and boundary conditions and the choices of zig-zag and global representation functions.

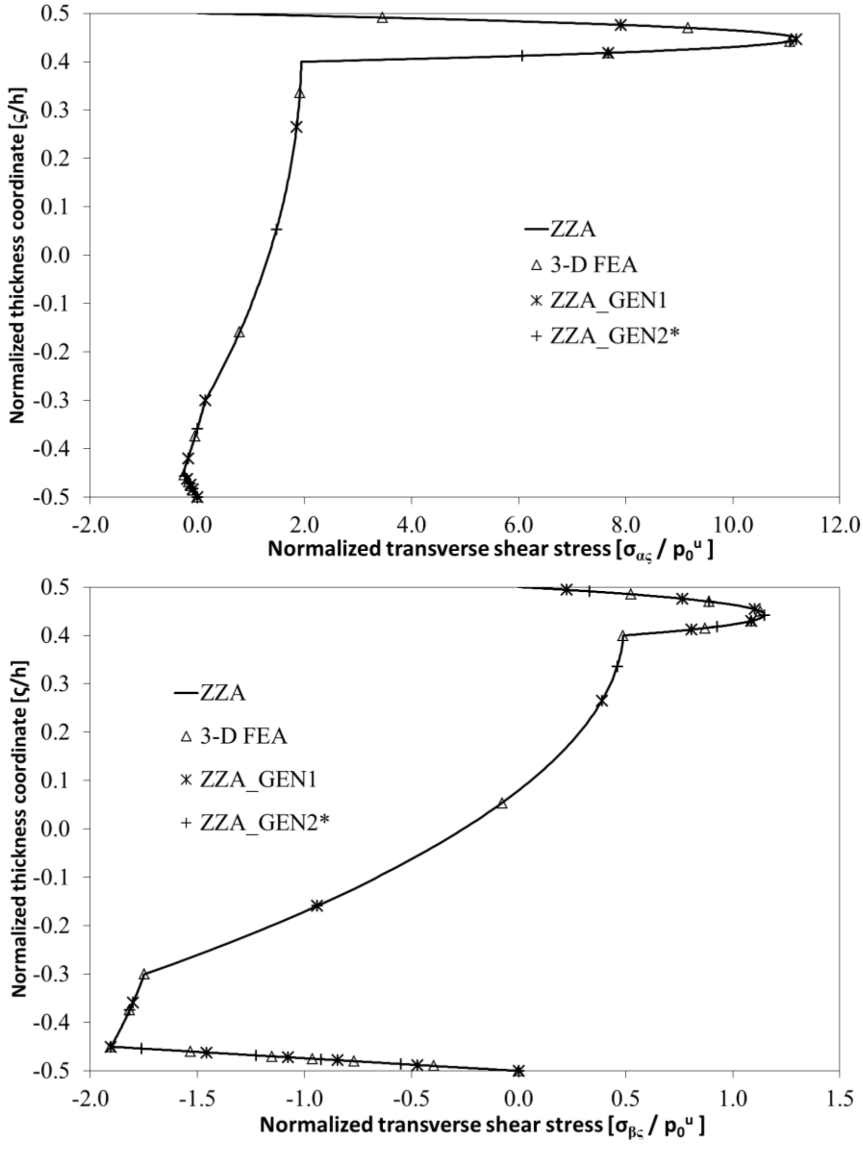

Figure 4.6a: Transverse shear stresses, case f

4.7 Cases g to j

Four simply-supported sandwich laminates under non-classical loading are analyzed, which are retaken from [15]. Like the previous case, only ZZA_GEN1 and ZZA_GEN2* are reported in Figures 4.7.

Regarding case g, it is a simply-supported sandwich beam under a sinusoidal loading (two half-waves). The length-to-thickness ratio is 10 and the same lay-up of parent case d is assumed. For this case, results of in-plane displacement and transverse shear stress are reported in Figure 4.7a (other quantities in Appendix 1) and the following normalizations are assumed:

$$\overline{u_{\alpha}}=\frac{u_{\alpha}\left(0,\varsigma\right)}{hp^{o}}\quad \overline{\sigma_{\alpha\varsigma}}=\frac{\sigma_{\alpha\varsigma}\left(0,\varsigma\right)}{p^{o}} \tag{4.7}$$

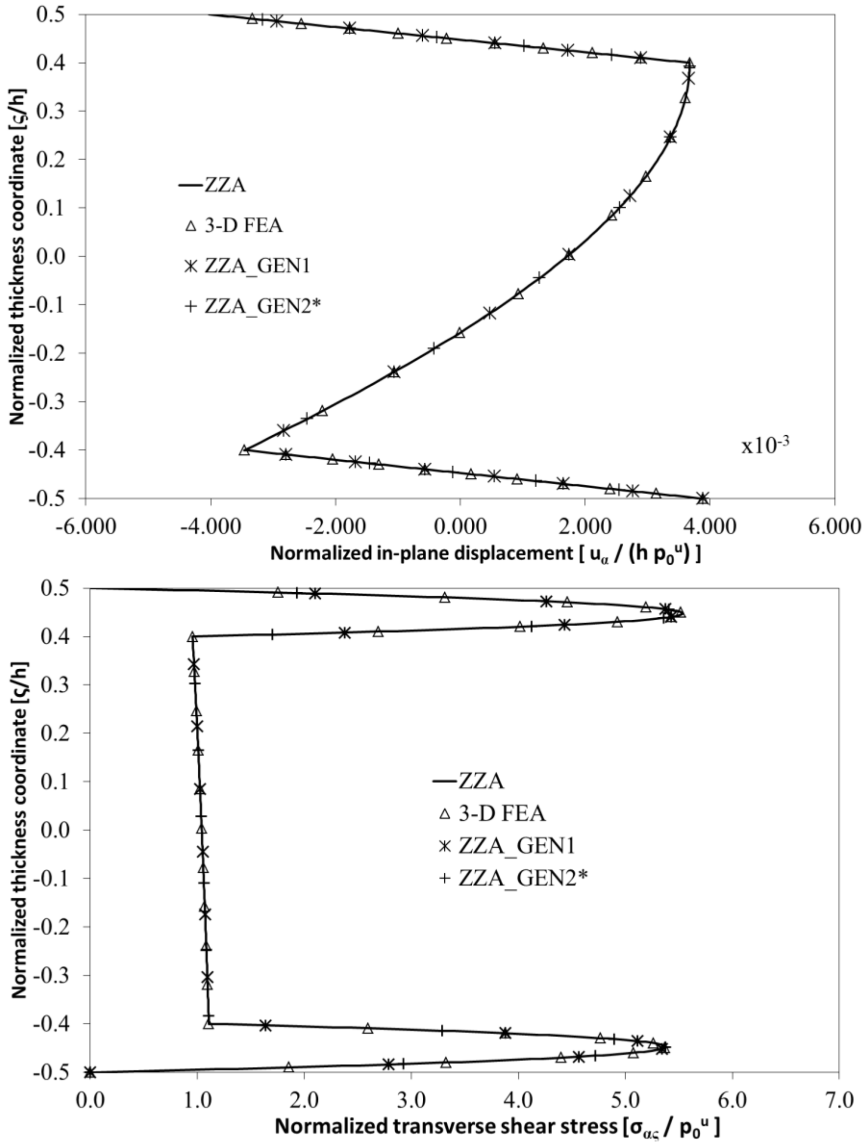

Figure 4.7a: In-plane displacement and transverse shear stress, case g

Differently to case d, because of the effect of loading, 3-D effects rise and lower-order theories calculate displacements and stresses with higher percentage errors respect to 3-D FEA, used as reference, while higher-order zig-zag adaptive theories are again accurate [15].

Anyway, very strong layerwise effects are shown in the following cases because of the application of localized step loading. For the following cases h to j, a further mechanical boundary condition on transverse shear stress have to be imposed using Lagrange multiplier method (section 1.4), in order to improve accuracy. Similarly to case e, there is no need to impose further conditions on bending moment, because numerical experiment have shown that this does not affect accuracy for these cases.

Regarding case h, an eleven-layer sandwich beam with a length-to-thickness ratio of 4 under a uniform step loading that is applied on the upper layer at $0 \le \alpha < L_\alpha / 2$ and on the bottom one at $L_\alpha / 2 \le \alpha \le L_\alpha$ with an opposite sign is analyzed. Each face is laminated (five layers) and made of materials whose features are described in section 1.7.1. Results of transverse displacement and transverse shear stress (other quantities in Appendix 1) are reported in Figure 4.7b and normalized as:

$$\overline{u_\varsigma} = \frac{u_\varsigma\left(\frac{L_\alpha}{2}, \varsigma\right)}{hp^o} \quad \overline{\sigma_{\alpha\varsigma}} = \frac{\sigma_{\alpha\varsigma}\left(0, \varsigma\right)}{p^o} \tag{4.8}$$

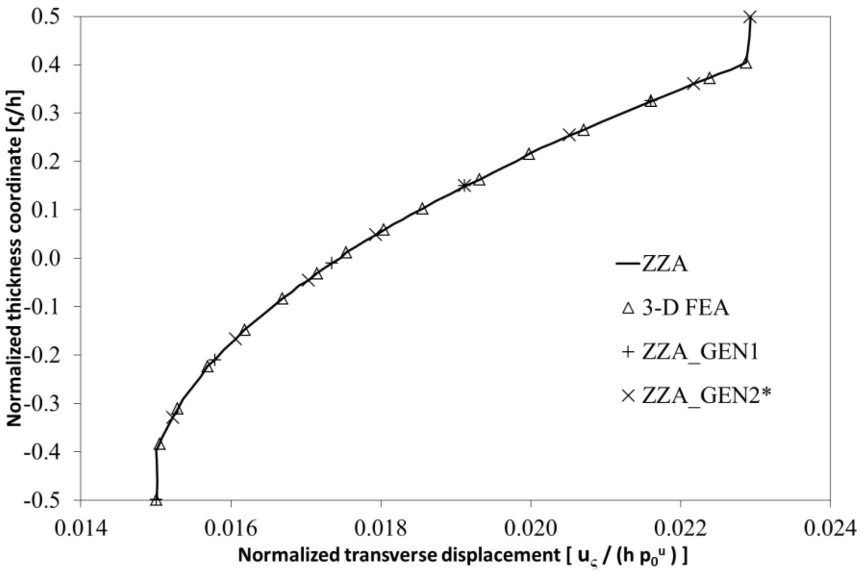

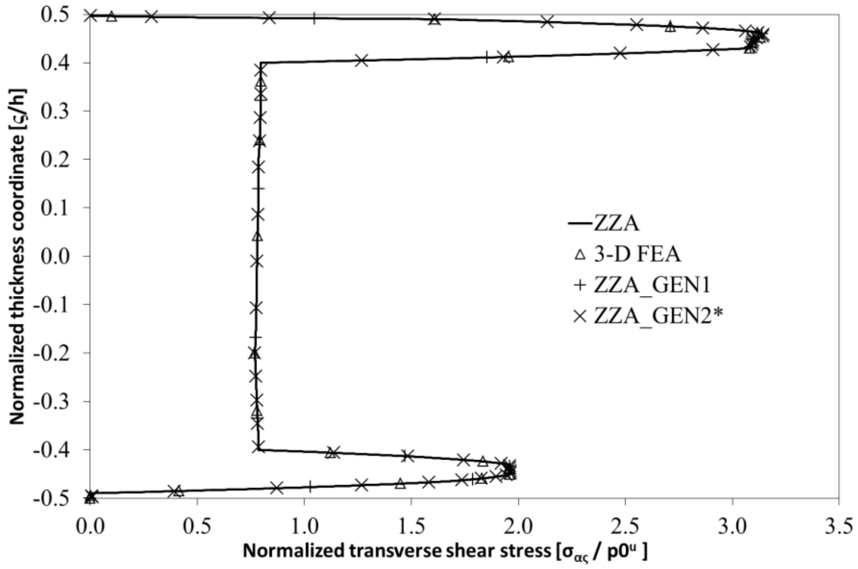

Figure 4.7b: Transverse displacement and transverse shear stress, case h

Localized step loading strongly increase layerwise effects, indeed displacements and stresses assume strongly asymmetric trends across the thickness. As a result, a great dispersion of results is showed by lower-order theories, especially by kinematic-based ones, because the Murakami's rule is not respected [15]. Again, only higher-order adaptive theories are very accurate and very close to reference results.

Case i is a simply-supported sandwich beam with a length-to-thickness ratio of 5.714 under a uniform step loading that is applied on the upper layer at $L_\alpha/8 \le \alpha < 3L_\alpha/8$ and on the bottom layer at $5L_\alpha/8 \le \alpha \le 7L_\alpha/8$ with an opposite sign. The same materials and lay-up of case e are assumed, but core (E_{1122} E_{2222} E_{1212} E_{1313} E_{2323} are reduced by $1\cdot10^{-1}$) and upper face (E_{1111} E_{1122} E_{2222} E_{1212} reduced by $4\cdot10^{-2}$) are damaged. In-plane and transverse shear stresses (other quantities in Appendix 1) are reported in Figure 4.7c and normalized as:

$$\overline{\sigma_{\alpha\alpha}} = \frac{\sigma_{\alpha\alpha}\left(L_\alpha/4,\varsigma\right)}{p^o(L_\alpha/h)^2} \quad \overline{\sigma_{\alpha\varsigma}} = \frac{\sigma_{\alpha\varsigma}\left(0,\varsigma\right)}{p^o} \tag{4.9}$$

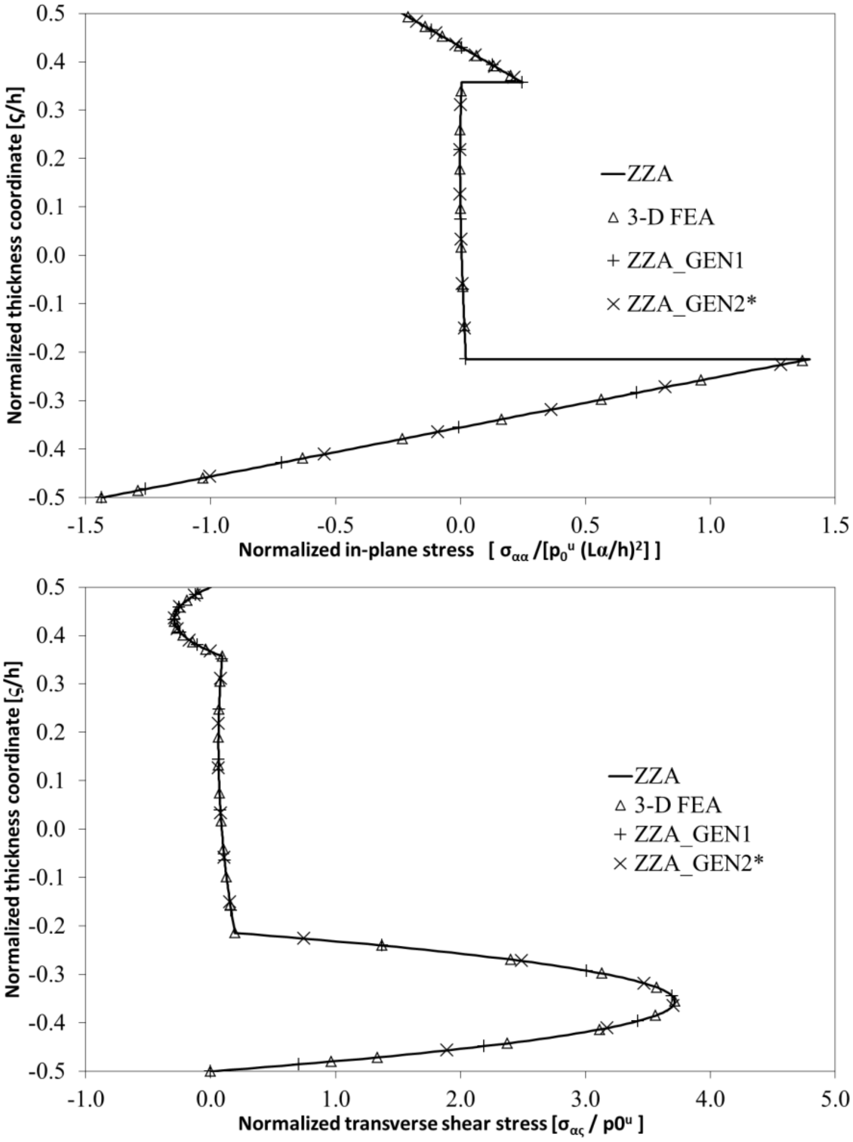

Figure 4.7c: In-plane stress and transverse shear stress, case i

Because of lay-up and localized step loading, strong 3-D effects rise and displacements and stresses assume very asymmetric behavior across the thickness. Similarly to case e, transverse shear stress assumes a different sign for each face that is difficult to be described by theories. Similarly to the previous cases of this section, lower-order theories cannot reach the accuracy of higher-order adaptive ones [15], the only always very close to reference solutions, because of their too simple kinematics.

Case j is a simply-supported square sandwich plate under a uniform localized step loading that is applied at the upper face at $L_\alpha / 4 \le \alpha \le 3L_\alpha / 4$ and $L_\beta / 4 \le \beta \le 3L_\beta / 4$. Faces are thin and length-to-thickness ratio is 5. Because of all constituent materials are isotropic and geometrical symmetries, the following relations apply $u_\alpha = u_\beta$, $\sigma_{\alpha\alpha} = \sigma_{\beta\beta}$, $\sigma_{\alpha\varsigma} = \sigma_{\beta\varsigma}$. Transverse shear stress (other quantities in Appendix 1) is reported in Figure 4.7d and the following normalization is used:

$$\overline{\sigma_{\alpha\varsigma}} = \frac{\sigma_{\alpha\varsigma}(0,\varsigma)}{p^o} \tag{4.10}$$

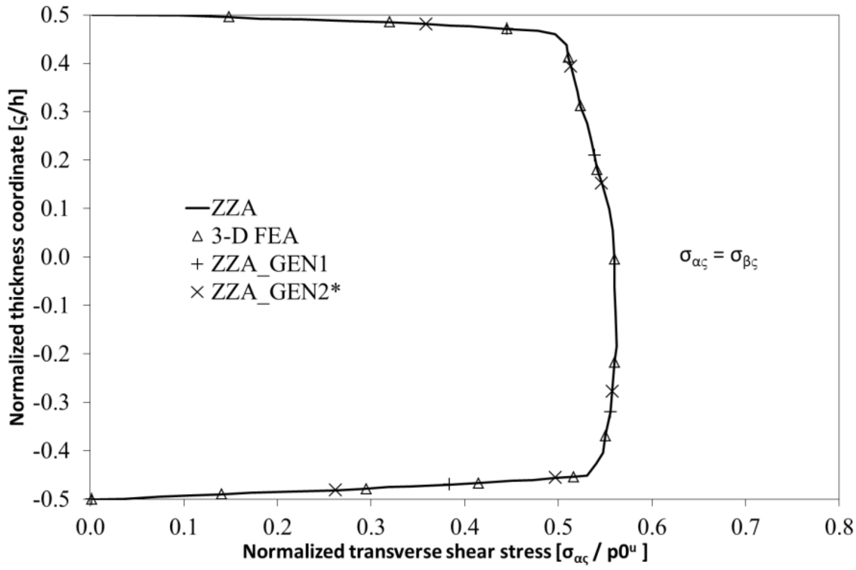

Figure 4.7d: Transverse shear stresses, case j

Nevertheless lay-up is symmetric and laminate is quite thin, asymmetries are shown, because of the application of localized step loading. So, similar findings of previous cases still apply [15].

For all cases of this section, higher-order adaptive theories ZZA_GEN1 and ZZA_GEN2* appear always accurate and very close to reference 3-D FEA solutions, being the exact one not available. Because of these models do not include any zig-zag, assume different functions to describe transverse variation of displacements across the thickness, do not include linear contribution by FSDT and obtain indistinguishable results, it is again confirmed that these choices are immaterial, whenever coefficients are redefined for each layer across the thickness and the full set of physical constraints (1.15)-(1.20) is imposed. The same findings also apply to other higher-order zig-zag theories (ZZA, HWZZ, ZZA_RDF, HWZZ_RDF, HSDT_34, ZZM, HWZZM, ZZA*, HWZZM*, ZZA****, ZZA_XN1 to ZZA_XN10).

4.8 Case k

Another propped cantilever sandwich beam is analyzed, whose lay-up is the same of case e but a length-to-thickness ratio of 20 is assumed. This case is retaken from [15] and transverse displacement and transverse shear stress are reported in Figure 4.8a, using the following normalizations (other quantities in Appendix 1):

$$\overline{u_{\varsigma}} = \frac{u_{\varsigma}\left(L_{\alpha},\varsigma\right)}{hp^{0}} \quad \overline{\sigma_{\alpha\varsigma}} = \frac{A\sigma_{\alpha\varsigma}\left(L_{\alpha},\varsigma\right)}{L_{\alpha}p^{0}} \tag{4.11}$$

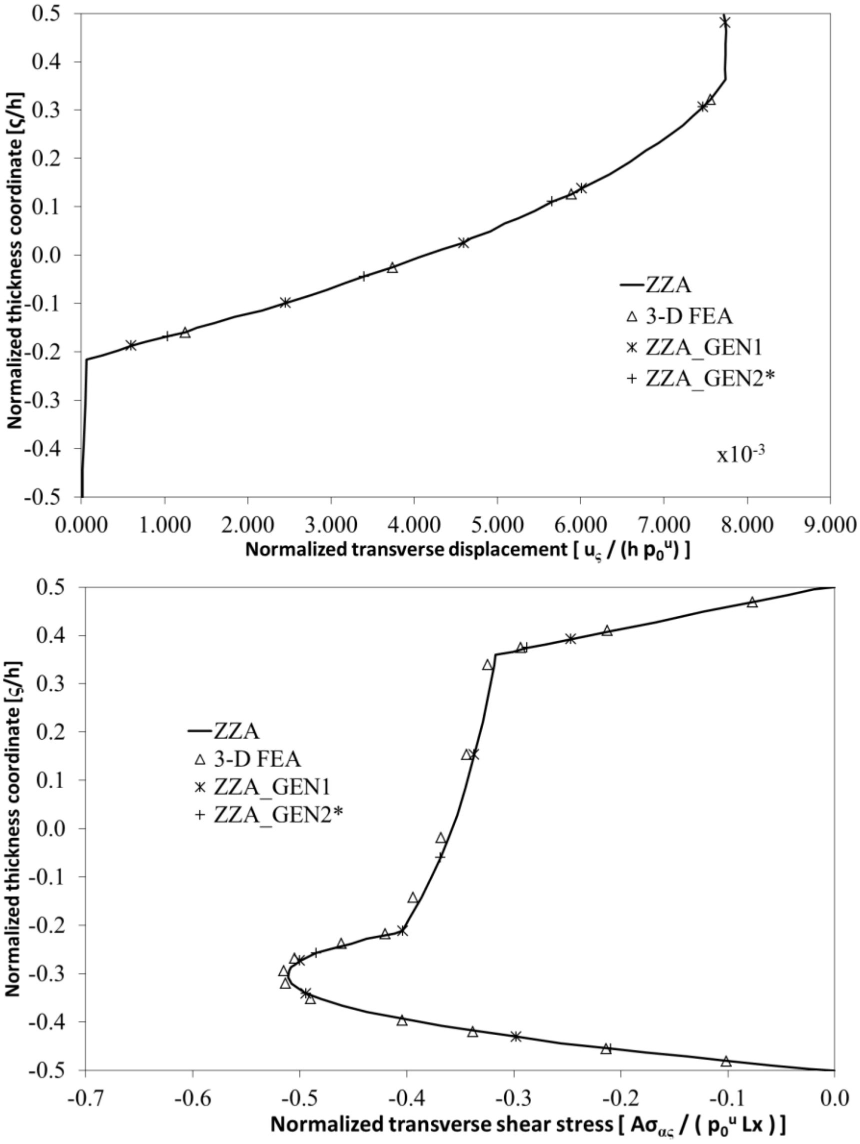

Figure 4.8a: Transverse displacement and transverse shear stress, case k

This case is very interesting, because, nevertheless it is thin, displacements and stresses show strong asymmetries, so, ESL theories cannot describe them properly. Again lower order theories cannot reach the same accuracy of higher-order adaptive theories, but percentage errors are lower than parent case, because layerwise effects are not very strong [15].

Again, ZZA_GEN1 and ZZA_GEN2* are very close to reference results by 3-D FEA, so, all statements and conclusions about their accuracy still apply also for this case. In the next section, a sandwich plate with functionally graded core is analyzed.

4.9 Case l

Accuracy of most advanced ZZA_GEN1 and ZZA_GEN2* higher-order zig-zag theories is assessed, considering a simply-supported sandwich plate with a graded core. This case is very interesting, because material properties of constituent layers are not uniform within layer and it is retaken from paper by Kashtalyan and Menshykova [82], assuming a length-to-thickness ratio of 3. It should be noticed that these results are new, because no functionally-graded laminates were considered in previous papers [15] to [23].

G^f is shear modulus of faces and a strong variation of properties is imposed, assuming shear modulus of core at ς=0 as $G^c = 0.1\, G^f$. So, the following through-thickness variation of modulus is assumed:

$$G_i(\varsigma) = \alpha_i\; G^f \tag{4.12}$$

For faces, α_i=1, while for core, the following α_i are assumed:

$$\begin{aligned} &G_{c1}(\varsigma) = \alpha_{c1}(\varsigma)\; G^f \qquad for\;\; \varsigma < 0 \\ &G_{c2}(\varsigma) = \alpha_{c2}(\varsigma)\; G^f \qquad for\;\; \varsigma > 0 \end{aligned} \tag{4.13}$$

$$\alpha_{c1}(\varsigma) = \frac{G^c}{G^f} e^{\frac{\beta_1\, \varsigma}{h}} \qquad \beta_1 = +\frac{2h}{h_c} \ln\left(\frac{G^c}{G^f}\right)$$

$$\alpha_{c2}(\varsigma) = \frac{G^c}{G^f} e^{\frac{\beta_2\, \varsigma}{h}} \qquad \beta_2 = -\frac{2h}{h_c} \ln\left(\frac{G^c}{G^f}\right)$$

The through-the-thickness variation of shear modulus is reported in Figure 4.9a:

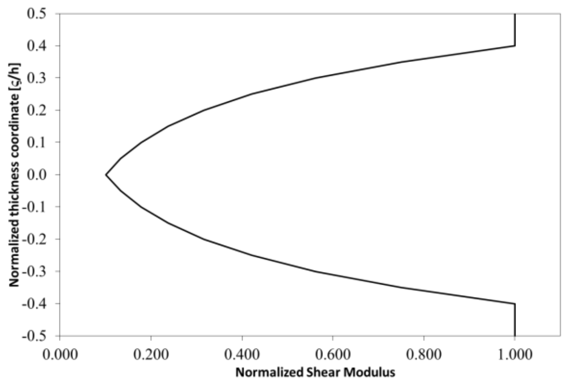

Figure 4.9a: Through-thickness variation of the shear modulus, case l

The same law is assumed for Young modulus. Because of all constituent materials are isotropic and geometrical symmetries, the following relations apply $u_\alpha = u_\beta$, $\sigma_{\alpha\alpha} = \sigma_{\beta\beta}$, $\sigma_{\alpha\varsigma} = \sigma_{\beta\varsigma}$. The following normalizations are used for displacements and stresses:

$$\overline{u_i} = \frac{G^f \ u_i}{hp^0} \qquad \overline{\sigma_{ij}} = \frac{\sigma_{ij}}{p^0} \tag{4.14}$$

In order to solve this case, two different strategies are used:

- the overall laminate is assumed as a unique layer, where mechanical properties of constituent layer are assumed to vary approximating (4.13) with a polynomial interpolation (up to ninth order). In this case, ZZA_GEN1 is expanded across the thickness up to 14^{th} order for transverse displacement and up to 13^{th} for in-plane ones and it will be indicated as ZZA_GEN1_mono in Figure 4.9b. Results, that are compared with 3-D solution by [82] are very accurate, but a very high expansion order across the thickness is required.
- Otherwise, the core is split into two parts that are further subdivided into four mathematical layers, in order to increase the number of equilibrium points and accuracy. So, using this strategy, the total number of layers is ten and no polynomial interpolation of mechanical properties is used to approximate transverse variation of Young and shear moduli.

Results obtained by parent theory ZZA and by ZZA_GEN1 and ZZA_GEN2* are in a very good agreement with those provided by three-dimensional solution by Kashtalyan and Menshykova [82], see Figures 4.9b.

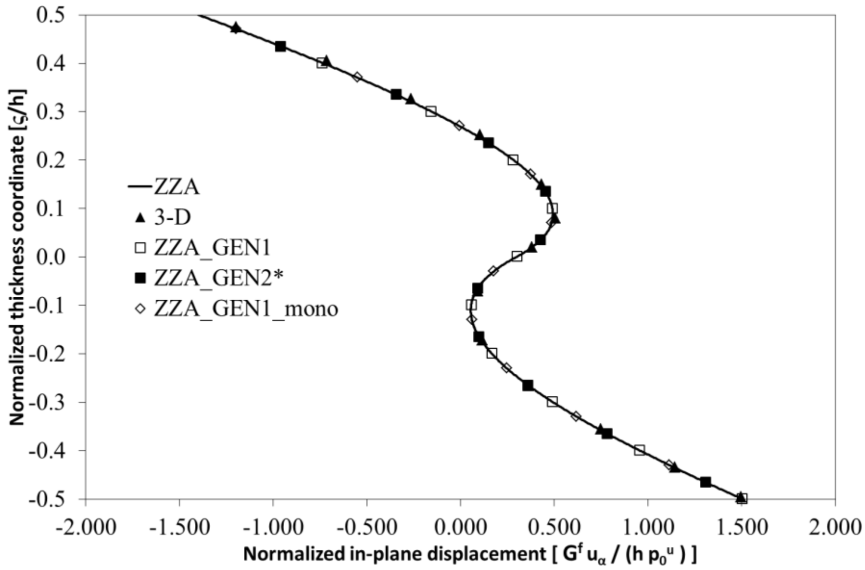

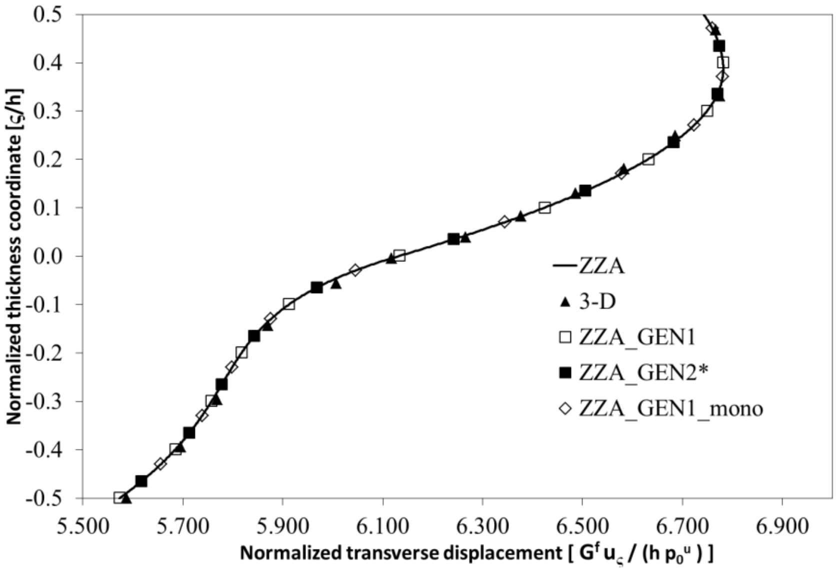
Normalized thickness coordinate [ς/h]
Normalized transverse displacement [$G^f u_ς / (h\, p_0^u)$]
ZZA
3-D
ZZA_GEN1
ZZA_GEN2*
ZZA_GEN1_mono

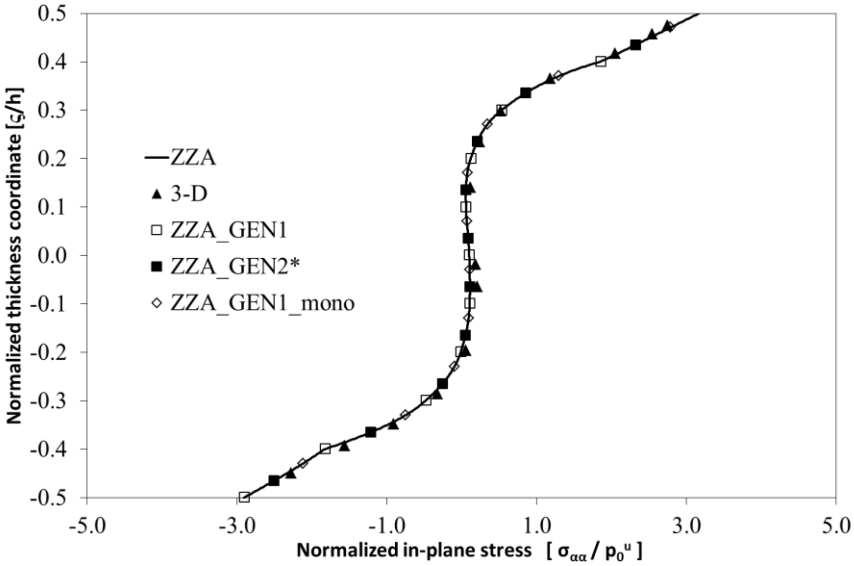
Normalized thickness coordinate [ς/h]
Normalized in-plane stress [$σ_{αα} / p_0^u$]
ZZA
3-D
ZZA_GEN1
ZZA_GEN2*
ZZA_GEN1_mono

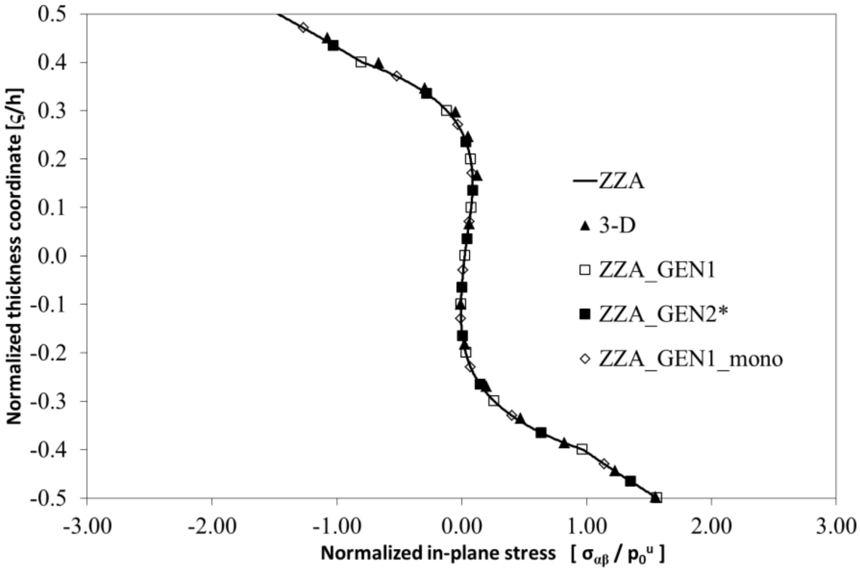
Normalized thickness coordinate [ς/h]
Normalized in-plane stress [$σ_{αβ} / p_0^u$]
ZZA
3-D
ZZA_GEN1
ZZA_GEN2*
ZZA_GEN1_mono

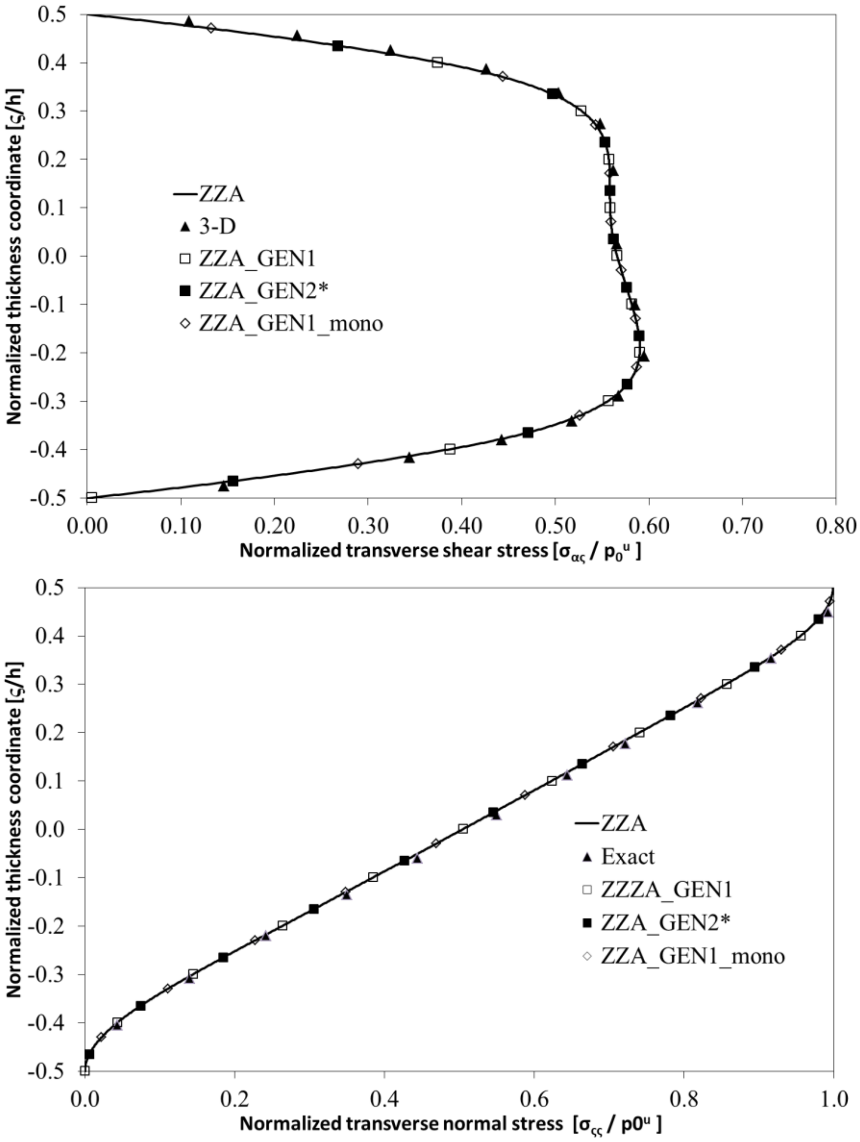

Figure 4.9b: Normalized displacements and stresses, case l

It should be noticed that higher-order theories (ZZA, ZZA_GEN1, ZZA_GEN2*) are always able to accurate calculate displacement and stress fields, even when functionally graded and extreme high length-to-thickness ratios are considered. Results by ZZA, ZZA_GEN1, ZZA_GEN2* are indistinguishable so, also for functionally graded problems, it is demonstrated that if coefficients are redefined for each layer across the thickness and the full set of physical constraints (1.15)-(1.20) is imposed:

- zig-zag functions can be changed or omitted without any loss of accuracy;
- functions that describe variation of displacements across the thickness can be changed, so, exponential, power series and sinusoidal functions, or a combination of them, can be assumed differently for

each displacement and from point to point across the thickness, without any loss of accuracy;
- the role of coefficients can be freely switched;
- linear contribution by FSDT are not necessary to obtain precise displacements and stresses

Otherwise accuracy of theories is strongly dependent by assumptions made, confirming what widespread in Literature.

4.10 Processing time of elastostatic cases

Table 4.4 reports processing time for theories of chapter 2 and 3 for elastostatic cases. It should be noticed that MHR, MHR4 are very cheap, but since they are inaccurate (if Murakami's rule is not respected or very strong layerwise effects occur), their use should be avoided. As a general rule, mixed theories show very little cost savings, so, these technique should not be used because they are not convenient, neither from the standpoint of accuracy, nor for processing time. Mixed HWZZ is accurate, but time calculations are similar to those of ZZA, because of its zig-zag functions. Instead, DZZ whose zig-zag functions are omitted, show very good processing time. Particularly, the most general physically-based higher-order adaptive theories ZZA_GEN and ZZA_X are the best theories of this thesis, because their particularizations (such as ZZA_GEN1 and ZZA_GEN2*) always get accurate results (irrespective layerwise and representation functions) with a great efficiency. In the next chapter, the accuracy of theories of chapters 2 and 3 is assessed for dynamic calculations.

	a	b	c	d	e	f	g	h	i	j	k
ZZA	13.5620	19.9740	10.6297	10.5768	15.0671	10.3465	4.9770	17.5977	5.0712	10.9591	15.9719
HWZZ	12.0193	18.4149	9.6997	9.6664	14.4271	9.5745	4.4949	16.1594	5.1993	9.7755	14.8490
HRZZ	14.9182	20.9727	11.6926	12.1633	18.2312	11.6618	5.3990	20.9194	7.9113	12.5887	18.2261
HRZZ4	14.7821	20.9727	11.6649	12.9170	18.2237	11.4963	5.4094	21.1942	11.5603	12.5681	18.4891
MHR	8.1514	11.7768	6.5659	6.5138	6.9574	6.8583	4.3663	12.0285	4.5774	6.6732	6.6258
MHR4	8.6564	11.7603	6.4724	6.8826	6.4946	6.2430	4.3310	12.5987	4.6969	6.5056	6.9702
MHWZZA	10.7396	16.8825	8.2006	8.5096	7.2359	8.3921	4.4726	14.1698	5.3375	8.6730	7.6952
MHWZZA4	10.2451	16.7948	8.6045	8.1205	7.8365	8.0087	4.6211	14.2118	5.8352	8.9862	7.5861
MHR±	8.4385	12.5376	6.5810	6.6179	9.4716	6.4682	3.1054	10.8977	3.1668	6.8371	9.9350
MHR4±	8.5114	12.5969	6.6603	6.7103	9.5769	6.5766	3.1022	11.0719	3.2121	6.8344	10.0833
ZZA_RDF	13.0935	19.1586	10.2809	10.2247	14.4071	9.9657	4.7515	16.8998	4.8881	10.5372	15.4189
HWZZ_RDF	12.1410	17.8027	9.4631	9.4295	13.2845	9.1373	4.4164	15.6738	4.5312	9.7334	14.1751
HSDT_32	8.3084	12.2156	6.4949	6.4672	9.2081	6.3308	3.0110	10.7097	3.0605	6.6572	9.6222
HSDT_33	8.8493	13.0538	6.8598	6.8360	9.8530	6.7005	3.2542	11.3976	3.2998	7.1135	10.4649
HSDT_34	10.3040	15.1162	8.0368	7.9790	11.4757	7.8000	3.7599	13.2485	3.8450	8.2522	12.1252
ZZM	10.3149	15.0518	8.0396	7.9872	11.4347	7.8241	3.7988	13.4239	3.8656	8.3257	12.2106
HWZZM	11.1021	16.4152	8.7214	8.7167	12.3112	8.4187	4.0771	14.4948	4.1248	9.0171	13.0365

ZZA*	10.2855	15.1293	8.0794	7.9890	11.5227	7.7923	3.7726	13.4473	3.8660	8.3105	12.0343
HWZZM*	10.1479	14.7512	7.8923	7.8381	11.2749	7.7784	3.6859	13.1859	3.7557	8.1946	11.9370
ZZA_GEN1	10.2978	15.2325	8.0963	8.1610	11.4330	7.8830	3.8223	13.3491	3.8652	8.3416	12.1530
ZZA_GEN2*	10.4859	15.2488	8.1289	8.1568	11.6423	7.8740	3.8564	13.5747	3.8728	8.4149	12.2901
ZZA_XN1	10.2824	15.1142	8.1034	8.0551	11.3860	7.8793	3.7824	13.3791	3.8552	8.3100	12.2904
ZZA_XN2	10.6858	15.5807	8.3856	8.2485	11.7541	8.1023	3.9210	13.6985	4.0075	8.6336	12.4686
ZZA_XN3	10.6999	15.7233	8.4473	8.4404	11.9836	8.2971	3.9464	14.1156	4.0321	8.6869	12.8044
ZZA_XN4	10.8286	15.9166	8.3966	8.3672	11.8920	8.2454	3.9764	13.9771	4.0290	8.7513	12.6875
ZZA_XN5	10.3529	15.2664	8.0889	8.0770	11.3887	7.8703	3.7716	13.5314	3.8735	8.3644	12.0899
ZZA_XN6	10.7037	15.6507	8.3252	8.3356	11.8630	8.0781	3.8961	13.7857	3.9937	8.5530	12.5852
ZZA_XN7	10.4029	15.3707	8.1084	8.0920	11.5681	7.8424	3.7880	13.4132	3.8802	8.3601	12.1415
ZZA_XN8	10.6837	15.6680	8.2701	8.2456	11.8590	8.1415	3.9068	13.7022	4.0048	8.5028	12.5226
ZZA_XN9	10.8340	15.8636	8.4505	8.3288	11.9881	8.1579	3.9839	14.0419	4.0272	8.7323	12.7934
ZZA_XN10	10.6611	15.7749	8.3820	8.3294	11.8764	8.2384	3.9240	13.9478	4.0316	8.6666	12.7244
FSDT	2.7860	4.2943	4.9372	5.4858	7.3303	5.0712	2.3014	6.5481	2.3261	4.0778	4.0522

Table 4.4: Processing time [s]

A graphical, condensed comparison of computing times is reported in Figure 4.10 (processing times are reported normalized to ZZA ones).

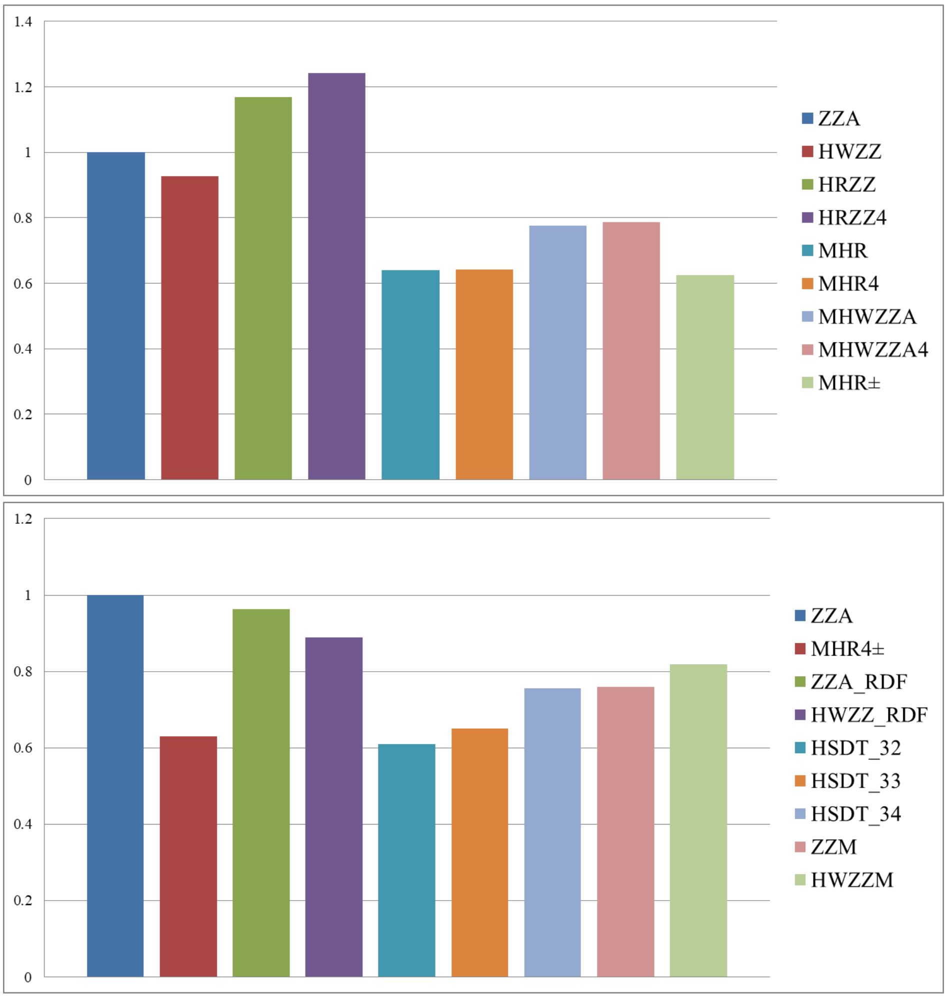

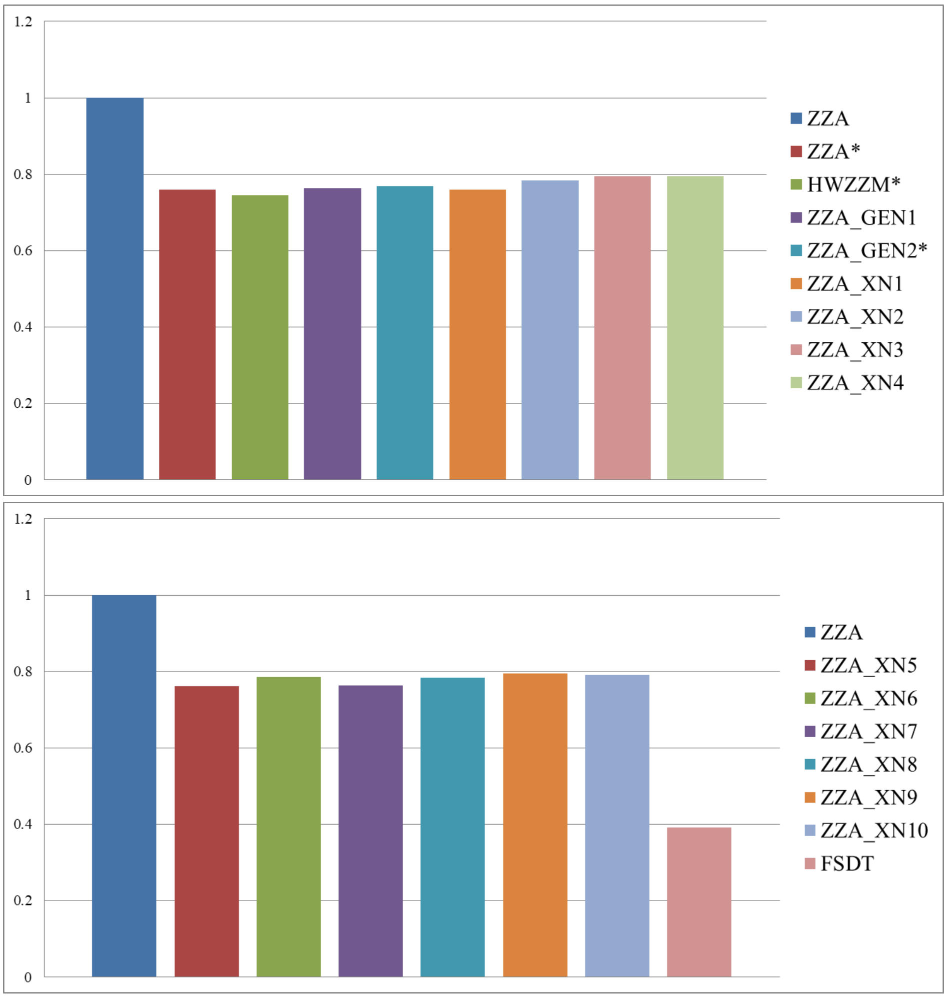

Figure 4.10: Graphical, condensed comparison of computing times of theories for elastostatic cases. Results are normalized to processing time of ZZA.

4.11 Concluding remarks

In this chapter a lot of challenging elastostatic cases are analyzed considering different loading and boundary conditions, that in conjunction with strong variation of mechanical properties of constituent layers across the thickness enhance strong layerwise effects. Moreover, the accuracy of theories of chapter 2 and 3 for functionally graded plates is deepened.

Regarding zig-zag theories, kinematic-based ones provide results with low processing time. However, because of their coefficients of displacement field are not redefined and the full set of physical constraints is not imposed, they cannot obtain the same accuracy of ZZA and other higher-order adaptive theories, especially when Murakami's rule is not respected and/or when there are strong layerwise effects.

MHR±, MHR4± (where Murakami's slope is determined on a physical basis), MHWZZA and MHWZZA4 (where strains and stresses are assumed as like as physically-based zig-zag theories) provide better results than MHR and MHR4 with similar processing time, but accuracy of higher-order theories cannot be obtained because of their simplified kinematics. So, also MHR±, MHR4±, MHWZZA and MHWZZA4 should be used to analyze quite thick laminates and sandwiches, without strong variation of mechanical properties across the thickness. Main features of MHR, MHR4, MHR±, MHR4±, MHWZZA and MHWZZA4 are reported in Tables 4.5a to 4.5c:

MHR, MHR4	
Type:	Kinematic-based zig-zag theories
Displacement field:	Piecewise cubic (in-plane displacements) Fourth-order polynomial (transverse displacement of MHR) Piecewise fourth-order polynomial (transverse displacement of MHR4)
Physical constraints:	Full set of physical constraints of ZZA is not imposed
Coefficients:	Not redefined (no adaptive)
Accuracy:	Strongly case-dependent; particularly, very wrong results could be provided if Murakami's rule is not respected or there are strong layerwise effects
Recommended usage:	Only for cases without strong layerwise effects (e.g. cross-ply laminated thin beams and plates)

Table 4.5a: Main features of MHR and MHR4

MHR±, MHR4±	
Type:	Kinematic-based zig-zag theories (slope of Murakami's zig-zag function is obtained on a physical basis)
Displacement field:	Piecewise cubic (in-plane displacements) Fourth-order polynomial (transverse displacement of MHR±) Piecewise fourth-order polynomial (transverse displacement of MHR4±)
Physical constraints:	Full set of physical constraints of ZZA is not imposed
Coefficients:	Not redefined (no adaptive)
Accuracy:	Strongly case-dependent; better than MHR and MHR4 counterpart but very wrong results could be provided if there are strong layerwise effects
Recommended usage:	Only for cases without strong layerwise effects (e.g. not extremely thick laminates and sandwiches without strong variation of properties across the thickness)

Table 4.5b: Main features of MHR± and MHR4±

MHWZZA, MHWZZA4	
Type:	Mixed zig-zag theories; displacements from MHR, strains and stresses apart from HWZZ
Displacement field:	Piecewise cubic (in-plane displacements) Fourth-order polynomial
Physical constraints:	Full set of physical constraints of ZZA is not imposed
Coefficients:	Coefficients of displacement field are not redefined (no adaptive)
Accuracy:	Strongly case-dependent; better than MHR and MHR4 counterpart but very wrong results could be provided if there are strong layerwise effects
Recommended usage:	Only for cases without strong layerwise effects (e.g. not extremely thick laminates and sandwiches without strong variation of properties across the thickness)

Table 4.5c: Main features of MHWZZA and MHWZZA4

Regarding physically-based adaptive zig-zag theories, HSDT_32 and HSDT_33 that assume a parabolic and cubic piecewise transverse displacement respectively are not always accurate, because the full set of physical constraints of ZZA is not enforced. These theories demonstrate that a piecewise cubic-fourth-order displacement field is the minimum expansion order to get the maximal precision. These results are also corroborated by those provided by HRZZ and HRZZ4, that are mixed physically-based adaptive lower order theories, where a uniform and a polynomial (not piecewise) transverse displacement is assumed. For HRZZ and HRZZ4 stresses are assumed apart (transverse normal stress is the same of ZZA), but despite this the accuracy of higher-order theories cannot be reached because the full set of physical constraints is not imposed and a simplified transverse deformability is described. It should be noticed that results provided by HSDT_32, HSDT_33, HRZZ and HRZZ4 are a little better than MHR and MHR4 ones, so, they could be used to analyze laminated and sandwiches with quite strong layerwise effects (see Tables 4.6a and 4.6b for their main features).

HSDT_32, HSDT_33	
Type:	Displacement-based physically-based zig-zag theories
Displacement field:	Piecewise cubic (in-plane displacements) Piecewise parabolic (transverse displacement of HSDT_32) Piecewise cubic (transverse displacement of HSDT_33)
Physical constraints:	Full set of physical constraints of ZZA is not imposed
Coefficients:	Coefficients of displacement field are redefined (adaptive)
Accuracy:	Case-dependent; better than kinematic-based theories but wrong results could be provided if there are very strong layerwise effects
Recommended usage:	They are able to accurately analyse also thick laminated and sandwiches with quite strong layerwise effects; anyway, they should be avoided if a very accurate description of transverse deformability is required (e.g. propped cantilever beams)

Table 4.6a: Main features of HSDT_32 and HSDT_33

HRZZ, HRZZ4	
Type:	Mixed physically-based zig-zag theories
Displacement field:	Piecewise cubic (in-plane displacements) Uniform (transverse displacement of HRZZ) Fourth-order polynomial (transverse displacement of HRZZ4)
Physical constraints:	Full set of physical constraints of ZZA is not imposed
Coefficients:	Coefficients of in-plane displacement are redefined (no adaptive)
Accuracy:	Case-dependent; better than kinematic-based theories but wrong results could be provided if there are very strong layerwise effects
Recommended usage:	They are able to accurately analyze also thick laminated and sandwiches with quite strong layerwise effects; anyway, they should be avoided if a very accurate description of transverse deformability is required (e.g. propped cantilever beams)

Table 4.6b: Main features of HRZZ and HRZZ4

Regarding higher-order physically-based adaptive theories ZZA, HWZZ, ZZA_RDF, HWZZ_RDF, HSDT_34, ZZM, HWZZM, ZZA*, HWZZM*, ZZA_GEN1, ZZA_GEN2*, ZZA_XN1 to ZZA_XN10, they always provide very accurate results, very close to reference results (percentage errors are always lower than 3% for all displacements and stresses) for all loading and boundary conditions considered. Because of coefficients are redefined for each layer across the thickness (adaptive) and the full set of physical constraints is enforced all these theories provide the same results irrespective zig-zag and global representation functions assumed. Particularly, particularizations of the most general physically-based higher-order adaptive theory (ZZA_GEN) are the best theories of this thesis, by virtue of their great efficiency (over 20% time less than ZZA). ZZA, HWZZ, ZZA_RDF, HWZZ_RDF, HSDT_34, ZZM, HWZZM, ZZA*, HWZZM*, ZZA_GEN1, ZZA_GEN2*, ZZA_XN1 to ZZA_XN10 can be used to successfully analyze both thick and thin laminates and sandwiches with also strong layerwise effects. Their features are briefly reported in Tables 4.7a and 4.7c. Regarding HWZZ, HWZZ_RDF, HWZZM and HWZZM*, which are mixed version of other higher-order adaptive theories, the cost saving is too low respect to their counterparts, so, mixed theories won't be used for develop further theories.

ZZA, ZZA_RDF, HSDT_34, ZZM, ZZA*	
Type:	Displacement-based physically-based zig-zag theories
Displacement field:	Piecewise cubic (in-plane displacements) Piecewise fourth-order (transverse displacement)
Physical constraints:	Full set of physical constraints of ZZA is imposed
Coefficients:	Coefficients of displacements are redefined (adaptive)
Accuracy:	Always very accurate and close to reference solutions
Recommended usage:	Always

Table 4.7a: Main features of ZZA, ZZA_RDF, HSDT_34, ZZM, ZZA*

HWZZ, HWZZ_RDF, HWZZM and HWZZM*	
Type:	Mixed physically-based zig-zag theories
Displacement field:	Piecewise cubic (in-plane displacements) Piecewise fourth-order (transverse displacement)
Physical constraints:	Full set of physical constraints of ZZA is imposed
Coefficients:	Coefficients of displacements are redefined (adaptive)
Accuracy:	Always very accurate and close to reference solutions
Recommended usage:	Always; they allow a little cost saving than theories of Table 4.7a

Table 4.7b: Main features of HWZZ, HWZZ_RDF, HWZZM and HWZZM*

ZZA_GEN1, ZZA_GEN2*, ZZA_XN1 to ZZA_XN10	
Type:	Displacement-based physically-based generalized zig-zag theories
Displacement field:	Piecewise cubic (in-plane displacements) Piecewise fourth-order (transverse displacement) User can choose layerwise and representation functions as an input of analysis.
Physical constraints:	Full set of physical constraints of ZZA is imposed
Coefficients:	Coefficients of displacements are redefined (adaptive)
Accuracy:	Always very accurate and close to reference solutions
Recommended usage:	Always; they allow a good cost saving (over 20%) than theories of Table 4.7a

Table 4.7c: Main features of ZZA_GEN1, ZZA_GEN2*, ZZA_XN1 to ZZA_XN10

Finally, equivalent single layer theories, as like as FSDT, provide the lower processing time, but their accuracy is too poor, so, they should not be used unless very thin laminates are analyzed.

FSDT	
Type:	Equivalent single layer theory
Displacement field:	Linear (in-plane displacements) Uniform (transverse displacement)
Physical constraints:	No physical constraints are imposed; out-of-plane stresses are post-processed after analysis
Coefficients:	No additional coefficients than d.o.f.
Accuracy:	Very poor, they are not able to analyse sandwiches
Recommended usage:	Only for very thin laminated beams and plates; they should not be used to analyse sandwiches

Table 4.8: Main features of FSDT

Chapter 5 – Dynamic assessment of theories

5.1 Introduction

In this chapter the accuracy of theories of chapters 2 and 3 is assessed for dynamic calculations and particularly, their capability to get global quantities such as natural frequencies (cases a to k) and their behaviour under impulsive blast loading (cases l and m). All cases are retaken from previous papers by author; different boundary conditions are assumed and both laminated and sandwich beams and plates are considered (both thick and thin). Lay-up, geometry, trial functions, expansion order ad material properties of constituent layer are reported in Tables 5.1a to 5.1c.

Case	Lay-up	Layer thickness	Material	BCS	$L\alpha/h$	$L\beta/L\alpha$
a	[0/90/0]	$[(h/3)]_3$	$[p]_3$	SS	4,10,20	-
b	[0/90/0]	$[(h/3)]_3$	$[m]_3$	SS	4	-
c	[0/90/0]	$[(h/3)]_3$	$[p]_3$	SSSS	10	1
d	[0/90/0]	$[(h/3)]_3$	$[p]_3$	CCCC	10	1
e	[0/90/0]	$[(h/3)]_3$	$[p]_3$	CSCS	10	1
f	[0]	[h]	♣	SSSS	10	1
g	[0/90/0/0/90]	[(h/24)2 / (5h/12)]$_S$	[r1/r2/s/r1/r2]	SSSS	5	1
h	[0/90/0/0/90]	$[(h/24)_2 / (5h/12)]_S$	[r1/r2/t/r1/r2]	SSSS	5	1
i	$[0_5]$	$[(h/24)_2 / (5h/12)]_S$	[u1/u2/v/u1/u2]	SSSS	4	1
j	$[0_5]$	$[(h/24)_2 / (5h/12)]_S$	[u1/u2/w/u1/u2]	SSSS	4	1
k	$[0_6]$	$[(h/24)_2 / (30h/48) / (10h/48) / (h/24)_2]$	[u1/u2/v/z/u1/u2]	SSSS	4	1
l	$[(45/-45)_2/45/0]_S$	$[(0.381mm)_5/ (12.7mm)]_S$	$[o1_5/o2]_S$	SSSS	20.8696	1
m	$[(0/90)_2/0_2]_S$	$[(0.381mm)_5 / (12.7mm)]_S$	$[o1_5/o2/o3/o1_5]$	SSSS	10	1
♣ material properties are specified in text (section 5.3)						

Table 5.1a. List of dynamic cases

Case	Trial Functions	Expansion Order
a b	$u_\alpha^0(\alpha)=\sum_{m=1}^{M}A_m\cos\left(\frac{m\pi\alpha}{L_\alpha}\right);\quad w^0(\alpha)=\sum_{m=1}^{M}C_m\sin\left(\frac{m\pi\alpha}{L_\alpha}\right);\quad \Gamma_\alpha^0(\alpha)=\sum_{m=1}^{M}D_m\cos\left(\frac{m\pi\alpha}{L_\alpha}\right)$	5 5
c f g h i j k l m	$u_\alpha^0(\alpha,\beta)=\sum_{m=1}^{M}\sum_{n=1}^{N}A_{mn}\cos\left(\frac{m\pi}{L_\alpha}\alpha\right)\sin\left(\frac{n\pi}{L_\beta}\beta\right);\quad u_\beta^0(\alpha,\beta)=\sum_{m=1}^{M}\sum_{n=1}^{N}B_{mn}\sin\left(\frac{m\pi}{L_\alpha}\alpha\right)\cos\left(\frac{n\pi}{L_\beta}\beta\right);$ $w^0(\alpha,\beta)=\sum_{m=1}^{M}\sum_{n=1}^{N}C_{mn}\sin\left(\frac{m\pi}{L_\alpha}\alpha\right)\sin\left(\frac{n\pi}{L_\beta}\beta\right);$ $\Gamma_\alpha{}^0(\alpha,\beta)=\sum_{m=1}^{M}\sum_{n=1}^{N}D_{mn}\cos\left(\frac{m\pi}{L_\alpha}\alpha\right)\sin\left(\frac{n\pi}{L_\beta}\beta\right);\quad \Gamma_\beta{}^0(\alpha,\beta)=\sum_{m=1}^{M}\sum_{n=1}^{N}E_{mn}\sin\left(\frac{m\pi}{L_\alpha}\alpha\right)\cos\left(\frac{n\pi}{L_\beta}\beta\right);$	4 10 10 10 15 15 15 11 11
c d e	$u_\alpha{}^0(\alpha,\beta)=\sum_{j=1}^{J}\sum_{i=1}^{I}A_{\alpha i}\left(\frac{\alpha}{L_\alpha}\right)^i\left(\frac{\beta}{L_\beta}\right)^j;\ \Gamma_\alpha^0(\alpha,\beta)=\sum_{j=1}^{J}\sum_{i=1}^{I}D_{\alpha i}\left(\frac{\alpha}{L_\alpha}\right)^i\left(\frac{\beta}{L_\beta}\right)^j;$	4 4 4

Table 5.1b. Trial functions and expansion order.

Material name	m *	o1	o2	o3	p	r1	r2	s	t	u1	u2	v	w	z
E1[GPa]	E1	206.84	0.138	0.0138	172.4	33.5	139	6.89	0.035	36.23	190	0.036	0.070	0.020
E2[GPa]	E2	5.171	0.138	0.0138	6.89	8	3.475	6.89	0.035	10.62	7.7	0.036	0.070	0.020
E3 [GPa]	E2	5.171	0. 138	0. 0138	6.89	8	3.475	6.89	0.035	7.21	7.7	0.036	0.070	0.020
G12 [GPa]	0.5E2	2.551	0.1027	0.01027	3.45	2.26	1.7375	3.45	0.0123	5.6	4.2	0.013	0.019	0.012
G13 [GPa]	0.5E2	2.551	0.1027	0.01027	3.45	2.26	1.7375	3.45	0.0123	5.68	4.2	0.013	0.019	0.012
G23 [GPa]	0.2E2	2.551	0.06205	0.006205	1.378	3	0.695	3.45	0.0123	3.46	2.96	0.013	0.019	0.012
υ12	0.25	0.25	0.35	0.35	0.25	0.35	0.25	0	0.4	0.26	0.3	0.38	0.3	0.3
υ13	0.25	0.25	0.35	0.35	0.25	0.35	0.25	0	0.4	0.33	0.3	0.38	0.3	0.3
υ23	0.25	0.25	0.02	0.02	0.25	0.35	0.25	0	0.4	0.48	0.3	0.38	0.3	0.3
ρ	1558.35	1558.35	16.3136	16.3136	1558.35	1627	1627	97	32	1800	1600	32	52.1	39.7

* El/E2=3,25,40 for case b

Table 5.1c. Material properties.

Similarly to the previous chapter, the purpose of these benchmarks is to demonstrate that if coefficients are redefined for each layer across the thickness and the full set of physical constraints (1.15)-(1.20) is imposed:

- zig-zag functions can be changed or omitted without any loss of accuracy;
- functions that describe variation of displacements across the thickness can be changed, so, exponential, power series and sinusoidal functions, or a combination of them, can be assumed differently for each displacement and from point to point across the thickness, without any loss of accuracy;
- the role of coefficients can be freely switched;
- linear contribution by FSDT are not necessary to obtain precise displacements and stresses

On the contrary, accuracy becomes strongly dependent by assumptions made and results provided by lower-order theories become strongly case dependent.

5.2 Test cases a to e (natural frequencies)

Firstly, the capability of theories to accurately calculate natural frequencies is assessed for standard cases retaken from Literature. For all cases, also results provided by FSDT and HSDT theories are reported (see section 1.6), with the intended aim to test their capacity to get at least the fundamental frequency. Regarding FSDT, a shear correction factor of 5/6 is assumed. For all cases of this section, theories that provide very similar results (discrepancies < 1%) are grouped together, with the purpose to contain thesis length.

Regarding case a, the first three natural frequencies of a simply-supported [0/90/0] laminated beam, retaken from [39], are reported in Table 5.2a, where three different length to thickness ratios (4, 10, 20) are assumed, in order to test the accuracy of theories to varying thickness of laminates. The following normalization is used for this case:

$$\bar{\omega} = \omega h \sqrt{\frac{\rho_{\_MATp}}{G_{12\_MATp}}} \tag{5.1}$$

Regarding the thinner case (Lx/h=20), it should be noticed that all theories, except that FSDT, HSDT, HSDT_32 are very accurate and in very good agreement with 3-D FEA, that is used as reference when exact solution is not available, as like as elastostatic cases. Anyway, greater percentage errors are provided for the thickest cases, confirming what widespread in Literature. Particularly, for Lx/h=4, also MHR, MHR4, MHR±, MHR4±, MHWZZA and MHWZZA4 are not able to reach the accuracy of other theories, especially for the third frequency, because their kinematics is too simple. FSDT and HSDT are unable to get also the fundamental frequencies, also for moderately thick laminates (Lx/h=10), so they should not be used. Only HRZZ, HRZZ4, ZZA, HWZZ, ZZA_RDF, HWZZ_RDF, ZZM, HWZZM, ZZA*, HWZZM*, ZZA_GEN1, ZZA_GEN2*, ZZA****, ZZA_XN1 to ZZA_XN10, HSDT_33, HSDT_34 are always accurate for this case. Particularly, indistinguishable and accurate results provided by higher-order zig-zag adaptive theories demonstrate that they can be successfully used also for dynamic case, irrespective the choice of zig-zag functions and ones used to represent the transverse variation of displacements across the thickness.

	Lα/h=4			Lα/h=10			Lα/h=20		
Theories	**Mode 1**	**Mode 2**	**Mode 3**	**Mode 1**	**Mode 2**	**Mode 3**	**Mode 1**	**Mode 2**	**Mode 3**
3-D FEA	0.5175	1.1888	1.8911	0.1464	0.3901	0.6490	0.0449	0.1464	0.2653
♠	0.5176	1.1954	1.9011	0.1463	0.3897	0.6486	0.0449	0.1461	0.2652
MHR	0.5235	1.2540	2.0802	0.1463	0.3921	0.6601	0.0449	0.1462	0.2658
MHR4	0.5246	1.2634	2.1011	0.1463	0.3925	0.6623	0.0449	0.1462	0.2659
MHR±	0.5235	1.2540	2.0802	0.1463	0.3921	0.6601	0.0449	0.1462	0.2658
MHR4±	0.5246	1.2634	2.1011	0.1463	0.3925	0.6623	0.0449	0.1462	0.2659
HRZZ	0.5171	1.1910	1.8978	0.1462	0.3895	0.6475	0.0449	0.1462	0.2651
HRZZ4	0.5172	1.1920	1.9062	0.1462	0.3895	0.6478	0.0449	0.1462	0.2651
MHWZZA	0.4331	1.2283	1.8657	0.1458	0.3852	0.6542	0.0449	0.1461	0.2644
MHWZZA4	0.4523	1.2984	2.2496	0.1459	0.3881	0.6553	0.0449	0.1462	0.2651
HSDT_32	0.6553	1.7022	2.9648	0.1621	0.4770	0.8447	0.0466	0.1621	0.3111
FSDT	0.5686	1.2409	1.8951	0.1564	0.4299	0.7057	0.0461	0.1564	0.2907
HSDT	0.5373	1.2317	2.0517	0.1510	0.4061	0.6700	0.0455	0.1510	0.2763
♠ ZZA, HWZZ, ZZA_RDF, HWZZ_RDF, HSDT_34, ZZM, HWZZM, ZZA*, HWZZM*, ZZA_GEN1, ZZA_GEN2*, ZZA****, ZZA_XN1 to ZZA_XN10, HSDT_33, HSDT_34, (error < 1%); Modes with 1,2,3 halfwaves									

Table 5.2a. Case a

Regarding case b, the first three natural frequencies of a simply-supported [0/90/0] laminated beam, retaken from [39], are reported in Table 5.2b, where three different orthotropy ratios (3, 25, 40) are assumed, where the length-to-thickness ratio is 4. The following normalization is used for this case:

$$\bar{\omega} = \omega h \sqrt{\frac{\rho_{\_MATm}}{G_{12\_MATm}}} \tag{5.2}$$

	E1/E2=3			E1/E2=25			E1/E2=40		
Theories	**Mode 1**	**Mode 2**	**Mode 3**	**Mode 1**	**Mode 2**	**Mode 3**	**Mode 1**	**Mode 2**	**Mode 3**
3-D FEA	0.4505	1.0912	1.7769	0.5175	1.1888	1.8911	0.5463	1.2337	1.9173
♠	0.4504	1.0939	1.7804	0.5176	1.1954	1.9011	0.5467	1.2407	1.9706
MHR	0.4518	1.1151	1.8553	0.5235	1.2540	2.0802	0.5578	1.3290	2.2076
MHR4	0.4520	1.1191	1.8676	0.5246	1.2634	2.1011	0.5599	1.3414	2.2332
MHR±	0.4518	1.1151	1.8553	0.5235	1.2540	2.0802	0.5578	1.3290	2.2076
MHR4±	0.4520	1.1191	1.8676	0.5246	1.2634	2.1011	0.5599	1.3414	2.2332
HRZZ	0.4501	1.0885	1.7596	0.5171	1.1910	1.8978	0.5461	1.2373	1.9637
HRZZ4	0.4501	1.0895	1.7656	0.5172	1.1920	1.9062	0.5462	1.2389	1.9721
MHWZZA	0.4334	1.0582	1.6250	0.4331	1.2283	1.8657	0.6310	1.3421	1.9666
MHWZZA4	0.4389	1.1044	1.8119	0.4523	1.2984	2.2496	0.6424	1.4535	2.6059
HSDT_32	0.5276	1.4123	2.4616	0.6553	1.7022	2.9648	0.7212	1.8585	3.2266
FSDT	0.4944	1.1846	1.8539	0.5686	1.2409	1.8951	0.5929	1.2560	1.9057
HSDT	0.4694	1.1268	1.8253	0.5373	1.2317	2.0517	0.5641	1.3021	2.2374
♠ ZZA, HWZZ, ZZA_RDF, HWZZ_RDF, HSDT_34, ZZM, HWZZM, ZZA*, HWZZM*, ZZA_GEN1, ZZA_GEN2*, ZZA****, ZZA_XN1 to ZZA_XN10, HSDT_33, HSDT_34, (error < 1%); Modes with 1,2,3 halfwaves									

Table 5.2b. Case b

A greater dispersion of results is obtained than the previous case and MHR, MHR4, MHR±, MHR4±, MHWZZA, MHWZZA4, HSDT_32, FSDT and HSDT are inaccurate, with percentage errors that increase with increasing the orthotropy ratio and the number of frequency, confirming what widespread in Literature. Instead, HRZZ, HRZZ4, ZZA, HWZZ, ZZA_RDF, HWZZ_RDF, HSDT_34, ZZM, HWZZM, ZZA*, HWZZM*, ZZA_GEN1, ZZA_GEN2*, ZZA****, ZZA_XN1 to ZZA_XN10, HSDT_33, HSDT_34 are in very good agreement with results provided by 3-D FEA, used as reference solution. Similar findings about the previous case still apply.

Cases c to e are three laminated [0/90/0] square plates, which are retaken from [83] and whose length-to-thickness ratio is 10. Results of fundamental frequencies for three different boundary conditions (all simply-supported edges SSSS, all clamped edges CCCC, two opposite edges parallel to α-axis supported, while the others are clamped CSCS) are reported in Table 5.2c, where the following normalizations are used:

$$\bar{\omega} = \omega \frac{L_\alpha}{h} \sqrt{\frac{L_\alpha^2 \, \rho_{\_MATp}}{E_{2\_MATp}}} \tag{5.3}$$

Regarding case c, all theories (except FSDT and HSDT, whose percentage errors are greater than 3%) accurately calculate fundamental frequency. Nevertheless layerwise effects are not strong and this case is not particularly thick, FSDT and HSDT demonstrate that they should not be used, because there are not capable to capture even the first natural frequency.

A bigger scatter of results is obtained for cases d and e, because of clamped edges. Particularly, MHWZZA and MHWZZA4 are very inaccurate (percentage errors greater than 10%) but also HRZZ, HRZZ4, MHR, MHR4, MHR±, MHR4±, HSDT_32, HSDT_33, FSDT and HSDT (errors between 3% and 10%) are not able to obtain the precision of higher-order adaptive theories (ZZA, HWZZ, ZZA_RDF, HWZZ_RDF, HSDT_34, ZZM, HWZZM, ZZA*, HWZZM*, ZZA_GEN1, ZZA_GEN2*, ZZA****, ZZA_XN1 to ZZA_XN10), which are in a very good agreement with 3-D FEA solution. Anyway, these cases are not particularly probative, so, more challenging cases will be considered in the following section.

Theories	Case c SSSS	Case d CCCC	Case e CSCS	Theories	Case c SSSS	Case d CCCC	Case e CSCS
3-D FEA [48]	11.4306	16.6658	15.3895	MHR4	11.6644	18.4802	16.9713
♠	11.4583	16.4575	15.1875	MHR±	11.4647	18.0505	16.6145
HRZZ	11.4502	17.5659	16.1304	MHR4±	11.6644	18.4802	16.9713
HRZZ4	11.4569	17.6134	16.1481	HSDT_32	11.4575	18.0908	16.3905
MHWZZA	9.1000	20.8865	6.0313	HSDT_33	11.4652	18.1088	16.9934
MHWZZA4	9.1054	21.0304	6.3368	HSDT	11.7900	18.5237	17.4157
MHR	11.4647	18.0505	16.6145	FSDT	12.1630	17.5603	16.4436

♠ ZZA, HWZZ, ZZA_RDF, HWZZ_RDF, HSDT_34, ZZM, HWZZM, ZZA*, HWZZM*, ZZA_GEN1, ZZA_GEN2*, ZZA****, ZZA_XN1 to ZZA_XN10, HSDT_34, (error < 1%);

Table 5.2c. Cases c to e

5.3 Cases f to k (natural frequencies)

Regarding case f, a monolayer retaken from [84] is analysed and results of first seven modes are reported in Table 5.3a. The following orthotropic stiffness properties are assumed: Q11=10^5MPa, Q12=23319Mpa, Q13=1077.6MPa, Q22=54310.3MPa, Q23=9827.6MPa, Q33=53017.2MPa, Q55=26681MPa, Q44=15991.4MPa, Q66=26293.1MPa, density=1627 kg/m^3 and the following normalization is adopted:

$$\overline{\omega} = \omega h \sqrt{\frac{\rho}{Q_{11}}} \tag{5.4}$$

This case is interesting because nevertheless it is a monolayer, pumping modes occur (numbers in bold in Table 5.3a). Pumping modes show asymmetric trend of transverse displacement respect to middle plane of laminate and in-plane displacements are symmetric. Instead, other modes (bending) show a symmetric trend of transverse displacement, while in-plane displacements are asymmetric. As a general rule, the latter ones are better represented by theories, because transverse deformability could not be of primary importance. Indeed, following cases show that very big errors are provided by lower-order theories regarding pumping modes, while higher-order zig-zag adaptive models are always accurate.

Theories	**Mode with (n, m) waves**					**(n,m) waves**	**Mode with (n, m) waves**					**(n,m) waves**
Exact	0.0474	**0.2170**	**0.3941**	1.3077	1.6530		0.1033	**0.3450**	**0.5624**	1.3331	1.7160	
♠	0.0474	**0.2169**	**0.3940**	1.3085	1.6543	(1,1)	0.1033	**0.3450**	**0.5624**	1.3339	1.7184	(1,2)
HSDT	0.0474	-	-	1.3086	1.6549		0.1031	-	-	1.3339	1.7208	
FSDT	0.0473	-	-	1.3078	1.6540		0.1031	-	-	1.3331	1.7201	
Exact	0.1188	**0.3515**	**0.6728**	1.4205	1.6805		0.1694	**0.4338**	**0.7880**	1.4316	1.7509	
♠	0.1188	**0.3515**	**0.6728**	1.4215	1.6819	(2,1)	0.1694	**0.4338**	**0.7880**	1.4324	1.7535	(2,2)
HSDT	0.1187	-	-	1.4215	1.6826		0.1692	-	-	1.4323	1.7560	
FSDT	0.1185	-	-	1.4209	1.6817		0.1698	-	-	1.4316	1.7554	
Exact	0.1888	**0.4953**	**0.7600**	1.3765	1.8115		0.2180	**0.5029**	**0.9728**	1.5778	1.7334	
♠	0.1888	**0.4953**	**0.7601**	1.3772	1.8156	(1,3)	0.2180	**0.5029**	**0.9728**	1.5788	1.7351	(3,1)
HSDT	0.1884	-	-	1.3772	1.8207		0.2180	-	-	1.5788	1.7360	
FSDT	0.1881	-	-	1.3764	1.8203		0.2172	-	-	1.5782	1.7353	
Exact	0.3320	**0.6504**	**1.1814**	1.5737	1.9289							
♠	0.3321	**0.6504**	**1.1816**	1.5744	1.9338	(3,3)						
HSDT	0.3315	-	-	1.5744	1.9390							
FSDT	0.3302	-	-	1.5736	1.9388							

♠ ZZA, HWZZ, ZZA_RDF, HWZZ_RDF, HSDT_34, ZZM, HWZZM, ZZA*, HWZZM*, ZZA_GEN1, ZZA_GEN2*, ZZA****, ZZA_XN1 to ZZA_XN10, HRZZ, HRZZ4, MHR, MHR4, MHWZZA, MHWZZA4, MHR±, MHR4±, HSDT_32, HSDT_33

Table 5.3a. Case f

Anyway, because of a monolayer is analyzed, all theories of chapter two are very accurate and provide indistinguishable results, so, ZZA, HWZZ, ZZA_RDF, HWZZ_RDF, HSDT_34, ZZM, HWZZM, ZZA*, HWZZM*, ZZA_GEN1, ZZA_GEN2*, ZZA****, ZZA_XN1 to ZZA_XN10, HRZZ, HRZZ4, MHR,

MHR4, MHWZZA, MHWZZA4, MHR±, MHR4±, HSDT_32, HSDT_33 are in very good agreement with exact solution. Regarding FSDT and HSDT, they are able to reproduce bending modes, while they cannot calculate pumping ones because of their uniform transverse displacement. However, the following cases will demonstrate that pumping modes could occur between the first modes for thick sandwiches, so, their use in application should be discouraged. Nevertheless this case constitutes a standard test for accuracy of sandwich theories, results demonstrate that it is not probative, because 3-D zig-zag effects are disregarded.

Challenging cases g to k are reported here with the intended aim to test the accuracy of theories of chapter two to capture pumping modes and strong layerwise effects, for dynamic applications. So, these benchmarks are five soft-core sandwich plates, whose laminated faces are made up of different materials whose mechanical properties are similar to those of materials that are used for industrial applications. Low length-to-thickness ratios are considered, so, Lx/h=5 is assumed for cases g and h, while 4 is adopted for cases i to k. Five different lay-ups, either symmetrical and non-symmetrical, are considered, for which pumping modes occur for cases g, i and k.

Regarding case g, the first six modes of a simply-supported soft-core sandwich plate (retaken from [17]) are reported in Table 5.3b. Its faces are laminated while a length-to-thickness ratio of 5 and the following normalizations are adopted:

$$\overline{\omega}=\omega\frac{L_{\alpha}^{2}}{h}\sqrt{\frac{\rho_{\_MATr2}}{E_{2\_MATr2}}}\quad \overline{u_i}=\frac{u_i}{\left|u_i\right|_{\max}}\quad \overline{\sigma_{ij}}=\frac{\sigma_{ij}}{\left|\sigma_{ij}\right|_{\max}} \tag{5.5}$$

Theories	Mode 1	Mode 2	Mode 3	Mode 4	Mode 5	Mode 6 Pumping
3D FEA	1.6882	2.8796	3.4723	4.3033	4.6899	5.7441
♠	1.6898	2.8855	3.4777	4.3171	4.7030	5.7500
HRZZ	1.6823	2.8517	3.3940	4.1648	4.5907	34.3046
HRZZ4	1.6821	2.8525	3.3965	4.1720	4.5948	34.1832
MHWZZA	11.7654	2.7153	2.7264	3.7526	6.8737	1.4635
MHWZZA4	1.1776	3.9325	4.3165	4.3950	4.5656	5.6519
MHR	12.7147	15.1380	16.4288	27.1626	27.6009	64.6322
MHR4	12.7626	16.6121	22.2689	27.7771	27.8687	75.2673
MHR±	1.6959	2.9097	3.4919	4.3405	4.7643	61.7387
MHR4±	5.1510	5.8356	6.7704	7.2618	7.2672	66.5689
HSDT_32	1.7083	3.7725	5.5851	6.5974	6.8196	7.6773
HSDT	3.9263	5.9589	6.8677	8.2366	8.4810	-
FSDT	11.0783	17.6361	20.9784	25.0619	25.3697	-
♠ ZZA, HWZZ, ZZA_RDF, HWZZ_RDF, HSDT_34, ZZM, HWZZM, ZZA*, HWZZM*, ZZA_GEN1, ZZA_GEN2*, ZZA****, ZZA_XN1 to ZZA_XN10, HSDT_33 (error < 1%)						

Table 5.3b. Normalized natural frequencies, case g

Thick core is weaker and less stiff than materials of faces, so, as a consequence of strong variation of properties across the thickness, strong layerwise effects rise. So, all lower-order theories except HSDT_33 (whose results are in good agreement those provided by higher-order zig-zag theories) are inadequate.

Particularly, the first five bending modes are inaccurately predicted by MHWZZA, MHWZZA4, MHR, MHR4, MHR4±, HSDT_32, FSDT and HSDT, while good results are provided by HRZZ, HRZZ4 and MHR±. Anyway, all these theories calculate the sixth mode (pumping) with very high percentage errors, because their kinematic is too simple, while an accurate description of transverse deformability is required to precisely capture this mode.

Figure 5.3a reports modal transverse shear stress provided by all theories for the first mode (bending). For all figures of this chapter, results provided by higher-order zig-zag adaptive theories (ZZA, HWZZ, ZZA_RDF, HWZZ_RDF, HSDT_34, ZZM, HWZZM, ZZA*, HWZZM*, ZZA****, ZZA_XN1 to ZZA_XN10) are grouped together, because practically indistinguishable results are obtained (discrepancies lower than 0.5% from each other). It should be noticed that a great dispersion of results is obtained and a very inaccurate stress is calculated by MHR, MHR4, MHR±, MHWZZA, MHWZZA4, FSDT and HSDT because of their kinematics, confirming what previously stated.

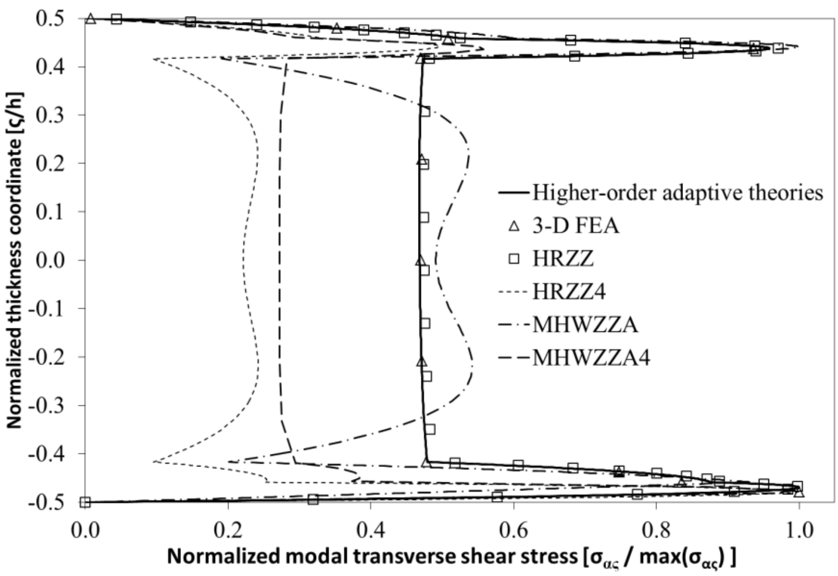

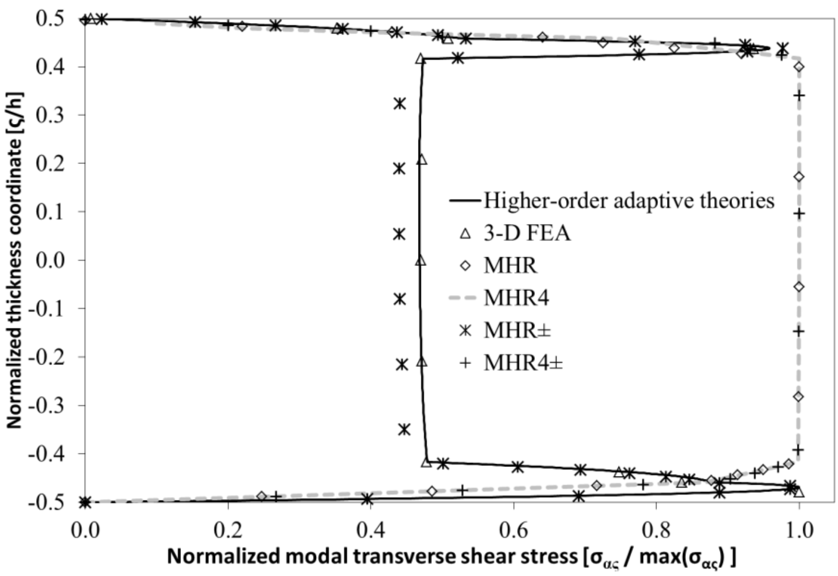

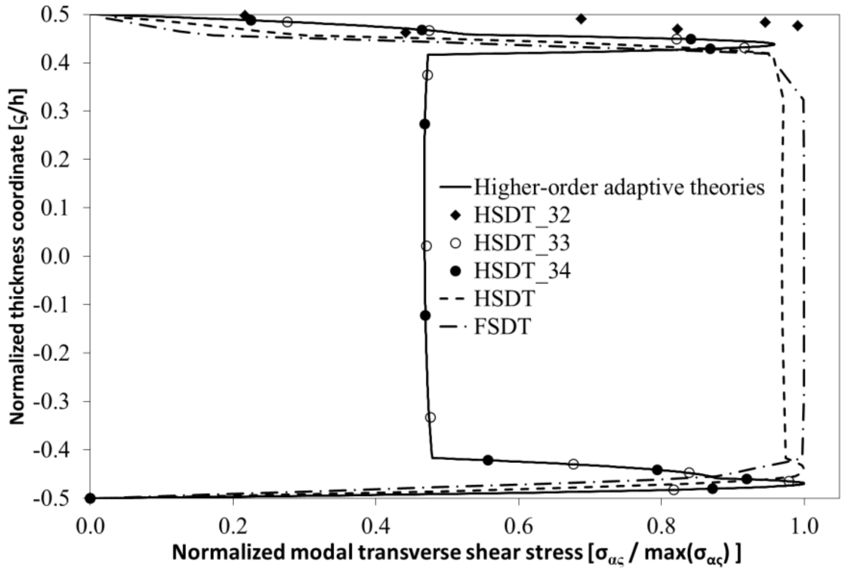

Figure 5.3a: Transverse shear modal stress, mode 1, case g

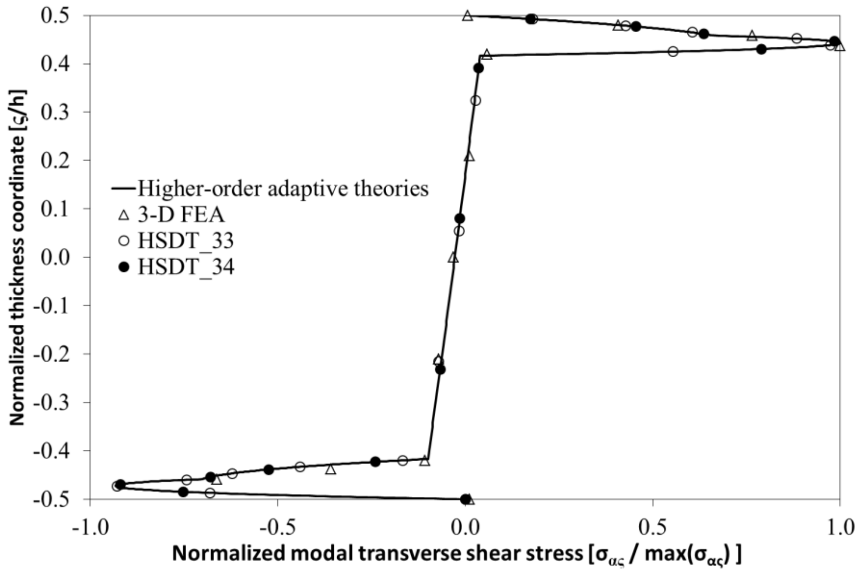

Figure 5.3b: Transverse shear modal stress, mode 6, case g

Figure 5.3b reports modal transverse shear stress of the sixth mode (pumping) provided by HSDT_33, HSDT_34 and higher-order adaptive theories (ZZA, HWZZ, ZZA_RDF, HWZZ_RDF, HSDT_34, ZZM, HWZZM, ZZA*, HWZZM*, ZZA****, ZZA_XN1 to ZZA_XN10), while results by other models are not reported being too inaccurate. Because of higher-order theories always obtain results in a very well agreement with 3-D FEA or other reference solutions, it is demonstrated that these theories can be successfully used also for dynamic calculations, without any loss of accuracy, irrespective the zig-zag and representation functions used, demonstrating that these choices are not important if the full set of physical constraints is imposed and coefficients are redefined for each layer across the thickness (adaptivity). Moreover, under these conditions, it is unnecessary to assign a specific role a priori to coefficients. Instead, the precision of lower-order theories is strongly case-dependent and pumping modes constitute very challenging test cases for theories, because a very accurate description of transverse deformability is required. ESL theories, FSDT and HSDT, are very inaccurate, so, their use should be avoided and limited to structures whose 3-D effects are irrelevant.

Regarding case h, a simply-supported sandwich plate with a length-to-thickness ratio of 5 is analyzed. This case is retaken from [19] and the same lay-up of the previous case is assumed, while a different and less stiff material is used for the core. The first six modes are reported in Table 5.3c and the following normalizations are assumed:

$$\overline{\omega} = \omega \frac{L_\alpha^2}{h} \sqrt{\frac{\rho_{\_MATr2}}{E_{2\_MATr2}}} \quad \overline{u_i} = \frac{u_i}{|u_i|_{\max}} \quad \overline{\sigma_{ij}} = \frac{\sigma_{ij}}{|\sigma_{ij}|_{\max}} \tag{5.6}$$

Theories	**Mode 1 (1,1)**	**Mode 2 (2,1)**	**Mode 3 (1,2)**	**Mode 4 (2,2)**	**Mode 5 (3,1)**	**Mode 6 (3,2)**
3D FEA	3.1542	5.1028	5.5209	6.8629	7.5472	8.8919
♠	3.1633	5.1395	5.5511	6.9273	7.6341	9.0113
HRZZ	3.1479	5.0779	5.4561	6.7539	7.4598	8.6694
HRZZ4	3.1514	5.0913	5.4767	6.7941	7.4976	8.7509
MHWZZA	1.3295	2.3539	2.9193	3.1509	3.5257	8.2946
MHWZZA4	1.3279	3.6122	3.7515	3.8117	4.1134	5.4391
MHR	13.8886	16.7596	18.6062	29.6763	30.2885	30.6550
MHR4	13.9395	18.3181	24.6705	30.3678	30.5640	33.9737
MHR±	3.1738	5.1859	5.5979	7.0148	7.7790	9.1996
MHR4±	8.1940	9.0023	10.5224	12.2961	12.5958	14.3421
HSDT_32	3.3692	5.6590	7.2343	8.6884	9.1652	11.4630
HSDT	4.9605	7.6850	8.5441	10.4062	10.9805	13.0905
FSDT	12.1820	19.4765	23.1196	27.6664	28.0848	34.2690
♠ ZZA, HWZZ, ZZA_RDF, HWZZ_RDF, HSDT_34, ZZM, HWZZM, ZZA*, HWZZM*, ZZA_GEN1, ZZA_GEN2*, ZZA****, ZZA_XN1 to ZZA_XN10, HSDT_33 (error < 1%)						

Table 5.3c. Normalized natural frequencies, case h

Because of the different material used for the core, there are no pumping modes between the first six ones (bending). This suggests that pumping modes can occur among the first modes depending on the combination of mechanical properties and densities of faces and core. Anyway, there are quite strong layerwise effects and Murakami’s rule is not respected, so, MHR, MHR4, calculate frequencies with high percentage errors. Anyway, also MHR±, MHWZZA, MHWZZA4, HSDT_32, FSDT and HSDT are inaccurate, because their too simple kinematic. Only HRZZ, HRZZ4, HSDT_33, MHR± and higher-order adaptive theories (ZZA, HWZZ, ZZA_RDF, HWZZ_RDF, HSDT_34, ZZM, HWZZM, ZZA*, HWZZM*, ZZA****, ZZA_XN1 to ZZA_XN10) are in good agreement with 3-D FEA that is used as reference solution for this case.

Figure 5.3c shows the through-the-thickness variation of modal in-plane displacement for the fourth mode (bending) predicted by theories of chapters 2 and 3. A great dispersion of results is showed, like in the previous case and all lower-order theories except HSDT_33 and HSDT_34 calculate this quantity with a wrong trend. Also HRZZ and HRZZ4 are erroneous across the thickness, nevertheless their percentage errors of fourth frequency are not very big.

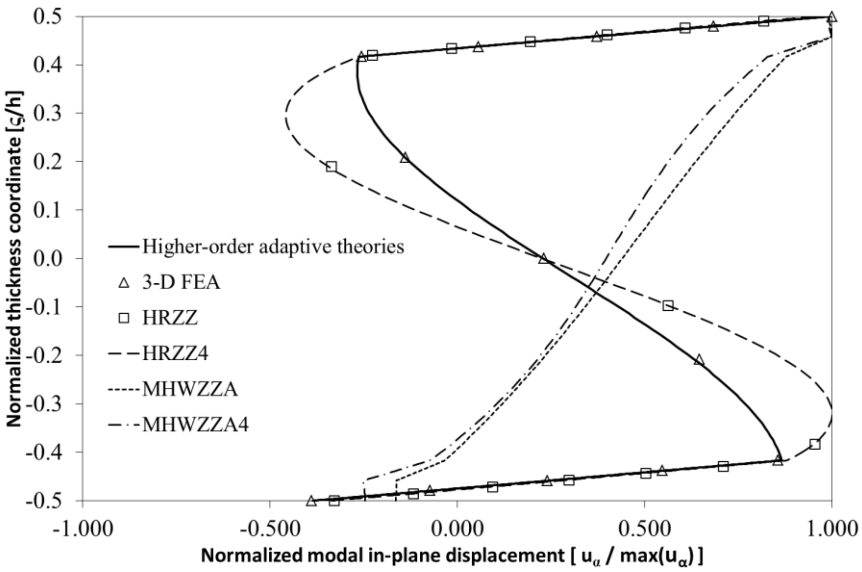

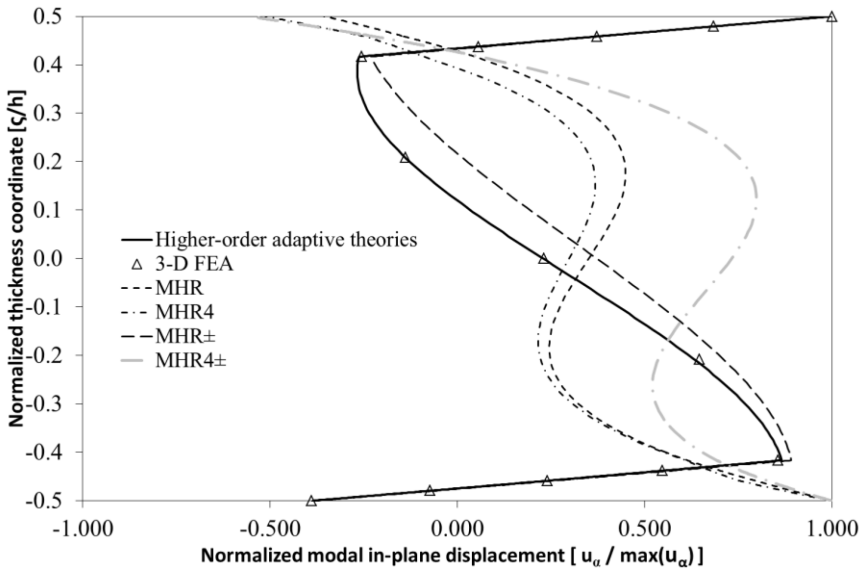

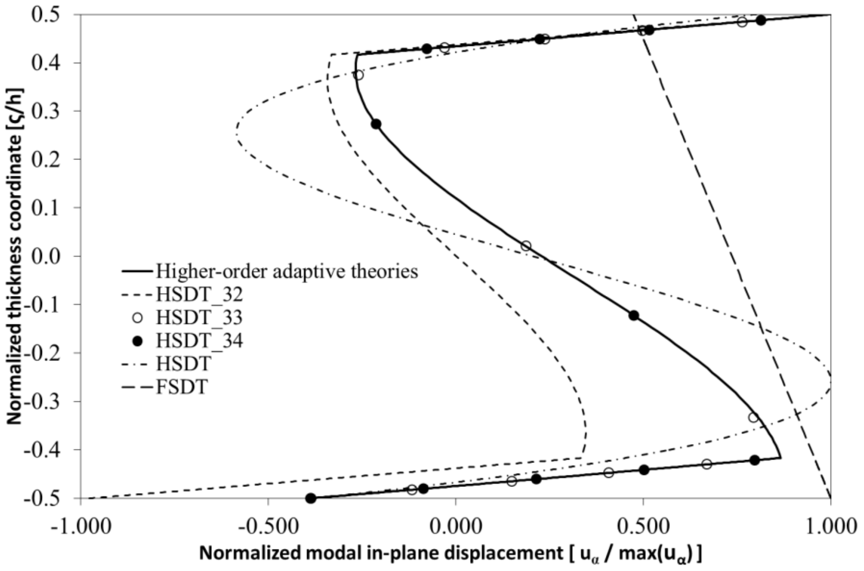

Figure 5.3c: In-plane modal displacement, mode 4, case h

Again, higher-order adaptive theories (ZZA, HWZZ, ZZA_RDF, HWZZ_RDF, HSDT_34, ZZM, HWZZM, ZZA*, HWZZM*, ZZA****, ZZA_XN1 to ZZA_XN10) prove their superiority, being always in very good agreement with 3-D FEA, irrespective the choices of zig-zag and representation functions. Moreover, zig-zag functions and linear contribution by FSDT can be also omitted and role of coefficients can be changed without any loss of accuracy.

Regarding case i, a simply-supported sandwich plate with a length to thickness ratio of 4 (retaken from [19]) is analyzed. Laminated faces are thin, whose constituent layers are made of glass/epoxy and rayon/epoxy. Instead, soft core is thick and it is made of a foam with more rigid properties than the previous case. The first ten normalized natural frequencies are reported in Table 5.3d

$$\overline{\omega} = \omega \frac{L_\alpha^2}{h} \sqrt{\frac{\rho_{\_MATu2}}{E_{2\_MATu2}}} \quad \overline{u_i} = \frac{u_i}{|u_i|_{\max}} \quad \overline{\sigma_{ij}} = \frac{\sigma_{ij}}{|\sigma_{ij}|_{\max}} \tag{5.7}$$

As a consequence of strong differences among properties of constituent layers, very strong layerwise effects rise and similarly to case g, pumping modes occur among the first ten frequencies (eighth to tenth, in bold in Table 5.3d).

Theories	Mode 1 (1,1)	Mode 2 (1,2)	Mode 3 (2,1)	Mode 4 (1,3)	Mode 5 (2,2)	Mode 6 (2,3)	Mode 7 (1,4)	Mode 8 (1,2) pumping	Mode 9 (1,3) pumping	Mode 10 (1,1) pumping
3D FEA	1.8250	2.9115	3.8103	4.3378	4.5581	5.7563	6.1051	**6.4866**	**6.6342**	**6.7820**
Theories with identical results♠	1.8302	2.9306	3.8184	4.3758	4.5813	5.7983	6.1442	**6.5052**	**6.6158**	**6.8955**
HRZZ	1.8116	2.8521	3.6589	4.1144	4.2849	5.1317	5.3547	**13.3111**	**15.6067**	**22.8002**
HRZZ4	1.8160	2.8702	3.6892	4.1721	4.3456	5.2736	5.5271	**15.6428**	**16.6538**	**22.9738**
MHWZZA	0.6942	2.3977	2.6214	3.0188	3.9030	4.5651	6.1380	**7.7168**	**10.9624**	**13.5256**
MHWZZA4	0.6980	2.0240	2.4328	3.2701	3.4373	3.6584	3.8426	**6.2970**	**21.3296**	**28.1332**

MHR	9.5006	12.2412	15.1366	17.2619	17.6349	17.9766	18.3084	**18.8505**	**37.6813**	**52.1934**
MHR4	9.5609	13.3372	18.6770	18.9136	20.7667	24.6293	25.1072	**15.6264**	**25.7609**	**34.6050**
MHR±	1.8389	2.9673	3.8584	4.4778	4.6501	5.9317	6.3553	**16.9912**	**31.6639**	**45.3776**
MHR4±	5.0499	5.9727	6.7604	7.1795	7.2376	7.8740	7.9708	**31.6309**	**36.3794**	**41.6820**
HSDT_32	2.0354	3.1806	4.8855	5.2842	6.0359	7.1412	7.3720	**7.5825**	**8.7272**	**12.6639**
HSDT_33	1.8301	2.9303	3.8175	4.3750	4.5800	5.7964	6.1428	**6.7578**	**6.8938**	**7.1157**
HSDT	3.3835	5.1523	6.0926	7.2858	7.3239	9.0389	9.7357	-	-	-
FSDT	8.7966	13.4532	17.2541	19.7304	20.0760	24.7239	26.4143	-	-	-
♠ ZZA, HWZZ, ZZA_RDF, HWZZ_RDF, HSDT_34, ZZM, HWZZM, ZZA*, HWZZM*, ZZA_GEN1, ZZA_GEN2*, ZZA****, ZZA_XN1 to ZZA_XN10, HSDT_33 (error < 1%)										

Table 5.3d. Normalized natural frequencies, case i

So, all lower-order theories are inaccurate and very high percentage errors are provided by HRZZ, HRZZ4, MHWZZA, MHWZZA4, MHR, MHR4, MHR±, MHR4±, HSDTD_32, HSDT_33 (for this theory, unlike other lower-order ones, only pumping modes are wrong), FSDT and HSDT. These latter two ESL models confirm their unreliability to analyze thick soft core sandwiches. Anyway, all the previous cited models are not precise, because of their too simple kinematics and their incorrect description of transverse deformability. It is also confirmed that percentage errors increase for higher frequency, so, the only fundamental frequency (which is accurately predicted by HRZZ, HRZZ4, MHR± and HSDT_32 and higher-order theories) is not probative about the accuracy of theories. It should be also noticed that Murakami's rule is not respected, so, MHR and MHR4 are erroneous, but the incorporation of strains and stresses from DZZ (MHWZZA, MHWZZA4) or the calculation of sign on a physical basis (MHR± and MHR4±) cannot improve performance, for the reason given above.

Figure 5.3d reports the modal transverse normal stress, for the tenth mode (pumping) as predicted by higher-order adaptive theories and by HSDT_32 and HSDT_33. These two latter models are the only reported in Figures because other ones show very inaccurate trend for pumping modes. Similar findings regarding natural frequencies still apply. Results demonstrate that higher-order theories (ZZA, HWZZ, ZZA_RDF, HWZZ_RDF, HSDT_34, ZZM, HWZZM, ZZA*, HWZZM*, ZZA****, ZZA_XN1 to ZZA_XN10) are the only able to accurately calculate natural frequencies and modal displacements and stresses, irrespective the zig-zag and representation functions chosen, demonstrating that these choices are not important if the full set of physical constraints from elasticity theory is imposed and coefficients are redefined for each layer across the thickness (adaptivity). Moreover, under these conditions, it is unnecessary to assign a specific role to coefficients.

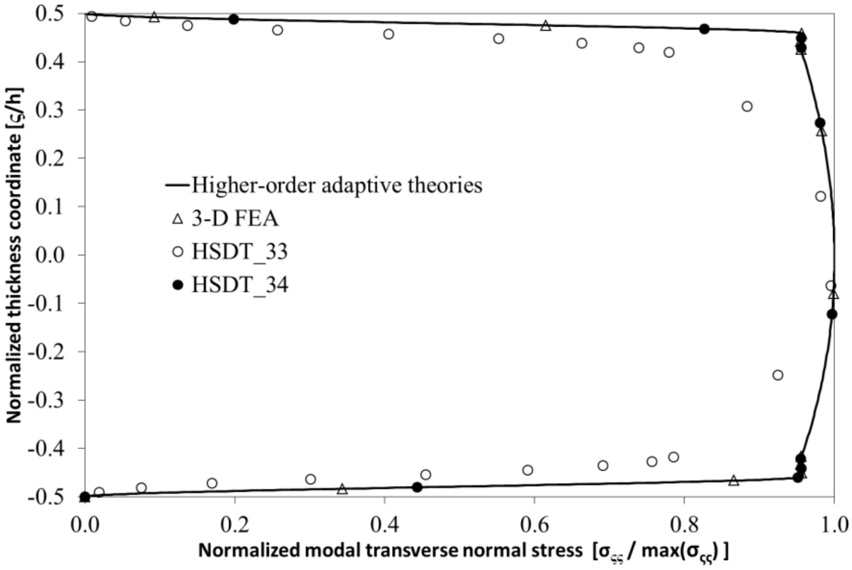

Figure 5.3d: Transverse normal modal stress, mode 10 (pumping), case i

Regarding <u>case j</u>, a simply-supported sandwich plate with a length-to-thickness ratio of 4 is analyzed. Like the previous case, faces are laminated and made of glass/epoxy and rayon/epoxy, but a more rigid and a more dense core is considered. The first tenth natural frequencies are reported in Table 5.3e and the following normalizations are adopted:

$$\overline{\omega}=\omega\frac{L_{\alpha}^{2}}{h}\sqrt{\frac{\rho_{\_MATu2}}{E_{2\_MATu2}}}\quad \overline{u_i}=\frac{u_i}{|u_i|_{\max}}\quad \overline{\sigma_{ij}}=\frac{\sigma_{ij}}{|\sigma_{ij}|_{\max}} \tag{5.8}$$

Differently to case i, no pumping modes occur among reported ones, because of the different properties of the core and as a consequence percentage errors provided by lower order theories are smaller than the previous case, because there are less strong layerwise effects. Anyway, because of their simplified kinematics, HRZZ, HRZZ4, HSDT_32, FSDT and HSDT are inaccurate, especially for higher frequencies. It should be noticed that HRZZ and HRZZ4 give a precise value of fundamental frequency, while the tenth is obtained with a mistake greater than 10%, demonstrating that the first natural frequency is not probative about accuracy of theories. Moreover, because of Murakami's rule is not respected, MHR and MHR4 are inadequate and MHWZZA, MHWZZA4, MHR4± are not able to improve their performance. Nevertheless this, MHR± appear quite accurate, as like as HSDT_33, demonstrating that the precision of lower-order theories is strongly case dependent. Only higher-order adaptive theories (ZZA, HWZZ, ZZA_RDF, HWZZ_RDF, HSDT_34, ZZM, HWZZM, ZZA*, HWZZM*, ZZA****, ZZA_XN1 to ZZA_XN10) appear always very accurate, irrespective the zig-zag and representation functions chosen, demonstrating that these choice is not important if the full set of physical constraints from elasticity theory is imposed and coefficients are redefined for each layer across the thickness (adaptivity).

Theories	Mode 1 (1,1)	Mode 2 (1,2)	Mode 3 (2,1)	Mode 4 (1,3)	Mode 5 (2,2)	Mode 6 (2,3)	Mode 7 (1,4)	Mode 8 (3,1)	Mode 9 (3,2)	Mode 10 (2,4)
3D FEA	2.0795	3.3263	4.1141	4.9108	4.9759	6.3078	6.8086	7.4053	8.0236	8.0545
Theories with identical results♠	2.0796	3.3265	4.1004	4.9036	4.9648	6.2918	6.7699	7.3228	7.9472	8.0112
HRZZ	2.0555	3.2287	3.9386	4.6061	4.6658	5.6683	6.0051	6.2595	6.4412	6.6360
HRZZ4	2.0616	3.2539	3.9753	4.6830	4.7377	5.8248	6.2043	6.4185	6.6973	6.9919
MHWZZA	0.6897	2.5190	2.8355	3.2094	4.0947	4.7940	5.2636	6.3369	10.2714	11.2195
MHWZZA4	0.6916	2.1904	2.5936	3.4786	3.6347	3.8856	4.0466	5.6961	8.6553	8.7156
MHR	9.2783	11.9900	14.8886	17.0729	17.2357	17.6067	18.5309	19.4935	21.3978	21.7227
MHR4	9.3355	13.0453	18.2477	18.5238	20.3075	24.1139	24.6192	26.5227	28.1148	29.0030
MHR±	2.0873	3.3592	4.1351	4.9964	5.0251	6.4125	6.9726	7.4450	8.0906	8.2465
MHR4±	5.1728	6.5043	7.5808	7.6859	7.8535	8.8055	9.2334	8.2442	8.9815	10.1505
HSDT_32	2.2404	3.5104	5.2991	5.4004	6.2323	7.5868	7.6496	9.6758	10.9591	11.5818
HSDT	3.4532	5.2974	6.1860	7.4331	7.5539	9.2594	9.6431	10.0533	10.5555	11.4844
FSDT	8.5977	13.1629	16.8641	19.3114	19.6340	24.1875	25.2568	25.8551	27.2188	29.6662
♠ ZZA, HWZZ, ZZA_RDF, HWZZ_RDF, HSDT_34, ZZM, HWZZM, ZZA*, HWZZM*, ZZA_GEN1, ZZA_GEN2*, ZZA****, ZZA_XN1 to ZZA_XN10, HSDT_33 (error < 1%)										

Table 5.3e. Normalized natural frequencies, case j

Regarding case k, a simply-supported sandwich plate is analyzed. Again a length-to-thickness ratio of 4 is assumed and faces are made of glass/epoxy and rayon/epoxy like cases i and j. Soft core is made of two different industrial foams, where the ¾ of thickness from below are made of Rohacell 31 (like case i), while the remaining part is made of a less rigid and more dense Rohacell foam. Because of these choices, strongly asymmetries (greater than those of cases i and j) rise. It should be noticed that sandwich theories in literature are often developed by imposing symmetric limitations, anyway, also asymmetries should be considered because they could be caused by a damage during service life. A big scatter of results is shown in Table 5.3f, that contains the first tenth natural frequencies for this case, where the seventh, the ninth and the tenth are pumping modes (in bold in Table 5.3f). The following normalizations are adopted:

$$\overline{\omega} = \omega \frac{L_{\alpha}^{2}}{h} \sqrt{\frac{\rho_{\_MATu2}}{E_{2\_MATu2}}} \quad \overline{u_i} = \frac{u_i}{|u_i|_{\max}} \quad \overline{\sigma_{ij}} = \frac{\sigma_{ij}}{|\sigma_{ij}|_{\max}} \tag{5.9}$$

Regarding lower-order theories, very large errors, especially for pumping modes, are provided by HRZZ, HRZZ4, MHR, MHR4, MHR±, MHR4±, MHWZZA, MHWZZA4, HSDT_32, HSDT and FSDT, because their kinematics is too simple. HSDT_33 obtain natural frequencies with percentage errors up 5%, but the accuracy of higher-order adaptive ones (ZZA, HWZZ, ZZA_RDF, HWZZ_RDF, HSDT_34, ZZM, HWZZM, ZZA*, HWZZM*, ZZA****, ZZA_XN1 to ZZA_XN10) cannot be reached.

Theories	Mode 1 (1,1)	Mode 2 (1,2)	Mode 3 (2,1)	Mode 4 (1,3)	Mode 5 (2,2)	Mode 6 (2,3)	Mode 7 (1,2) pumping	Mode 8 (1,4)	Mode 9 (1,1) pumping	Mode 10 (1,3) pumping
3D FEA	1.8088	2.8905	3.8226	4.3159	4.5659	5.7612	**5.8607**	6.0359	**6.0584**	**6.1857**
Theories with identical results♠	1.8078	2.8887	3.7844	4.3068	4.5319	5.7260	**5.8201**	6.0452	**6.0635**	**6.1789**
HRZZ	1.8069	2.8837	3.7376	4.2738	4.4553	5.5480	**15.8071**	5.8823	**28.4136**	**28.7126**
HRZZ4	1.8067	2.8826	3.7339	4.2671	4.4484	5.5302	**15.6286**	5.8443	**27.3772**	**27.9550**
MHWZZA	0.7246	0.9179	3.3407	3.3479	3.5688	4.3557	**6.1238**	4.0545	**7.9043**	**16.7350**
MHWZZA4	0.6978	0.8651	3.5557	6.3966	6.8917	9.7175	**6.2385**	10.1841	**6.8404**	**23.3498**
MHR	10.9702	12.9657	15.3170	17.2175	19.5764	19.5866	**12.4103**	20.1339	**12.9515**	**25.9401**
MHR4	11.1870	14.7950	22.6656	22.9203	26.2358	33.1135	**15.4831**	34.9702	**27.0792**	**28.0628**
MHR±	2.1762	3.5080	4.3617	5.2810	5.3128	6.8076	**20.4583**	7.3859	**27.0941**	**39.0589**
MHR4±	2.4204	4.0933	4.8042	5.9706	6.1081	7.6269	**25.1892**	8.3280	**29.2856**	**48.0530**
HSDT_32	2.8859	5.3262	6.8437	8.8258	9.9568	34.1067	**41.9080**	42.6294	**50.1473**	**53.2910**
HSDT_33	1.8076	2.8884	3.7832	4.3069	4.5306	5.7250	**5.8278**	6.0465	**6.3980**	**6.4500**
HSDT	3.3705	5.1307	6.0685	7.2555	7.2900	8.9979	-	9.6855	-	-
FSDT	8.7728	13.4157	17.2080	19.6752	20.0217	24.6560	-	26.3410	-	-
♠ ZZA, HWZZ, ZZA_RDF, HWZZ_RDF, HSDT_34, ZZM, HWZZM, ZZA*, HWZZM*, ZZA_GEN1, ZZA_GEN2*, ZZA****, ZZA_XN1 to ZZA_XN10 (error < 1%)										

Table 5.3f. Normalized natural frequencies, case k

Figure 5.3e reports the through-the-thickness variation of transverse normal stress for the ninth mode (pumping), where only results provided by higher-order theories and HSDT_33 are reported (the others are omitted being too inaccurate) confirming what previously stated about the accuracy of theories of chapter two for natural frequencies.

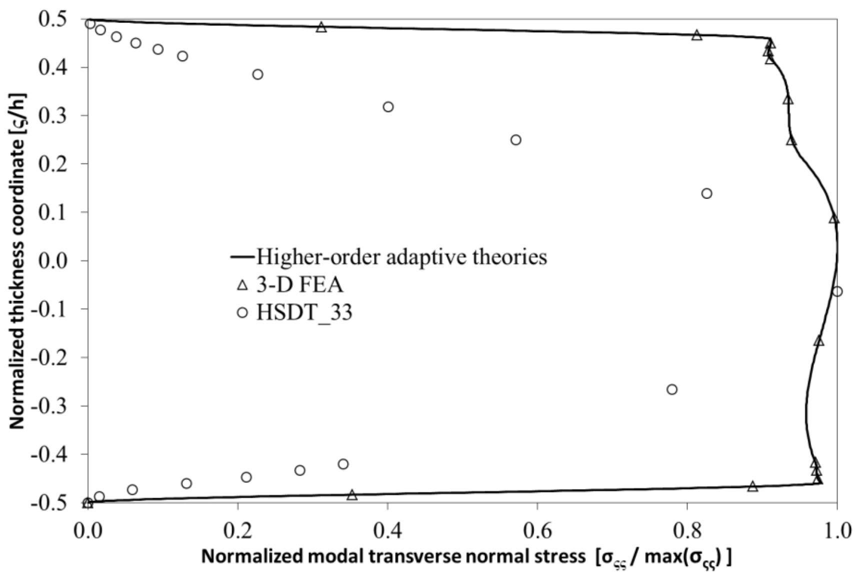

Figure 5.3e: Transverse normal modal stress, mode 9 (pumping), case k

Again, it is confirmed that only higher-order adaptive theories (ZZA, HWZZ, ZZA_RDF, HWZZ_RDF, HSDT_34, ZZM, HWZZM, ZZA*, HWZZM*, ZZA****, ZZA_XN1 to ZZA_XN10) appear always very accurate, irrespective the zig-zag and representation functions chosen, demonstrating that these choices are not important if the full set of physical constraints from elasticity theory is imposed and coefficients are redefined for each layer across the thickness (adaptivity). Moreover, under these conditions, it is unnecessary to assign a specific role to coefficients. All higher-order adaptive theories are able to successfully obtain accurate results also for dynamic cases and especially general ZZA_GEN theories demonstrates its superiority, being very efficient (see processing time of its particularizations ZZA_GEN1 and ZZA_GEN2*) and therefore able to compete with more famous and used examples in Literature.

5.4 Cases l and m: response to blast pulse loading

In this section, responses of two laminated sandwich plates under impulsive blast pulse loadings are reported. Study of this problem is important because this pressure pulse creates a shock wave that generates a pressure peak in the structures, which comes down with time and that could have harmful effects during service life. Papers [85], [86], [87], [88], [89], [90] are reported as remarkable examples regarding this argument.

According to the last cited papers, the following general expression of pressure for explosive blast pulse loading is adopted:

$$P(t) = P_m\left(1-\frac{t}{t_p}\right)e^{-a't/t_p} \tag{5.10}$$

where P_m is peak reflected pressure in excess to the ambient one, t_p is the positive phase duration of the pulse measured from the time of impact of the structure, while a' is a decay parameter. Regarding sonic boom problems, the following general expression is adopted:

$$P(t) = \begin{cases} P_m\left(1-\dfrac{t}{t_p}\right) & \text{for } 0<t<rt_p \\ 0 & \text{for } t<0 \text{ and } t>rt_p \end{cases} \tag{5.11}$$

where r is the shock pulse length factor, while P_m and t_p assume the same meaning of (5.10). Impulsive step, triangular, or exponential loading can be obtained from (5.10) and (5.11). In numerical applications, loading will be uniformly applied to the upper face of cases l and m. In the following subsection, Newmark implicit time integration scheme is briefly described, being used for calculations.

5.4.1 Newmark implicit time integration scheme

In this section, Newmark implicit time integration scheme is presented, because it is used for cases l and m. Explicit time integration scheme are not used in this thesis, because they could require very small time steps to be stable, even if very little ones are also used for this implicit method in numerical applications. However, this choice is not particularly heavy for computational costs, because only linearity are considered in numerical applications.

In order to use this method, firstly, dynamic problem is rewritten into matrix form, assuming $\{U(t)\}$ as the vector that contain the d.o.f. and $\{P(t)\}$ as the column of vector of applied load, which are function of the time t:

$$[M]\{\ddot{U}(t)\}+[K]\{U(t)\}=\{P(t)\} \tag{5.12}$$

$[M]$ is the mass matrix, while $[K]$ is the stiffness matrix (no damping is considered in numerical applications). The following boundary conditions on displacement vector $\{U(t)\}$ and its first time derivative, the velocity vector $\{\dot{U}(t)\}$, are assumed:

$$\begin{cases}\{U(0)\}=\{0\}\\ \{\dot{U}(0)\}=\{0\}\end{cases} \tag{5.13}$$

So, the following matrix system is obtained:

$$\begin{cases}[M]\{\ddot{U}(t)\}+[K]\{U(t)\}=\{P(t)\}\\ \{U(0)\}=\{0\}\\ \{\dot{U}(0)\}=\{0\}\end{cases} \tag{5.14}$$

Assuming Δt as the chosen time step, a total of m steps are obtained. Considering $n-th$ step, the following expressions of velocity and acceleration vectors are obtained after Δt (they are indicated as $\{\dot{U}\}_{n+1}$ and $\{\ddot{U}\}_{n+1}$ respectively), starting from $\{U\}_n$, $\{\dot{U}\}_n$ and $\{\ddot{U}\}_n$.

$$\begin{aligned}\{\dot{U}\}_{n+1}&=\frac{\gamma}{\beta\Delta t}\left(\{U\}_{n+1}-\{U\}_n\right)+\left(1-\frac{\gamma}{\beta}\right)\{\dot{U}\}_n+\left(1-\frac{\gamma}{2\beta}\right)\Delta t\{\ddot{U}\}_n\\ \{\ddot{U}\}_{n+1}&=\frac{1}{\beta\Delta t^2}\left(\{U\}_{n+1}-\{U\}_n\right)-\frac{1}{\beta\Delta t}\{\dot{U}\}_n+\left(1-\frac{1}{2\beta}\right)\{\ddot{U}\}_n\end{aligned} \tag{5.15}$$

where 2β and γ are assumed as 0.5, because in order to make this procedure unconditionally stable, the following inequality have to be respected [91], [92]:

$$2\beta\geq\gamma\geq 0.5 \tag{5.16}$$

A linear algebraic system of equations is obtained by substituting (5.15) into (5.14), obtaining $\{U\}_{n+1}$. So, using these same steps is possible to obtain $\{\ddot{U}\}_{n+2}$, $\{\dot{U}\}_{n+2}$, $\{U\}_{n+2}$ and so on.

5.4.2 Cases l and m

Results provided by theories for two simply-supported sandwich square plates under a step blast pulse are reported in this section. For both cases, the following expression of loading (that is uniform and applied on the top face) is assumed:

$$p = \begin{cases} p^0 & if \quad t < 5ms \\ 0 & if \quad t \geq 5ms \end{cases} \tag{5.17}$$

For both cases no effect of damping are taken into considerations and according to the previous section, Newmark implicit time integration method is used, where a time step of 30μs.

Regarding case l, that is retaken from [88] and has a length-to-thickness ratio of 20.8696, sandwich faces are laminated (five layers) and normalized transverse displacement is reported in Figure 5.4a and Table 5.4a, where the following normalization is used:

$$\overline{u_\varsigma} = \frac{u_\varsigma}{h} \tag{5.18}$$

It should be noticed that Murakami's rule is not respected, so, MHR and MHR4 are very inaccurate. For this reasons, their results are reported only in Table while they are omitted in Figure 5.4a.

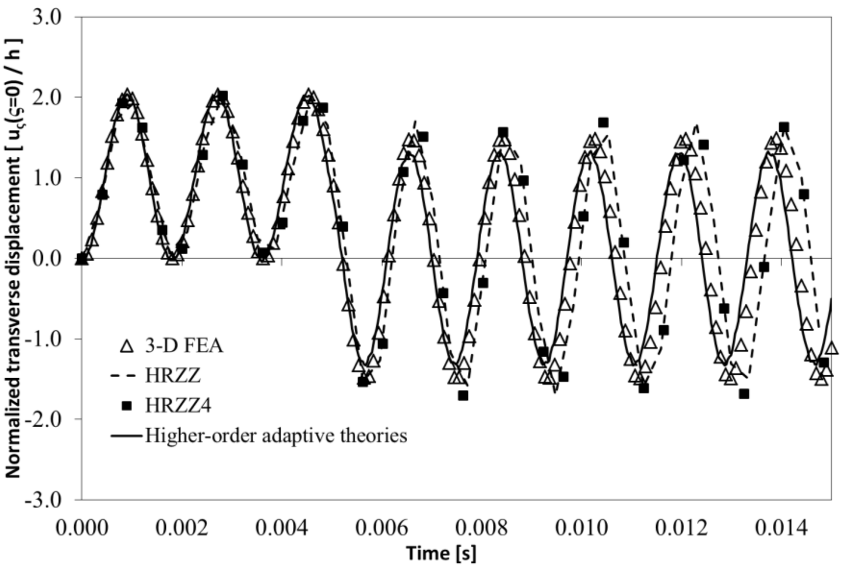

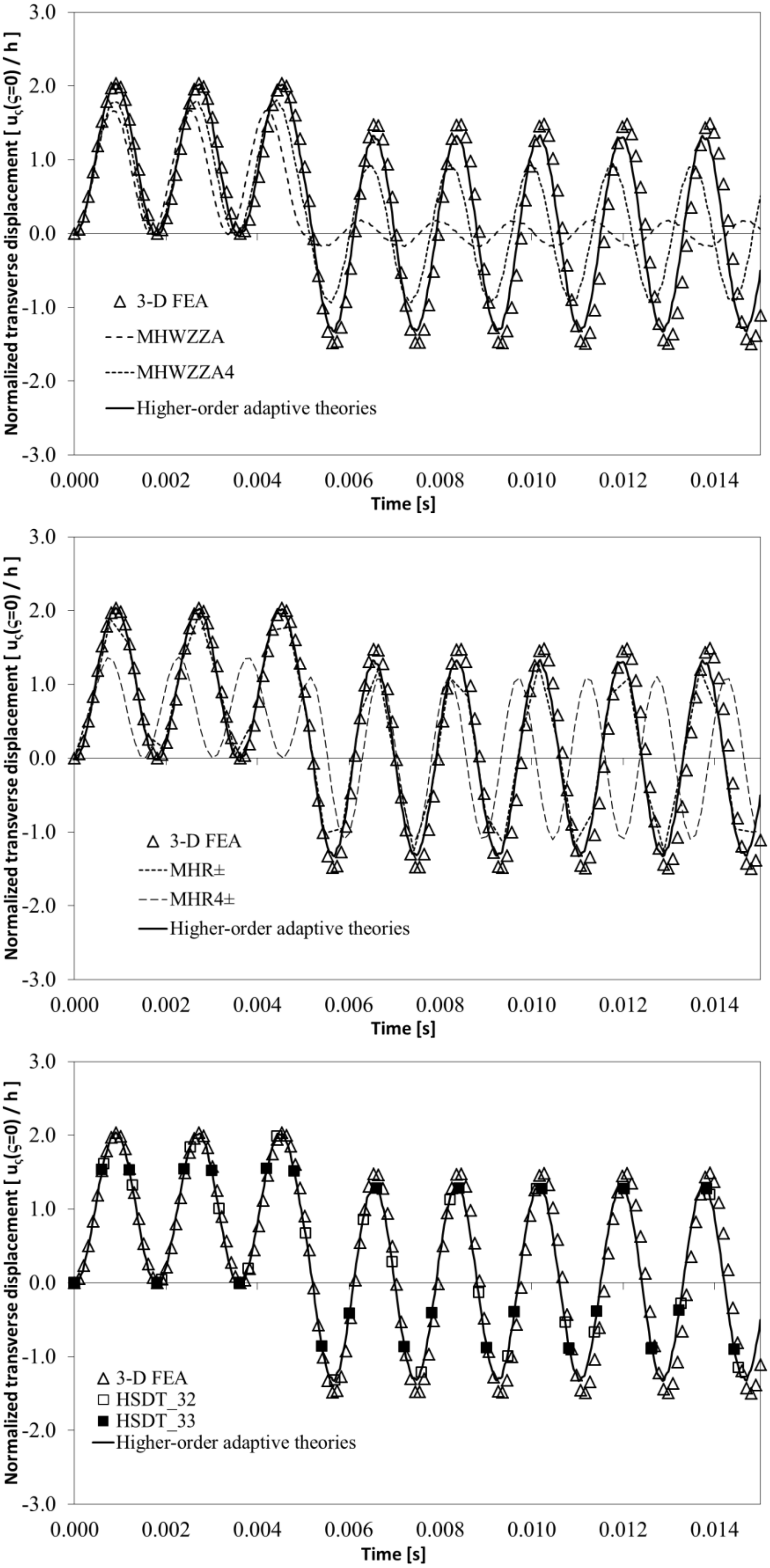

Figure 5.4a: Normalized transverse displacement, case I

MHR4± is not adequate for this case, while HRZZ, HRZZ4, MHWZZA, MHWZZA4 and MHR± are quite accurate during the first instants, but their percentage errors increase with increasing time. HSDT_32 and HSDT_33 are adequate, because their results are similar to those provided by higher-order adaptive theories (ZZA, HWZZ, ZZA_RDF, HWZZ_RDF, HSDT_34, ZZM, HWZZM, ZZA*, HWZZM*, ZZA****, ZZA_XN1 to ZZA_XN10, ZZA_GEN1 and ZZA_GEN2*) that are in very good agreement with 3-D FEA ones. Anyway, because of layerwise effects are not particularly high, other cases should be considered, in order to test the accuracy of theories regarding the response to blast pulse.

Theories	t[s]	0.0009	0.0045	0.0056	0.0065	0.0074
3-D FEA [48]		2,0268	2.0165	-1.3291	1.3278	-1.3174
Higher-order adaptive theories		2,0399	2.0179	-1.3298	1.3286	-1.3181
HRZZ		2,0219	1.9176	-1.6341	1.4543	-1.5171
HRZZ4		2,0212	1.9175	-1.6332	1.4540	-1.5169
MHWZZA		1,6544	1.1687	-0.0994	0.1028	-0.0331
MHWZZA4		1,7847	1.7135	-0.8618	0.8970	-0.8344
MHR		0,7774	0.9828	-0.4954	-0.0765	0.7464
MHR4		0,7320	1.0386	-0.2750	-0.2267	0.5604
MHR±		1,9734	1.9659	-1.2595	1.2568	-1.2586
MHR4±		1,2527	0.0008	-0.6226	0.8942	-1.0796
HSDT_32		2.0376	2.0376	-1.2797	1.2803	-1.2809
HSDT_33		2.0398	2.0396	-1.2744	1.2756	-1.2767

Table 5.4a. Case l

Regarding case m, that is retaken from [19], a length-to-thickness ratio of 10 is considered. Similarly to the previous case, faces are laminated (five layers), but a different orientation of layers is assumed and core is split into two parts and the half from above is made of a very slender material. Results of normalized transverse displacement of the middle plane are reported in Figure 5.4b, while those of upper and lower faces are reported in Figures 5.4c and 5.4d respectively, where the following normalization is assumed:

$$\overline{u_{\varsigma}} = \frac{u_{\varsigma}}{w} \quad w \text{ static response} \tag{5.19}$$

Because of asymmetries and properties of constituent layers, strong layerwise effects rise, so, there is a very big scatter of results. Again, MHR and MHR4 are very inaccurate and not reported in Figures because they are too inaccurate (since Murakami's rule is not respected), but also MHR±, MHR4±, MHWZZA, MHWZZA4, HRZZ, HRZZ4 and HSDT_32 are inadequate, because of their kinematic is too poor. Quite accurate results are provided by HSDT_33, even if percentage errors increase with increasing time (see Figure 5.4b). Higher-order theories (ZZA, HWZZ, ZZA_RDF, HWZZ_RDF, HSDT_34, ZZM, HWZZM, ZZA*, HWZZM*, ZZA****, ZZA_XN1 to ZZA_XN10, ZZA_GEN1 and ZZA_GEN2*) give always very accurate results, very close to 3-D FEA ones and indistinguishable from each other. So, it is demonstrated that the choice of zig-zag functions is immaterial (they can be also omitted) and that other representations across the thickness than polynomial one can be used without any loss of accuracy, if the whole set of physical constraints (1.15)-(1.20) is imposed and coefficients are redefined for each layer across the thickness. Under these conditions, it is confirmed that the role of coefficients can be changed and also linear contribution by FSDT can be omitted, otherwise accuracy of models depends on these choices and results become strongly case dependent.

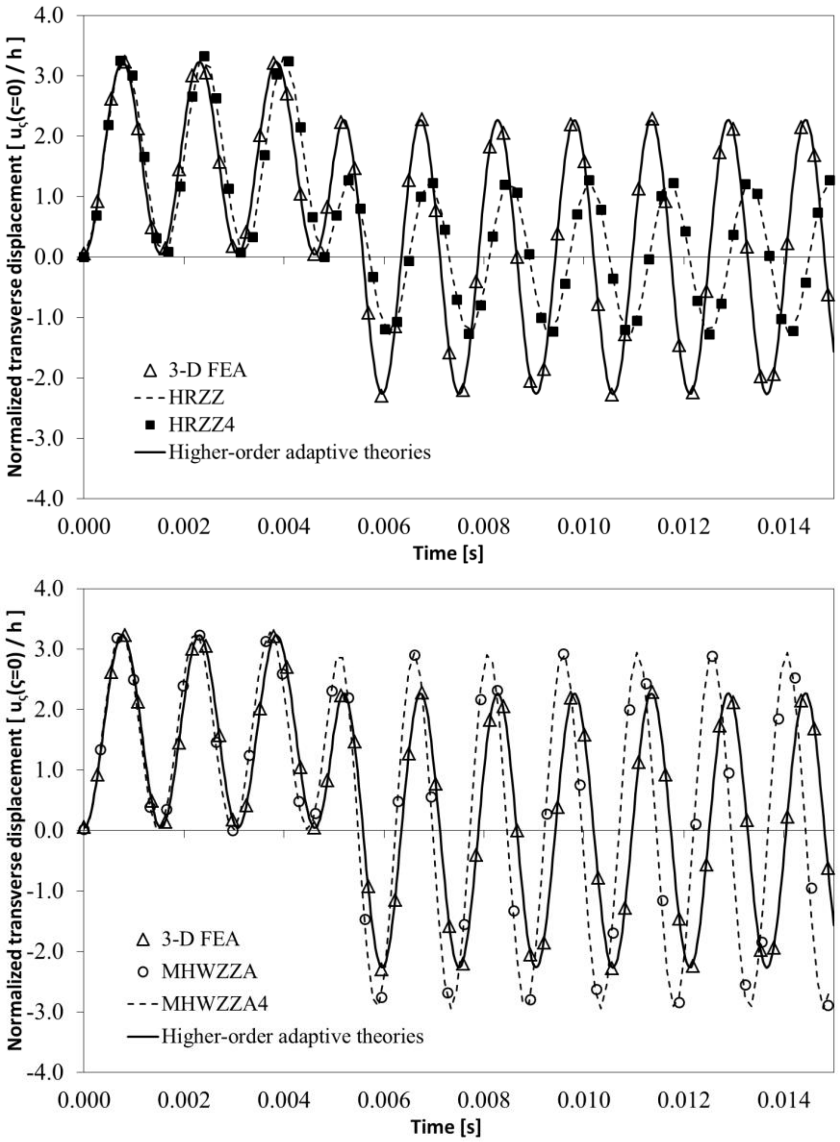

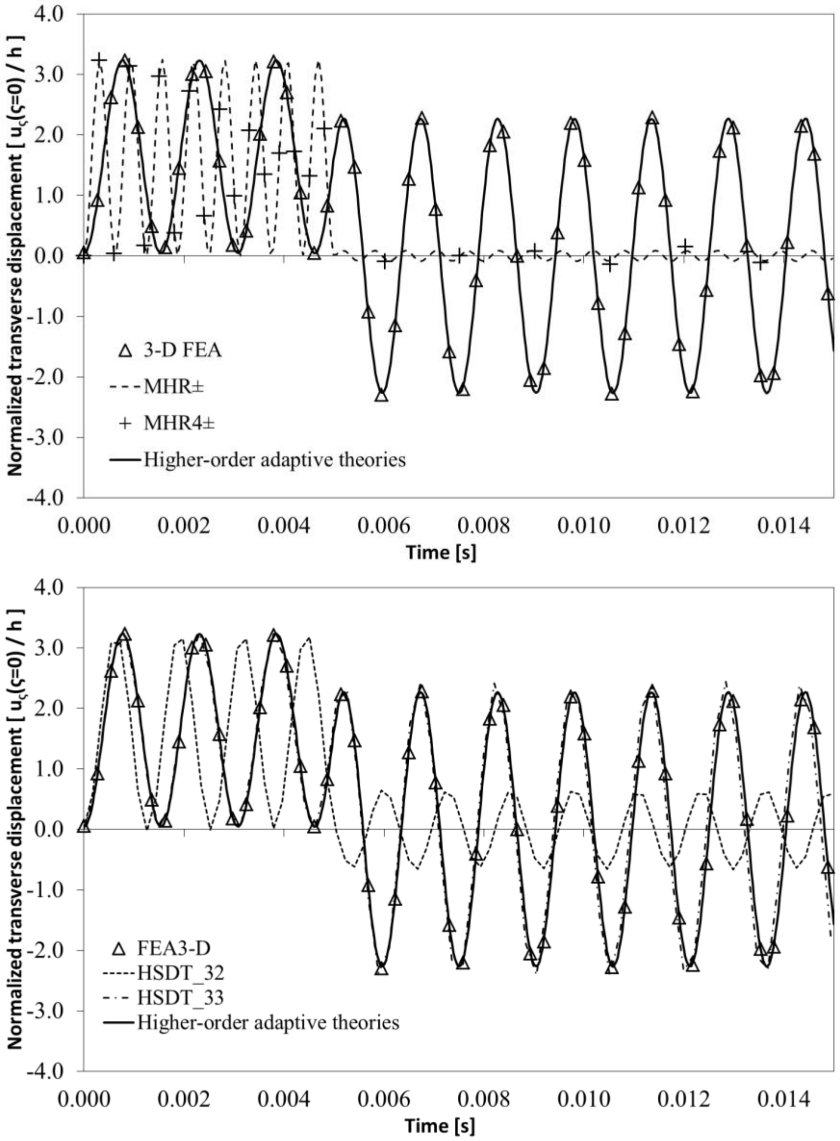

Figure 5.4b: Normalized transverse displacement, case m

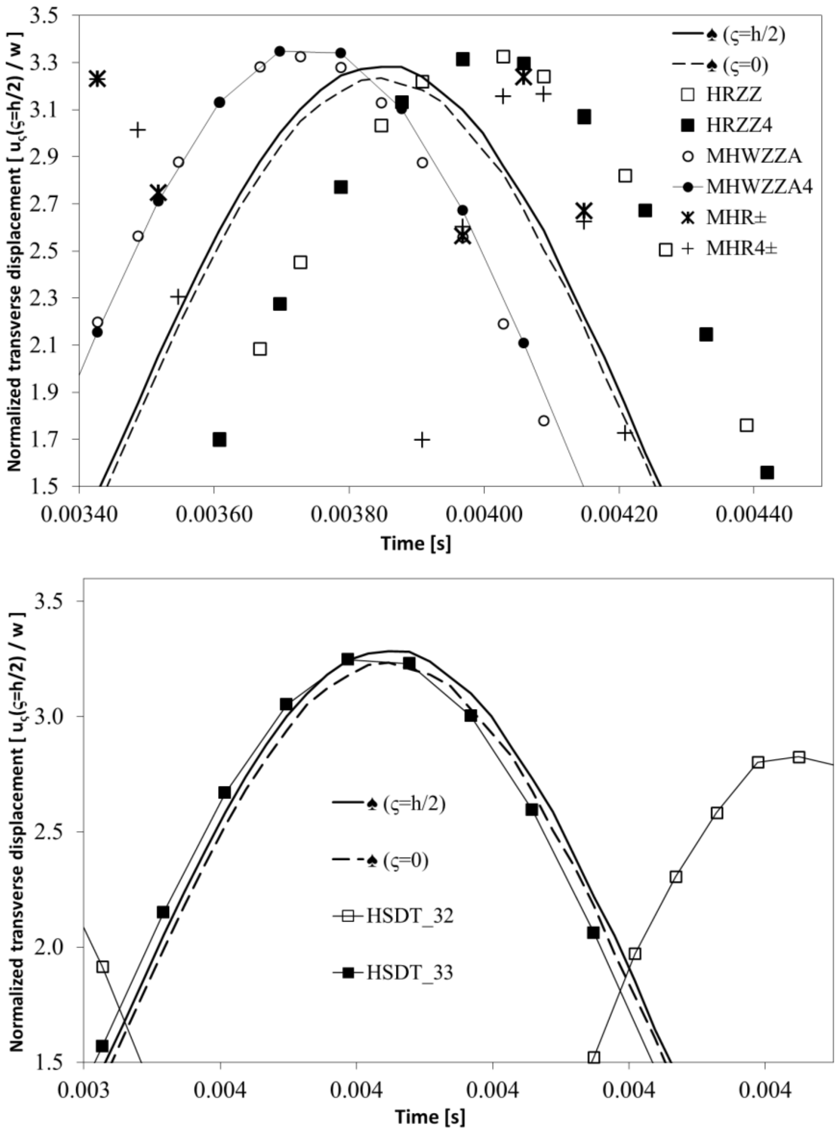

Figure 5.4c: Normalized transverse displacement, ♠ higher-order adaptive theories, case l (upper face)

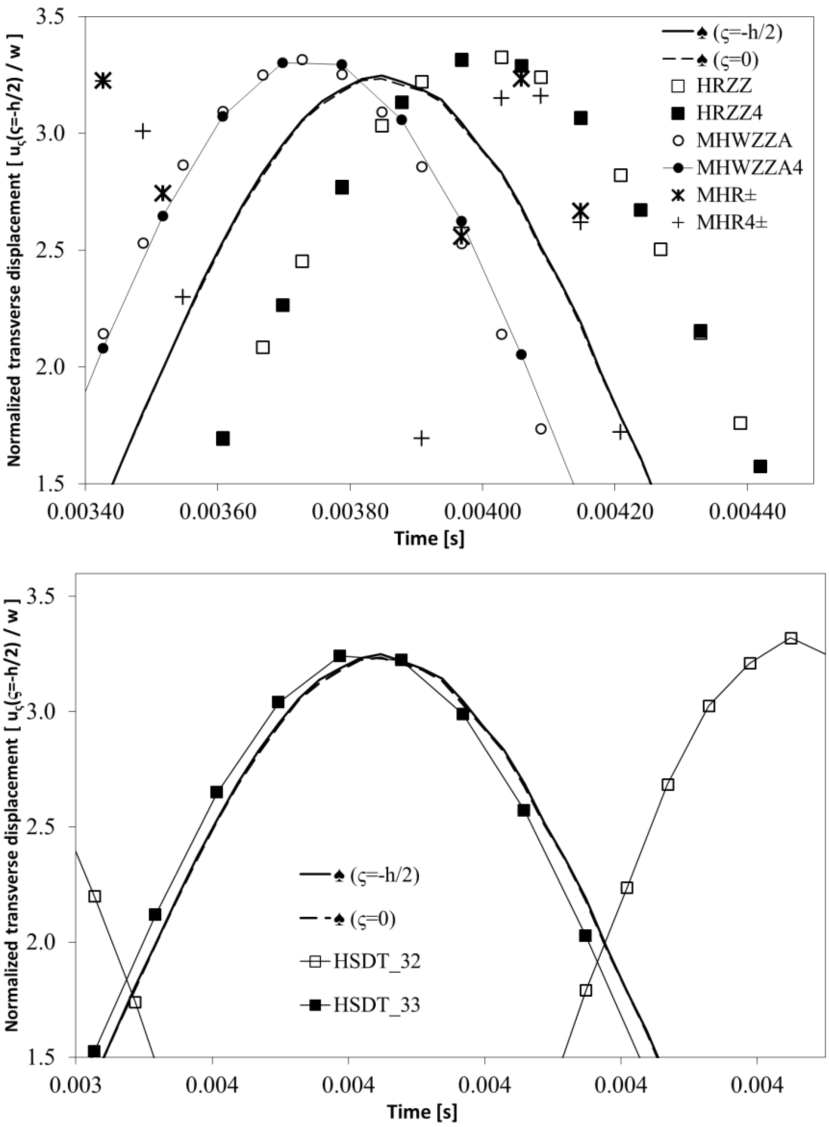

Figure 5.4d: Normalized transverse displacement, ♠ higher-order adaptive theories, case l (lower face)

5.5 Processing time of dynamic cases

Table 5.5 reports processing time for theories of chapter 2 and 3 for dynamic cases. Similar findings of Table 4.4 still apply. Mixed theories, MHR, MHR4, MHWZZA, MHWZZA4, HRZZ, HRZZ4, MHR± and MHR4± show low processing time but they are very inaccurate, especially when a precise description of transverse deformability is required (e.g. for pumping modes). So, the cost saving does not justify their usage. Higher-order adaptive DZZ whose zig-zag functions are omitted, show very good processing time. Particularly, because of the particularizations (ZZA_GEN1 and ZZA_GEN2*) of most general physically-based higher-order adaptive theory ZZA_GEN are always accurate (irrespective layerwise and representation functions chosen) with low processing time, this theory represents the best and efficient model of this thesis.

	a	b	c	d	e	f	g	h	i	j	k	l	m
ZZA	5.1194	5.1194	27.3202	27.3202	27.3202	7.0182	57.4363	46.4055	43.3751	45.7840	54.5138	147.6859	143.1814
HWZZ	4.8679	4.8679	25.3396	25.3396	25.3396	6.4877	53.2725	42.8977	40.0964	42.3232	50.3931	136.9795	138.1438
HRZZ	4.8988	4.8988	25.0022	25.0022	25.0022	6.2076	52.5631	41.0461	38.3657	40.4964	48.2179	135.1555	130.4250
HRZZ4	5.0302	5.0302	27.2240	27.2240	27.2240	6.7541	57.2341	44.6591	41.7428	44.0610	52.4623	147.1661	150.2565
MHR	2.7918	2.7918	17.9456	17.9456	17.9456	4.1177	37.7277	27.2271	25.4491	26.8625	31.9844	97.0092	93.0318
MHR4	2.6853	2.6853	18.4395	18.4395	18.4395	4.2454	38.7660	28.0714	26.2383	27.6955	32.9763	99.6791	100.9251
MHWZZA	3.6640	3.6640	21.2093	21.2093	21.2093	5.1634	44.5891	34.1415	31.9120	33.6843	40.1070	114.6519	117.1169
MHWZZA4	3.6636	3.6636	21.2350	21.2350	21.2350	5.1663	44.6430	34.1607	31.9299	33.7032	40.1295	114.7906	116.9716
MHR±	2.8197	2.8197	18.0423	18.0423	18.0423	4.2840	37.9309	28.3264	26.4767	27.9471	33.2758	97.5317	93.5817
MHR4±	2.7122	2.7122	18.5385	18.5385	18.5385	4.3450	38.9742	28.7299	26.8538	28.3451	33.7498	100.2145	98.4607
ZZA_RDF	4.7539	4.7601	25.6791	25.4221	25.5688	6.5151	53.4237	43.4723	40.3448	42.6023	50.7220	137.9143	133.4312
HWZZ_RDF	4.4366	4.4057	23.5791	23.4724	23.3803	6.0751	49.3126	39.7600	37.1489	39.7076	46.6893	127.1806	123.7666
HSDT_32	3.1214	3.0795	16.5601	16.4988	16.4814	4.2328	34.8655	28.2441	26.2932	27.5588	32.8362	89.4214	86.1535
HSDT_33	3.3112	3.3242	17.8197	17.7763	17.7350	4.5421	37.5871	30.0267	28.3671	29.7902	35.6805	95.9062	93.3321
HSDT_34	3.7431	3.7435	20.0323	20.0299	19.9865	5.1326	42.2194	34.2272	31.9077	33.4257	40.2768	108.7112	105.0458
ZZM	3.8297	3.8680	20.5380	20.5733	20.5855	5.2703	43.1540	34.7094	32.8187	34.5179	41.1493	111.9573	107.9893
HWZZM	4.0014	4.0014	22.8133	22.8133	22.8133	5.6511	47.9613	37.3664	34.9263	36.8660	43.8954	123.3228	119.6847
ZZA*	3.8378	3.8378	21.6727	21.6727	21.6727	5.2398	44.6040	34.6466	32.3841	34.1826	40.7003	114.6902	112.7978
HWZZM*	3.8013	3.8013	20.3723	20.3723	20.3723	5.1532	42.3786	34.0740	31.8489	33.6177	40.0277	106.6619	106.5141
ZZA_GEN1	3.5569	3.5491	19.0559	18.9772	19.0349	4.8361	40.1153	32.2075	30.0466	31.7805	37.8997	103.1445	98.8547
ZZA_GEN2*	3.6201	3.5965	19.2806	19.3764	19.3245	4.9542	40.5806	32.5930	30.7501	32.3397	38.3453	104.5919	101.0792
ZZA_XN1	3.7803	3.7858	20.4074	20.1397	20.1462	5.2368	42.8075	34.3507	32.0218	34.1440	40.1400	109.7420	105.9616
ZZA_XN2	3.8975	3.8740	20.9015	20.7122	20.8252	5.3416	43.8740	35.4183	33.0627	34.8716	41.4219	111.7069	109.3585
ZZA_XN3	3.9570	3.9495	21.1959	20.9241	20.9588	5.3773	44.5795	36.0181	33.1871	35.5023	41.9697	114.3735	110.8409
ZZA_XN4	3.9293	3.9587	21.1564	21.0065	21.0164	5.4229	44.5232	35.7340	33.5520	35.0233	42.2088	112.9965	110.4083
ZZA_XN5	3.7968	3.8007	20.2992	20.2979	20.3000	5.2353	42.4996	34.3229	32.1621	34.0502	40.4440	108.9201	106.7728
ZZA_XN6	3.8990	3.8929	20.7787	20.8844	20.8002	5.3402	43.6445	35.4531	33.2025	34.7651	41.4882	112.4237	108.9681
ZZA_XN7	3.8110	3.8069	20.1892	20.3330	20.3107	5.2042	42.3192	34.6114	32.0761	33.9686	40.3171	109.1296	105.8898
ZZA_XN8	3.8793	3.8928	20.6669	20.7793	20.8406	5.3412	43.9535	35.1104	33.1230	34.8843	41.2046	112.3614	109.3573
ZZA_XN9	3.9335	3.9732	20.9319	21.0504	21.1069	5.3733	44.3578	35.7088	33.3426	35.4412	41.8453	113.4169	109.8425
ZZA_XN10	3.9383	3.9689	21.1843	20.9980	21.1488	5.4134	44.2240	35.8335	33.2524	35.0769	41.8385	114.1747	110.3408
FSDT	2.6100	2.6100	12.0963	12.0963	12.0963	3.5504	25.4307	23.4756	21.9426	23.1613	27.5775	65.3900	64.1452
HSDT	2.6134	2.6134	13.6169	13.6169	13.6169	3.8809	28.6275	25.6612	23.9855	25.3175	30.1449	73.6099	75.5128

Table 5.5: Processing time [s]

Similarly to section 5.5, condensed comparisons of processing time provided for dynamic cases are reported in Figure 5.5.

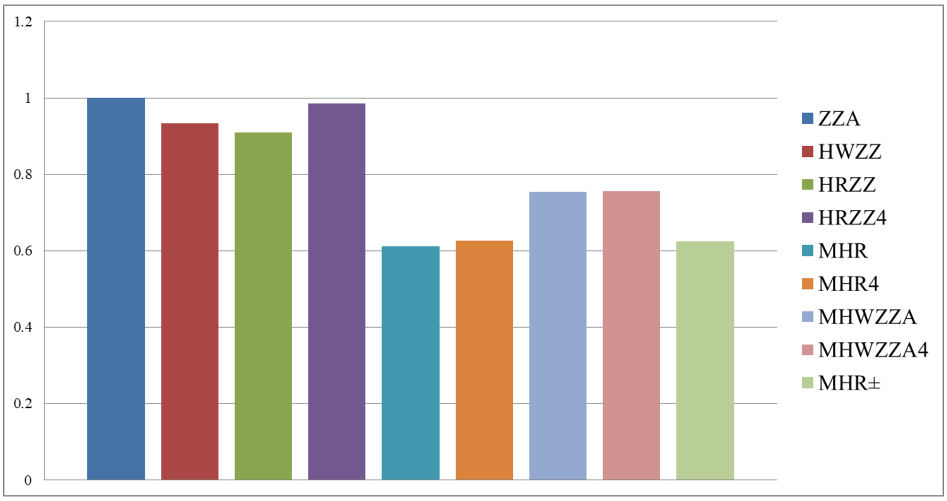
1.2
1
0.8
0.6
0.4
0.2
0
ZZA
HWZZ
HRZZ
HRZZ4
MHR
MHR4
MHWZZA
MHWZZA4
MHR±

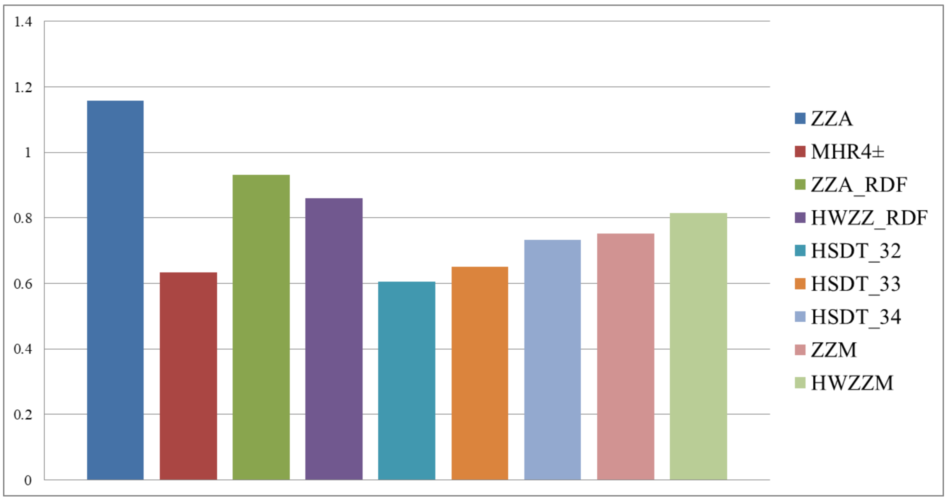
1.4
1.2
1
0.8
0.6
0.4
0.2
0
ZZA
MHR4±
ZZA_RDF
HWZZ_RDF
HSDT_32
HSDT_33
HSDT_34
ZZM
HWZZM

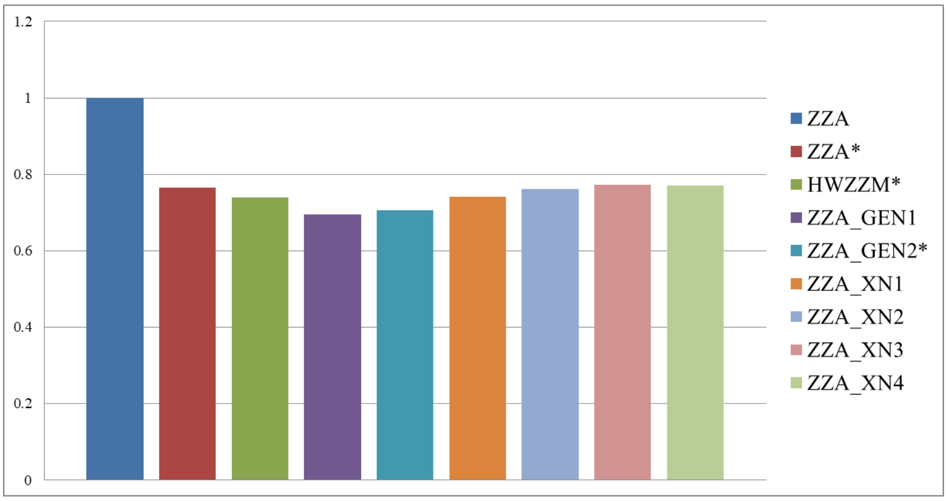
1.2
1
0.8
0.6
0.4
0.2
0
ZZA
ZZA*
HWZZM*
ZZA_GEN1
ZZA_GEN2*
ZZA_XN1
ZZA_XN2
ZZA_XN3
ZZA_XN4

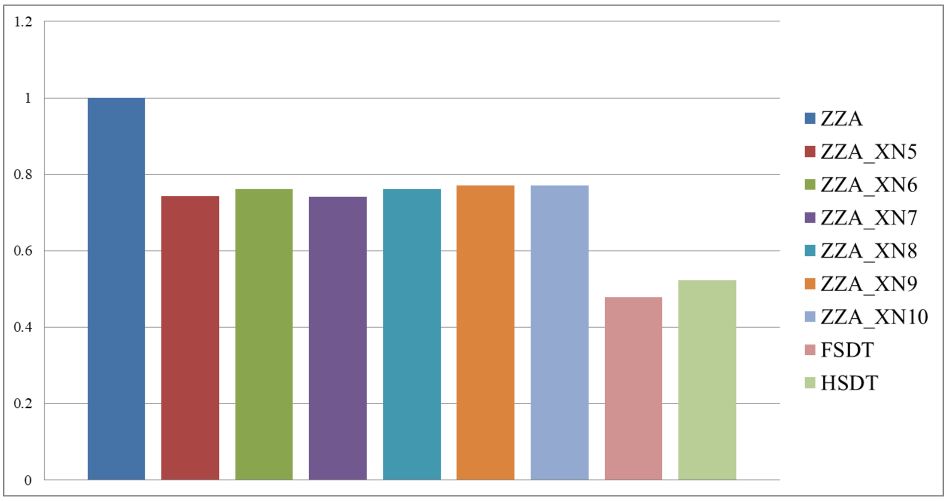

Figure 5.5: Graphical, condensed comparison of computing times of theories for dynamic cases. Results are normalized to processing time of ZZA.

5.6 Concluding remarks

In this chapter a lot of challenging dynamic cases are analyzed. Particularly the capability of theories to accurately provide natural frequencies and calculate forced response to blast pulse loadings, as like as pumping modes is thoroughly tested.

Differently to elastostatic benchmarks of the previous chapter, all lower-order mixed theories, both physically- and kinematic-based, MHR, MHR4, MHWZZA, MHWZZA4, HRZZ, HRZZ4, MHR± and MHR4± prove to be inaccurate, especially when a precise description of transverse deformability is required. despite their processing time is lower than ZZA and other higher-order theories, the cost saving does not justify their usage for dynamic analysis of structures, especially thick sandwiches (which could have pumping modes among their first natural frequencies).

MHR, MHR4, MHR±, MHR4±, MHWZZA, MHWZZA4, HRZZ, HRZZ4	
Type:	Mixed zig-zag theories (both physically- and kinematic-based)
Displacement field:	Piecewise cubic (in-plane displacements) Fourth-order polynomial (transverse displacement of MHR, MHR±, MHWZZA) Piecewise fourth-order polynomial (transverse displacement of MHR4, MHR4±, MHWZZA4, HRZZ4) Uniform (transverse displacement of HRZZ)
Physical constraints:	Full set of physical constraints of ZZA is not imposed
Coefficients:	Not redefined (no adaptive) for MHR, MHR4, MHR±, MHR4±, MHWZZA, MHWZZA4 Redefined only for in-plane displacement for HRZZ, HRZZ4
Accuracy:	Strongly case-dependent
Recommended usage:	Only for thin laminated and sandwich plates without strong variation of mechanical properties of constituent layers across the thickness. So, their usage for dynamic analysis of structures should be avoided, especially

	when a precise description of transverse deformability is required (pumping modes).

Table 5.6: Main features of MHR, MHR4, MHR±, MHR4±, MHWZZA, MHWZZA4, HRZZ, HRZZ4

Displacement-based physically-based adaptive zig-zag theories, HSDT_32 and HSDT_33 that assume a parabolic and cubic piecewise transverse displacement respectively are not always accurate, because the full set of physical constraints of ZZA is not enforced. These theories demonstrate that also for dynamic cases, a piecewise cubic-fourth-order displacement field is the minimum expansion order to get the maximal precision. So, similarly to theories of Table 5.6, their usage should be avoided when a precise description of transverse displacement is required (e.g. pumping modes).

HSDT_32, HSDT_33	
Type:	Displacement-based physically-based zig-zag theories
Displacement field:	Piecewise cubic (in-plane displacements) Piecewise parabolic (transverse displacement of HSDT_32) Piecewise cubic (transverse displacement of HSDT_33)
Physical constraints:	Full set of physical constraints of ZZA is not imposed
Coefficients:	Coefficients of displacement field are redefined (adaptive)
Accuracy:	Case-dependent; better than theories of Table 5.6 but less accurate than higher-order theories
Recommended usage:	Only for thin laminated and sandwich plates without strong variation of mechanical properties of constituent layers across the thickness. So, their usage for dynamic analysis of structures should be avoided, especially when a precise description of transverse deformability is required (pumping modes).

Table 5.7: Main features of HSDT_32 and HSDT_33

Similar findings of section 4.11 regarding accuracy higher-order physically-based adaptive theories ZZA, HWZZ, ZZA_RDF, HWZZ_RDF, HSDT_34, ZZM, HWZZM, ZZA*, HWZZM*, ZZA_GEN1, ZZA_GEN2*, ZZA_XN1 to ZZA_XN10 still apply also for dynamic calculations. Because of coefficients are redefined for each layer across the thickness (adaptive) and the full set of physical constraints is enforced all these theories provide the same results irrespective zig-zag and global representation functions assumed. Particularly, particularizations of the most general physically-based higher-order adaptive theory (ZZA_GEN) are the best theories of this thesis, by virtue of their great efficiency (over 20% time less than ZZA). Usage of this kind of theories is strongly suggested, in order to prevent unacceptable loss of accuracy.

ZZA, ZZA_RDF, HSDT_34, ZZM, ZZA*, HWZZ, HWZZ_RDF, HWZZM and HWZZM*	
Type:	Mixed and displacement-based physically-based zig-zag theories
Displacement field:	Piecewise cubic (in-plane displacements) Piecewise fourth-order (transverse displacement)
Physical constraints:	Full set of physical constraints of ZZA is imposed
Coefficients:	Coefficients of displacements are redefined (adaptive)
Accuracy:	Always very accurate and close to reference solutions

Recommended usage:	Always; moreover, mixed theories allow a little cost saving than ZZA, ZZA_RDF, HSDT_34, ZZM, ZZA*

Table 5.8: Main features of ZZA, ZZA_RDF, HSDT_34, ZZM, ZZA*, HWZZ, HWZZ_RDF, HWZZM and HWZZM*

ZZA_GEN1, ZZA_GEN2*, ZZA_XN1 to ZZA_XN10	
Type:	Displacement-based physically-based generalized zig-zag theories
Displacement field:	Piecewise cubic (in-plane displacements) Piecewise fourth-order (transverse displacement) User can choose layerwise and representation functions as an input of analysis.
Physical constraints:	Full set of physical constraints of ZZA is imposed
Coefficients:	Coefficients of displacements are redefined (adaptive)
Accuracy:	Always very accurate and close to reference solutions
Recommended usage:	Always; they allow a good cost saving (over 20%) than theories of Table 5.8

Table 5.9: Main features of HWZZ, HWZZ_RDF, HWZZM and HWZZM*

Similarly to findings of the previous chapter, equivalent single layer theories FSDT and HSDT demonstrate their inability to accurately obtain also overall quantities, such as first natural frequencies, because of their too simple displacement field. So, despite they provide very low processing time, their usage should be avoided.

FSDT, HSDT	
Type:	Equivalent single layer theories
Displacement field:	Linear (in-plane displacements of FSDT) Cubic (in-plane displacements of HSDT) Uniform (transverse displacement)
Physical constraints:	Regarding FSDT no physical constraints are imposed. Regarding HSDT, only boundary conditions on transverse shear stresses are enforced. Out-of-plane stresses are post-processed after analysis
Coefficients:	No additional coefficients for FSDT Two additional no-redefined coefficients for HSDT
Accuracy:	Very poor, they are not able to analyse sandwiches
Recommended usage:	Only for very thin laminated beams and plates; they should not be used to analyse sandwiches

Table 5.10: Main features of FSDT, HSDT

Chapter 6 – Theory VK-ZZ for impact damage study

6.1 Introduction

As stated in the previous chapters, composite are used in a lot of engineering fields, thanks to their great specific properties. Composite and sandwiches structures are very vulnerable to low-velocity impacts (see [93], [94], [95], [96] and [97]) that could occur during the production or service life of component. However, even though they are not evident (barely visible impact damages) they are always responsible for a relevant strength degradation. Because of warping, shearing and straining deformations, local micro-failure and damages may form. Their dimensions can increase during service life of components, causing loss of strength and stiffness. Although the velocities and the energies indicated in literature have a rather large range of variation, all the authors agree that the incoming energy is mainly absorbed as strain energy and through local failures. They also agree that for this type of impacts strain-rate dependent properties are unnecessary.

Among many others, an in-depth description of damage mechanisms and of failure criteria for impacted structures are given by Chai and Zhu [98], Garnich and Akula Venkata [99]; Liu and Zheng [100] and Berthelot [101] proposed different damage models, while studies on damaged or impacted honeycomb sandwiches were proposed by Horrigan and Staal [102]. Interesting studies about the effects of stacking sequence on the impact and post-impact behaviour were investigated by Aktas et al. [103], those of the impactor shape by Mitrevski et al. [104], while those of multiple impacts by Damanpack et al. [105] and Chakraborty [106].

Papers by by Chakrabarti et al. [107], Chen and Wu [34], Kreja [108], Zhang and Yang [109], Tahani [110], Matsunaga [111], Chao and Tu [112] and Zhou and Stronge [113] are cited as examples of structural models for impact studies, which must have low computational effort, with the intended aim to analyse structures of industrial interest. As a consequence, 3-D FEA and discrete layers models are less suitable, because of their too many unknowns. For these reasons, equivalent single layers and zig-zag theories are more appropriate for impact studies (see papers by Icardi and Sola [4], Icardi and Ferrero [10], Palazotto et al. [114], Kärger et al. [115], Diaz Diaz et al. [116], Oñate et al. [117], [118].

Previous studies by Icardi and Sola [4], [119] and by Icardi and Urraci [24], proposed modified versions of zig-zag adaptive theory ZZA with additional zig-zag functions, without any increase of d.o.f., in order to make stresses continuous also along in-plane directions. These modifications successfully improved accuracy of theories for impact studies and also allow the analysis of structures with different mechanical properties along in-plane directions (two material wedge problem). In this chapter, a modified version of the theories proposed in [4]- [24] is developed, whose formulation is completely new: layerwise functions will be omitted, with the intended aim to test if previous statements about the immaterial choice of zig-zag and representation functions are still valid. This theory, referred as ZZA_GEN_INP will be presented as an extension of general formulation ZZA_GEN of chapter 3. Accuracy of its particularizations and of VK-ZZ from [24], will be compared for some challenging benchmarks. The results show the importance of in-plane stress continuity to obtain accurate predictions. It should be noticed that the development of ZZA_GEN_INP represents the largest contribution and the main focus of this chapter.

Regarding the application on impact problems, the analysis makes use of stress-based criteria, in order to progressively extend damaged area to portions where ultimate conditions are reached for each step. Mesomechanic model by Ladevèze et al. [120] is used, that takes into account the effects of discontinuities by assuming a modified version of the strain energy. After that transverse cracking rate and delamination ratios are calculated by stress-based criteria for each step, homogenized energy can be obtained and used to evaluate stresses. Modified Hertzian contact law of Icardi and Ferrero [10] is used in numerical calculations, because of Yigit and Christoforou [121] and Choi [122] (among many others) demonstrate its accuracy and contact model by Palazotto et al. [114] is adopted for sandwiches. All geometric nonlinearity is taking into account using Lagrangian approach, but also non-linear strains could be assumed, according to [10]. Even though low-velocity impact studies could be carried out also in static form (Li et al. [123]), the Newmark's implicit time integration method is used because it could be applied in a wider range of applications (e.g. progressively increasing velocity of impactor). Moreover, it is not very heavy from the computational standpoint of view (see section 5.4.1 for a more detailed description of this method). Regarding sandwiches, according to the rest of thesis, honeycomb core is modelled as a thick homogenized layer, whose elastic moduli during damaging are assumed a part from 3-D finite element analysis, according to Icardi and Sola [124].

6.2 Hertzian contact force

As previously stated, in numerical applications the impactor is assumed spherical, while distribution of contact stress is described by Hertzian law [114]:

$$\sigma(r) = \sigma(0)\sqrt{1-\left(r^2 / R_{contact}^2\right)} \text{ if } (\sigma(r) = 0 \text{ if } r > R_{contact}) \tag{6.1}$$

$\sigma(0)$ is Hertzian stress at centre, while $\sigma(r)$ is the Hertzian stress far of r from the centre. $R_{contact}$ is the radius of contact area. $R_{contact}$ is assumed fixed for laminates and it is calculated apart by 3-D FEA analysis. Regarding sandwiches, assumption of a constant $R_{contact}$ is not adequate [114] and a modified version of the Newton-Raphson method is used to calculate it for any load increment, making impact area conform to impactor shape. Approaches used to solve the problem are explained in section 6.3.

6.3 Solution Procedure

In this section the solution procedure [24] is described. Regarding laminates, in the loading phase, the contact force is assumed as:

$$F = K_c \alpha^{\upsilon} \tag{6.2}$$

K_c is the contact stiffness that is calculated apart by 3-D FEA analysis (see Figure 6.1), while α is the indentation depth. The same 3-D FEA analysis is used to calculate $R_{contact}$ for laminates, while for sandwiches it is computed as explained in section 6.2 (see [24] for details).

Regarding the unloading phase, contact force is assumed as:

$$F = F_m \left(\frac{\alpha - \alpha_0}{\alpha_m - \alpha_0} \right)^q \tag{6.3}$$

F_m is the maximum of the contact force, α_m is the relative indentation depth at each loading and α_0 is the permanent indentation, while α is still the indentation depth. Exponents υ and q are obtained experimentally.

Finally, contact force assumes a different expression for bounces:

$$F = K_c^b (\alpha - \alpha_0)^p \tag{6.4}$$

The same procedure previously described is used to calculate the contact stiffness K_c^b, while α and α_0 assume the same meaning of (6.2) and (6.3). Again, exponent p is calculated experimentally.

The following values of exponents are assumed in numerical applications:

$$\upsilon = p = 1.5 \qquad q = 2.5 \tag{6.4a}$$

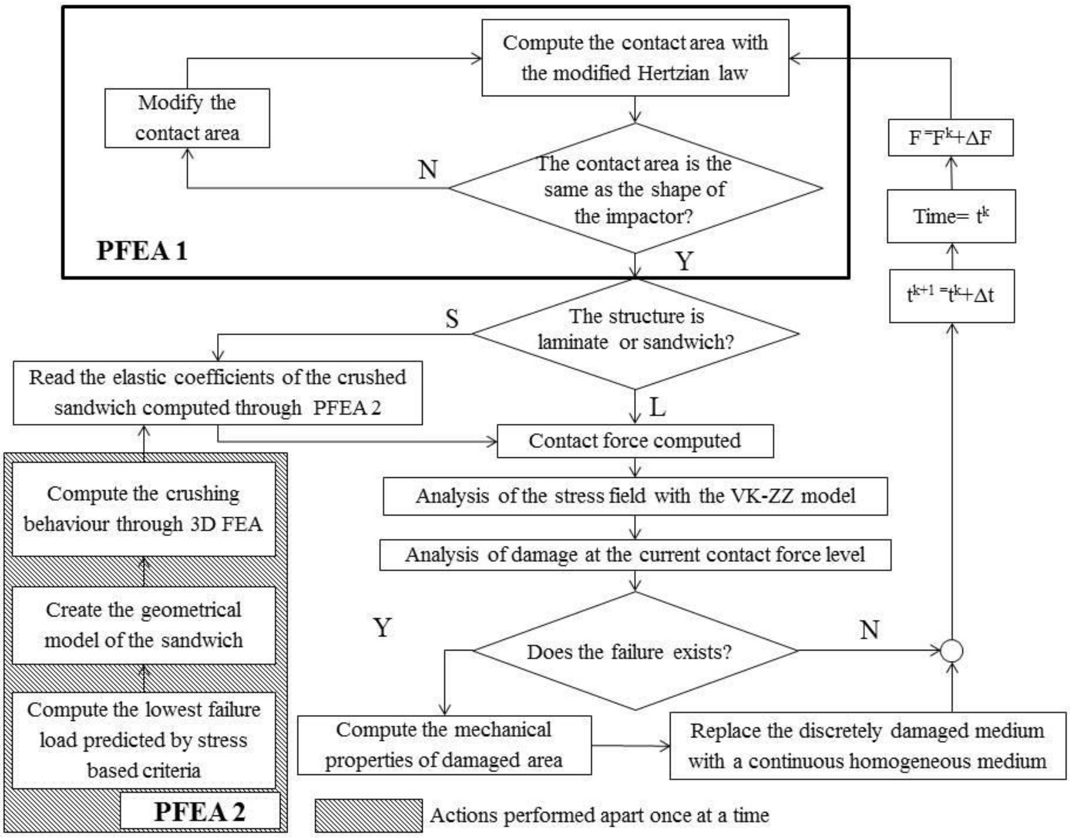

Figure 6.1: Procedure to solve the problem

Regarding sandwiches, because of a constant $R_{contact}$ is not adequate, the iterative algorithm of Palazotto et al. [114], making impact area conform to impactor shape, is used to calculate the contact radius for any load increment. This is accomplished through a modified version of the Newton-Raphson method:

$$\delta^i = \left[\mathbf{K}\left(d^{(i-1)}\right)\right]_S d^{(i-1)} - \mathbf{F}_c^{(i-1)} \neq 0 \tag{6.4b}$$

where $\left[\mathbf{K}\left(d^{(i-1)}\right)\right]_S$ is the secant stiffness matrix computed by using VK-ZZ or ZZA_GEN_INP theories, $d^{(i-1)}$ is the converged solution at the previous load increment $\mathbf{F}_c^{(i-1)}$, while δ^i is the residual force and $d^{(i-1)}$ is the displacement amplitude vector. In order to respect the equilibrium with $\mathbf{F}_c^i$ it is updated by Δd^i, so:

$$\delta^i = \left[\mathbf{K}\left(d^{(i-1)}\right)\right]_T \Delta d^i \tag{6.4c}$$

$\left[\mathbf{K}\left(d^{(i-1)}\right)\right]_T$ being the tangent stiffness matrix obtained using the VK-ZZ and ZZA_GEN_INP theories.

The updated displacement amplitude vector is computed as

$$d^i = d^{(i-1)} + \Delta d^i \tag{6.4d}$$

This process is repeated until the convergence tolerance is reached. It is verified comparing the percentage of variation of the solution, from the current to the previous iteration. In applications $D \le 1\%$ is assumed, whose expression is:

$$D = \frac{\left[\overline{d}^{i+1} - \overline{d}^{i} \right]}{\overline{d}^{i}} \tag{6.4e}$$

and $\overline{d}^{i}$ is the norm of displacements:

$$\overline{d}^{i} = \sqrt{\sum_n \left(d_j^n \right)^2} \tag{6.4f}$$

In the next section, stress-based failure criteria are briefly reminded, because they are used during analysis in order to progressively extend damaged area to portions where ultimate conditions are reached for step by step.

6.4 Stress-based failure criteria

3-D criterion by Hashin and Rotem [125]:

It is used to predict fiber/matrix failure. Regarding tensile failure of fibers $\sigma_{11} > 0$:

$$\left(\frac{\sigma_{11}}{X^t} \right)^2 + \frac{1}{S_{12=13}{}^2} \left(\tau_{12}{}^2 + \tau_{13}{}^2 \right) = 1 \tag{6.5}$$

X^t is the tensile strength of fibers, while $S_{12=13}$ is the in-situ shear strength of the matrix. In-plane and transverse shear stresses on fibers are indicated as σ_{11}, τ_{12} and τ_{13}.

For compressive failure of fibers ($\sigma_{11} < 0$):

$$\sigma_{11} = -X^c \tag{6.6}$$

X^c is the compressive strength of fibers, while σ_{11} has the same meaning of (6.5).

Regarding matrix failure, the following expression is used under traction, where $\sigma_{22} + \sigma_{33} > 0$:

$$\left(\frac{\sigma_{22} + \sigma_{33}}{Y^t} \right)^2 + \frac{1}{S_{23}{}^2} (\tau_{23}{}^2 - \sigma_{22}\sigma_{33}) + \left(\frac{\tau_{12}}{S_{12=13}} \right)^2 + \left(\frac{\tau_{13}}{S_{12=13}} \right)^2 = 1 \tag{6.7}$$

While, the following expression is used under compression, where $\sigma_{22} + \sigma_{33} < 0$:

$$\frac{1}{Y^c}\left[\left(\frac{Y^c}{2S_{23}}\right)^2-1\right](\sigma_{22}+\sigma_{33})+\frac{(\sigma_{22}+\sigma_{33})^2}{4S_{23}{}^2}+\frac{(\tau_{23}{}^2-\sigma_{22}\sigma_{33})}{S_{23}{}^2}+\frac{(\tau_{12}{}^2+\tau_{13}{}^2)}{S_{12=13}{}^2}=1 \tag{6.8}$$

Y^t and Y^c are tensile and compressive strength of matrix, respectively, while other symbols assume the same meaning of (6.6) to (6.8).

Criterion for delamination failure by Choi and Chang [126]:

Is used for delamination failure of laminates under low-velocity impact:

$$e_d^2 = D_a \left[\frac{\overline{\sigma}_{\beta\varsigma}^n}{S_i^n}+\frac{\overline{\sigma}_{\alpha\varsigma}^{n+1}}{S_i^{n+1}}+\frac{\overline{\sigma}_{\beta\beta}^{n+1}}{Y^{n+1}}\right]^2>1 \tag{6.9}$$

D_a is an empirical constant that depends from material properties, while the following formula is used for calculate the mean stress $\overline{\sigma}_{ij}$ (n is the number of layer):

$$\overline{\sigma}_{ij}^{n+1}=\frac{1}{h_{n+1}}\int_{t_{n-1}}^{t_n}\sigma_{ij}dt \tag{6.10}$$

Letter i in symbols means in-situ property, while Y^{n+1} is assumed Y_t^{n+1} for traction ($\overline{\sigma}_{\beta\beta}\geq 0$) or Y_c^{n+1} for compression ($\overline{\sigma}_{\beta\beta}<0$).

Criterion of Besant et al. for honeycomb core failure [127]:

It is used for honeycomb core failure under compression and transverse shear stresses:

$$e_{core}=\left(\frac{\sigma_{\varsigma\varsigma}}{\sigma_{cu}}\right)^n+\left(\frac{\sigma_{\alpha\varsigma}}{\tau_{lu}}\right)^n+\left(\frac{\sigma_{\beta\varsigma}}{\tau_{lu}}\right)^n>1 \tag{6.11}$$

σ_{cu} is the core compression strength, while τ_{lu} is transverse shear strength. Exponent n is assumed as 1.5 in numerical applications.

Criterion for failure of foam core by Evonik [128] and Li et al. [129]:

It is estimated as:

$$\begin{aligned}
&\sigma_v=\frac{\sqrt{(12a_2+12a1+12)I_2+[4a_2{}^2+(4a_1+4)a_2+a_1{}^2]I_1{}^2}+a_1I_1}{2a_2+2a_1+2}\\
&I_1=\sigma_{11}+\sigma_{22}+\sigma_{33}\\
&I_2={}^1\!/_3\left[\sum_{i=1}^{3}\sigma_{ii}^2-\sigma_{11}\sigma_{22}-\sigma_{11}\sigma_{33}-\sigma_{22}\sigma_{33}+3\sum_{ij=12,13,23}\sigma_{ij}{}^2\right]\\
&a_1=k^2(d-1)/d\\
&a_2=(k^2/d)-1\\
&d=R_{11}^-/R_{11}^+\\
&k=\sqrt{3}R_{12}/R_{11}^+
\end{aligned} \tag{6.12}$$

Parameters a_1, a_2, d, k are determined experimentally, while R_{11}^{+}, R_{11}^{-}, R_{12} are tensile, compressive and shear strength.

Criterion for core crushing failure by Lee and Tsotsis [130]:

It is used to determine core crushing of core under transverse shear and compressive stresses:

$$\frac{\sigma_{zz}}{Z^c}=1\ ,\ \frac{\sigma_{xz}}{S^x}=1\ ,\ \frac{\sigma_{yz}}{S^y}=1 \tag{6.13}$$

Z^c, S^x and S^y are compressive and transverse shear stresses strength, respectively.

As both criteria (6.11) and (6.13) refer to honeycomb failure, the failed region is computed as the envelope of failures predicted by each of these two criteria.

6.5 Mesoscale damage model

With the intended aim to take into considerations discontinuities due to impact, Mesoscale model by Ladevèze et al, [120] is chosen, which substitutes the discretely damaged portion of laminate with a continuous homogeneous medium that have the same energy. Indeed, strain energy contains damage indicators $\bar{I}_{22},\bar{I}_{12},\bar{I}_{23},\bar{I}_{13},\bar{I}_{33}$ calculated as the homogenized result of damage micromodels.

At microscale, displacements U^m, strains ε^m and stress σ^m fields are calculated as superposition of solutions of an undamaged problem and a residual one (residual stress around damage).

According to [120], homogenized potential energy of each ply is calculated as:

$$\begin{aligned}\frac{2E_p^S}{|S|} &= [\pi\bar{\varepsilon}\pi]^t[\bar{M}_1(\bar{I}_{22},\bar{I}_{12})][\pi\bar{\varepsilon}\pi]+\tilde{\sigma}_{33}[\bar{M}_2(\bar{I}_{22},\bar{I}_{12})]\tilde{\sigma}_{33}+\tilde{\sigma}_{33}[\bar{M}_3(\bar{I}_{22},\bar{I}_{12})][\pi\bar{\varepsilon}\pi]+\\ &-\frac{(1+\bar{I}_{23})\tilde{\sigma}_{23}^2}{\tilde{G}_{23}}-\frac{(1+\bar{I}_{13})\tilde{\sigma}_{13}^2}{\tilde{G}_{23}}-\frac{(1+\bar{I}_{33})<\tilde{\sigma}_{33}^2>_+^2}{\tilde{E}_3}\end{aligned} \tag{6.14}$$

Where $\bar{I}_{22},\bar{I}_{12},\bar{I}_{23},\bar{I}_{13},\bar{I}_{33}$ are calculated as the integral of the strain energy of the elementary cell for each basic residual problem under the five possible elementary loads in the directions 22, 12, 23, 13, 33, while $[\bar{M}_1],[\bar{M}_2],[\bar{M}_3]$ depend from material properties and symbol $<.>_+$ is the positive part of $\tilde{\sigma}_{33}^2$. (6.14) is rewritten for interfaces, assuming elastic stiffness coefficients $\tilde{k}_1,\tilde{k}_2,\tilde{k}_3$ and damage indicators $\bar{I}^1,\bar{I}^2,\bar{I}^3$:

$$\frac{2E_p^j}{|\gamma_j|}=-\frac{(1+\bar{I}^1)\tilde{\sigma}_{13}}{\tilde{k}_1}-\frac{(1+\bar{I}^2)\tilde{\sigma}_{23}}{\tilde{k}_2}-\frac{(1+\bar{I}^3)\tilde{\sigma}_{33}}{\tilde{k}_3} \tag{6.15}$$

Where γ_j is the deformation. So, coefficients of (6.14) and (6.15) are elastic properties of equivalent model.

According to [24], $\overline{I}_{22}, \overline{I}_{12}, \overline{I}_{23}, \overline{I}_{13}, \overline{I}_{33}$ are calculated apart by using 3-D FEA to simulate elementary cell, assuming discrete values of fibre failure, matrix ρ and τ for various load levels, by using (6.5)-(6.9). $\rho = L/H$ is the crackling rate, calculated as ratio of distance L between two adjacent cracks and the length of the crack across the thickness H, while $\tau = l/h$ is delamination ratio, obtained as the ratio of length of the microcrack. In applications ρ and τ assume values [0; 0.7] and [0; 0.4] respectively. Once modified elastic properties are calculated, they are provided to analytical model.

At each time step, progressive failure analysis is used and damaged area is computed by applying criteria (6.5)-(6.13) under loading (6.1)-(6.4) and it is extended at the next step. It should be noticed that with the intended aim to simplify calculations, a discrete representation of the domain is assumed (see Figure 6.3), which is subdivided into fictitious small square cells, where the damage state is computed at the central point and assumed uniform for the rest of the cell. So, it is possible to determine damaged area, that is made of cells where ultimate stress is reached. Dimension of cells is chosen in order to strike the right balance between accuracy and computational effort. More details can be found [24], while in the following section, VK-ZZ theory retaken from literature is reported.

6.6 VK-ZZ theory

This adaptive theory is retaken from [24] and its displacement field is:

$$
\begin{aligned}
u_\alpha(\alpha,\beta,\varsigma) &= u_\alpha{}^0(\alpha,\beta) + \varsigma(\Gamma_\alpha^0(\alpha,\beta) - w^0(\alpha,\beta)_{,\alpha}) + U_\alpha^{ZZA}(\alpha,\beta,\varsigma) + \sum_{j=1}^{s}\sum_{k=1}^{n_l} {}_u^j\theta_\alpha^k(\beta)(\alpha-\alpha_k)H_k + \\
&\quad + \sum_{j=1}^{t}\sum_{k=1}^{n_l} {}_u^j\theta_\beta^k(\alpha)H_k + \sum_{j=1}^{t}\sum_{k=1}^{n_l} {}_u^j\lambda_\alpha^k(\alpha)(\beta-\beta_k)H_k \\
u_\beta(\alpha,\beta,\varsigma) &= u_\beta{}^0(\alpha,\beta) + \varsigma(\Gamma_\beta^0(\alpha,\beta) - w^0(\alpha,\beta)_{,\beta}) + U_\beta^{ZZA}(\alpha,\beta,\varsigma) + \sum_{j=1}^{t}\sum_{k=1}^{n_l} {}_v^j\theta_\beta^k(\alpha)(\beta-\beta_k)H_k + \\
&\quad + \sum_{j=1}^{s}\sum_{k=1}^{n_l} {}_v^j\theta_\alpha^k(\beta)H_k + \sum_{j=1}^{s}\sum_{k=1}^{n_l} {}_v^j\lambda_\beta^k(\beta)(\alpha-\alpha_k)H_k \\
u_\varsigma(\alpha,\beta,\varsigma) &= w^0(\alpha,\beta) + U_\varsigma^{ZZA}(\alpha,\beta,\varsigma) + \sum_{j=1}^{s}\sum_{k=1}^{n_l} {}_w^j\eta_\alpha^k(\beta)(\alpha-\alpha_k)H_k + \sum_{j=1}^{t}\sum_{k=1}^{n_l} {}_w^j\eta_\beta^k(\alpha)H_k + \sum_{j=1}^{s}\sum_{k=1}^{n_l} {}_w^j\Upsilon_\alpha^k(\beta)H_k + \\
&\quad + \sum_{j=1}^{t}\sum_{k=1}^{n_l} {}_w^j\Upsilon_\beta^k(\alpha)(\beta-\beta_k)H_k
\end{aligned}
\tag{6.16}
$$

U_α^{ZZA}, U_β^{ZZA} and U_ς^{ZZA} are the same of ZZA, whose expressions are:

$$U_{\alpha}^{ZZA}(\alpha,\beta,\varsigma)=\left[\varsigma^{2}C_{\alpha}^{i}(\alpha,\beta)+z^{3}D_{\alpha}^{i}(\alpha,\beta)+\sum_{k=1}^{n_{i}}\Phi_{\alpha}^{k}(\alpha,\beta)(\varsigma-\varsigma_{k})H_{k}(z)+\sum_{k=1}^{n_{i}}{}_{\alpha}C_{u}^{k}(\alpha,\beta)H_{k}(\varsigma)\right]$$
$$U_{\beta}^{ZZA}(\alpha,\beta,\varsigma)=\left[\varsigma^{2}C_{\beta}^{i}(\alpha,\beta)+z^{3}D_{\beta}^{i}(\alpha,\beta)+\sum_{k=1}^{n_{i}}\Phi_{\beta}^{k}(\alpha,\beta)(\varsigma-\varsigma_{k})H_{k}(\varsigma)+\sum_{k=1}^{n_{i}}{}_{\beta}C_{u}^{k}(\alpha,\beta)H_{k}(\varsigma)\right] \quad (6.17)$$
$$U_{\varsigma}^{ZZA}(\alpha,\beta,\varsigma)=\left[\varsigma\, b^{i}(\alpha,\beta)+\varsigma^{2}c^{i}(\alpha,\beta)+\varsigma^{3}d^{i}(\alpha,\beta)+\varsigma^{4}e^{i}(\alpha,\beta)+\sum_{k=1}^{n_{i}}\Psi^{k}(\alpha,\beta)(\varsigma-\varsigma_{k})H_{k}(\varsigma)+\right.$$
$$\left.+\sum_{k=1}^{n_{i}}\Omega^{k}(\alpha,\beta)(\varsigma-\varsigma_{k})^{2}H_{k}(\varsigma)+\sum_{k=1}^{n_{i}}C_{\varsigma}^{k}(\alpha,\beta)H_{k}(\varsigma)\right]$$

So, similarly to ZZA $C_{\alpha}^{i},C_{\beta}^{i},D_{\alpha}^{i},D_{\beta}^{i},b^{i},c^{i},d^{i},e^{i}$ are calculated by imposing (1.15)-(1.18), while $\Phi_{\alpha}^{k},\Phi_{\beta}^{k},\Psi^{k},\Omega^{k}$ by (1.19) and ${}_{\alpha}C_{u}^{k}$, ${}_{\beta}C_{u}^{k}$, C_{ς}^{k} by (1.20).

Additional zig-zag contributions make continuous the stresses under in-plane variation of properties. So, additional zig-zag functions depend from in-plane coordinates. The number of in-plane interfaces is assumed to be s along α-direction and t along β-direction. ${}_{u}^{j}\theta_{\alpha}^{k}$, ${}_{u}^{j}\theta_{\beta}^{k}$, ${}_{u}^{j}\lambda_{\alpha}^{k}$, ${}_{v}^{j}\theta_{\alpha}^{k}$, ${}_{v}^{j}\theta_{\beta}^{k}$, ${}_{v}^{j}\lambda_{\beta}^{k}$, ${}_{w}^{j}\eta_{\alpha}^{k}$, ${}_{w}^{j}\eta_{\beta}^{k}$, ${}_{w}^{j}\Upsilon_{\alpha}^{k}$, ${}_{w}^{j}\Upsilon_{\beta}^{k}$ terms are redefined after each in-plane interface j and are assumed to be zero in the first *in-plane layer* before the first in-plane interface, both from α- and β-directions. ${}_{u}^{j}\theta_{\alpha}^{k}$ and ${}_{u}^{j}\theta_{\beta}^{k}$ are calculated by imposing the continuity of in-plane stress $\sigma_{\alpha\alpha}$ along α and β directions:

$$\sigma_{\alpha\alpha}({}^{(j)}\alpha^{+})=\sigma_{\alpha\alpha}({}^{(j)}\alpha^{-})$$
$$\sigma_{\alpha\alpha}({}^{(j)}\beta^{+})=\sigma_{\alpha\alpha}({}^{(j)}\beta^{-}) \quad (6.18a)$$

Similarly, the in-plane continuity of $\sigma_{\beta\beta}$ is imposed by ${}_{v}^{j}\theta_{\alpha}^{k}$ and ${}_{v}^{j}\theta_{\beta}^{k}$:

$$\sigma_{\beta\beta}({}^{(j)}\alpha^{+})=\sigma_{\beta\beta}({}^{(j)}\alpha^{-})$$
$$\sigma_{\beta\beta}({}^{(j)}\beta^{+})=\sigma_{\beta\beta}({}^{(j)}\beta^{-}) \quad (6.18b)$$

Instead, ${}_{u}^{j}\lambda_{\alpha}^{k}$ and ${}_{u}^{j}\lambda_{\beta}^{k}$ are calculated by imposing:

$$\sigma_{\alpha\beta}({}^{(j)}\alpha^{+})=\sigma_{\alpha\beta}({}^{(j)}\alpha^{-})$$
$$\sigma_{\alpha\beta}({}^{(j)}\beta^{+})=\sigma_{\alpha\beta}({}^{(j)}\beta^{-}) \quad (6.19)$$

Finally, ${}_{w}^{j}\eta_{\alpha}^{k}$, ${}_{w}^{j}\eta_{\beta}^{k}$ are calculated by imposing:

$$\sigma_{\alpha\varsigma}({}^{(j)}\alpha^{+})=\sigma_{\alpha\varsigma}({}^{(j)}\alpha^{-})$$
$$\sigma_{\alpha\varsigma}({}^{(j)}\beta^{+})=\sigma_{\alpha\varsigma}({}^{(j)}\beta^{-}) \quad (6.20)$$

While ${}_{w}^{j}\Upsilon_{\alpha}^{k}$, ${}_{w}^{j}\Upsilon_{\beta}^{k}$ impose:

$$\sigma_{\beta\varsigma}({}^{(j)}\alpha^{+})=\sigma_{\beta\varsigma}({}^{(j)}\alpha^{-})$$
$$\sigma_{\beta\varsigma}({}^{(j)}\beta^{+})=\sigma_{\beta\varsigma}({}^{(j)}\beta^{-}) \quad (6.21)$$

There is no need to impose in-plane continuity of transverse normal stress or of its gradient. Obviously, if a beam is considered, ${}^{j}_{u}\theta^{k}_{\beta}$, ${}^{j}_{u}\lambda^{k}_{\beta}$ and ${}^{j}_{w}\Upsilon^{k}_{\beta}$ are null because there are no interfaces along β-direction. Numerical results will show the importance of in-plane continuity to obtain accurate results. A generalized version of VK-ZZ is developed and assessed into this thesis. It should be considered as a new original contribution and an extension of ZZA_GEN for applications that require in-plane continuity of stresses.

6.7 ZZA_GEN_INP theory

A generalized version of VK-ZZ can be obtained, considering the following displacement field, whose coefficients are redefined for each after each interface along α-, β- and ς- directions:

$$u_{\alpha}^{\,j\,k\,l}(\alpha,\beta,\varsigma)=\sum_{i=0}^{n_{\alpha}=5}{}^{k}_{l}A^{\alpha}_{ij}(\alpha,\beta)\,\mathrm{F}^{i}_{\alpha}(\varsigma)+\sum_{i=i_{\alpha 2}}^{n_{\alpha 2}}{}^{k}_{l}B^{\alpha}_{ij}(\beta)\,\mathrm{G}^{i}_{\alpha}(\alpha)+\sum_{i=i_{\alpha 3}}^{n_{\alpha 3}}{}^{k}_{l}C^{\alpha}_{ij}(\alpha)\,\mathrm{H}^{i}_{\alpha}(\beta)$$
$$u_{\varsigma}^{\,j\,k\,l}(\alpha,\beta,\varsigma)=\sum_{i=0}^{n_{\varsigma}=5}{}^{k}_{l}D_{ij}(\alpha,\beta)\,\mathrm{F}^{i}_{\varsigma}(\varsigma)+\sum_{i=0}^{n_{\varsigma 2}=1}{}^{k}_{l}E_{ij}(\beta)\,\mathrm{G}^{i}_{\varsigma}(\alpha)+\sum_{i=0}^{n_{\varsigma 3}=1}{}^{k}_{l}F_{ij}(\alpha)\,\mathrm{H}^{i}_{\varsigma}(\beta) \qquad (6.22)$$

Symbols j,k,l refers to j-th, k-th and l-th layer along ς-, α- and β-directions. Obviously, before the first interfaces along α and β are reached, terms B_{ij}, C_{ij}, E_{ij} and F_{ij} are null. The following coefficients of the bottom layer ${}^{1}_{1}A^{\alpha}_{01}$, ${}^{1}_{1}A^{\alpha}_{11}$, ${}^{1}_{1}D_{01}$ are assumed as fixed d.o.f. and other coefficients are calculated as function of ${}^{1}_{1}A^{\alpha}_{01}$, ${}^{1}_{1}A^{\alpha}_{11}$, ${}^{1}_{1}D_{01}$ and their derivatives. In order to compare results by ZZA_GEN_INP and VK-ZZ, ${}^{1}_{1}A^{\alpha}_{01}$, ${}^{1}_{1}A^{\alpha}_{11}$, ${}^{1}_{1}D_{01}$ are assumed as:

$${}^{1}_{1}A^{\alpha}_{01}=u^{0}_{\alpha} \quad , \quad {}^{1}_{1}A^{\alpha}_{11}=\Gamma^{0}_{\alpha}-w^{0},_{\alpha} \quad , \quad {}^{1}_{1}D^{\alpha}_{01}=w^{0} \qquad (6.23)$$

Moreover, the following choices are made for particularization of ZZA_GEN_INP for numerical calculation:

$$\begin{aligned}
&\mathrm{F}^{i}_{\alpha}(\varsigma)=\mathrm{F}^{i}_{\varsigma}(\varsigma)=\varsigma^{i}\\
&\mathrm{G}^{i}_{\alpha}(\alpha)=\mathrm{G}^{i}_{\varsigma}(\alpha)=\alpha^{i}\\
&\mathrm{H}^{i}_{\alpha}(\beta)=\mathrm{H}^{i}_{\varsigma}(\beta)=\beta^{i}\\
&for\;\; u_{\alpha} \quad\rightarrow\quad i_{\alpha 3}=0;\;\; i_{\alpha 2}=n_{\alpha 2}=n_{\alpha 3}=1\\
&for\;\; u_{\beta} \quad\rightarrow\quad i_{\beta 2}=0;\;\; i_{\beta 3}=n_{\beta 2}=n_{\beta 3}=1
\end{aligned} \qquad (6.24)$$

Differently to ZZA_GEN, there is no need to change reference frame position, because terms B_{ij}, C_{ij}, E_{ij} and F_{ij} can't vanish.

As previously stated, in the portion of laminate before any interface along α- and β- directions, B_{ij}, C_{ij}, E_{ij} and F_{ij} are null and the remaining terms ${}^{1}_{1}A^{\alpha}_{ij}$ and

${}_1^1D_{ij}$, are calculated for $i > 1$ or $j > 1$ by imposing the fulfilment of (1.15)-(1.20) as function of d.o.f. ${}_1^1A_{01}^{\alpha}$, ${}_1^1A_{11}^{\alpha}$, ${}_1^1D_{01}$ and their derivatives.

For the other portions of laminate where $k > 1$ or $l > 1$, additional terms B_{ij}, C_{ij}, E_{ij} and F_{ij} are calculated by imposing (6.17)-(6.21), while terms ${}_1^1A_{ij}^{\alpha}$ and ${}_1^1D_{ij}$ are obtained still by imposing (1.15)-(1.20). Differently from the previous portion of laminate, for the bottom layer, additional equations that restore the in-plane continuity of displacements along α- and β- directions are needed to determine ${}_{l>1}^{k>1}A_{01}^{\alpha}$ and ${}_{l>1}^{k>1}D_{01}$:

$$\begin{aligned}
&u_\alpha({}^{(j)}\alpha^+) = u_\alpha({}^{(j)}\alpha^-)\\
&u_\alpha({}^{(j)}\beta^+) = u_\alpha({}^{(j)}\beta^-)\\
&u_\varsigma({}^{(j)}\alpha^+) = u_\varsigma({}^{(j)}\alpha^-)\\
&u_\varsigma({}^{(j)}\beta^+) = u_\varsigma({}^{(j)}\beta^-)
\end{aligned} \tag{6.25}$$

An additional equilibrium point is needed to calculate ${}_{l>1}^{k>1}A_{11}^{\alpha}$. This is done to keeping the number of d.o.f. fixed to five, like VK-ZZ theory. It should be noticed that the only substantial differences between ZZA_GEN_INP and the parent theory is omission of explicit zig-zag functions and summations. This latter feature allows ZZA_GEN_INP to be more efficient than parent theory, because it obtains indistinguishable results than VK-ZZ, with lower processing time (see section 6.9), demonstrating that the choice of zig-zag functions is immaterial and they can be also omitted also for in-plane continuity, obviously, if coefficients are redefined after each interface along in-plane and transverse directions. Obviously, terms that restore in-plane continuity along y-direction are not taken into account if a beam is considered.

For both previous theories, in order to account for core crushing mechanism, a finite element analysis is done, to determine the apparent elastic moduli of the core at each magnitude of transverse loading. It is done apart once and for all and then results are provided to the VK-ZZ model for the analysis. Honeycomb structure is accurately simulated using a very refined mesh, where elastic-plastic isotropic material and (6.8)-(6.11) are used for each loading. Solid elements are used for foam core, whose material has nonlinear properties determined from experiments and materials databases. An in-depth description of this technique can be found in [124] and it is used because obtains accurate predictions for sample cases.

Similarly to previous application, Rayleigh-Ritz method is used where the following trial functions are assumed for simply-supported edges:

$$u_\alpha^0(\alpha,\beta,t) = \sum_{m=1,2,3}^{M} \sum_{n=1,2,3}^{N} A_{mn}(t) \sin\left(\frac{m\pi}{L_\alpha}\alpha\right)\cos\left(\frac{n\pi}{L_\beta}\beta\right);$$
$$u_\beta^0(\alpha,\beta,t) = \sum_{m=1,2,3}^{M} \sum_{n=1,2,3}^{N} B_{mn}(t) \cos\left(\frac{m\pi}{L_\alpha}\alpha\right)\sin\left(\frac{n\pi}{L_\beta}\beta\right); \quad (6.26)$$
$$w^0(\alpha,\beta,t) = \sum_{m=1,2,3}^{M} \sum_{n=1,2,3}^{N} C_{mn}(t) \sin\left(\frac{m\pi}{L_\alpha}\alpha\right)\sin\left(\frac{n\pi}{L_\beta}\beta\right);$$
$$\Gamma_\alpha^0(\alpha,\beta,t) = \sum_{m=1,2,3}^{M} \sum_{n=1,2,3}^{N} D_{mn}(t) \sin\left(\frac{m\pi}{L_\alpha}\alpha\right)\cos\left(\frac{n\pi}{L_\beta}\beta\right);$$
$$\Gamma_\beta^0(\alpha,\beta,t) = \sum_{m=1,2,3}^{M} \sum_{n=1,2,3}^{N} E_{mn}(t) \cos\left(\frac{m\pi}{L_\alpha}\alpha\right)\sin\left(\frac{n\pi}{L_\beta}\beta\right);$$

The following trial functions are assumed for clamped edges:

$$u_\alpha^0(\alpha,\beta,t) = \sum_{m=1,2,3}^{M} \sum_{n=1,,2,3}^{N} A_{mn}(t) \sin\left(\frac{m\pi}{L_\alpha}\alpha\right)\sin\left(\frac{n\pi}{L_\beta}\beta\right);$$
$$u_\beta^0(\alpha,\beta,t) = \sum_{m=1,2,3}^{M} \sum_{n=1,2,3}^{N} B_{mn}(t) \sin\left(\frac{m\pi}{L_\alpha}\alpha\right)\sin\left(\frac{n\pi}{L_\beta}\beta\right); \quad (6.27)$$
$$w^0(\alpha,\beta,t) = \sum_{m=2,4}^{M} \sum_{n=2,4}^{N} C_{mn}(t) \left[\cos\left(\frac{m\pi}{L_\alpha}\alpha\right) - (-1)^{m/2}\right]\left[\cos\left(\frac{n\pi}{L_\beta}\beta\right) - (-1)^{n/2}\right];$$
$$\Gamma_\alpha^0(\alpha,\beta,t) = \sum_{m=1,2,3}^{M} \sum_{n=1,2,3}^{N} D_{mn}(t) \sin\left(\frac{m\pi}{L_\alpha}\alpha\right)\sin\left(\frac{n\pi}{L_\beta}\beta\right);$$
$$\Gamma_\beta^0(\alpha,\beta,t) = \sum_{m=1,2,3}^{M} \sum_{n=1,2,3}^{N} E_{mn}(t) \sin\left(\frac{m\pi}{L_\alpha}\alpha\right)\sin\left(\frac{n\pi}{L_\beta}\beta\right);$$

Where also the following mechanical boundary conditions are imposed uniformly on the contour C (it should be noticed that this hypothesis is valid only for thin laminates):

$$Q_\alpha = \oint_C \sigma_{\alpha\varsigma} d\alpha d\varsigma; \quad Q_\beta = \oint_C \sigma_{\beta\varsigma} d\beta d\varsigma \quad (6.28)$$

As previously stated, Newmark's time integration scheme is used and amplitudes are computed and for each step and used as input of damage analysis, while (6.21) and (6.21) are used to calculate linear, secant and tangent stiffness matrices. The consistent mass matrix is used, because according to [24], this choice guarantees accuracy. In the following sections, accuracy of VK-ZZ and ZZA_GEN_INP is assessed for numerical applications retaken from [10] and [131].

6.8 Assessment of VK-ZZ and ZZA_GEN_INP for two material wedge

Accuracy of theories is firstly tested for two material wedge problem. This problem was previously studied by Hein and Erdogan [132], where a 3-D beam is analysed. Beam is subdivided into two plates, which have a length-to-width ratio of 50. One plate is made of a rigid isotropic material ($E_1 = 730GPa \quad \nu$=0.3), while the other one is made of an elastic material ($E_1 = 7.3GPa \quad \nu$=0.3). Two semi-infinite sectors are bonded together to form an interface angle at the free edge of 90°, as shown in the figure 6.1. For this reason, the variation of displacements and stresses along thickness direction is not important. Results of in-plane shear stress provided by VK-ZZ and ZZA_GEN_INP are compared to exact solution by [132] and reported in Figure 6.1, which impose the continuity of $\sigma_{\alpha\beta}$ along x-direction. The following normalization is used:

$$\overline{\sigma_{\alpha\beta}} = \frac{\sigma_{\alpha\beta}}{\max(\sigma_{\alpha\beta})} \tag{6.29}$$

It should be noticed that there is a strong stress concentration between the two plates, because of singularity of material properties, which can cause loss during service life if it is not taken into account. Thanks to additional terms of (6.16) and (6.22) VK-ZZ and ZZA_GEN_INP are very accurate and indistinguishable results are obtained, demonstrating that also in-plane zig-zag functions are immaterial and they can be omitted, once coefficients are redefined after each interface along α-, β- and ς- directions. In the next section, more challenging cases are analyzed, in order to test accuracy of new ZZA_GEN_INP theory.

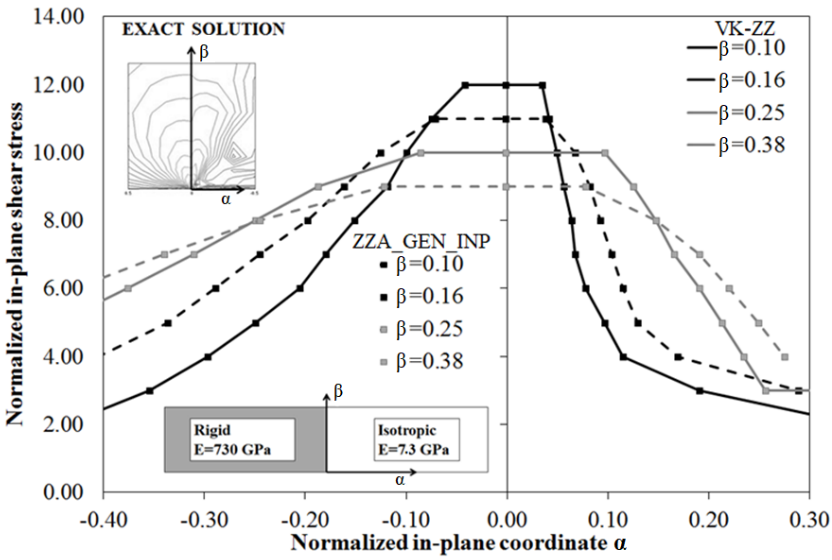

Figure 6.1: Normalized in-plane stress for two material wedge problem

6.9 Assessment of VK-ZZ and ZZA_GEN_INP for impacted panels

6.9.1 Case a

In order to show the importance of in-plane continuity to predict accurate results, an impact study, whose results are compared to analytical and experimental ones retaken from paper by Icardi and Zardo [131] is now performed.

The intended aim of this study is to replicate the numerical analysis, preserving all the previous formulations [131], [24] with the same procedures [24], without trying to improve any of them. Indeed the goal is to highlight the effects of assuming in-plane continuities omitting them by discarding in-plane zig-zag functions.

Panel is composite with I stiffeners having a length of 800mm (L_α), a width of 330mm (L_β) and an overall thickness (h) of 3mm and its short edges are clamped, while the others are free. The panel is impacted at its centre with a steel spherical impactor (E= 210GPa, ν= 0.3, radios=12.7mm, mass=5.45kg) with a velocity of 3.83m/s and an energy of 40J. All layers have the same thickness (0.25mm) and are made of the same material, whose properties are E_1=130GPa, E_2= E_3=8GPa, G_{12}= G_{13}=5GPa, G_{23}=2.5 GPa, ν_{12}= ν_{13}= ν_{23}=0.3, ρ= 1557 kg/m^3. The following lay-up is used [45°/-45°/0°/0°/45°/-45°/-45°/45°/0°/0°/-45°/45] and the following strengths are assumed:

- Tensile strengths S_{tii} along i-direction:
    - S_{t11}=1.67GPa, S_{t22}=0.06GPa
- Compressive strengths S_{cii} along i-direction:
    - S_{c11}=1.08GPa, S_{c22}=0.17GPa
- Shear strengths S_{ij}:
    - S_{12}=S_{13}=S_{23}=0.07GPa

Results of contact force estimated by present simulation and by those of [131] are reported in Figure 6.2. Because of the only difference between VK-ZZ of [131] and ZZA_GEN_INP is that this latter theory omits zig-zag functions (that are substituted with power series functions of in-plane coordinates, which it has been proven in the previous case to provide completely identical results) and the same procedure of the reference paper is followed, the same estimated contact force is obtained, which is in a well agreement with experimental one.

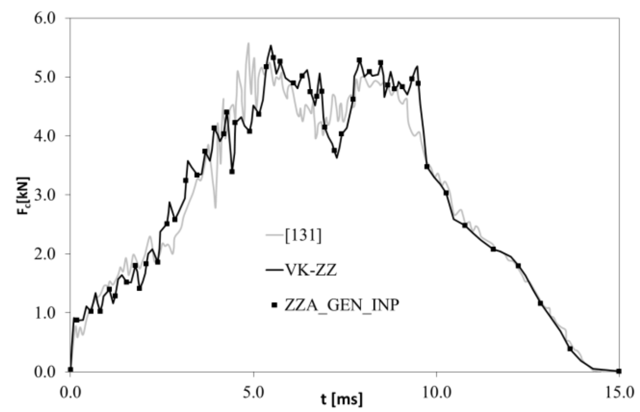

Figure 6.2: Contact force

Accordingly to [24], in this case the results with and without enforcement of the target to conform the shape of the impactor are undistinguishable, as is to be expected because laminates do not shrink like the faces of sandwiches which rest on a soft core. Figure 6.3 shows the estimated damaged area, which is calculated, according to sections 6.2 to 6.5. The overall area is subdivided into square subregions, where criteria of section 6.3 are applied to the centre point of each square and if any of the damage criteria predicts failure, all the sub-region is considered damaged. It should be noticed that stresses are calculated by using mesoscale model through a modified strain energy expression, where damage indicators are calculated apart, accordingly to section 6.5. Capability of VK-ZZ and ZZA_GEN to calculate damaged area is compared to that of theory by [131] (where in-plane continuity of stresses was not enforced) and to experimental results, which are used as reference solutions (see Figure 6.3). It should be noticed that indistinguishable results provided by VK-ZZ and ZZA_GEN (light grey) are in very good agreement with experimental results (dashed lines). Note that just delamination damage is reported. So, the previous findings about the choice of zig-zag functions are confirmed. Instead, a minor precision is obtained not considering in-plane continuity of stresses (dark grey) [131], even if errors are not very big for this case.

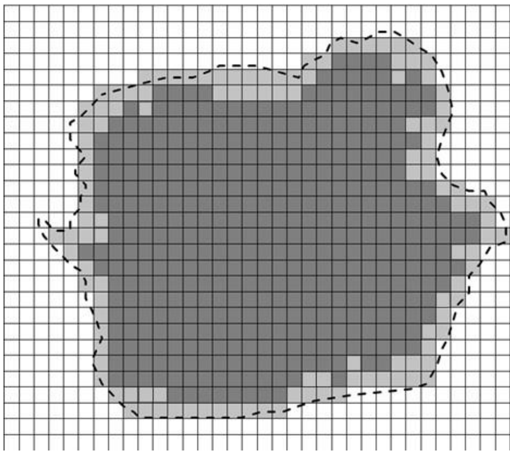

Figure 6.3: Overlap induced damage

This is also corroborated by delaminated area predicted at each interface and compared to experimental one (see Table 6.1):

Physical interface	Experimental [131]	VK-ZZ ZZA_GEN_INP	VK-ZZ No in-plane continuity	Analytical [131]
1st	960	950	930	950
2nd	790	758	740	258
3rd	430	400	380	376
4th	310	250	210	143
5th	160	115	107	114
6th	135	102	98	108
7th	95	75	62	75
8th	50	44	38	43

Table 6.1. Delaminated area [mm^2] predicted by various theories

It should be noticed that better results are obtained by VK-ZZ and ZZA_GEN_INP, demonstrating that in-plane stress continuity is important to get accurate results. Moreover, ZZA_GEN_INP has demonstrating to be more efficient than the parent theory, with a reduction of processing time of 40%.

6.9.2 Case b

This case is retaken from [10] and it is a $[0]_8$ laminated plate (dimensions are 100x100x2mm). The plate is supported at the sides along a strip 1.3 cm wide. Material properties of constituent layers are E_1=53.7GPa, E_2=53.88GPa E_3=10.00GPa, G_{12}= G_{13}=4.462GPa, G_{23}=3.0 GPa, ν_{12}= ν_{13}= 0.0502 ν_{23}=0.06. The plate is impacted by a steel sphere (radius of 6.35mm, mass of 0.36kg) with a velocity of 4.49m/s and an energy of 3.63J. The time history of contact force, retaken from [10] is reported in Figure 6.4.

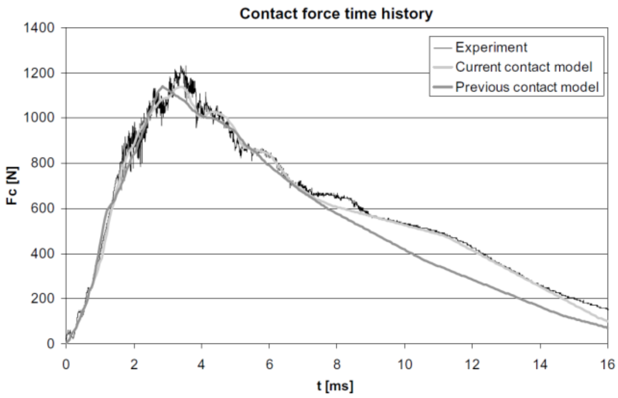

Figure 6.4: Contact force [10]

The curve indicated as “Previous” in Figure 6.4 represents the contact force obtained with a different contact law (from a former paper than [10]), while the light-grey curve indicated as “Current” in figure, represents the results obtained in [10] using an improved contact law. It should be noticed that this latter one is in a quite well agreement with experimental results.

Again, the capability of ZZA_GEN_INP to calculate damaged area is compared to that of theory by [10] and reported in Figure 6.5.

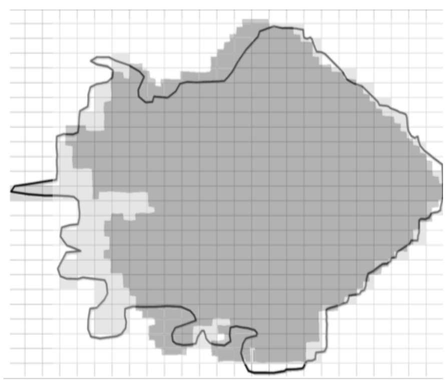

Figure 6.5: Overlap damage

Results obtained by ZZA_GEN_INP are in very good agreement with experimental ones (dashed lines), while a minor precision is obtained by previous theory [10] (dark grey), so, the importance to consider also in-plane continuities is reiterated.

Chapter 7 – Approximate 3-D solutions

A lot of 3-D exact solutions for multi-layered structures were proposed in Literature. Papers by Pagano [57] and [133] (for beams and plates), Ren [134] (plates in cylindrical bending), Brischetto [135] (multi-layered plates and shells), Icardi [54] (damaged sandwich beams), Kashtalyan and co-workers [82], [136], [137], [138] (3-D elasticity solution for graded isotropic plates, sandwich panels with functionally graded cores, distributed, concentrated and point loadings) are cited as notable examples.

Even though these solutions are very useful terms to comparisons in order to test accuracy of theories, they often show strong limitations regarding the choice of loading, boundary conditions and material properties of constituent layers. Indeed, lay-ups are usually symmetric and simply-supported beams and plates under sinusoidal or bi-sinusoidal loading are analysed. Anyway, closed-form 3-D solutions should be obtained for other more realistic loading and boundary conditions and for industrial lay-ups, that can be used as reference solutions in addition to finite elements solutions. Indeed displacement-based 3-D FEA cannot a priori satisfy local equilibrium equations, while mixed finite elements are very sensitive to local effects and some boundary conditions, such as clamped edges.

With the intended aim to overcome limitations of exact 3-D solutions, Reddy and Chao [139] and Yakimov [140] proposed approximate 3-D solutions. So, to obtain solutions that can be used as further reference to finite element results, accuracy of approximated theories is in-depth evaluated in this chapter, according to [20], [21], [23], renouncing to have exact solutions. Symbolic calculus is used to develop this approximate 3-D theory, starting from results of previous chapters, whose coefficients are redefined for each layers, in order to preserve adaptivity. Expression of displacements is completely general, similar to ZZA_GEN one. Anyway, differently to zig-zag theories, all coefficients are d.o.f. of this theory, some of which are calculated by imposing the fulfillment of physical constraints of theory of elasticity as function of the remaining ones, calculated by applying Rayleigh-Ritz method (Vel and Batra [25]). So, the solution is sought by assuming an appropriate in-plane expression for each displacement, that a priori fulfill kinematic boundary conditions. Also natural ones can be enforced without any difficulty; it should be noticed that Lagrange multiplier method is not mandatory, because these boundary conditions could be obtained through an adequate expansion across the thickness. Two different approaches are shown, with the aim to contain the number of d.o.f.

Results will demonstrate that an approximate 3-D theory can be obtained, able to analyze structures with any loading and boundary conditions. Similarly to previous chapters, thanks to symbolic calculus, analytical expression of loading is used in numerical applications and a series expansion is not needed. So, these approximate 3-D theories assume different and more d.o.f. than zig-zag theories of chapters 2 and 3. It should be noticed that DL are not used because their high number of unknowns.

In the next section, approximate 3-D theory (3D-AP) is reported, while results of some challenging benchmarks of chapter 4 are reported in section 7.2.

7.1 Approximate 3-D theory

A general approximate 3-D theory, referred as 3D-AP, with features similar to ones previously presented by author in [18], [21] and [23] is developed. The main purpose is to obtain solutions that can be used as further reference to finite element results, whose displacement field is:

$$\begin{aligned} u_\alpha{}^j &= \left(\sum_{k=0}^{n_\alpha} \left[{}^j a_k^\alpha \; {}_\alpha H_k(\varsigma) \right] \right) F(\alpha,\beta) \\ u_\varsigma{}^j &= \left(\sum_{k=0}^{n_\varsigma} \left[{}^j b_k^\alpha \; {}_\varsigma H_k(\varsigma) \right] \right) G(\alpha,\beta) \end{aligned} \tag{7.1}$$

n_α and n_ς represent the expansion order across the thickness of in-plane and transverse displacements. Their choice is free and performed by user, anyway, $n_\alpha = 4$ and $n_\varsigma = 5$ are assumed in numerical applications because it is sufficient to get accurate results. Coefficients ${}^j a_k^\alpha$ and ${}^j b_k^\alpha$ are redefined for each layer across the thickness, while the following expressions of ${}_\alpha H_k(\varsigma)$ and ${}_\varsigma H_k(\varsigma)$ are used for its particularization of numerical assessment of section 7.3:

$${}_\alpha H_k(\varsigma) = {}_\varsigma H_k(\varsigma) = \varsigma^{(k-1)} \tag{7.2}$$

Any other expressions of ${}_\alpha H_k(\varsigma)$ and ${}_\varsigma H_k(\varsigma)$ could be assumed, anyway, their assessment will be performed in future studies. Trial functions $F(\alpha,\beta)$ and $G(\alpha,\beta)$ a priori respect boundary conditions. They are assumed as a series expansion, whose expression is:

$$\begin{aligned} F(\alpha,\beta) &= \sum_{m=1}^{M} \sum_{p=1}^{P} A_{p\,m} \, F_{p\,m}(\alpha,\beta) \\ G(\alpha,\beta) &= \sum_{m=1}^{M} \sum_{p=1}^{P} B_{p\,m} \, G_{p\,m}(\alpha,\beta) \end{aligned} \tag{7.3}$$

M and P are two index of series of functions $F_{p\,m}(\alpha,\beta)$ and $G_{p\,m}(\alpha,\beta)$ along α and β axes, while $A_{p\,m}$ and $B_{p\,m}$ are the amplitudes constitute d.o.f. of this theory. So, the explicit expression of 3D-AP is:

$$
\begin{aligned}
u_{\alpha}{}^{j} &= \left(\sum_{k=0}^{n_{\alpha}} \left[{}^{j}a_k^{\alpha} \;\; {}_{\alpha}H_k(\varsigma) \right] \right) \sum_{m=1}^{M} \sum_{p=1}^{P} A_{p\,m} \, F_{p\,m}(\alpha,\beta) \\
u_{\varsigma}{}^{j} &= \left(\sum_{k=0}^{n_{\varsigma}} \left[{}^{j}b_k^{\alpha} \;\; {}_{\varsigma}H_k(\varsigma) \right] \right) \sum_{m=1}^{M} \sum_{p=1}^{P} B_{p\,m} \, G_{p\,m}(\alpha,\beta)
\end{aligned}
\tag{7.4}
$$

and two different approaches can be used to solve the boundary value problems.

Using the first procedure, amplitudes $A_{p\,m}$ and $B_{p\,m}$ constitute the d.o.f. of the problem. All coefficients ${}^{j}a_k^{\alpha}$ and ${}^{j}b_k^{\alpha}$ are calculated as functions of $A_{p\,m}$ and $B_{p\,m}$ by imposing the full set of physical constraints of ZZA (1.15)-(1.20). It should be noticed that the total number of ${}^{j}a_k^{\alpha}$ and ${}^{j}b_k^{\alpha}$ is greater than the number of coefficients of ZZA, so, they are saturated by imposing the fulfillment of local equilibrium equations for more equilibrium points. When the computation of all coefficients ${}^{j}a_k^{\alpha}$ and ${}^{j}b_k^{\alpha}$ is obtained, $A_{p\,m}$ and $B_{p\,m}$ are calculated by using Rayleigh-Ritz method. Anyway, this procedure should be avoided, even tough is possible to solve the algebraic system, because the products of $A_{p\,m}\,{}^{j}a_k^{\alpha}$ and $B_{p\,m}\,{}^{j}b_k^{\alpha}$ are non-linear and a lot of time could be required to compute them. Alternatively ${}^{j}a_k^{\alpha}$ and ${}^{j}b_k^{\alpha}$ could be calculated for each amplitude $A_{p\,m}$ and $B_{p\,m}$ by imposing M x P times physical constraints (1.15)-(1.20), however, further conditions have to be imposed for all no-homogenous conditions using Lagrange multiplier technique, so, also this alternative method is discarded.

So, the second procedure is performed, in order to overcome algebraic issue, assuming the products $A_{p\,m}\,{}^{j}a_k^{\alpha} = {}_{p\,m}^{\;j}c_k^{\alpha}$ and $B_{p\,m}\,{}^{j}b_k^{\alpha} = {}_{p\,m}^{\;j}d_k^{\varsigma}$ as new unknowns of this problem, so, (7.4) is rewritten as:

$$
\begin{aligned}
u_{\alpha}{}^{j} &= \sum_{m=1}^{M} \sum_{p=1}^{P} \sum_{k=0}^{n_{\alpha}} \left[{}_{p\,m}^{\;j}c_k^{\alpha} \; F_{p\,m}(x,y) \; z^{(k-1)} \right] \\
u_{\varsigma}{}^{j} &= \sum_{m=1}^{M} \sum_{p=1}^{P} \sum_{k=0}^{n_{\varsigma}} \left[{}_{p\,m}^{\;j}d_k^{\varsigma} \; G_{p\,m}(x,y) \; z^{(k-1)} \right]
\end{aligned}
\tag{7.5}
$$

This passage may appear trivia, but it is sufficient to remove all algebraic non-linarites and to reduces time required for computations. Differently to ZZA_GEN and other zig-zag theories particularized starting from ZZA, any number of coefficients ${}_{p\,m}^{\;j}c_k^{\alpha}$ and ${}_{p\,m}^{\;j}d_k^{\varsigma}$ could be assumed as d.o.f. However, in numerical applications, a part of ${}_{p\,m}^{\;j}c_k^{\alpha}$ and ${}_{p\,m}^{\;j}d_k^{\varsigma}$ are calculated by imposing the full set of physical constraints of ZZA (1.15)-(1.20), so, the remaining ones constitute the d.o.f. of this problem that are obtained similarly to previous theories by Rayleigh-Ritz method. There is no need to assign a specific role to coefficients, so, user can freely decide which are used to impose physical constraints and which are d.o.f., differently to ZZA and other zig-zag theories.

Thanks to symbolic calculus, it is again possible to assume the exact formula of the load acting on upper or lower faces, without any series expansion. In the following section, some results obtained by this theory for some challenging cases of chapter 4 are reported.

7.2 Application of 3D-AP

Results obtained by present 3D-AP theory is compared to findings provided by 3-D FEA and ZZA for cases a, c, e and h retaken from chapter 4. The same lay-up, loading, boundary conditions are assumed, as well as the same trial functions and in-plane expansion order. For all cases, n_α and n_ς are assumed as three and four respectively, because numerical assessment of [18], [21] and [23] demonstrate that these choices are sufficient to get accurate results,

Regarding case a, that is a simply-supported laminated [0/90/0/90] beam under a sinusoidal loading, the following results are obtained (Figure 7.1):

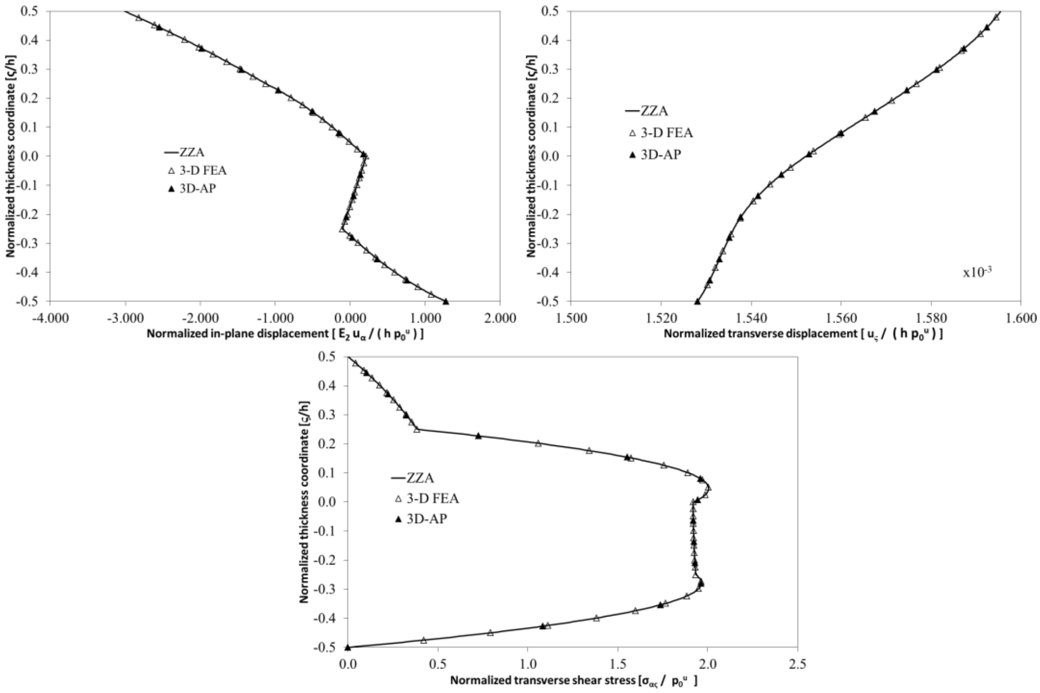

Figure 7.1: Normalized displacements and stresses, case a

Results obtained by 3D-AP, where M=1 (one term along x-axis) is assumed, are very close to 3-D FEA solutions, so, it could be used as reference solution, along with mixed finite elements by Icardi and Atzori when exact solution is not available. This is also reiterated for case c, that is a simply-supported asymmetric sandwich plate under a bisinusoidal loading (Figure 7.2):

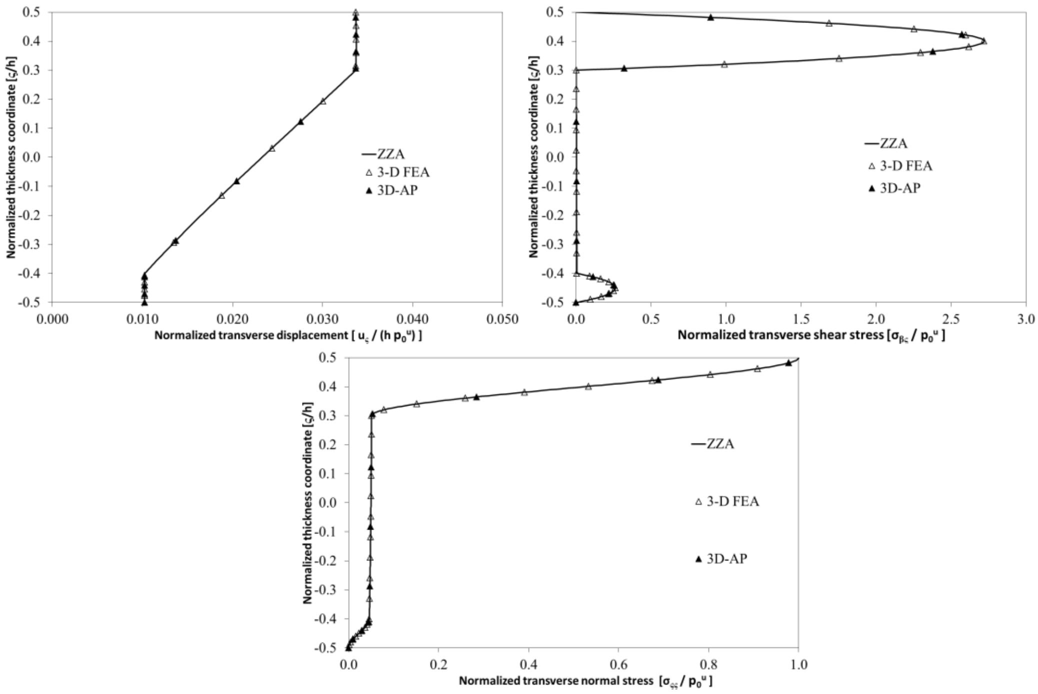

Figure 7.2: Normalized displacements and stresses, case c

In this case M=1 and P=1 but it is confirmed that 3D-AP can compete with mixed 3-D FEA, because of indistinguishable results are obtained. However, the next two cases are considered, with the intended aim to test accuracy of 3D-AP also for other loading and boundary conditions.

The same propped cantilever sandwich beam of case e of chapter 4 is considered and results are reported in Figure 7.3:

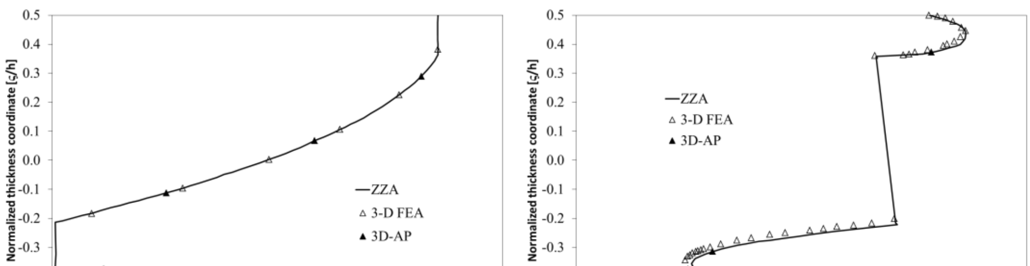

Figure 7.3: Normalized displacements and stresses, case e

For this case, M=9 is assumed, in order to compare results under the same conditions of ZZA, but it should be noticed that a good level of accuracy is already obtained with M=3, thanks to higher number of d.o.f. and redefinition of coefficients of 3D-AP for each term of in-plane expansion respect to zig-zag theory. Again, 3D-AP is in well agreement with 3-D FEA, also for this very challenging case. Particularly, 3D-AP is able to accurately describe transverse displacement and deformability and accordingly to [71], accurate transverse shear stress is obtained. This demonstrate that 3D-AP is able to describe displacements and stresses also when a high in-plane expansion is assumed. Obviously, processing time required is quite high for this case, having a lot of more d.o.f. than ZZA. However, good results obtained confirm that this theory can be used as reference if exact solution is not available, also for other boundary conditions than ZZA. In the next case h, an eleven-layer simply-supported sandwich beam under a uniform loading that is applied on the top face for half of beam and on the bottom face for the remaining part, but with an opposite sign (Figure 7.4):

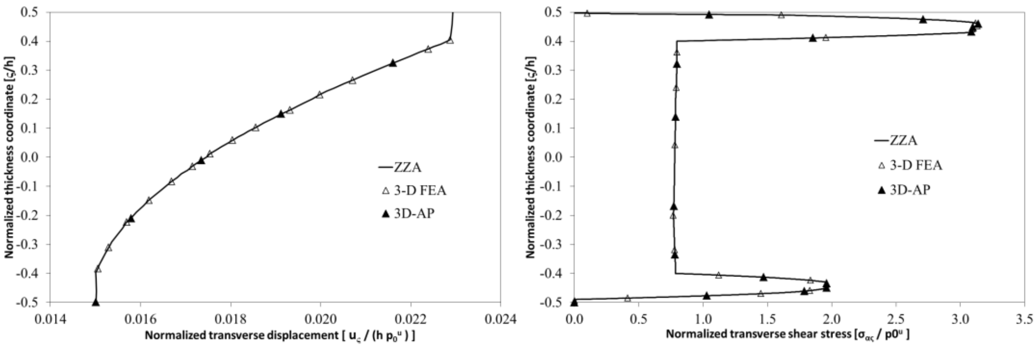

Figure 7.4: Normalized displacements and stresses, case h

Again, M=1 is assumed also for this case and the same findings on accuracy of 3D-AP still apply also for this case.

Because of 3D-AP demonstrates its great accuracy for considered cases, according to [18], [21] and [23], it is demonstrated that 3-D approximate solutions can be used as alternative references when exact results are not available, irrespective loading and boundary conditions of analyzed lay-up. It should be also noticed that this approach is able to overcome strong limitations of exact 3-D solutions, which are in any case an important instrument of validations of numerical procedures.

Chapter 8 – Strain Energy Update Technique

As shown in previous chapters, accuracy of ZZA (and higher-order theories obtained from it) is very high. Anyway, it is not able to analyse complex structures of industrial interests, e.g. wings, as like as any other analytical model. In order to overcome this issue, finite elements can be obtained by this theory. However, because of its layerwise and higher-order terms that impose physical constraints there are a lot of derivatives into strain energy (see Icardi and Ferrero [5]). As a consequence, finite elements obtained from theories of chapters 2, should contain a high number of nodal d.o.f., so, they could require very high computational burden if very complex structures are analyzed. Mixed finite elements able to obtain accurate displacements and stresses can be developed (see Icardi and Atzori [6]). Anyway, even though their shape functions are simple, they still require a greater number of d.o.f. than commercial ones.

Over the years, various techniques were proposed to eliminate derivatives of d.o.f., see Zhen and Wanji [141] and Sahoo and Singh [142]. Strain Energy Update Technique (SEUPT) proposed by Icardi and Sola [13] is discussed in this chapter because of its efficiency. Regarding its original form (see Icardi [9] and Icardi and Ferrero [10]), precision of results by commercial finite elements was improved using an iterative post-processing tool. This procedure was modified and upgraded by Icardi and Sola (see [11], [12], [13]). Unlike the previous version, the intended aim is to update the strain energy and the work of forces through a priori calculation of corrective terms. In this way, energy contributions of an original theory (e.g. ZZA or ZZA_GEN) are equalled to ones of an equivalent theory without derivatives of d.o.f. In this way, a C0 finite element can be obtained; its shape functions are the same of commercial elements, but its precision is similar to a layerwise model [13].

A further and new version of SEUPT is also theorized into this section. It consists of a novel approach that strongly integrates commercial finite elements software in the improvement process, without any iterative post-processing tool.

It should be noticed that all these techniques will be applied to a particularization of ZZA_GEN, thanks to its particular efficient and optimized expression of displacements. Application of SEUPT technique will be assessed considering benchmarks retaken from literature. This chapter contains only preliminary studies and results regarding the application of this technique.

8.1 Iterative SEUPT technique

Firstly, the iterative original form of SEUPT [9]- [10] is here retaken. The purpose is to increase accuracy of results by commercial finite elements; in order to apply this version of SEUPT, the next steps have to be followed:

- User choices the region to which apply SEUPT;
- Polynomial spline of results (displacements, strains, stresses) by finite elements;
- Energy contributions are calculated by an accurate zig-zag theory, using finite element results;
- Also energy contributions of finite elements are calculated;
- Corrective terms are introduced into energy contribution by finite elements and are calculated through an iterative process and an energy balance;
- When the convergence has been achieved, nodal d.o.f. of finite elements are updated;
- A great improvement of results is obtained.

It should be noticed that this technique will not be used into this thesis. In the next chapter, a modified version of SEUPT will be discussed to obtain an accurate C0 finite element.

8.2 Modified SEUPT technique by Icardi and Sola

This version of SEUPT (see Icardi and Sola [11], [12], [13]) is a modified and an upgraded version of that presented in section 8.1 with the intended aim to obtain an accurate C0 Lagrangian finite element.

Firstly a higher-order theory (ZZA_GEN in applications) is chosen as “original theory” and it will be indicated with the superscript ^{OT}. Displacement field, which is explained in (3.18) can be rewritten as:

$$\begin{aligned} u_\alpha^{j\,OT}(\alpha,\beta,\varsigma) &= \sum_{i=0}^{n_\alpha=3} \left[{}^jC_\alpha^i(\alpha,\beta) F^i(\varsigma) \right] = U_\alpha^{0\;OT}(\alpha,\beta,\varsigma) + U_\alpha^{1\;OT}(\alpha,\beta,\varsigma) \\ u_\varsigma^{j\,OT}(\alpha,\beta,\varsigma) &= \sum_{i=0}^{n_\varsigma=4} \left[{}^jC_\varsigma^i(\alpha,\beta) G^i(\varsigma) \right] = U_\varsigma^{0\;OT}(\alpha,\beta,\varsigma) + U_\varsigma^{1\;OT}(\alpha,\beta,\varsigma) \end{aligned} \tag{8.1}$$

Where $U_\alpha^{0\;OT}$ and $U_\varsigma^{0\;OT}$ contain all terms that are functions of d.o.f., while $U_\alpha^{1\;OT}$ and $U_\varsigma^{1\;OT}$ contain terms that are functions of derivatives of d.o.f. These latter ones appear into displacement field as a consequence of enforcement of physical constraints. For this reason, the development of a finite element starting from (8.1) is not considered.

Another theory is designated as equivalent theory (and indicated as ^{ET}), whose displacement field does not contain any derivative of d.o.f.:

$$u_\alpha^{j\ ET}(\alpha,\beta,\varsigma)=U_\alpha^{0\ ET}(\alpha,\beta,\varsigma)$$
$$u_\varsigma^{j\ ET}(\alpha,\beta,\varsigma)=U_\varsigma^{0\ ET}(\alpha,\beta,\varsigma) \tag{8.2}$$

So, the purpose is to obtain a modified expression of ET displacements, without any d.o.f. derivatives, through corrective terms $\Delta U_\alpha^{0\ ET}$ and $\Delta U_\varsigma^{0\ ET}$ able to balance strain energy and work of external and inertial forces between OT and ET. So, the following displacement field is assumed for ET:

$$u_\alpha^{j\ ET}(\alpha,\beta,\varsigma)=U_\alpha^{0\ ET}(\alpha,\beta,\varsigma)+\Delta U_\alpha^{0\ ET}$$
$$u_\varsigma^{j\ ET}(\alpha,\beta,\varsigma)=U_\varsigma^{0\ ET}(\alpha,\beta,\varsigma)+\Delta U_\varsigma^{0\ ET} \tag{8.3}$$

The following balances are imposed:

$$[\delta E]^{OM}=[\delta E]^{u^0 EM}=0 \tag{8.4}$$

From which a corrective terms for each d.o.f. ($\Delta u_\alpha^0, \Delta w^0, \Delta\Gamma_\alpha^0$ and so, $\Delta U_\alpha^{0\ ET}$ and $\Delta U_\varsigma^{0\ ET}$) are obtained. E in (8.4) is the sum of strain energy and work of external and inertial forces:

$$E=\frac{1}{2}\int_V\{\sigma\}^T\{\varepsilon\}dV-\left[\int_V\{b\}\{u\}dV+\int_S\{t\}\{u\}dS\right]+\int_V-\rho\left\{\ddot{u}\right\}\{u\}dV \tag{8.5}$$

It should be noticed that modified expression of displacements of ET (8.3) have the same amount of energy, so, the same functional d.o.f. are calculated. Differently from the previous techniques, corrective terms are calculated once and for all, in closed form by using symbolic calculus and no iterative post-processing technique is required. So, the following steps have to be followed:

- Coefficients of OT are calculated in closed form by imposing physical constraints;
- D.o.f. derivatives are substituted with unknown corrective terms (ET);
- Strain energy and the works of external and inertial forces are computed;
- Corrective terms are calculated, once and for all in a closed form, using symbolic calculus tool, by energy balances between OT and ET.

Corrective terms are calculated by integrating by part energy balance. In this way, strain energy of OT is rewritten without any d.o.f. derivatives. As a consequence, a C0 finite element can be obtained. Its shape functions are the same of commercial elements (Lagrangian polynomial), but its precision is similar to a layerwise model. It should be noticed that these elements provide a very good approximation of the correct value of functional d.o.f. of ZZA_GEN along in-plane directions, but, because of their intrinsic simplicity, they are not able to reproduce trend of displacements and stresses across the thickness. So, in order to accurately reproduce them a post-processing is needed. Results provided by these elements are substituted into a higher-order theory (ZZA or ZZA_GEN) and assumed as trial functions (both amplitudes and trend along in-plane directions) in order to plot trend of displacements and stresses across the thickness. It should be noticed that analytical model is only used to plot quantities across the thickness.

8.2.1 Development of finite element

Accordingly to Icardi and Sola [11], the following vector of nodal d.o.f. is assumed for the eight-node finite element obtained by energy of ET:

$$\{Q\} = \left\{\left[u_{\alpha 1}^0, u_{\beta 1}^0, w_1^0, \Gamma_{\alpha 1}^0, \Gamma_{\beta 1}^0\right], ..., \left[u_{\alpha 8}^0, u_{\beta 8}^0, w_8^0, \Gamma_{\alpha 8}^0, \Gamma_{\beta 8}^0\right]\right\}^T \tag{8.6}$$

A polynomial Lagrangian representation is assumed to increase accuracy and to obtain precise results also for coarse meshing. The separate representations of Γ_α^0 and w^0 prevent shear locking (see Prathap [143]) while the following shape functions are assumed:

$$N_i = \begin{cases} \frac{1}{4}(1+\xi\xi_i)(1+\eta\eta_i)(\xi\xi_i+\eta\eta_i-1) & \text{for corners } (i=1,2,3,4) \\ \frac{1}{2}(1-\xi^2)(1+\eta\eta_i) & \text{for mid-side nodes } (i=5,7) \\ \frac{1}{2}(1-\eta^2)(1+\xi\xi_i) & \text{for mid-side nodes } (i=6,8) \end{cases} \tag{8.7}$$

Similarly to section 1.8, the topological transformation from physical to natural volume is used, in order to simplify and harmonize calculus of integrals of strain energy, so:

$$x_i = \mathbf{N}\{Q\} \tag{8.8}$$

As regards derivative, the following relations apply:

$$\begin{Bmatrix} \dfrac{\partial}{\partial \xi} \\ \dfrac{\partial}{\partial \eta} \end{Bmatrix} = [J] \begin{Bmatrix} \dfrac{\partial}{\partial \alpha} \\ \dfrac{\partial}{\partial \beta} \end{Bmatrix} \longrightarrow \begin{Bmatrix} \dfrac{\partial}{\partial \alpha} \\ \dfrac{\partial}{\partial \beta} \end{Bmatrix} = [J]^{-1} \begin{Bmatrix} \dfrac{\partial}{\partial \xi} \\ \dfrac{\partial}{\partial \eta} \end{Bmatrix} \tag{8.9}$$

where $[J]$ is Jacobian matrix and $[J]^{-1}$ its inverse:

$$[J] = \begin{bmatrix} \dfrac{\partial \alpha}{\partial \xi} & \dfrac{\partial \beta}{\partial \xi} \\ \dfrac{\partial \alpha}{\partial \eta} & \dfrac{\partial \beta}{\partial \eta} \end{bmatrix} \tag{8.10}$$

So, strains and stresses are expressed as:

$$\{\varepsilon\} = [B]\{Q\} \rightarrow \{\sigma\} = [D]\{\varepsilon\} = [D][B]\{Q\} \tag{8.11}$$

And the following expression of stiffness and mass matrixes and of vector of nodal loads are gotten, using standard techniques:

$$\begin{aligned}
&[K] = \int_V [B]^T [D][B] dV \\
&[M] = \int_V \rho [N]^T [N] dV \\
&\{Fe\} = \int_V [N]^T \{\bar{X}\} dV
\end{aligned} \tag{8.12}$$

Regarding $\{Fe\}$, also punctual forces or ones applied to a surface could be considered with a few changes. In the next sections, accuracy of finite elements obtained by ZZA_GEN (assuming the particularization of (8.13)) will be compared to results provided by finite elements obtained from ZZA.

$$\begin{aligned}
&\text{d.o.f.:} \quad {}^1C_\alpha^0 = u_\alpha^0,\ {}^1C_\alpha^1 = \Gamma_\alpha^0 - w_{,\alpha}^0,\ {}^1C_\varsigma^0 = w^0 \\
&F_\alpha^i(\varsigma) = G^i(\varsigma) = \varsigma^i
\end{aligned} \tag{8.13}$$

Moreover, also a mixed version of this finite element could be obtained [11].

8.3 Numerical results of C0 finite element generated from ZZA_GEN

Case a

This case is retaken from [141] and it is a square sandwich plate under a bisinusoidal loading, whose mechanical properties are reported in Table 8.1:

Material name	Face	Core	Lay-up
E1[GPa]	172.4	0.276	
E2[GPa]	6.89	0.276	[Core/Face/Core]
E3 [GPa]	6.89	345	[0.1h/0.8h/0.1h]
G12 [GPa]	3.45	0.1104	
G13 [GPa]	3.45	0.414	Lβ=Lα
G23 [GPa]	1.378	0.4141	Lα/h=4,10,20
υ12	0.25	0.25	
υ13	0.25	0.25	ρ=1558.35 kg/m^3
υ23	0.25	0.25	

Table 8.1. Material properties and Lay-up, case a.

As previously explained, finite elements described in section 8.2 obtain an approximate value of d.o.f. of ZZA_GEN that are suddenly substituted into parent theory, in order to compute displacements and stresses (without solving analytical problem). Results reported in Table 8.2 are compared to those provided by finite elements obtained from ZZA by Icardi and Sola, where the following normalizations are used:

$$\bar{\sigma}^{u}_{\alpha\alpha} = \frac{\sigma_{\alpha\alpha}\left(0,0,\frac{h}{2}\right)h^2}{q^0 L_\alpha^2}; \bar{\sigma}^{l}_{\alpha\alpha} = \frac{\sigma_{\alpha\alpha}\left(0,0,-\frac{h}{2}\right)h^2}{q^0 L_\alpha^2}$$
$$\bar{\sigma}_{\alpha\varsigma} = \frac{\sigma_{\alpha\varsigma}\left(\frac{L_\alpha}{2},0,0\right)h}{q^0 L_\alpha}; \bar{\sigma}_{\beta\varsigma} = \frac{\sigma_{\beta\varsigma}\left(0,\frac{L_\beta}{2},0\right)h}{q^0 L_\alpha} \quad (8.14)$$

Lx/h		$\sigma_{\alpha\alpha}^U$	$\sigma_{\alpha\alpha}^L$	$\sigma_{\alpha\varsigma}$	$\sigma_{\beta\varsigma}$
4	[141]	1.5622	-1.5622	0.1505	0.1325
	ZZA	1.5622	-1.5300	0.1505	0.1363
	Icardi and Sola (9x9 mesh)	1.5622	-1.5250	0.1505	0.1375
	Present (9x9 mesh)	1.5622	-1.5250	0.1505	0.1375
10	[141]	1.1686	-1.1686	0.2957	0.0506
	ZZA	1.1686	-1.1650	0.2957	0.0506
	Icardi and Sola (9x9 mesh)	1.1686	-1.1599	0.2957	0.0506
	Present (9x9 mesh)	1.1686	-1.1599	0.2957	0.0506
20	[141]	1.1101	-1.1101	0.3174	0.0360
	ZZA	1.1101	-1.1101	0.3174	0.0360
	Icardi and Sola (9x9 mesh)	1.1101	-1.1101	0.3174	0.0360
	Present (9x9 mesh)	1.1101	-1.1101	0.3174	0.0360

Table 8.2. Results for case a.

Results confirm that there is no shear locking and indistinguishable findings are provided by present finite elements obtained by ZZA_GEN and finite elements by Icardi and Sola. It should be noticed that a 9x9 mesh (only a quarter of plate is analysed because of its in-plane symmetric properties) is sufficient to obtain accuracy comparable to ZZA. These findings still apply to case b for natural frequencies.

Case b

Natural frequencies of a simply-supported laminated square plate from [144] are analysed, where different orthotropic ratios are assumed:

Material name	p	Lay-up
E1[GPa]	E1	$[p_4]$ $[(0.25h)_4]$ $L\beta=L\alpha$ $L\alpha/h=5$
E2[GPa]	E2	
E3 [GPa]	E2	
G12 [GPa]	0.6 E2	
G13 [GPa]	0.6 E2	
G23 [GPa]	0.5 E2	
υ12	0.25	
υ13	0.25	
υ23	0.25	

Table 8.3. Material properties and Lay-up, case b.

Results of natural frequencies are normalized as:

$$\bar{f} = f\frac{L_x^2}{h}\sqrt{\frac{\rho}{E_2}} \quad (8.15)$$

E1/ E2		f	E1/ E2		f
3	[144]	6.618	20	[144]	9.560
	ZZA	6.506		ZZA	9.351
	Icardi and Sola (9x9 mesh)	6.599		Icardi and Sola (9x9 mesh)	9.558
	Present (9x9 mesh)	6.599		Present (9x9 mesh)	9.558
10	[144]	8.210	30	[144]	10.272
	ZZA	8.096		ZZA	10.107
	Icardi and Sola (9x9 mesh)	8.225		Icardi and Sola (9x9 mesh)	10.275
	Present (9x9 mesh)	8.225		Present (9x9 mesh)	10.275

Table 8.4. Results for case b.

Finite elements of section 8.2 are again in good agreement with those obtained from ZZA by Icardi and Sola. Accuracy of finite elements obtained starting from other particularizations of ZZA_GEN or to other more challenging cases are left for future research. However, it is important to emphasize that SEUPT technique demonstrate that it is possible to obtain a simple and efficient finite element, which could be used also to analyse structures of industrial interests. A preliminary study about a new version of SEUPT is reported in the next chapter.

8.4 New direct version of SEUPT

A further version of SEUPT, reported into this section, consists of a novel approach that strongly integrates commercial finite elements software in the improvement process. Firstly, structure is analyzed by using commercial tools, so, the next steps are followed:

- Choice of the region to which apply SEUPT;
- Polynomial spline interpolation of displacements calculated by finite elements;
- Spline functions are normalized and then they are assumed as trial functions of a higher-order theory (e.g. ZZA or ZZA_GEN), whose amplitudes are unknowns;
- Equivalent external load are applied to the model;
- Amplitudes are calculated by applying Rayleigh-Ritz method;
- Corrective elastic moduli (as material properties of a fictitious material) are calculated, in order to equal strain energies of higher-order theory and of finite elements;
- Corrective elastic moduli are substituted into commercial finite elements software; a new calculation is done, improving results because the same energy of a higher-order models is obtained.

8.4.1 Preliminary assessment of commercial finite element software

Firstly, results by commercial finite element software are compared to ZZA_GEN (the following functions $F^i(\varsigma) = G^i(\varsigma) = \varsigma^i$ are assumed) and 3D-FEA ones for simply-supported square plates. Regarding 3-D FEA, a mesh of 8x8 elements along α and β directions is adopted, because it is sufficient to get accurate results for examined benchmarks.

Regarding case c, the following lay-up and mechanical properties are assumed:

Material Name	q	Lay-Up
E1= E2= E3 [GPa]	73	[q]
G12=G13=G23 [GPa]	28.076	[h]
υ12=υ13=υ23	0.3	Lβ=Lα Lα/h=4 to 100

Table 8.5. Material properties and lay-up, case c.

The following results are obtained for transverse displacement at the center of the plate (a mesh of 120x120 elements is used to discretize the plate using commercial finite elements tool), where a L=100mm is assumed for each edge:

Lα/h	3D-FEA	ZZA_GEN	Commercial FEA
4	$3.38\cdot10^{-3}$	$3.38\cdot10^{-3}$	$3.38\cdot10^{-3}$
10	$3.92\cdot10^{-2}$	$3.92\cdot10^{-2}$	$3.92\cdot10^{-2}$
25	$5.62\cdot10^{-1}$	$5.62\cdot10^{-1}$	$5.62\cdot10^{-1}$
50	4.40	4.40	4.40
100	$3.48\cdot10^{1}$	$3.48\cdot10^{1}$	$3.48\cdot10^{1}$

Table 8.6. Transverse displacement [mm], case c.

Regarding isotropic plates, there is no need of post-processing, because commercial finite elements are able to correctly provide an accurate solution irrespective length to thickness ratios considered.

Regarding cases d and e, the following lay-ups and material properties are assumed:

Material name	p	Case d	Case e
E1[GPa]	172.4		
E2[GPa]	6.89		
E3 [GPa]	6.89	$[p_3]$	$[p_2]$
G12 [GPa]	3.45	$[(h/3)_3]$	$[(h/2)_2]$
G13 [GPa]	3.45		
G23 [GPa]	1.378	Lβ=Lα	Lβ=Lα
υ12	0.25	Lα/h=4 to 50	Lα/h=4 to 50
υ13	0.25		
υ23	0.25		

Table 8.7. Material properties and Lay-up, case b.

The following results are obtained for transverse displacement at the center of plate, where a length of L=100mm is assumed for each edge:

	$L\alpha/h$	3D-FEA	ZZA_GEN	Commercial FEA
Case d	4	$1.89\cdot10^{-2}$	$1.86\cdot10^{-2}$	$1.90\cdot10^{-2}$
	10	$1.11\cdot10^{-1}$	$1.09\cdot10^{-1}$	$1.02\cdot10^{-1}$
	25	1.11	1.10	1.00
	50	8.10	8.07	7.29
Case e	4	$1.95\cdot10^{-2}$	$1.92\cdot10^{-2}$	$1.98\cdot10^{-2}$
	10	$1.80\cdot10^{-1}$	$1.78\cdot10^{-1}$	$1.83\cdot10^{-1}$
	25	2.50	2.47	2.32
	50	19.6	19.4	17.8

Table 8.8. Transverse displacement [mm], cases d and e.

It should be noticed that percentage errors increase than previous case, anyway, commercial finite element software is still able to quite accurately predict transverse displacement.

This does not apply for case f, where the same sandwich of section 4.4 is analyzed (again a length of L=100mm is assumed for each edge where a length to thickness ratio of 10 is assumed):

$L\alpha/h$	3D-FEA	ZZA_GEN	Commercial FEA
10	3.93	3.93	2.7

Table 8.9. Transverse displacement [mm], case f.

In this case, very inaccurate results are obtained by plate elements. Three-dimensional finite elements could be used, but a lot of elements are required to get precise results, so SEUPT technique will be applied in the next section, with the intended aim to increase accuracy of results obtained by commercial tools.

8.4.2 Updating of results by direct version of SEUPT

Firstly, the region to which apply SEUPT technique is chosen. Regarding case f, the entire plate is chosen and results of in-plane and transverse displacements are interpolated by using polynomial spline. Results obtained are normalized and assumed as trial functions, whose amplitudes are unknowns and are calculated by solving the structural problem. Interpolated trial function is indicated with symbol $w^0_{\mathrm{int}er}(\alpha,\beta)$ in this section.

Since Rayleigh-Ritz method is used, the convergence of results is guaranteed if natural boundary conditions are fulfilled by trial functions. The original trial functions (indicated as $w^0_{orig}(\alpha,\beta)$) for simply-supported plates under a bi-sinusoidal loading are:

$$w^0_{orig}(\alpha,\beta)=\sin\left(\frac{\pi\alpha}{L_\alpha}\right)\sin\left(\frac{\pi\beta}{L_\beta}\right) \qquad (8.16)$$

$w_{orig}^0(\alpha,\beta)$ is able to a priori fulfill all the following natural boundary conditions:

$$u_\varsigma(0,\beta)=u_\varsigma(L_\alpha,\beta)=0$$
$$u_\varsigma(\alpha,0)=u_\varsigma(\alpha,L_\beta)=0$$
$$u_{\varsigma,\alpha}\left(\frac{L_\alpha}{2},\beta\right)=u_{\varsigma,\beta}\left(\alpha,\frac{L_\beta}{2}\right)=0$$
$$u_{\varsigma,\alpha\alpha}(0,\beta)=u_{\varsigma,\alpha\alpha}(L_\alpha,\beta)=0$$
$$u_{\varsigma,\beta\beta}(\alpha,0)=u_{\varsigma,\beta\beta}(\alpha,L_\beta)=0$$

(8.17a)

The polynomial trial function obtained through spline interpolation of results provided by finite elements $w_{inter}^0(\alpha,\beta)$ is reported in Figure 8.1a (in red) and compared to $w_{orig}^0(\alpha,\beta)$ (in black) of (8.16):

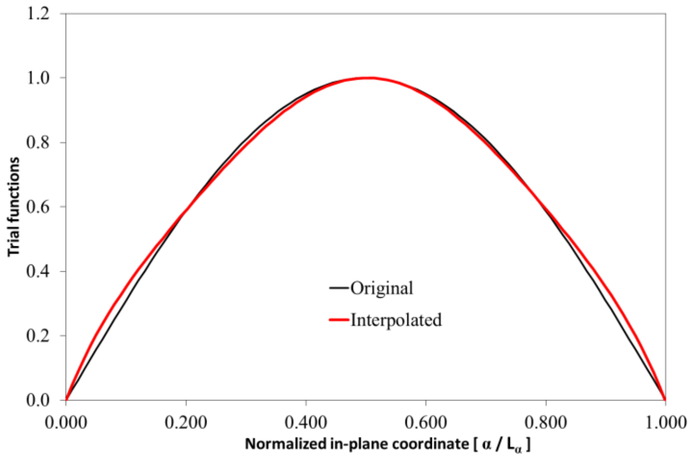

Figure 8.1a: Comparison between interpolated trial function and original one (8.16)

$w_{inter}^0(\alpha,\beta)$ is very close to $w_{orig}^0(\alpha,\beta)$ of (8.16) and it is able to fulfill the following boundary conditions:

$$u_\varsigma(0,\beta)=u_\varsigma(L_\alpha,\beta)=0$$
$$u_\varsigma(\alpha,0)=u_\varsigma(\alpha,L_\beta)=0 \qquad (8.17b)$$

However, also boundary conditions on the first and second derivatives of trial functions of (8.17a) have to be fulfilled, in order to get convergent results through the application of Rayleigh-Ritz method.

Comparisons of the first and the second derivatives of $w_{orig}^0(\alpha,\beta)$ respect to the first and the second derivatives of the interpolated one $w_{inter}^0(\alpha,\beta)$ (in red) are reported in Figure 8.1b:

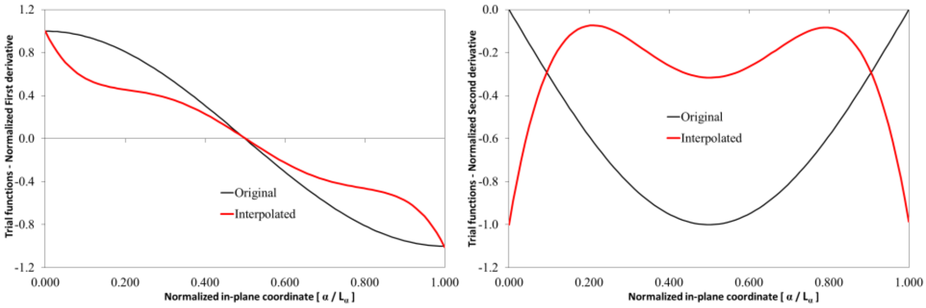

Figure 8.1b: Comparison between first and second derivatives of trial function and original one (8.16)

First and second derivatives of $w^0_{inter}(\alpha,\beta)$ cannot guarantee the fulfilment of:

$$\begin{aligned} &u_{\varsigma,\alpha}\left(\frac{L_\alpha}{2},\beta\right)=u_{\varsigma,\beta}\left(\alpha,\frac{L_\beta}{2}\right)=0 \\ &u_{\varsigma,\alpha\alpha}(0,\beta)=u_{\varsigma,\alpha\alpha}(L_\alpha,\beta)=0 \\ &u_{\varsigma,\beta\beta}(\alpha,0)=u_{\varsigma,\beta\beta}(\alpha,L_\beta)=0 \end{aligned} \tag{8.17c}$$

Moreover, their trend along in-plane directions is also wrong, compared to those of first and second derivatives of $w^0_{orig}(\alpha,\beta)$. As a consequence, $w^0_{inter}(\alpha,\beta)$ cannot be used directly as trial functions for Rayleigh-Ritz method. Indeed, six additional corrective terms have to be added to $w^0_{inter}(\alpha,\beta)$, in order to get the following corrected trial function:

$$w^0_{corr}(\alpha,\beta)=\left(w^0_{inter}\left(\alpha,\frac{L_\beta}{2}\right)+\alpha C_0+\alpha^2 C_1+\alpha^3 C_2\right)\left(w^0_{inter}\left(\frac{L_\alpha}{2},\beta\right)+\beta D_0+\beta^2 D_1+\beta^3 D_2\right) \tag{8.17d}$$

These corrective terms are calculated by imposing (8.17c), through symbolic calculus tool. In this way, $w^0_{corr}(\alpha,\beta)$ is able to fulfil all boundary conditions (8.17a) and it can be used as trial function. Indeed, Figure 8.2 shows that $w^0_{corr}(\alpha,\beta)$ and its first and second derivatives are able to reproduce $w^0_{orig}(\alpha,\beta)$ and its derivatives:

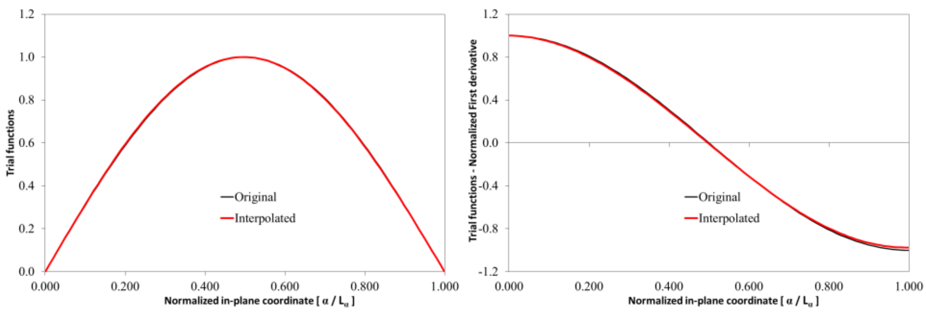

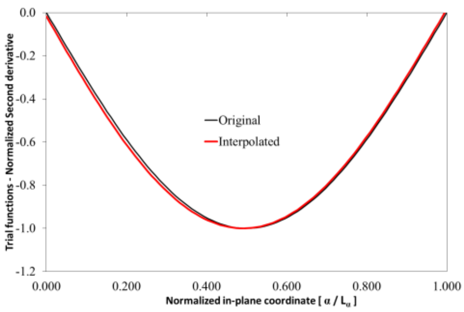

Figure 8.2: Comparison between corrected trial function and original one

So, new corrected trial functions $w^0_{corr}(\alpha, \beta)$ can be used for calculation and substituted into ZZA_GEN symbolic procedure. An equivalent external loading is applied and amplitudes of corrected trial functions are calculated by Rayleigh-Ritz method. Results obtained by ZZA_GEN (with $F^i(\varsigma) = G^i(\varsigma) = \varsigma^i$), assuming the previous corrected trial functions are reported in Table 8.10:

Lα/h	3D-FEA	ZZA_GEN	Commercial FEA	ZZA_GEN with trial functions obtained from commercial finite elements
10	3.93	3.93	2.70	3.92

Table 8.10. Transverse displacement [mm], case f.

Moreover, the following displacements and stresses are obtained:

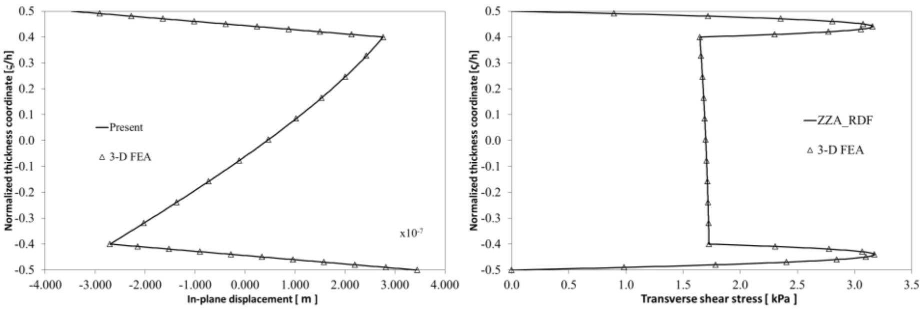

Figure 8.3: Displacements and stresses, case f

A great improvement of results is obtained, so, approach here preliminary proposed can be used to increase accuracy of results obtained by commercial finite elements. The same procedure could be also applied also to other structures, such as wings. On-going studies are in progress, whose purpose is to obtain a modified expression of elastic moduli as the next step of this procedure, through strain energy balances, which could be used into commercial finite element software to increase their performances when complex structures (e.g. wings) are analyzed. However, this will be developed in future studies.

Conclusions and major findings

The accuracy of several zig-zag theories, developed as variants of the adaptive zig-zag one by Icardi and Sola (ZZA) is assessed. The purpose was the development a simplified and generalized version of ZZA, with low computational cost but keeping the accuracy of the parent theory. Many challenging benchmarks were considered, both elastostatic and dynamic, assuming different boundary conditions. Both distributed and localized loading, symmetric and strongly asymmetric lay-ups (also with damaged properties of constituent layers) were taken into account, because these choices could increase layerwise effects. Moreover, the precision of theories to describe pumping modes, response to blast pulse loading, material wedge and impact problems are tested. Results are compared to exact solutions, if available, or to 3-D FEA by Icardi and Atzori.

Moreover, also approximate 3-D theories were created, for which (differently to zig-zag theories) user can a priori choose the number of d.o.f. as an input of analysis and any expansion order along in-plane and thickness directions. A portion of coefficients is calculated through fulfilment of physical constraints, while the remaining part is assumed as d.o.f. of this theory, whose number depends on expansion orders chosen and physical constraints enforced. These theories are more expensive than zig-zag theories, but they can be used as reference results if exact ones are not available.

Results confirm that higher-order theories, whose coefficients are redefined for each layers across the thickness and calculated by imposing the same full set of physical constraints of ZZA provide results that are indistinguishable from those obtained by the parent theory. Moreover, under these conditions:

- zig-zag functions can be changed or omitted without any loss of accuracy;
- functions that describe variation of displacements across the thickness can be changed, so, exponential, power series and sinusoidal functions, or a combination of them, can be assumed differently for each displacement and from point to point across the thickness, without any loss of accuracy;
- there is no need to assign a specific role to each coefficient and so, there is no need to calculate coefficients in order to fulfil a specific physical constraint. In other words, differently to ZZA, there is no need to a priori subdivide coefficients into categories (e.g. higher-order, continuity terms, …) because numerical results have proved that their role can be switched.

- linear contribution by FSDT is not necessary to obtain precise displacements and stresses

Otherwise, the accuracy of different approaches is strongly dependent on the simplifying assumptions made and on the choices of layerwise and global representation functions. Particularly, lower-order mixed theories that assume a simplified kinematics are not able to get the same precision of higher-order theories, when an accurate description of transverse deformability is required. Moreover, the superiority of mixed physically-based theories on kinematic-based ones is demonstrated if Murakami's rule is not respected. For such cases the kinematic-based theories require very high expansion order across the thickness to get comparably accurate results. Furthermore, numerical tests demonstrate that a piecewise cubic and a piecewise fourth-order description for in-plane and transverse displacements respectively is sufficient to get precise results, as long as coefficients are redefined for each layer and physical constraints are imposed.

Generalized version of ZZA, here referred as ZZA_GEN, is the best theory of this thesis, because its particularizations have the same accuracy of parent theory but very low computational burden. This theory is very interesting, because, thanks to its simple expression of displacements it requires very low expansion order across the thickness and this is optimal for the SEUPT and advantageous compared to similar widespread formulations in literature. Moreover, it was demonstrated that thanks to SEUPT technique is possible to develop Lagrangian C0 finite elements with accuracy of a layerwise models and to improve the results obtained by commercial finite elements, without any iterative process.

Summarizing, ZZA_GEN and its particularizations represent very appealing numerical tools by virtue of their accuracy and efficiency, which can provide considerable support for design and analysis of structures of industrial interest.

Appendix 1

In this appendix are reported displacements and stresses not previously included into chapter 4, where comments and analysis of results are reported.

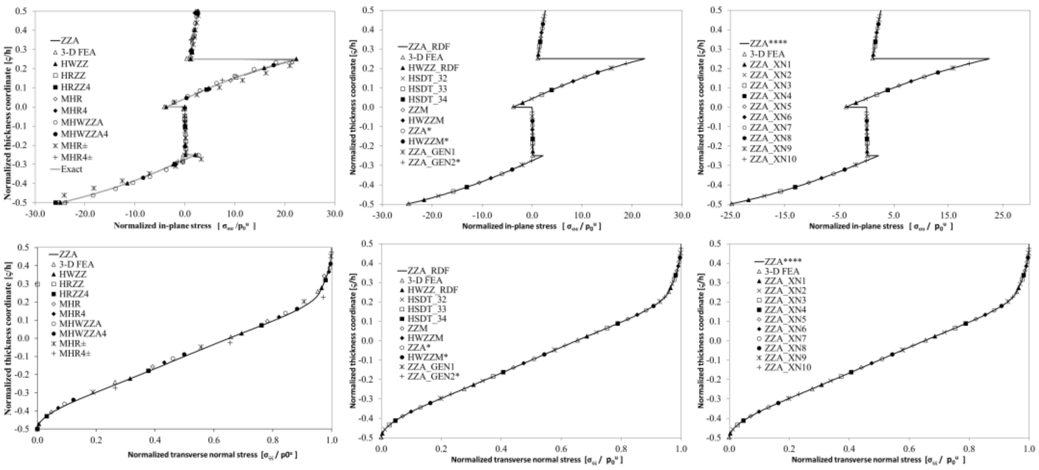

Figure A1.1: Normalized displacements and stresses, case a

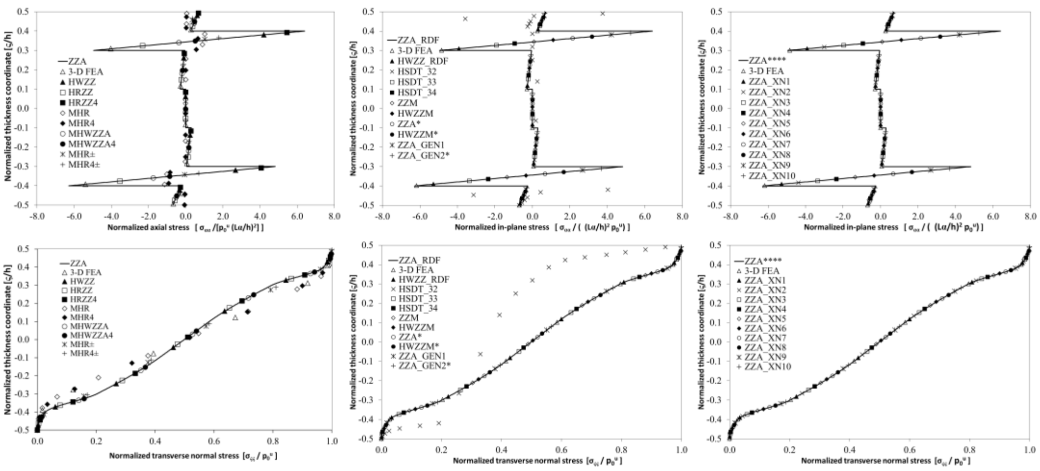

Figure A1.2: Normalized displacements and stresses, case b

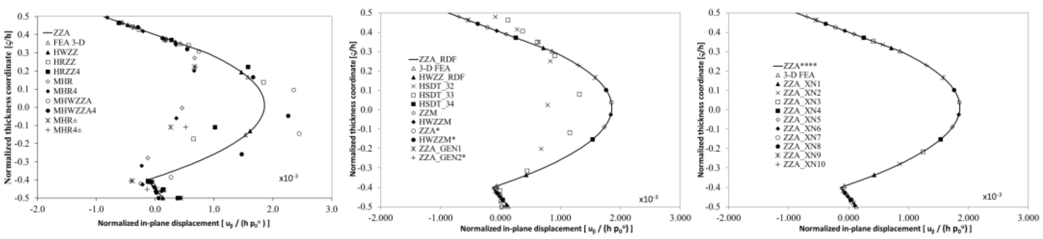

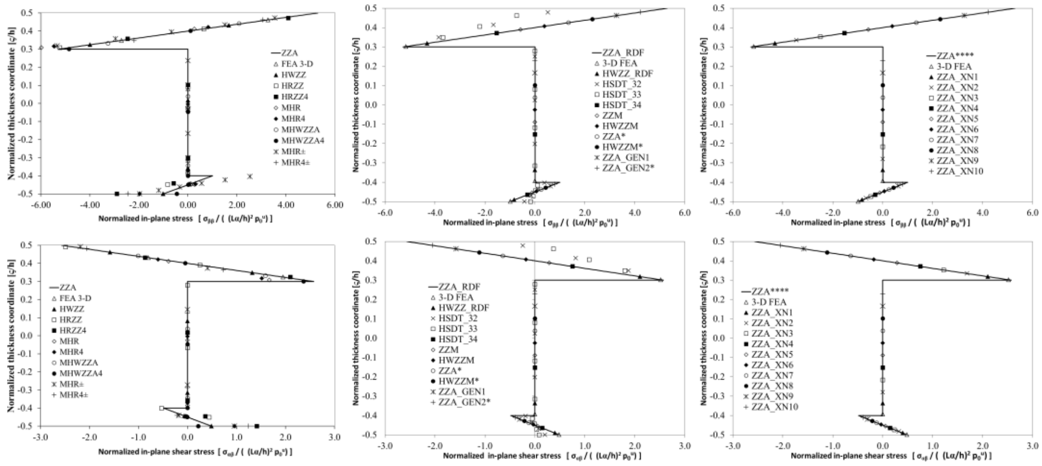

Figure A1.3: Normalized displacements and stresses, case c

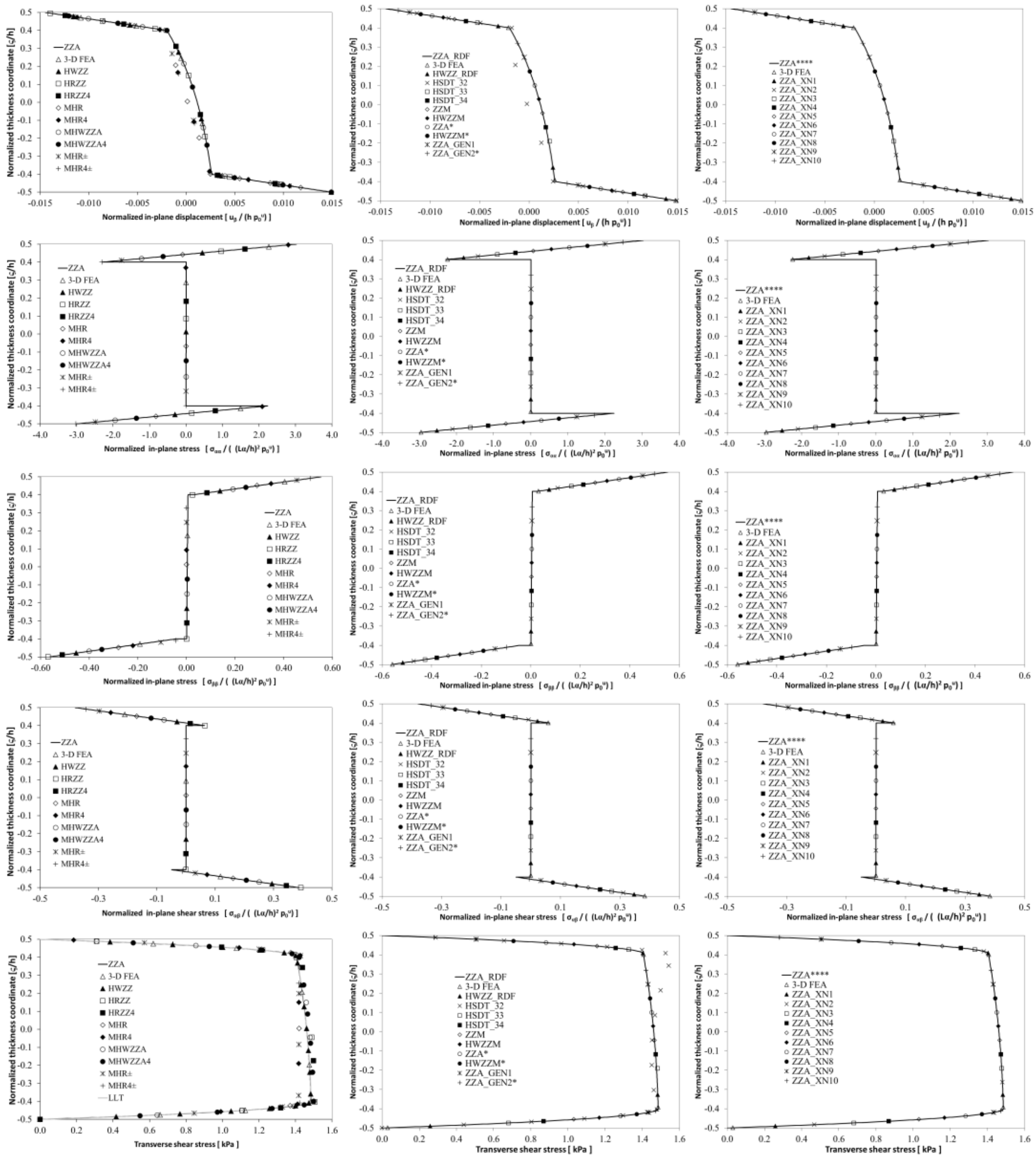

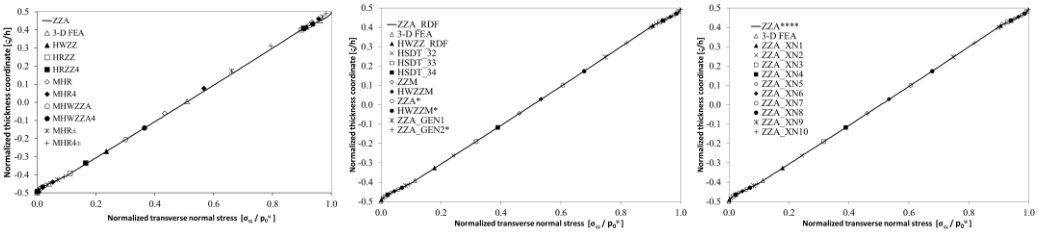

Figure A1.4: Normalized displacements and stresses, case d

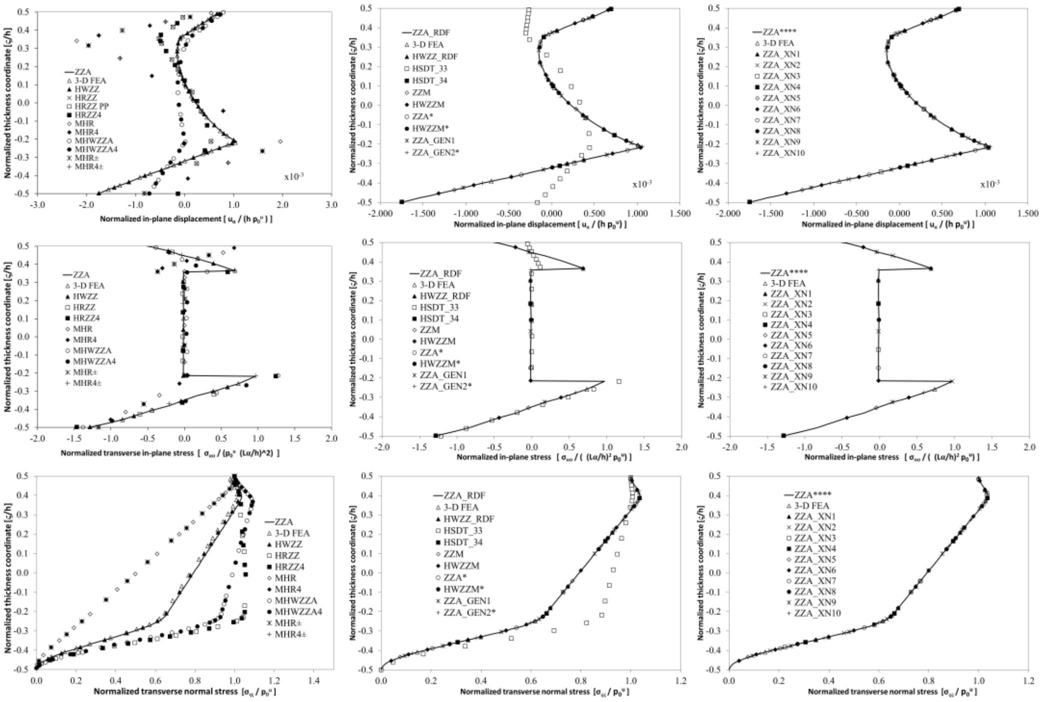

Figure A1.5: Normalized displacements and stresses, case e

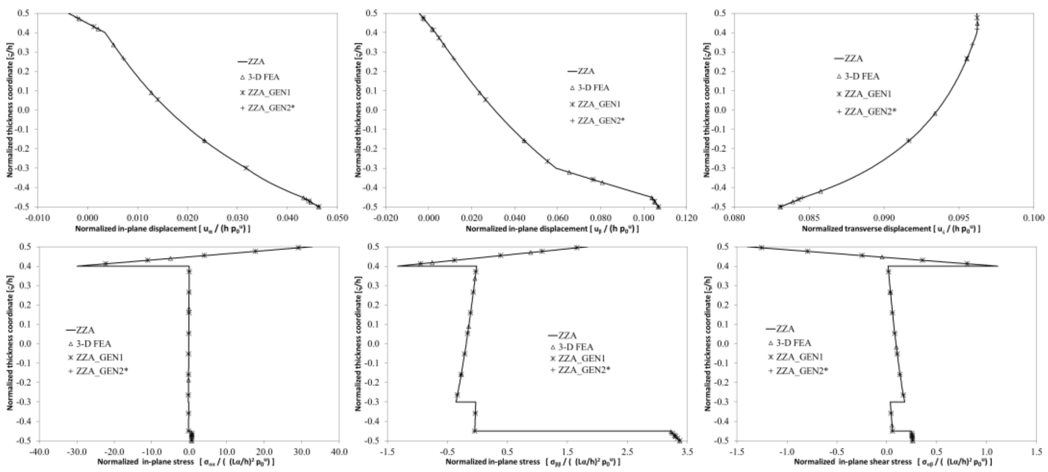

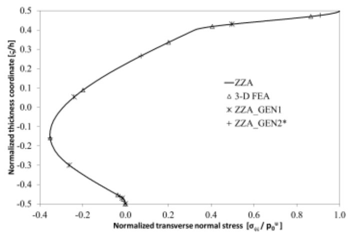

Figure A1.6: Normalized displacements and stresses, case f

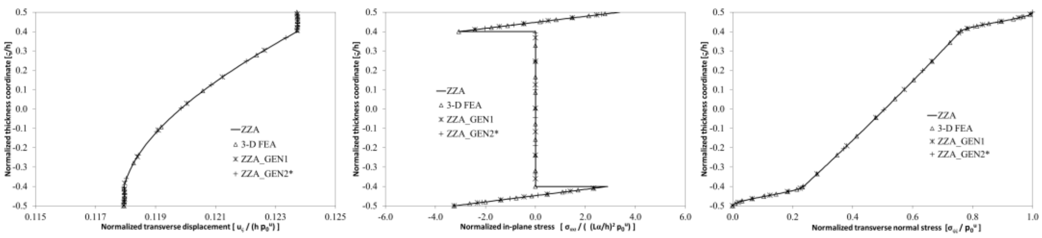

Figure A1.7: Normalized displacements and stresses, case g

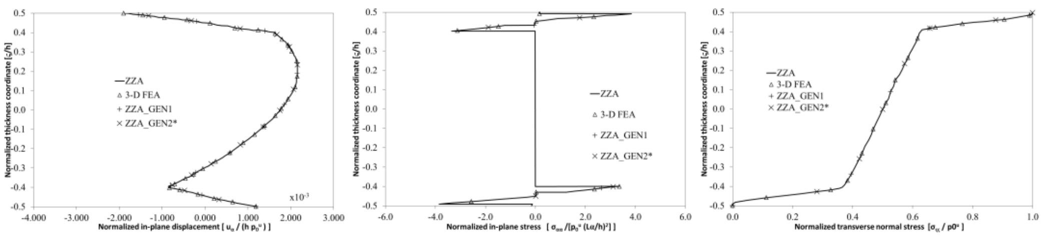

Figure A1.8: Normalized displacements and stresses, case h

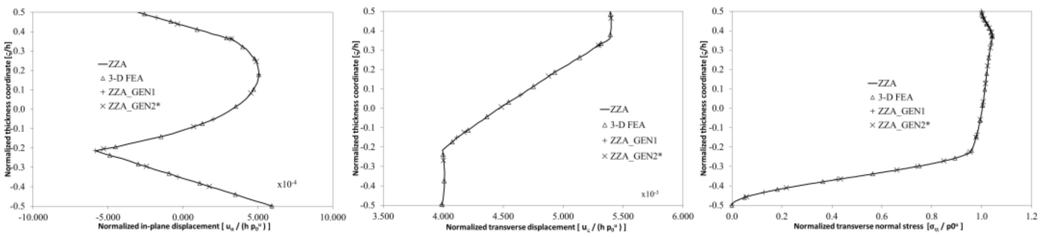

Figure A1.9: Normalized displacements and stresses, case i

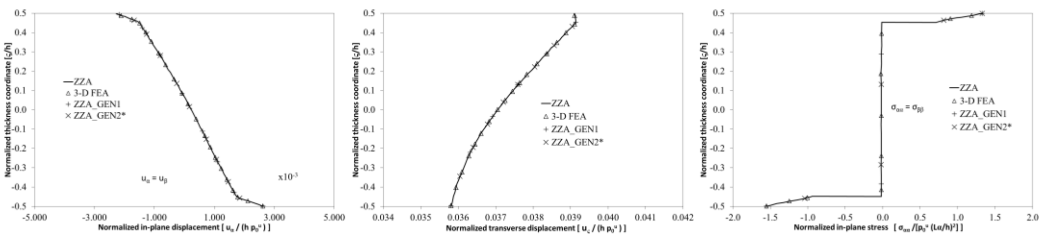

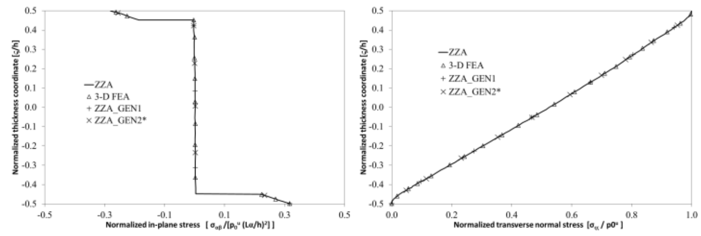

Figure A1.10: Normalized displacements and stresses, case j

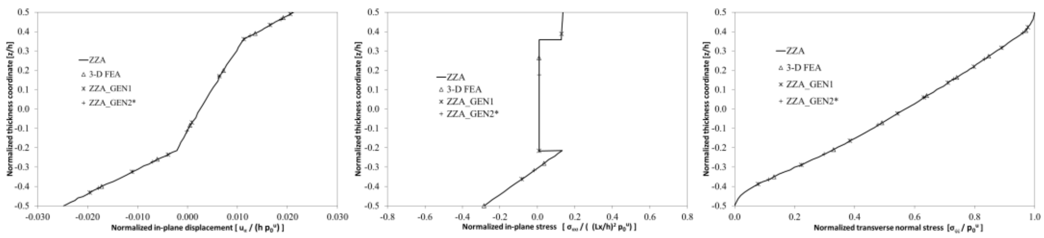

Figure A1.11: Normalized displacements and stresses, case k

Appendix 2

This appendix was created as guideline in order to help aerostructural engineers to choose appropriate models depending on problem.

Firstly, use of Equivalent Single Layer theories should be avoided. Indeed, they are very simple, but they are not able to accurately describe displacements and stresses. It should be noticed that they cannot obtain accurate trend of stresses, even if they are post-processed by recalculating out-of-plane stresses through local equilibrium equations, especially when thick laminates or sandwiches are analysed. Moreover they are not suitable to get also overall quantities such as fundamental frequencies.

Regarding zig-zag theories, as a general rule, use of kinematic-based should be avoided, being proved to be less efficient than physically-based ones. Moreover, it should be noticed that very high expansion order of displacements across the thickness are required, in order to limit errors when Murakami's rule is not respected, whose fulfilment is not easily deducible a priori. However, displacements could be wrongly calculated also when very high orders are assumed across the thickness [80]. Lower-order physically-based zig-zag theories are more accurate than kinematic-based counterparts, if the same expansion order across the thickness is used, anyway, they cannot accurately describe transverse deformability. As a consequence, use of these lower-order ones should be limited to elastostatic calculations of not extremely thick cross-ply laminates and thin sandwiches (without strong variation of mechanical properties of constituent material across the thickness) or to get first natural frequencies of these lay-ups.

Anyway, it should be also noticed that an accurate description of transverse displacement or deformability could be required:

- for elastostatic cases:
  - to analyse thick composite and sandwich laminates;
  - to analyse lay-up with very strong variation of mechanical properties of constituent layers;
  - to analyse very asymmetric lay-ups;
  - under boundary conditions (e.g. clamped edges);
  - under localized step loadings;
- for dynamic benchmarks:
  - to get high frequency vibrations;
  - also to get first natural frequencies, if pumping modes are present among the first modes of thick sandwiches;
  - for transient response to impulsive loadings, such as blast pulse;
- for piezo-actuating loadings;
- under temperature gradients;
- for impact damage analysis;
- delamination;

For these cases use of physically-based higher-order theories is mandatory to prevent any loss of accuracy caused by simplifications and assumptions.

Appendix 3

In this appendix the symbolic procedure that is used for all physically-based zig-zag theories is reported in Figure A3.1:

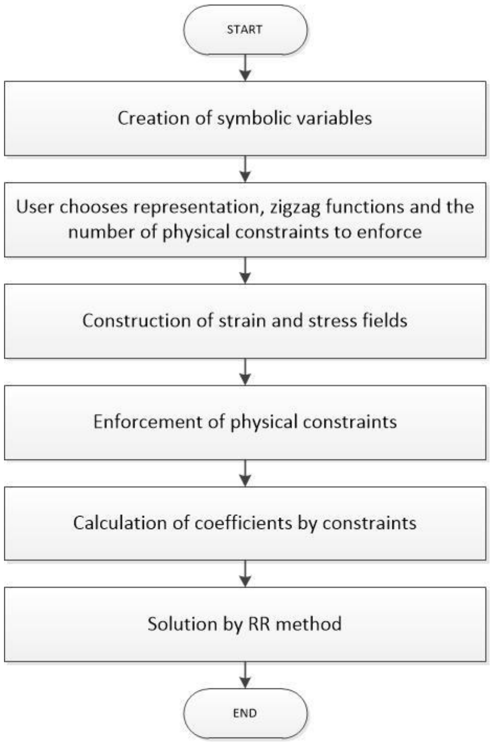

Figure A3.1: Normalized displacements and stresses, case k

Firstly, symbolic variables (e.g. in-plane and thickness coordinates, symbolic amplitudes) that are used in all next steps are created. In this step, the number of halfwaves along in-plane directions is chosen by user.

```
%% CREATION OF SYMBOLIC VARIABLES (example refers to a beam)
  for i=1:M    %M is the number of terms of in-plane expansion
    vettAmn(i)=sym(strcat('Amn_',num2str(i)),'real');
    vettCmn(i)=sym(strcat('Cmn_',num2str(i)),'real');
    vettDmn(i)=sym(strcat('Dmn_',num2str(i)),'real');
  end
dofRR=[vettAmn,vettCmn,vettDmn]';
%example for a beam
p0u=sym('p0u','real');   %symbolic loading
```

Subsequently, user choices the expansion order of displacements across the thickness (note that three different expansion order could be assumed), the functions that represent the variation of displacements across the thickness, the number of physical constraints that have to be imposed and the in-plane function of loading.

This is the only things that user must specify, which is the only thing that characterizes theories

As a consequence, displacements are developed automatically, so, strain and stress fields are calculated.

```
%% CONSTRUCTION OF STRAIN FIELD
%diff: Differentiate symbolic expression or function respect the indicate variable
epsx=diff(u,x);
epsz=diff(w,z);
epsxz=diff(u,z)+diff(w,x);
…
```

```
%% CONSTRUCTION OF STRESS FIELD
 for i=1:nl
   layer_Q=Q(:,:,i);
   epsilon=[epsx(i) … ]';
   sigmax(i)=(layer_Q(1,:)*epsilon)';
   …
end
```

Afterwards, physical constraints can be imposed and coefficients can be calculated, which depend on d.o.f. and their derivatives.

```
%% ENFORCEMENT OF PHYSICAL CONSTRAINTS
%e.g. sigmaxz=0 at upper and lower layers
 %posxz_x: definition of in-plane position where constraint is imposed (numerical
variable)
cont=1;  %counter
sigmaxzL=sigmaxz(1);
F(cont,1)=sigmaxzL;  %equivalent to imposition of sigmaxzL=0;
F(cont,1)=subs(F(cont,1),x,posxz_x);
F(cont,1)=subs(F(cont,1),z,-0.5*h);
cont=cont+1;
…
```

```
%% CALCULATION OF COEFFICIENTS BY CONSTRAINTS
 %Cost_sist contains the coefficients that are calculated  by imposing the fulfillment of
conditions F
 %The number and which coefficients are contained in Cost_sist is chosen by user.
 %Number of equations of F must be the same of Cost_sist
 F=subs(vpa(F), p0u,p0u_num );  %p0u_num is the numerical value of load
solut=vpasolve(F,Cost_sist);
```

Actually the displacement field is completely defined, by substituting back expressions *solut*.

Once all coefficients are calculated, Rayleigh-Ritz method is used to calculate d.o.f. It should be noticed that, thanks to symbolic calculus, work of external forces is computed exactly, regardless its expression, and no series expansions (e.g. Fourier series) are needed.

```
%% SOLUTION BY RR METHOD
 %TOT_POT: total potential energy
%Symbolic integration may be carried out by int function, but a numerical approach is
%equally accurate and requires a lower effort. dofRR contains the remaining unknown
amplitudes that are not yet determined by solving the previous system of equations F.
  cont=1;
 for i=1:length(dofRR)
    F2(cont,1)=diff(TOT_POT,dofRR(i));
    cont=cont+1;
 end
 F2=subs(vpa(F2),p0u,p0u_num);
soluz=vpasolve(F2,dofRR);
```

Once d.o.f. are obtained, problem is solved and results can be plotted and analysed.

References

1. **E. Carrera, E. Zappino, T. Cavallo.** *Accurate Free Vibration Analysis of Launcher Structures Using Refined 1D Models.* s.l. : International Journal of Aeronautical and Space Sciences , 2015. pp. 206-222. Vol. 16.
2. **E. Carrera, A. Pagani.** *Evaluation of the accuracy of classical beam FE models via locking-free hierarchically refined elements.* s.l. : International Journal of Mechanical Sciences, 2015. pp. 169-179. Vol. 100.
3. **E. Carrera, M. Boscolo.** *Classical and mixed finite elements for static and dynamic analysis of piezoelectric plates.* s.l. : International Journal for numerical methods in engineering, 2007. pp. 1135-1181. Vol. 70.
4. **U. Icardi, F. Sola.** *Development of an efficient zig-zag model with variable representation of displacements across the thickness.* s.l. : J. of Eng. Mech., 2014. pp. 531-541. Vol. 140.
5. **U. Icardi, L. Ferrero.** *Layerwise zig-zag model with selective refinement across the thicknes.* s.l. : International Journal for numerical methods in engineering, 2010. pp. 1085–1114. Vol. 84.
6. **U. Icardi, A. Atzori.** *Simple, efficient mixed solid element for accurate analysis of local effects in laminated and sandwich composites.* s.l. : Advances in Eng. Software, 2004. pp. 843-859. Vol. 35.
7. **Icardi, U.** *Layerwise mixed element with sublaminates approximation and 3D zig-zag field, for analysis of local effects in laminated and sandwich composites.* s.l. : International Journal for Numerical Methods in Engineering , 2006. pp. 94-125. Vol. 70.
8. **U. Icardi, F. Sola.** *Variable Singularity Power Wedge Element for Multilayered Composites.* s.l. : Universal Journal of Engineering Science, 2014. pp. 16-29. Vol. 2.
9. **Icardi, U.** *C0 plate element based on strain energy updating and spline interpolation, for analysis of impact damage in laminated composites.* s.l. : International Journal of Impact Engineering, 2007. pp. 1835–1868. Vol. 34.
10. **U. Icardi, L. Ferrero.** *Impact analysis of sandwich composites based on a refined plate element with strain energy updating.* s.l. : Composite Structures, 2009. pp. 35-51. Vol. 89.
11. **U. Icardi, F. Sola.** *C0 Mixed Layerwise Quadrilateral Plate Element with Variable in and Out-Of-Plane Kinematics and Fixed D.O.F.* s.l. : International Journal of Computational Engineering Research, 2015. pp. 6-25. Vol. 5.
12. —. *C0 Layerwise Model with Fixed Degrees of Freedom and Variable In- and Out-of-Plane Kinematics by Strain Energy Updating Technique.* s.l. : Aerospace, 2015. pp. 637-672. Vol. 2.

13. —. *C0 Fixed Degrees of Freedom Zigzag Model with Variable In-Plane and Out-of-Plane Kinematics and Quadrilateral Plate Element.* s.l. : Journal of Aerospace Engineering, 2015. Vol. 28.

14. **E., Carrera.** *Developments, ideas, and evaluations based upon Reissner's mixed variational theorem in the modeling of multilayered plates and shells.* s.l. : Appl. Mech. Rev., 2001. pp. 301–329. Vol. 54.

15. **U. Icardi, A. Urraci.** *Novel HW mixed zig-zag theory accounting for transverse normal deformability and lower-order counterparts assessed by old and new elastostatic benchmarks.* s.l. : Aerospace Science and Technology, 2018. pp. 541–571 . Vol. 80.

16. —. *Elastostatic assessment of several mixed/displacement-bases laminated plate theories, differently accounting for trasverse normal deformability.* s.l. : Aerospace Science and Technology, 2020. Vol. 98.

17. —. *Free and Forced Vibration of Laminated and Sandwich Plates by Zig-Zag Theories Differently Accounting for Transverse Shear and Normal Deformability.* s.l. : Aerospace, 2018. p. 108. Vol. 5(4).

18. —. *Considerations about the choice of layerwise and through-thickness global functions of 3-D physically-based zig-zag theories.* s.l. : Under Review, 2019.

19. —. *Free Vibration of flexible soft-core sandwiches according to layerwise theories differently accounting for the transverse normal deformability.* s.l. : Latin American Journal of Solids and Structures, 2019. pp. 1-35. Vol. 16.

20. **A. Urraci, U. Icardi.** *New 3-D zig zag theories: elastostatic assessment of strategies differently accounting for layerwise effects of laminated and sandwich composites.* s.l. : International Journal of Engineering Research and Application, 2019. pp. 1-25. Vol. 9.

21. —. *Approximate 3-D model for analysis of laminated plates with arbitrary lay-ups, loading and boundary conditions.* s.l. : International Journal of Engineering Research & Science, 2019. pp. 21-39. Vol. 5.

22. —. *Zig-zag theories differently accounting for layerwise effects of multilayered composites.* s.l. : International Journal of Engineering Research & Science, 2019. pp. 21-42. Vol. 5.

23. —. *Approximate 3-D models for laminated plates with arbitrary lay-ups, loading and constraints.* s.l. : Under Review.

24. **U. Icardi, A. Urraci.** *Impact Damage Analysis with Stress Continuity Constraints Fulfilment at Damaged-Undamaged Regions and at Layer Interfaces.* s.l. : Latin American Journal of Solids and Structures, 2017. pp. 1416-1442. Vol. 14.

25. **Reddy, J.N.** *Mechanics of laminated composite plates and shells: theory and analysis. 2nd Edition.* Boca Raton : CRC Press, 2003.

26. **J.N. Reddy, D.H. Robbins.** *Theories and computational models for composite laminates.* s.l. : Appl Mech Rev 1994, 1994. pp. 147-169. Vol. 47.

27. **J.N. Reddy, R.A. Arciniega.** *Shear deformation plate and shell theories: from Stavsky to present.* s.l. : Mech Adv Mater Struct, 2004. pp. 535–582. Vol. 11.

28. **V.V. Vasilive, A.A. Lur'e.** *On refined theories of beams, plates and shells.* s.l. : J Compos Mat, 1992. pp. 422–430. Vol. 26.

29. **A.K. Noor, S.W. Burton, C.W. Bert.** *Computational model for sandwich panels and shells.* s.l. : Appl Mech Rev , 1996. pp. 155–199. Vol. 49.

30. **E., Carrera.** *Historical review of zig-zag theories for multilayered plates and shells.* s.l. : Appl. Mech. Rev., 2003. pp. 1-22. Vol. 56.

31. **Carrera, E.** *On the use of the Murakami's zig-zag function in the modeling of layered plates and shells.* s.l. : Compos. Struct., 2004. pp. 541–554. Vol. 82.

32. **Qatu, M.S.** *Recent research advances in the dynamic behavior of shells: 1989–2000, part 1: laminated composite shells.* s.l. : Appl Mech Rev, 2002. pp. 325–50. Vol. 55.

33. **M.S. Qatu, R.W. Sullivan, W. Wang.** *Recent research advances on the dynamic analysis of composite shells: 2000–2009.* s.l. : Compos Struct, 2010. pp. 14–31. Vol. 93.

34. **C. Wanji, W. Zhen.** *A selective review on recent development of displacement-based laminated plate theories.* s.l. : Recent Pat. Mech. Eng., 2008. pp. 29–44. Vol. 1.

35. **R. Khandan, S. Noroozi, P. Sewell, J. Vinney.** *The development of laminated composite plate theories: a review.* s.l. : J Mater Sci, 2012. pp. 5901-5910. Vol. 47.

36. **Burlayenko VN, Altenbach H, Sadowski T.** *An evaluation of displacement-based finite element models used for free vibration analysis of homogeneous and composite plates.* s.l. : Journal of Sound and Vibration, 2015. pp. 152–175. Vol. 358.

37. **Jun L, Xiang H, Li Xiaobin L.** *Free vibration analyses of axially loaded laminated composite beams using a unified higher-order shear deformation theory and dynamic stiffness method.* s.l. : Composite Structures, 2016. pp. 308–322. Vol. 158.

38. **Zhen W, Wanji C.** *Free vibration of laminated composite and sandwich plates using global–local higher-order theory.* s.l. : Journal of Sound and Vibration, 2006. pp. 333–349. Vol. 298.

39. **Kim, J. S.** *Free vibration of laminated and sandwich plates using enhanced plate theories.* s.l. : Journal of Sound and Vibration, 2007. pp. 268–286. Vol. 308.

40. **J.N. Reddy, E.J. Barbero, J.L. Teply.** *A plate bending element based on a generalized laminate theory.* s.l. : Int J Numer Meth Eng, 1989. pp. 2275–2292. Vol. 28.

41. **F.G. Rammerstorfer, K. Dorninger, A. Starlinger.** *Composite and sandwich shells.* s.l. : Nonlin An Shells Finite Elem, 1992. pp. 131–194. Vol. 328.

42. **Sciuva, M. Di.** *A refinement of the transverse shear deformation theory for multilayered orthotropic plates.* s.l. : L'Aerotecnica Missili e Spazio, 1984. pp. 84–9. Vol. 62.

43. **Murakami, H.** *Laminated composite plate theory with improved in-plane responses.* s.l. : ASME Appl Mech, 1986. pp. 661–666. Vol. 53.

44. **Gherlone, M.** *On the use of zigzag functions in equivalent single layer theories for laminated composite and sandwich beams: a comparative study and some observations on external weak layers.* s.l. : ASME Appl. Mech., 2013. pp. 1-19. Vol. 80(6).

45. **R.M.Jr, Groh, P.M.Weaver.** *On displacement-based and mixed-variational equivalent single layer theories for modeling highly heterogeneous laminated beams.* s.l. : Int J Solids and Struct, 2015. pp. 147-170. Vol. 59.

46. **G. Giunta, D. Crisafulli, S. Belouettar, E. Carrera.** *Hierarchical theories for the free vibration analysis of functionally graded beams.* s.l. : Comp Struct, 2011. pp. 68–74. Vol. 94.

47. **E. Carrera, A.G. de Miguel, A. Pagani.** *Hierarchical theories of structures based on Legendre polynomial expansions with finite element applications.* s.l. : Int J Mech Sci, 2017. pp. 286-300. Vol. 120.

48. **A. Catapano, G. Giunta, S. Belouettar, E. Carrera.** *Static analysis of laminated beams via a unified formulation.* s.l. : Comp. Struct., 2011. pp. 75-83. Vol. 94.

49. **A. G. de Miguel, E. Carrera, A. Pagani, E. Zappino.** *Accurate Evaluation of Interlaminar Stresses in Composite Laminates via Mixed One-Dimensional Formulation.* s.l. : AIAA Journal, 2018. pp. 4582-4594. Vol. 56.

50. **S. Candiotti, J.L. Mantari, J. Yarasca, M. Petrolo, E. Carrera.** *An axiomatic/asymptotic evaluation of best theories for isotropic metallic and functionally graded plates employing non-polynomic functions.* s.l. : Aerospace Science and Technology, 2017. pp. 179–192. Vol. 68.

51. **S. Brischetto, E. Carrera, L. Demasi.** *Improved response of asymmetrically laminated sandwich plates by using Zig-Zag functions.* s.l. : J. Sandwich Struct. & Mat, 2009. pp. 257- 26. Vol. 11.

52. **U. Icardi, F. Sola.** *Assessment of recent zig-zag theories for laminated and sandwich structures.* s.l. : Composites Part B, 2016. pp. 26-52. Vol. 97.

53. **Pagano, J M Whitney and N J.** *Shear deformation in heterogeneous anisotropic plates.* s.l. : ASME J. Appl. Mech., 1970. pp. 1031-1036. Vol. 37.

54. **Icardi, U.** *Higher-order zig-zag model for analysis of thick composite beams with inclusion of transverse normal stress and sublaminates approximations.* s.l. : Comp. Part B, 2001. pp. 343-354. Vol. 32.

55. **U. Icardi, F. Sola.** *C° fixed degrees of freedom zigzag model with variable in-plane and out-of plane kinematics and quadrilateral plate element.* s.l. : Journal Aerosp. Eng., 2014. pp. 040141351 - 0401413514. Vol. 28.

56. **Reddy, J N.** *A simple higher-order theory for laminated composite plates.* s.l. : ASME J. Appl. Mech., 1984. pp. 745-752. Vol. 51.

57. **Pagano, N.J.** *Exact Solutions for Composite Laminates in Cylindrical Bending.* s.l. : Journal of Composite Materials, 1969. pp. 398-411.

58. **X.Y. Li, D. Liu.** *Generalized laminate theories based on double superposition hypothesis.* s.l. : Int. J. Num. Mech. Eng., 1997. pp. 1197–212. Vol. 40.

59. **W. Zhen, C. Wanji.** *A study of global–local higher-order theories for laminated composite plates.* s.l. : Comp. Struct., 2007. pp. 44–54. Vol. 79.

60. **S. Kim, M. Cho.** *Enhanced first-order theory based on mixed formulation and transverse normal effect.* s.l. : International Journal of Solids and Structures, 2007. pp. 1256–1276. Vol. 44.

61. **A. Tessler, M. Di Sciuva, M. Gherlone.** *A refined zigzag beam theory for composite and sandwich beams.* s.l. : J. Compos. Mat., 2009. pp. 1051–1081. Vol. 43.

62. **L. Iurlaro, M. Gherlone, M. Di Sciuva.** *The (3,2)-mixed refined zigzag theory for generally laminated beams: theoretical development and C° finite element formulation.* s.l. : Int J of Solids and Struct, 2015. pp. 1–19. Vols. 73–74.

63. **Shariyat, M.** *A generalized global-local higher order theory for bending and vibration analyses of sandwich plates subjected to thermo-mecanical loads.* s.l. : Int J MechSci, 2010. pp. 495-514. Vol. 52.

64. **W. Zhen, C. Wanji.** *A global higher-order zig-zag model in terms of the HW variational theorem for multi-layered composite beams.* s.l. : Compos. Struct., 2016. pp. 128–136. Vol. 158.

65. **Demasi, L.** *Mixed plate theories based on the generalized unified formulation. Part IV: zig-zag theories.* s.l. : Compos. Struct., 2009. pp. 195–205. Vol. 87.

66. **J.D. Rodrigues, C.M.C. Roque, A.J.M. Ferreira, E. Carrera, M. Cinefra.** *Radial basis functions-finite differences collocation and a unified formulation for bending, vibration and buckling analysis of laminated plates, according to Murakami's zig-zag theory.* s.l. : Compos. Struct., 2011. pp. 1613–1620. Vol. 93.

67. **E., Carrera.** *An assessment of mixed and classical theories on global and local response of multilayered orthotropic plates.* s.l. : Compos Struct, 2000. pp. 183-198. Vol. 50.

68. —. *A priori vs. a posteriori evaluation of transverse stresses in multilayered orthotropic plates.* s.l. : Composite Structures, 2000. pp. 245-260. Vol. 48.

69. **E. Carrera, A. Ciuffreda.** *Bending of composites and sandwich plates subjected to localized lateral loadings: a comparison of various theories.* s.l. : Composite Structures, 2005. pp. 185–202. Vol. 68.

70. **C.S Rekatsinas, C.V. Nastos, T.C. Theodosiou, D.A. Saravanos.** *A time-domain high-order spectral finite element for the simulation of symmetric and anti-simmetric guided waves in laminated composite strips.* s.l. : Wave Motion, 2015. pp. 1-19. Vol. 53.

71. **O. Mattei, L. Bardella.** *A structural model for plane sandwich beams including transverse core deformability and arbitrary boundary conditions.* s.l. : European Journal of Mechanics Part A Solids, 2016. pp. 172-186. Vol. 58.

72. **E. Carrera, M. Filippi, E. Zappino.** *Laminated beam analysis by polynomial, trigonometric, exponential and zig-zag theories.* s.l. : European Journal of Mechanics Part A/Solids, 2013. pp. 58-69. Vol. 41.

73. **Matsunaga, H.** *Interlaminar stress analysis of laminated composite beams according to global higher-order deformation theories.* s.l. : Composite Structures, 2002. pp. 105-114. Vol. 55.

74. **K. Surana, S. Nguyen.** *Two-dimensional curved beam element with higher order hierarchical transverse approximation for laminated composites.* s.l. : Computers and Structures, 1990. pp. 499-511. Vol. 36.

75. **M.K. Rao, Y. Desai, M. Chistnis.** *Free vibrations of laminated beams using mixed theory.* s.l. : Composite Structures, 2001. pp. 149-160. Vol. 52.

76. **L. Jun, H. Hongxing.** *Dynamic stiffness analysis of laminated composite beams using trigonometric shear deformation theory.* s.l. : Composite Structures, 2009. pp. 433-442. Vol. 89.

77. **P. Vidal, O. Polit.** *Assessment of the refined sinus model for the non-linear analysis of composite beams.* s.l. : Composite Structures, 2009. pp. 370-381. Vol. 87.

78. **M. Karama, K. Afaq, S. Mistou.** *Mechanical behaviour of laminated composite beam by the new multi-layered laminated composite structures model with transverse shear stress continuity.* s.l. : International Journal of Solids and Structures, 2003. pp. 1525-1546. Vol. 40.

79. **J. Mantari, A. Oktem, C.G. Soares.** *A new higher order shear deformation theory for sandwich and composite laminated plates.* s.l. : Composites: Part B, 2012. pp. 1489-1499. Vol. 43.

80. **Brischetto S, Carrera E, Demasi L.** *Improved Response of Unsymmetrically Laminated Sandwich Plates by Using Zig-zag Functions* . s.l. : J. Sandw. Struct. Mater., 2009. pp. 257-267. Vol. 11.

81. **T.S. Plagianakos, D.A. Saravanos.** *Higher-order layerwise laminate theory for the prediction of interlaminar shear stresses in thick composite and sandwich com-posite plates.* s.l. : Compos. Struct., 2009. pp. 23-35. Vol. 87.

82. **M. Kashtalyan, M. Menshykova.** *Three-dimensional elasticity solution for sandwich panels with a functionally graded core.* s.l. : Composite Structures, 2009. pp. 36-43. Vol. 87.

83. **M. Di Sciuva, U. Icardi.** *Numerical studies on bending, free vibration and buckling of multilayered.* s.l. : L'aerotecnica, Missili e Spazio, 1993. pp. 1-2. Vol. 72.

84. **K.N. Cho, C.W. Bert, A.G. Striz.** *Free vibrations of laminated rectangular analyzed by higher order individual-layer theory.* s.l. : Journal of Sound and Vibration, 1991. pp. 429-442. Vol. 145.

85. **L. Librescu, S.Y. Oh, J. Hohe.** *Linear and non-linear dynamic response of sandwich panels to blast loading.* s.l. : Composites PartB: Engineering, 2004. pp. 673-683. Vol. 35.

86. **L. Librescu, S. Na, P. Marzocca, C. Chung, M.K. Kwak.** *Active aeroelastic control of 2-D wing-flap systems operating in an incompressible flowfield and impacted by a blast pulse.* s.l. : Journal of Sound and Vibration, 2005. pp. 685-706. Vol. 283.

87. **L. Librescu, S.Y. Oh, J. Hohe.** *Dynamic response of anisotropic sandwich flat panels to underwater and in-air explosions.* s.l. : International Journal of Solids and Structures, 2006. pp. 3794-3816. Vol. 43.

88. **T. Hause, L. Librescu.** *Dynamic response of anisotropic sandwich flat panels to explosive pressure pulses.* s.l. : International Journal of Impact Engineering, 2005. pp. 607-628. Vol. 31.

89. —. *Dynamic response of doubly-curved anisotropic sandwich panels impacted by blast loadings.* s.l. : International Journal of Solids and Structures, 2007. pp. 6678-6700. Vol. 44.

90. **O. Song, J.S. Ju, L. Librescu.** *Dynamic response of anisotropic thin-walled beams to blast and harmonically oscillating loads.* s.l. : International Journal of Impact Engineering, 1998. pp. 663-682. Vol. 21.

91. **Bathe, K.J.** *Finite element procedures.* Englewood Cliffs : Prentice-Hall, 1996.

92. **O.C. Zienkiewicz, R.L. Taylor.** *The Finite Element, Sixt Edition, Volume 1: The basis.* Oxford : Butterworth-Heinemann, 2000. Vol. 1.

93. **M.O.W. Richardson, M.J. Wisheart.** *eview of low-velocity impact properties of composite materials.* s.l. : Composites Part A. pp. 1123-1131. Vol. 27.

94. **F.D. Morinière, R.C. Alderliesten, R. Benedictus.** *Modelling of impact damage and dynamics in fibre-metal laminates-A review.* s.l. : International Journal of Impact Engineering, 2014. pp. 27-38. Vol. 67.

95. **Abrate, S.** *Modeling of impacts on composite structures.* s.l. : Composite Structures, 2001. pp. 129-138. Vol. 51.

96. —. *Impact on composite plates in contact with water.* s.l. : Procedia Engineering, 2014. pp. 2-9. Vol. 88.

97. **D.J. Elder, R.S. Thomson, M.Q. Nguyen, L. Scott.** *Review of delamination predictive methods for low speed impact of composite laminates.* s.l. : Composite Structures, 2004. pp. 677–683. Vol. 66.

98. **G.B. Chai, S. Zhu.** *A review of low-velocity impact on sandwich structures.* s.l. : Journal of Materials: Design & Applications, 2011. pp. 207-230. Vol. 225(4).

99. **M.R. Garnich, M.K. Akula Venkata.** *Review of degradation models for progressive failure analysis of fiber reinforced polymer composites.* s.l. : Appl. Mech. Reviews, 2009. pp. 1-35. Vol. 62.

100. **P.F. Liu, J.Y. Zheng.** *Review on methodologies of progressive failure analysis of composite laminates.* New York : Continuum mechanics, 2009.

101. **Berthelot, J.M.** *Transverse Cracking and Delamination in Cross-Ply Glass-Fiber and Carbon-Fiber Reinforced Plastic Laminates: Static and Fatigue Loading.* s.l. : Appl. Mech. Reviews, 2003. pp. 111–147. Vol. 56.

102. **D.P.W. Horrigan, R.A. Staal.** *Predicting failure loads of impact damaged honeycomb sandwich panels- A refined model.* s.l. : J of Sandwich Structures and Materials, 2011. pp. 111-133. Vol. 13.

103. **A. Aktas, M. Aktas, R. Turan.** *he effect of stacking sequence on the impact and post-impact behaviour of woven/knit glass/epoxy hybrid composites.* s.l. : Composite Structures, 2013. pp. 119-135. Vol. 103.

104. **T. Mitrevski, J.H. Marshall, R. Thomson, R. Jones, B. Whittingham.** *The effect of impactor shape on the impact response of composite laminates.* s.l. : Composite Structures, 2005. pp. 139–148. Vol. 67.

105. **A.R. Damanpack, M. Shakeri, M.M. Aghdam.** *A new finite element model for low-velocity impact analysis of sandwich beams subjected to multiple projectiles.* s.l. : Composite Structures, 2013. pp. 21–33. Vol. 104 .

106. **Chakraborty, D.** *Delamination of Laminated Fiber Reinforced Plastic Composites Under Multiple Cylindrical Impact.* s.l. : Materials & Design, 2007. pp. 1142-1153. Vol. 28.

107. **A. Chakrabarti, H.D. Chalak, M.A. Iqbal, A.H. Sheikh.** *A new FE model based on higher order zig-zag theory for the analysis of laminated sandwich beam soft core.* s.l. : Composite Structures, 2011. pp. 271-279. Vol. 93 .

108. **Kreja, I.** *A literature review on computational models for laminated composite and sandwich panels.* s.l. : Central European Journal of Engineering, 2001. pp. 59–80. Vol. 1.

109. **Y. Zhang, C. Yang.** *Recent Developments in Finite Element Analysis for Laminated Composite Plates.* s.l. : Composite Structures, 2009. pp. 147–157. Vol. 88.

110. **Tahani, M.** *Analysis of laminated composite beams using layerwise displacement theories.* s.l. : Composite Structures, 2007. pp. 535-547. Vol. 79.

111. **Matsunaga, H.** *A comparison between 2-D single-layer and 3-D layerwise theories for computing interlaminar stresses of laminated composite and sandwich plates subjected to thermal loadings.* s.l. : Composite Structures, 2004. pp. 161-177. Vol. 64.

112. **C.C. Chao, C.Y. Tu.** *Three-dimensional contact dynamics of laminated plates: Part 1. Normal Impact.* s.l. : Composites Part B, 1999. pp. 9-22. Vol. 30.

113. **D.W. Zhou, W.J. Stronge.** *Low velocity impact denting of HSSA lightweight sandwich panel.* s.l. : International Journal of Mechanical Sciences, 2006. pp. 1031–1045. Vol. 48.

114. **A.N. Palazotto, E.J. Herup, L.N.B. Gummadi.** *Finite Element Analysis of Low- Velocity Impact on Composite Sandwich Plates.* s.l. : Composite Structures, 2000. pp. 209–227. Vol. 49.

115. **L. Kärger, J. Baaran, J. Teßmer.** *Rapid Simulation of Impacts on Composite Sandwich Panels Inducing Barely Visible Damage.* s.l. : Composite Structures, 2007. pp. 527–534. Vol. 79.

116. **A. Diaz Diaz, J.J. Caron, A. Ehrlacher.** *Analytical Determination of the Modes I, II and III Energy Release Rates in a Delaminated Laminate and Validation of a Delamination Criterion.* s.l. : Composite Structures, 2007. pp. 424–432. Vol. 78.

117. **E. Oñate, A. Eijo, S. Oller.** *A numerical model of delamination in composite laminated beams using the LRZ beam element based on the refined zigzag theory.* s.l. : Composite Structures, 2012. pp. 270–280. Vol. 104.

118. —. *Delamination in laminated plates using the 4-noded quadrilateral QLRZ plate element based on the refined zigzag theory.* s.l. : Composite Structures, 2012. pp. 456–471. Vol. 108.

119. **U. Icardi, F. Sola.** *Analysis of bonded joints with laminated adherends by a variable kinematics layerwise model.* s.l. : Int. J. of Adhesion & Adhesives, 2014. pp. 244-254. Vol. 50.

120. **P. Ladevèze, G. Lubineau, D. Marsal.** *Towards a bridge between the micro- and mesomechanics of delamination for laminated composites.* s.l. : Compos. Sci. & Tech., 2006. pp. 698-712. Vol. 66.

121. **A.S. Yigit, A.P. Christoforou.** *On the impact between a rigid sphere and a thin composite laminate supported by a rigid substrate.* s.l. : Composite Structures, 1995. pp. 169-177. Vol. 30.

122. **Choi., I.H.** *Contact force history analysis of composite sandwich plates subjected to low-velocity impact.* s.l. : Composite Structures, 2006. pp. 582–586. Vol. 75.

123. **Y. Li, A. Xuefeng, Y. Xiaosu.** *Comparison with Low-Velocity Impact and Quasi-static Indentation Testing of Foam Core Sandwich Composites.* s.l. : International Journal of Applied Physics and Mathematics, 2012. pp. 58-62. Vol. 2.

124. **U. Icardi, F. Sola.** *Indentation of sandwiches using a plate model with variable kinematics and fixed degrees of freedom.* s.l. : Thin-Walled Structures, 2015. pp. 24-34. Vol. 86.

125. **Z. Hashin, A. Rotem.** *A Fatigue Criterion for Fiber-reinforced Materials.* s.l. : Journal of Composite Material, 1973. pp. 448–464. Vol. 7.

126. **H.Y. Choi, F.K. Chang.** *A model for predicting damage in graphite/epoxy laminated composites resulting from low velocity point impact.* s.l. : Journal of Composite Materials, 1992. pp. 2134–2169. Vol. 26.

127. **T. Besant, G.A.O. Davies, D. Hitchings.** *inite element modelling of low velocity impact of composite sandwich panels.* s.l. : Composites Part A, 2001. pp. 1189-1196. Vol. 32.

128. **WF, ROHACELL.** *Product Information.* s.l. : Evonik Röhm GmbH, 2011.

129. **Q.M. Li, R.A.W. Mines, R.S. Birch.** *The crush behaviour of Rohacell-51WF structural foam.* s.l. : International Journal of Solids and Structures, 2000. pp. 6321– 6341. Vol. 37.

130. **S.M. Lee, T.K. Tsotsis.** *Indentation failure behaviour of honeycomb sandwich panels.* s.l. : Composites Science and Technology, 2000. pp. 1147–1159. Vol. 60.

131. **U. Icardi, G. Zardo.** *C0 plate element for delamination damage analysis, based on a zig-zag model and strain energy updating.* s.l. : International Journal of Impact Engineering, 2005. pp. 579-606. Vol. 31.

132. **V.L. Hein, F. Erdogan.** *Stress singularities in a two-material wedge.* s.l. : International Journal of Fracture Mechanics, 1971. pp. 317-330. Vol. 7 .

133. **Pagano, N.J.** *Exact Solutions for Rectangular Bidirectional Composites and Sandwich Plates.* s.l. : Journal of Composite Materials, 1970. pp. 20-34. Vol. 4.

134. **Ren, J.G.** *Exact solutions for laminated cylindrical shells in cylindrical bending.* s.l. : Composites Science and Technology, 1987. pp. 169-187. Vol. 29.

135. **Brischetto, S.** *Exact three-dimensional static analysis of single- and multi-layered plates and shells.* s.l. : Composites Part B Engineering, 2017. pp. 230-252. Vol. 119.

136. **B. Woodward, M. Kashtalyan.** *3D elasticity analysis of sandwich panels with graded core under distributed and concentrated loadings.* s.l. : International Journal of Mechanical Sciences, 2011. pp. 872-885. Vol. 53.

137. **B. E. Abali, C. Voellmecke, B. Woodward, M. Kashtalyan, I. Guz, W.H. Mueller.** *Three-dimensional elastic deformation of functionally graded isotropic plates under point loading.* s.l. : Composite Structures, 2014. pp. 367-376. Vol. 118.

138. **B. Woodward, M. Kashtalyan.** *Three-dimensional elasticity analysis of sandwich panels with functionally graded transversely isotropic core.* s.l. : Archive of Applied Mechanics, 2019. pp. 1-22.

139. **J.N. Reddy, W.C. Chao.** *A comparison of closed-form and finite element solutions of thick laminated anisotropic rectangular plates.* s.l. : Nuclear Engineering and Design, 1981. pp. 153-167. Vol. 64.

140. **Yakimov, A.S.** *Analytical Solution Methods for Boundary Value Problems. 1st Edition.* s.l. : Academic Press, 2016.

141. **Wanji, W. Zhen and C.** *A C0-type higher-order theory for bending analysis of laminated composite and sandwich plates.* s.l. : Composite Structures, 2010. pp. 653-661. Vol. 92.

142. **R. Sahoo, B. N. Singh.** *A new shear deformation theory for the static analysis of laminated composite and sandwich plates.* s.l. : International Journal of Mech. Sci., 2013. pp. 324-336. Vol. 75.

143. **Prathap, G.** *The displacement-type finite element approach—from art to science.* s.l. : Prog. Aerospace Sci., 1994. pp. 295 - 405. Vol. 10.

144. **Mantari, J L, Oktem, A S and Guedes Soares, C.** *Static and dynamic analysis of laminated composite and sandwich plates and shells by using a new higher-order shear deformation theory.* s.l. : Composite Structures, 2011. pp. 37-49. Vol. 94.